

**IMPLANTABLE ANTINEOPLASTIC-LOADED ANTIBODY FUNCTIONALIZED
NANOMICELLES FOR HUMAN OVARIAN CARCINOMA CELL TARGETING BY
MOLECULAR AND IN VIVO INVESTIGATIONS**

JONATHAN MONWABISI PANTSHWA



A thesis submitted to the Faculty of Health Sciences, University of the
Witwatersrand,
in fulfillment of the requirements for the degree of
Doctor of Philosophy

Supervisors

Professor Viness Pillay
University of the Witwatersrand, Department of Pharmacy and Pharmacology,
Johannesburg, South Africa

Co-Supervisors:

Professor Yahya E. Choonara
Department of Pharmacy and Pharmacology, University of the Witwatersrand, South Africa
Professor Lisa C. du Toit
Department of Pharmacy and Pharmacology, University of the Witwatersrand, South Africa
and
Doctor Clem Penny
Department of Medical Oncology, University of the Witwatersrand, South Africa

Johannesburg, 2017

DECLARATION

I, Monwabisi Jonathan Pantshwa declare that this Thesis is my own work. It has being submitted for the degree of Doctor of Philosophy in the Faculty of Health Sciences at the University of the Witwatersrand, Johannesburg. It has not been submitted before for any degree or examination at this or any other University.

.....

Signature

Thisday of

RESEARCH PUBLICATIONS ARISING FROM THIS WORK

1. Jonathan Pantshwa, Viness Pillay, Yahya E Choonara, Lisa C du Toit, Lomas K Tomar, Charu Tyagi, Pradeep Kumar, Clement Penny 2015. Nanomicellar Technologies for Targeted Drug Delivery in Ovarian Cancer Chemotherapeutics. Submitted to Journal of Pharmaceutical Development and Technology.
2. Jonathan Pantshwa, Pradeep Kumar, Yahya Choonara, Lisa Du Toit, Clement Penny, Viness Pillay 2016. Synthesis of Novel Amphiphilic poly (N-isopropylacrylamide)-block-poly (aspartic acid) Nanomicelles for Potential Targeted Chemotherapy in Ovarian Cancer. Accepted by Journal of Drug Delivery Science and Technology.
3. Jonathan Pantshwa, Yahya Choonara, Pradeep Kumar, Lisa du Toit, Clement Penny, Viness Pillay 2016. Optimized Design of Combinational Poly (N-isopropylacrylamide)-block-Poly (Aspartic Acid) Nanomicelles for Tumor-Specific Microenvironmental Release of Methotrexate. Submitted to Journal of Pharmaceutical Sciences.
4. Jonathan Pantshwa, Yahya Choonara, Pradeep Kumar, Lisa du Toit, Clement Penny, Viness Pillay 2016. Anti-muc 16 Functionalized PNIPAAm-b-PAsp Nanomicelles for the Targeted Delivery of Methotrexate to Human Ovarian Carcinoma Cells. Submitted to Journal of Pharmaceutical Sciences.
5. Jonathan Pantshwa, Yahya Choonara, Pradeep Kumar, Lisa du Toit, Clement Penny, Viness Pillay 2016. *In-vitro* Synthesis, Characterization and Assessment of a Bio-responsive IPN nanomicelle/hydrogel Composite based Implant for Ovarian Carcinoma Treatment. To be submitted to International Journal of Pharmaceutics.
6. Jonathan Pantshwa, Khadija Rhoda, Sarah Clift, Divya Bijukumar, Yahya Choonara, Lisa Du Toit, Pradeep Kumar, Clement Penny, Viness Pillay 2016. An Optimal Mouse Model for Human Ovarian Carcinoma Research and Efficacy of various Chemotherapeutic Treatment Protocols: Submitted to the Journal of Biotechnology.

RESEARCH PRESENTATIONS ARISING FROM THIS WORK

- a. Jonathan Pantshwa, Viness Pillay, Yahya E. Choonara, Lisa C. du Toit and Clement Penny. Antibody Functionalized Nanomicelles for Ovarian Cancer Cell Targeting by Molecular and In Vivo Investigations. 6th Graduate Cross-Faculty Symposium, September 2015, University of the Witwatersrand, Johannesburg, South Africa. (Abstract in appendix B (6)).

- b. Jonathan Pantshwa, Viness Pillay, Yahya E. Choonara, Lisa C. du Toit and Clement Penny. Implantable Drug-Loaded Antibody Functionalized Nanomicelles for Ovarian Cancer Cell Targeting by Molecular and In Vivo Investigations. 1st prize winner of the Graduate Cross-Faculty Symposium. March 2016, University of the Witwatersrand, Johannesburg, South Africa. (Abstract in appendix B (6)).

RESEARCH ACCOLADES

Best Poster Presentation 1st prize Award

7th Cross-Symposium, University of the Witwatersrand, Johannesburg, South Africa, March 2016. Implantable Antineoplastic-Loaded Antibody Functionalized Nanomicelles for Ovarian Cancer Cell Targeting by Molecular and In Vivo Investigations. Jonathan Pantshwa, Viness Pillay, Yahya E. Choonara, Lisa C. du Toit and Clement Penny.

Postgraduates PhD Scholarship Awards

1. National Research Foundation (NRF) Scare Skill Doctoral Scholarship, South Africa, 2014-2015.
2. Postgraduate Merit Award, University of the Witwatersrand, 2014 and 2015.
3. Aspen Pharmacare Bursary Award 2014.

ACKNOWLEDGMENTS

First and foremost, I would like to express my deepest gratitude to my supervisor Viness Pillay, deep thanks for your continuous support, reassurance, guidance, encouragement, and for believing in me throughout the exciting phenomenal journey of acquiring my philosophy degree. Thank you also for being not only a supervisor in the lab but to be also there in the crucial moments of my personal life. With absolute assurance, my research career would not have been possible without him. I have also emulated his intolerance to incompetence. Deep thanks to my colleague Khadija Rhoda, through our rise and fall we have managed to make this study a great success.

I am honored to have had wonderful co-supervisory committee members. First and foremost: to my co-supervisors: Prof Yahya Choonara, Prof Lisa du Toit, many thanks for your assistance on research article publications and constant reminding me that we are not doing this for fun, publications must transpire out this research work. And that has prompted me to publish more than six research articles on international journals. Also deep thanks To Pradeep Kumar, Dr. Lomas Kumar Tomar, Dr.Divya Bijukumar, Dr Clem Penny, Dr Sarah Clift (and also for her good sense of consistent humor), my sincerest gratitude for your valuable input. My sincere appreciation for the work all of you have put into my research.

It also gives me great pleasure in acknowledging my friends, colleagues, associates, Felix Mashingaidze, Mpho Ngoepe, Mershen Govender, Pierre Kondiah, Maluta Steven Mufamadi, Olifemi Akilo, Sunaina Indermun, Bafana Themba and Derusha Frank. Without their motivation and support, I would not have accomplished anything; they taught me resilience, efficiency, independence, dedication and rigorously hard work in research. I am also grateful to my many wonderful, exceptional colleagues who supported me:, Ahmed Seedat, Kealeboga Mokolobate, Nonhlanhla Masina, Tebogo Kgesa, Martina Manyikana, Latavia Singh, Tasneem Rajan, Naeema Mayet, Famida Ghulam-Hoosain, Fatema Mia, Khuphukile Madida, Dr. Charu Tyagi. I would like to acknowledge all people that somehow were involved in my scientific work.

I also would like to express my gratitude to Mr. Sello Ramarumo for always being there to help. I would like to thank Central Animal Services staff of Wits University and Professor Kennedy Erlwanger for assistance and input not forgetting one my role models Sir Marcus Dagie who inspired me with excellence and would like to quote from his word “the difference between possible and impossible lies on one’s mind and determination, your attitude determines your

altitude Jonathan". Thank you to the National Research Foundation (NRF), University of the Witwatersrand Staff Bursary and Department of Education Clinical training (DoE) for the research grants.

DEDICATION

This thesis is dedicated to my late family Nozizwe Gladys Pantshwa (mother), George Pantshwa (brother), Thabo Zondi (brother), Hamilton luyanda Sishuba (Uncle). I know that I am not alone without family; you are with me in spirit. It is also indeed dedicated to all those, who strive and make their life, better even though the conditions don't allow them. To my aunt and uncle (Nkululeko and Nomvuyo Dlamini) deep thanks for your wisdom and believing in me, you always made me feel at home when I am with you.

ABSTRACT

Epithelial ovarian cancer (EOC) is the most insidious, fatal gynaecological malignancy that accounts for millions of deaths in female population. Globally, the five-year survival period is between 15–20% for patients with clinical late stage ovarian malignancy in spite of surgery and platinum treatment. This study aimed to design and develop a novel drug delivery system employing antibody-ligand functionalized antineoplastic-loaded nanomicelles encapsulated with Chitosan-Poly(vinylpyrrolidone)-Poly (N-isopropylacrylamide) (C-P-N) hydrogel to form an *in situ* forming Implant (ISFI) which is responsive to temperature (body temperature 37°C), pH (peritoneal fluid pH ~6.6) for cancer cell-targeting following intraperitoneal implantation to increase the residence time of the nanomicelles at tumor sites over a period exceeding one month, enhancing tumor uptake of drugs and prevent recurrence and chemo-resistance. An engineered-fabricated nanomicelle system (MTX)NM's was formed by a novel thermal ring opening co-polymerization of hydrophobic L-Aspartic acid-N-carboxyanhydride onto the backbone of hydrophilic PNIPAAm-NH₂ to form amphiphilic poly (N-isopropylacrylamide)-block-poly (aspartic acid) (PNIPAAm-b-PAsp) copolymer. PNIPAAm-b-PAsp copolymer exhibited competency in forming amphiphilic nanomicelles broadening areas of its nano-application in implantable drug delivery. Utilizing (PNIPAAm-b-PAsp) micelles, variables for an experimental design were obtained. A Face-Centred Central Composite experimental design approach generated thirteen formulations thoroughly screened in terms of variables (Amount of copolymer (mg) and homogenizer speed (rpm)) affecting responses (size (nm), drug entrapment efficiency (%) and mean dissolution time). Nanomicelles with sizes ranging from 51.67 to 76.45 nm, a yield/recovery of 46.8–89.8 mg and polydispersity index (PDI ≤ 0.5) were obtained. Drug encapsulation efficacy (DEE) was initially (65.3 ±0.5%) and was ultimately optimized to 80.6±0.3%. Optimal nanomicelle formulation was surface-functionalized with anti-MUC 16 (antibody) for the targeted delivery of methotrexate to human ovarian carcinoma (NIH:OVCAR-5) cells that expressed MUC 16 as a preferential form of intraperitoneal ovarian cancer chemotherapy. Furthermore, cross-linked interpenetrating C-P-N hydrogel was synthesized for the preparation of an *in situ* forming implant (ISFI) for ovarian carcinoma treatment. ISFI was fabricated by encapsulating a nanomicelle comprising of anti-MUC 16 (antibody) functionalized methotrexate (MTX)-loaded PNIPAAm-b-PAsp nanomicelles (AF(MTX)NM's) within C-P-N hydrogel. Ex vivo endocytotic internalization via confocal fluorescent microscopy and intracellular imaging studies in (NIH:OVCAR-5) cells showed positive cellular uptake in both optimal (MTX)NM's and (AF(MTX)NM's) with exemplary results for (AF(MTX)NM's) due to improved intracellular delivery. Chemotherapeutic efficacy of various treatment protocols including ISFI were *in vivo* tested on the optimal Athymic nude mouse model that was intraperitoneally and subcutaneously induced with human ovarian carcinoma cells (NIH:OVCAR-5) and tumors with associated severe ascites grew within 10 days of inoculation. Results demonstrated tumor regression including reduction in mouse weight and tumor size, as well as a significant ($p < 0.05$) reduction in mucin 16 levels in serum and ascitic fluid and improved survival of mice after treatment with the experimental anti-MUC16/CA125 antibody-bound nanotherapeutic implant drug delivery system ($p < 0.05$). Low quantities of drug were found in the plasma but elevated levels were observed in the peritoneal cavity. In addition, the drug was present in the surrounding tissue in high concentration even after 10 days. Based on the results of this study, the antibody-bound nanotherapeutic implant drug delivery system should be considered a potentially important immuno-chemotherapeutic agent that can be employed in human clinical trials of advanced, and/or recurring, metastatic epithelial ovarian cancer (EOC). The development of this novel implantable drug delivery system may circumvent the treatment flaws experienced with conventional systemic therapies, effectively manage recurrent disease and ultimately prolong disease-free intervals in ovarian cancer patients.

TABLE OF CONTENTS

DECLARATION.....	i
RESEARCH PUBLICATIONS ARISING FROM THIS WORK.....	ii
RESEARCH PRESENTATIONS ARISING FROM THIS WORK.....	iii
RESEARCH ACCOLADES.....	iv
ACKNOWLEDGMENTS.....	v
DEDICATION.....	vii
ABSTRACT.....	viii
TABLE OF CONTENTS.....	xi
LIST OF FIGURES.....	xxiv
LIST OF TABLES.....	xxxi
LIST OF EQUATIONS.....	xxxiii
LIST OF ABBREVIATIONS.....	xxxv

CHAPTER 1
INTRODUCTION

1.1. Introduction and Background on Ovarian Cancer.....1

1.2. Rationale and Motivation for this Research.....4

1.3. Novelty of this Research.....8

1.4. Aim and Objectives of this Research.....9

1.5. Overview of this Thesis.....10

CHAPTER 2
**LITERATURE REVIEW OF NANOMICELLAR TECHNOLOGIES FOR TARGETED DRUG
DELIVERY IN OVARIAN CANCER CHEMOTHERAPEUTICS**

2.1.	Introduction.....	12
2.2.	Current Nano-based Drug Delivery Approaches for Ovarian Cancer Therapy.....	13
2.3.	Critical Comparison of Nanosystems to Micelles for OC Treatment.....	15
2.4.	Micellar Morphology, Composition, and Mechanism of Formation.....	18
2.5.	Classification of Nanomicelles.....	19
2.5.1.	Amphiphilic Micelles.....	20
2.5.2.	Polycharged Composite Nanomicelles.....	21
2.5.3.	Non-covalently Connected Polymeric Micelles.....	21
2.4.	Polymers Used in Micelle Targeted Drug Delivery for Ovarian Cancer.....	21
2.5.	Preparation of Drug-loaded Micelles in Ovarian Cancer.....	24
2.6.	Applications of Nanomicelles in Ovarian Cancer.....	26
2.6.1.	Diagnosis of Ovarian Cancer Employing Nanomicelles.....	26
2.6.2.	Treatment of Ovarian Cancer via Nanomicelles.....	30
2.6.2.1	Delivery Routes of Nanomicelles.....	30
2.6.3.	Targeting strategies for nanomicelles.....	30
2.6.3.1.	Passive/Reactive targeting via improved permeability of tumor blood vessels.....	31
2.6.3.2.	Active targeting with ligand/antigen pairs.....	31
2.7.	Mucins as Targets for Antibodies in Cancer Chemotherapeutics.....	33
2.8.	Stimulus-responsive Nanomicelles.....	34
2.9.	Nanomicelles in Clinical Evaluations.....	35
2.10.	Patents in Nanomicellar Technologies for Targeted Drug Delivery.....	37

2.11.	Future Recommendations.....	39
2.12.	Concluding Remarks.....	39

CHAPTER 3
SYNTHESIS OF NOVEL AMPHIPHILIC POLY (N-ISOPROPYLACRYLAMIDE)-BLOCK-POLY
(ASPARTIC ACID) NANOMICELLES FOR POTENTIAL TARGETED CHEMOTHERAPY IN
OVARIAN CANCER

3.1. Introduction.....	41
3.2. Materials and Methods.....	42
3.2.1 Materials.....	42
3.2.2. Synthesis of amino poly (N- isopropylacrylamide) (PNIPAAm-NH ₂).....	42
3.2.3. Synthesis of L-aspartic acid-N-carboxyanhydride using a triphosgene approach.....	43
3.2.4. Synthesis of the amphiphilic poly-N-isopropylacrylamide-b-polyaspartic acid copolymer.....	43
3.2.5. Establishment of the copolymer molecular mass.....	43
3.2.6. Establishment of the nanomicellization process.....	44
3.2.7. Micelle size and stability determination.....	44
3.2.8. Determination of the MTX loading efficiency within the nanomicelles.....	44
3.2.9. Determination of the Critical Micelle Concentration of the PNIPAAm-b-PAsp nanomicelles.....	45
3.2.10. Investigation of the chemical structure integrity of the PNIPAAm-b-PAsp copolymer.....	46
3.2.11. Thermodynamic stability analysis of the PNIPAAm-b-PAsp copolymer.....	46
3.2.12. Thermogravimetric analysis of the PNIPAAm-b-PAsp copolymer.....	46
3.2.13. <i>In vitro</i> MTX release studies from the PNIPAAm-b-PAsp nanomicelles.....	47
3.2.14. <i>In vitro</i> Kinetic evaluation of drug release from the MTX-loaded Nanomicelles.....	47
3.3. Results and Discussion.....	48

3.3.1. Assessment of the copolymerization strategy and nanomicelle synthesis.....	48
3.3.2. Establishment of the molecular mass of the synthesized PNIPAAm-b-PAsp copolymer.....	51
3.3.3. Quantitative image assessment of PNIPAAm-b-PAsp copolymer morphology.....	52
3.3.4. Assessment of the nanomicellization process and MTX entrapment Efficiency.....	54
3.3.5. Analysis of the Critical Micelle Concentration value of the nanomicelles.....	55
3.3.6. Influence of nanomicelle size.....	57
3.3.6. Analysis of the copolymer chemical structure integrity and transformation.....	58
3.3.7. Assessment of the thermodynamic stability of the PNIPAAm-b-PAsp copolymer.....	59
3.3.8. Thermal degradation analysis of the PNIPAAm-b-PAsp copolymer.....	60
3.3.9. <i>In vitro</i> analysis of MTX release from the PNIPAAm-b-PAsp nanomicelles.....	62
3.3.10. <i>In vitro</i> kinetic evaluation of drug release from the MTX-loaded Nanomicelles.....	63
3.3.10. Conclusion Remarks.....	64

CHAPTER 4
OPTIMIZED DESIGN OF COMBINATIONAL POLY (N-ISOPROPYLACRYLAMIDE)-BLOCK
POLY (ASPARTIC ACID) NANOMICELLES FOR TUMOR-SPECIFIC
MICROENVIRONMENTAL RELEASE OF METHOTREXATE

4.1. Introduction.....	65
4.2. Materials and Methods.....	67
4.2.1. Materials.....	67
4.2.2. Determination of Critical Micelle Concentration of PNIPAAm-b-PAsp.....	68
4.2.3. Formulation of the Methotrexate-encapsulated PNIPAAm-b-Pasp Nanomicelles.....	68
4.2.4 Characterization of Nanomicelles.....	71
4.2.7. Optimization of the Nanomicelle Formulation.....	72
4.2.8. Characterization of the Optimum Nanomicelle Formulation.....	72
4.2.9. <i>In vitro</i> Kinetic evaluation of drug release from the optimum Nanoformulation.....	72
4.2.10. Fourier Transform Infrared spectroscopic characterization of the Nanomicelle Molecular Arrangement.....	72
4.2.11. Nanomicelle morphological characterization.....	72
4.2.12. Differential scanning calorimetry for elucidation of thermal events of the methotrexate-loaded nanomicelles.....	73
4.3. Results and Discussion.....	73
4.3.1 Critical Micelle Concentration Determination.....	73
4.3.2. Analysis of the Experimental Design Formulations and Statistical Optimization of the PNIPAAm-b-PAsp Nanomicelles.....	74
4.3.3. Influence of independent variables nanomicelle size, incorporation efficiency and drug release.....	76
4.3.4. Statistical analysis of the Face-Centred Central Composite Design.....	78
4.3.5. Statistical analysis of the residual error in the experimental design.....	80

4.3.5. Characterization of the Optimized Nanomicelle Formulation.....	85
4.3.6. Molecular transitions of the PNIPAAm- <i>b</i> -Pasp nanomicelles.....	85
4.3.7. PNIPAAm- <i>b</i> -PAsp micelle morphological characterization.....	87
4.3.8. Analysis of the thermal features of the drug-free and MTX-loaded PNIPAAm- <i>b</i> -PAsp nanomicelles.....	88
4.3.9. Methotrexate release behavior from the optimized nanomicelle under normal and tumoral conditions.....	89
4.3.10. <i>In vitro</i> kinetic evaluation of drug release from the optimum Nanoformulation.....	91
4.4 Conclusion Remarks.....	94

CHAPTER 5
ANTI-MUC 16 FUNCTIONALIZED PNIPAAm-B-PASP NANOMICELLES FOR THE
TARGETED DELIVERY OF METHOTREXATE TO HUMAN OVARIAN CARCINOMA CELLS

5.1. Introduction.....	95
5.2. Materials and Methods.....	96
5.2.1. Materials.....	96
5.2.2. Preparation of the Anti-MUC 16 Functionalized MTX-Loaded Nanomicelle.....	97
5.2.2.1. Synthesis of the amphiphilic PNIPAAm-b-PAsp copolymer for the Nanomicelle.....	97
5.2.2.2. Preparation of the MTX-loaded Nanomicelle.....	97
5.2.3. Evaluation of the Molecular Structural Integrity of the Functionalized Nanomicelles....	98
5.2.4. Particle Size, Zeta Potential and Morphological Analysis of the Nanomicelle.....	98
5.2.5. Determination of MTX Encapsulation into the Nanomicelle.....	98
5.2.6. <i>In vitro</i> cytotoxicity assay.....	99
5.2.7. Confocal Microscopic Analysis of the Nanomicelle on NIH: OVCAR-5.....	99
5.3. Results and Discussion.....	100
5.3.1. Analysis of the Molecular Structure Integrity of the Functionalized Nanomicelle.....	100
5.3.2. Assessment of Particle Size, Zeta Potential and Morphology of the Nanomicelle.....	102
5.3.3. Morphological Characterization of the Nanomicelle.....	104
5.3.4. Cell Culture and <i>In Vitro</i> Cytotoxicity Assay.....	104
5.3.5. Confocal Microscopy Analysis of the Nanomicelle.....	106
5.3.6. Mechanism of Synthesis of the Anti-MUC 16 MTX-Loaded Nanomicelle.....	107
5.4. Concluding Remarks.....	110

CHAPTER 6
IN-VITRO SYNTHESIS, CHARACTERIZATION AND EVALUATION OF A BIO-RESPONSIVE
IPN NANOMICELLE/HYDROGEL COMPOSITE BASED IMPLANT FOR OVARIAN
CARCINOMA TREATMENT

6.1.	Introduction.....	111
6.2.	Materials and Methods.....	113
6.2.1.	Materials.....	113
6.2.2.	Synthesis of Chitosan Poly(N-vinylpyrrolidone) Poly(N-isopropylacrylamide) (C-P-N) Hydrogel.....	113
6.2.3.	Physicochemical characterization of the cross-linked C-P-N hydrogel.....	114
6.2.3.1.	Nuclear Magnetic Resonance (NMR) Spectroscopic analysis of Polymeric C-P-N Hydrogel.....	114
6.2.3.2.	Determination of Polymeric Structural variations of the cross-linked C-P-N Hydrogel.....	114
6.2.3.3.	Differential Scanning Calorimetry (Thermalanalysis).....	115
6.2.3.4.	Thermogravimetric analysis of the cross-linked C-P-N hydrogel.....	115
6.2.4.	Physicomechanical characterization of the fabricated C-P-N hydrogel System.....	115
6.3.4.1.	Water content of the cross-linked C-P-N hydrogel.....	116
6.2.4.1.1.	Determination of the gelation temperature of the polymeric formulations utilizing oscillatory rheology.....	116
6.2.5.	Surface morphological characterization of the cross-linked C-P-N hydrogel.....	117
6.2.5.1.	Porositometric analysis.....	117
6.2.5.2.	Determination of the swelling and erosion behavior.....	118
6.2.6.	Preparation of bio-responsive IPN nanomicelle/hydrogel composite based implant (ISFI).....	119
6.2.7.	Drug encapsulation efficiency (DEE).....	119
6.2.8.	Determination of drug release from the ISFI at a simulated tumor site.....	119
6.2.9.	<i>Ex vivo</i> evaluation of the ISFI.....	120
6.2.9.1.	Cytotoxicity analysis of the polymer framework on cell culture.....	120

6.2.10.	Optical fluorescence imaging of fluorescence-labeled functionalized nanomicelles embedded within the C-P-N hydrogel framework system.....	120
6.3.	Results and Discussion.....	121
6.3.1	Synthesis of Chitosan-Poly (N-vinylpyrrolidone)-Poly(N-isopropylacrylamide) (C-P-N) hydrogel.....	121
6.3.2.	Assessment of polymeric structural variations of the cross-linked C-P-N Hydrogel.....	123
6.3.4.	Assessment of thermal degradation at various heating rates	124
6.3.5.	Physico-mechanical characterization of the fabricated cross-linked C-P-N hydrogel system.....	127
6.3.5.1.	Assessment of textural properties of the cross-linked C-P-N hydrogel.....	128
6.3.6.	Assessment of the gelation temperature using oscillatory rheology	129
6.3.7.	Assessment of Surface morphological properties	130
6.3.7.1.	Porositometric analysis.....	130
6.3.7.2.	Assessment of the swelling and erosion behavior.....	133
6.3.8.	Morphological characterization of the ISFI.....	134
6.3.9.	Assessment of drug release from the ISFI at a simulated tumor site.....	135
6.3.10	<i>Ex vivo</i> evaluation of the ISFI.....	136
6.3.10.1.	Cytotoxicity analysis of the polymer framework on cell culture.....	136
6.3.10.2.	Fluorescence imaging of the fluorescence-labeled ISFI.....	138
6.4.	Concluding Remarks.....	139

CHAPTER 7
AN OPTIMAL MOUSE MODEL FOR HUMAN OVARIAN CARCINOMA RESEARCH AND
EFFICACY OF VARIOUS CHEMOTHERAPEUTIC TREATMENT PROTOCOLS

7.1. Introduction.....	143
7.2. Materials and Methods.....	143
7.2.1. Materials.....	143
7.2.2. Mouse housing conditions and welfare.....	143
7.2.3. Cell Culture.....	146
7.2.4. Sterile preparation of ISFI formulations.....	146
7.2.5. Biocompatibility studies in mice.....	147
7.2.6. Establishment of a model for induction of ovarian cancer using Athymic nude mice: Pilot study.....	147
7.2.7. Experimental design.....	147
7.2.7.1. Intraperitoneal (IP) and Subcutaneous (SC) induction of Human Ovarian Carcinoma in Swiss Athymic Nude Mice – Pre-treatment Phase.....	149
7.2.7.2. Acquisition of adequate mice stock for human ovarian carcinoma Research.....	150
7.2.7.3. SC-inoculated mice.....	150
7.2.7.4. IP-inoculated mice.....	151
7.2.7.5. Description of the anaesthetics, analgesics and drugs employed.....	151
7.2.8. Experimental design.....	155
7.2.8.1. Chemotherapeutic Efficacy Studies in EOC-inoculated Nude (NU/NU) Mice.....	155
7.2.8.2. Athymic nude mice Blood Sampling.....	156
7.2.8.3. Quantification of MUC16/CA 125 levels in Plasma and Ascitic Fluid.....	157
7.2.8.4. Histopathology and IHC.....	158
7.2.8.5. Immunohistochemical Quantification of MUC16/CA125 antigens in FFPE tissue sections.....	159

7.2.9.	Applying Ultra Performance Liquid Chromatography (UPLC) to determine the Methotrexate content in blood and tissue samples.....	160
7.2.9.1.	UPLC analysis.....	160
7.2.9.2.	Preparation of weak and strong washes and mobile phases.....	161
7.2.9.3.	Determination of the optimal method of extraction of drug from plasma samples.....	162
7.2.9.4.	Treatment of actual plasma samples.....	163
7.2.9.5.	Construction of a calibration curve in order to quantify amounts of drug in actual plasma samples.....	163
7.2.9.6.	Construction of a calibration curve in PBS.....	163
7.2.9.7.	Determination of the drug content in surrounding tissue.....	164
7.2.9.8.	Statistical analysis.....	164
7.3.	Results and Discussion.....	165
7.3.1.	Sterile preparation of ISFI.....	165
7.3.2.	Bio-compatibility of the ISFI in the mouse model.....	165
7.3.2.1.	Implantation area and tissue-necrosis.....	165
7.3.3.	Establishment of a model for induction of ovarian cancer using Athymic nude mice: Pilot study.....	167
7.3.4	Main Study.....	169
7.3.4.1.	Intraperitoneal (IP) and Subcutaneous (SC) Induction of Human Ovarian Carcinoma in Athymic Swiss Nude Mice.....	169
7.3.4.2.	Chemotherapeutic efficacy in the Treatment of Human Ovarian Carcinoma.....	169
7.3.4.3.	Tumor size.....	169
7.3.4.4.	Whole mouse weight.....	172
7.3.4.5.	Quantification of plasma and ascitic fluid MUC16/CA125 antigen levels.....	174
7.3.4.6.	Histopathology and IHC.....	176
7.3.4.7.	SC and IP tumor Macropathology.....	176
7.3.4.8.	SC and IP tumor histopathology.....	176

7.3.4.9. Liver histopathology.....	176
7.3.4.10. Renal histopathology.....	177
7.3.4.11. Immunohistochemistry.....	179
7.3.4.12. MUC 16/CA125 IHC analysis on FFPE EOC tissue sections.....	180
7.3.5. Construction of a calibration curve in order to measure the quantity of methotrexate in blood and tissue samples and precision and accuracy of the UPLC method.....	182
7.3.5.1. Determination of methotrexate concentration in surrounding tissue.....	185
7.3.6. Mechanism of Intraperitoneal IFSI Delivery for human ovarian carcinoma targeting.....	185
7.4. Discussion.....	187
7.5. Conclusion Remarks.....	189

CHAPTER 8
CONCLUSION AND RECOMMENDATIONS

Conclusions.....	191
Recommendations and Future outlooks.....	191
REFERENCES.....	193
APPENDICES.....	223
Appendix A: ASSESSMENT OF C-P-N HYDROGEL PROPERTIES.....	224
Appendix B: RESEARCH PUBLICATION.....	225
B (1).....	226
B (2).....	227
B (3)	228
B (4)	229
B (5)	231
B (6)	233
Appendix C: ANIMAL ETHICS CLEARANCE.....	236
C (1)	236
C (2)	237
Appendix D: FELASA COURSE CERTIFICATE.....	239
Appendix E: IMPORT PERMITS AND SOP's	240
E (1)	241
E (2)	245
E (3)	245
E (4)	248
E (5)	250

LIST OF FIGURES

Figure 1.1: A diagrammatic illustration showing the expression of cancer-associated mucins accompanying the development of ovarian cancer and the intraperitoneal implant providing targeted therapy within the peritoneal cavity.....	3
Figure 1.2: A schematic of the proposed monoclonal antibody-mediated intraperitoneal drug delivery system.....	6
Figure 2.1: Schematic depicting examples of nano-sized delivery systems; liposomes (a-b), polymer drug conjugates (c-d), dendrimers (e-f) and solid lipid nanoparticles (g-h) and polymeric micelles (i-j) currently being exploited for transport of chemotherapeutic agents [(adapted from (a-b) (Jiang et al., 2014), (c-d) (Tong et al., 2010) , (e-f) Santos et al., 2010, (g-h) Pasc et al., 2011, (i) Palivan et al., 2012; (j) Ding et al.,2015).....	18
Figure 2.2: Schematic representation of the supramolecular structure of polymeric micelles (adapted from Lu and Park, 2012).....	19
Figure 2.3: Scheme of surfactant molecules aligning on water/air interface at pre and post 'CMC' point (adapted from Mukherjee et al., 2013).....	20
Figure 2.4: Main methods of drug loaded micelle preparation from copolymers.....	25
Figure 2.5: Schematic illustration of drug loaded nanomicelles (spheres) with imaging agent delivery from injection location to tumor tissue. After administration, nanomicelles (10–200 nm) display specific targeting of tumor growth and the nanomaterial collects at the solid cancer site due to the tumor vessels and passage through reticular endothelial system. Passive targeting is attained by cellular endocytotic uptake from exterior fluid to the cancer cells. Active targeting can be attained by attachment of antibody ligand molecule to the exterior of nanomicelles that encourage site-precise detection and attachment (Adapted from Chen et al., 2014).....	31
Figure 2.6: Schematic depicting (a) active targeting, (b-g) confocal images of A431 cellular uptake incubated with cetuximab encapsulated nanomicelles and lysotracker. The fluorescence intensity of A431 cells (b-d) treated with targeting nanomicelles was 1.45 times higher than in cells incubated with antibody-free nanomicelles (e-g) (Adapted from Zhou et al., 2013; Zhu et al., 2013).....	33
Figure 3.1: Calibration curve of the absorbance of Methotrexate in PBS (pH 7) using Cecil 3021 UV spectroscopy at 303 nm (in all cases n=3 and SD<0.025).....	45
Figure 3.2: ¹ H NMR spectra of PNIPAAm-b-PAsp in CDCl ₃ and peak assignment confirming the structure of the synthesized amphiphilic copolymer.....	49
Figure 3.3: Flow curves shear stress (τ), Viscosity (η) versus shear strain (γ) at various concentrations of amphiphilic copolymer synthesized.....	52

Figure 3.4: Scanning electron microscopy (SEM) images of synthesized copolymer in powder form (a-b), Surface of copolymer in film form (c-d), lyophilized copolymer displaying pore distribution and pore diameter variation (e-h).....	53
Figure 3.5: TEM (a) and SEM (b) images depicting self-assembled PNIPAAm-b-PAsp copolymeric nanomicellar formulation. The scale for all images is 90nm.....	55
Figure 3.6: (a) FITC emission spectra of PNIPAAm-b-PAsp solutions. (b) I_{390}/I_{290} intensity ratio for FITC as a function of the concentration of PNIPAAm-b-PAsp copolymer in deionized water. The CMC was obtained as the midpoint value of copolymer concentration at which the I_1/I_3 intensity ratio considerably decreases.....	56
Figure 3.7: (a) Zeta size graphs illustrating the hydrodynamic size of PNIPAAm-b-PASP nanomicelle formulation, (b) size intensity distribution for the optimized monotypic PNIPAAm-b-PASP nanomicelle.....	57
Figure 3.8: Overall Vibrational-Spectroscopy of Poly-N-isopropylacrylamide-block-poly aspartic acid (PNIPAAm-b-PASP), L-ASP-NCA, Poly NIPAAm-NH ₂ (descending order).....	58
Figure 3.9: (a) DSC scan plot of (a) L-ASP-NCA (b) PNIPAAm-NH ₂ and PNIPAAm-b-PASP copolymer combination of PNIPAAm-NH ₂ and L-ASP-NCA via ring opening polymerization.....	60
Figure 3.10: TGA properties of PNIPAAm-NH ₂ (A), L-ASP-NCA (B) and PNIPAAm-b-PASP (C) depicting various melting points.....	61
Figure 3.11: Methotrexate release from PNIPAAm-b-PASP copolymeric nanomicelles in acidic (pH 6.75) at 38 degrees and normal physiological conditions (pH 7.4) at 37 degrees. Each point depicts mean \pm SD (n=3).....	62
Scheme 1: Synthesis of amino terminated poly (N-isopropylacrylamide) by free-radical polymerization of NIPAm (a), carboxylation of aspartic acid (Asp) using triphosgene method (b) and thermal ring opening polymerization of Aspartic acid-N-carboxyanhydride using amino-terminated NIPAm to form the PNIPAAm-b-PASP amphiphilic copolymer product (c).....	50
Scheme 2: Incorporation of methotrexate with copolymer employing micellization process to form micelles which have potential application in cancer treatment as antineoplastic drug delivery systems, also included is the structural transformation due to changes in temperature and pH resulting in drug release.....	55
Figure 4.1: Methotrexate structure with IUPAC name (S)-2-(4-(((2,4-diaminopteridin-6-yl)methylamino) benzamido) pentanedioic acid, molar mass 454,46 g/mol, chemical formula C ₂₀ H ₂₂ N ₈ O ₅ with all possible binding sites also depicted (1,2,3 and 4).....	66
Figure 4.2: Schematic of amphiphilic PNIPAAm-b-PASP copolymer assemblage in aqueous media to form spherical nanomicelles.....	69

Figure 4.3: (a) FITC emission spectra of PNIPAAm-b-PASP solutions. (b) I_{390}/I_{290} intensity ratio for FITC as a function of the concentration of PNIPAAm-b-PASP copolymer in deionized water. The CMC was obtained as the midpoint value of copolymer concentration at which the I_1/I_3 intensity ratio considerably decreases.....	74
Figure 4.4: Desirability graphs for optimized 2(O1) showing the crucial variables for generating PNIPAAm-PASP micelles with the desired targeted responses.....	76
Figure 4.5: (a) Zeta size graphs illustrating the hydrodynamic size of PNIPAAm-b-PASP nanomicelle formulation, (b) size intensity distribution for the optimized monotype PNIPAAm-b-PASP nanomicelle.....	77
Figure 4.6: Three dimensional surface graphs produced by the 3^2 -Factorial Box-Behnken design approach investigating the influence of copolymer amount and homogenizer speed on size of the synthesized nanomicelles.....	77
Figure 4.7: Three dimensional response surface graphs produced by the 3^2 -Factorial Box-Behnken design approach investigating the influence of copolymer amount and homogenizer speed on DEE/DIE and MDT of the synthesized nanomicelles.....	84
Figure 4.8: FTIR spectrum of MTX, blank micelles and MTX- loaded PNIPAAm-b-PASP nanomicelles depicting the variations in the spectra.....	86
Figure 4.9: (a) Scanning electron microscopy (SEM) image showing the shell morphology of the optimized PNIPAAm-b-PASP nanomicelle formulation with average size of 65nm and (b) TEM images depicting of the optimized spherical MTX-loaded PNIPAAm-b-PASP nanomicelle formulation, also with average size of 65nm.....	87
Figure 4.10: DSC thermograms of (a) pure MTX (b) blank micelle nanoformulation (c) MTX-loaded micelle formulation and (d) temperature variations and shifts in the curves of MTX, blank micelles and MTX-loaded micelles.....	88
Figure 4.11: Methotrexate release from optimized PNIPAAm-b-PASP copolymeric nanomicelles in acidic (pH 6.75, ie tumor simulated micro-environment) at 38 °C and normal physiological conditions (pH 7.4) at 37 °C. Each point depicts mean \pm SD (n=3)....	90
Figure 4.12: <i>In vitro</i> Kinetic analysis of drug release, Zero Order kinetics, First Order release, Higuchi Hixson law and Crowell Korsmeyer law.....	93
Figure 5.1: FTIR spectra illustrating the molecular structural transitions of MTX, blank micelles, anti muc 16 MTX-loaded nanomicelles AF(MTX)NM's and MTX-loaded nanomicelles (MTX)NM's.....	101
Figure 5.2: Dynamic light scattering (DLS) plots of (MTX)NMs without (a) and (b) with anti-mucin 16 antibody modified including PNIPAAm-b-PASP micelle hydrodynamic size and monotype size distribution (c) (MTX)NMs (65 nm), AF(MTX)NMs (75 nm).....	103
Figure 5.3: Methotrexate release from (MTX)NM's and AF(MTX)NM's in PBS (pH 7.4) at 37 degrees. Each point depicts mean \pm SD (n=3).....	103

Figure 5.4: TEM (a and b) and SEM images (c and d) of native NMs (a and c) and antibody- functionalized NMs (b and d) for interaction with mucin 16 particles.....	104
Figure 5.5: Tetrazolium salt MTT assay to evaluate the effect of MTX, (MTX)NM's an AF(MTX)NM's formulations (a) on percentage viability of NIH:OVCAR-5 cells, blank micelles were utilized as control (b), invitro cytotoxicity of MTX-incorporated polymeric micelles with and without antibody including control against NIH:OVCAR-5 cells(c-d). All NM's were incubated with ovarian cells for 72 hours prior to cell viability evaluation in each treatment group. Each point depicts average \pm SD (n =3).....	106
Figure 5.6: Confocal fluorescence microscopy for determination and analysis of cell uptake with antibody binding on the surface of micelles [(a-b) control micelle transmission images, (b-f) fluorescence overlay images of NIH:OVCAR-5 cells treated with (MTX)NMs (b-c) and AF(MTX)NMs (e-f) formulations showing selective enhanced uptake following 24 hour incubation.....	107
Figure 5.7: A schematic illustration of monoclonal antibody-mediated methotrexate loaded nanomicelle drug delivery system.....	109
Figure 5.8: Schematic illustration of (antibody-antigen interaction) the anti-mucin 16 methotrexate loaded micelle interaction with mucin 16 (as known as CA 125) receptor.....	110
Figure 6.1: Illustration of possible constituent chemical structures and mechanism of synthesis of the physical C-P-N hybrid hydrogel structure.....	122
Figure 6.2: ¹ H-NMR spectra of Chitosan-Poly vinyl pyrrolidone-Poly N- isopropyl acrylamide (C-P-N) hydrogel (d) in the comparison of Poly N- isopropyl acrylamide (PNIPAAm) (c) Poly vinyl pyrrolidone (PVP) (b) Chitosan (CHT) (a).....	123
Figure 6.3: Overall Vibrational-Spectroscopy of Poly-N-isopropylacrylamide-block -poly aspartic acid (PNIPAAm-b-PASP), L-ASP-NCA, Chitosan (a), PVP (b), PNIPAAm (c) and combinational CHT-PVP-PNIPAAm hydrogel (d).....	124
Figure 6.4: TGA thermographs of the cross-linked C-P-N hydrogel; native a) CHT, b) PVP and c) PNIPAAm and d) cross-linked C-P-N hydrogel.....	126
Figure 6.5: Typical textual profiles of the cross-linked C-P-N hydrogel for determining, deformation energy, matrix resilience and matrix hardness.....	128
Figure 6.6: Typical profile obtained during rheological testing of samples. The black circle demarcates the crossover between the storage modulus (G') and the loss modulus (G'') and hence this value was used as the gelation temperature.....	130
Figure 6.7: Digital images of the surface of the C-P-N hydrogel (a-d) and representative cross sectional area of C-P-N hydrogel observed by scanning electron microscope (SEM) (e-f).....	134
Figure 6.8: Isotherm log plot of the polymerized C-P-N hydrogel.....	133

Figure 6.9: Weight loss profiles of the C-P-N hydrogels (F_1 - F_3) in simulated tumor condition over 30 days; a) non-cross-linked C-P-N hydrogel and b) cross-linked C-P-N hydrogel.....	134
Figure 6.10: Typical SEM micrographs and fluorescence images of the C-P-N (a&c) drug-loaded functionalized nanomicelles post encapsulated within the C-P-N at 50x magnification, b) high magnification 100x of the IFS.....	134
Figure 6.11: An optimized implantable antibody functionalized methotrexate loaded nanomicelles hydrogel composite delivery system.....	135
Figure 6.12: Folic acid and Methotrexate release outline from the optimized formulation over a month (30 days) period.....	136
Figure 6.13: Tetrazolium salt MTT assay to evaluate the effect of AF(MTX)NM's, IFSI and C-P-N formulations (a) on percentage viability of NIH:OVCAR-5 cells. AF(MTX)NM's formulation, IFSI and C-P-N elutes were incubated with ovarian cells for 72 hours prior to cell viability evaluation in each treatment group. Each point depicts average \pm SD (n =3).....	138
Figure 6.14: Confocal fluorescence images of the IFSI. Unlabelled control micelles image (a), FITC-labeled functionalized nanomicelles (b-d) and C-P-N hydrogel stained with DAPI or trypan blue.....	139
Figure 7.1: Athymic nude mice were placed in inside sterile IVC cages air flow systems in SPF room at 25°C with 60-70% relative humidity(RH), sterile fed ad libitum diet, water and bedding were also used to ensure the soothe-comfort and protection against infection.....	145
Figure 7.2: Schematic representing of the study design and number of mice required for the in vivo preclinical studies using PNIPAAm-b-PASP methotrexate-loaded with/without antibody nanomicelles for targeting ovarian cancer cells.....	149
Figure 7.3: a) Inoculation of 1×10^6 NIH:OVCAR-5 cells/ml into the flank (SC) and b) 2×10^8 cells/ml into the peritoneal cavity of immuno-deficient Swiss nude mice respectively.....	150
Figure 7.4: Digital-image of anaesthetized SC (neck region) inoculated mouse scanned for tumor development using ultra sound Vevo® 2100 Imaging system (Visualsonics Inc, Toronto, Canada).....	151
Figure 7.5: a, b, c and d are SC inoculated nude mice with a tumor diameter of 4mm, measured using an electronic digital Vernier caliper a) and Vevo® 2100 Imager d), respectively.....	154
Figure 7.6: a) An IP-inoculated nude mouse with a moderately distended abdomen due to tumor growth, dissemination and ascites. b) Refers to an ultrasound image taken using the Vevo® 2100 Imager indicating a tumor diameter of 100 mm ³ and c) is a 3D image of the circumference of the tumor. d) Reveals multiple coalescing tumor nodules disseminated throughout the peritoneal cavity (peritoneal carcinomatosis) as seen during the gross necropsy examination.....	154

Figure 7.7: Blood collection through the sephanus vein, during pre-inoculation, during the period of tumor growth, during the period of chemotherapeutic dosing (a-c), subsequently serum/plasma samples were extracted employing exxstat spin centrifuge from Idexx laboratories (d-e).....157

Figure 7.8: A) Scanned IP-implanted, AF(D)NM's-treated nude mouse tissue section showing a section (arrow) of ovarian carcinoma expressing MUC16/CA125 antigens (brown staining). MUC16/CA 125 IHC, DAB, chromogen, hematoxylin counterstain. B) Shows the region of interest/ROI delineated (yellow line) and MUC16-positive signal (red) within the ROI for quantification using the Olympus Count and Measure function (Olympus cellSens software).....159

Figure 7.9: PDA plot showing the absorbance of MTX (retention time= 1.5mins) and PYZ (retention time= 1.1.mins).....161

Figure 7.10: Intraperitoneal injected mice showing ISFI in the peritoneal cavity under biopsy microscope viewed with digital camera.....166

Figure 7.11: Histopathological analysis of tissue surrounding the site of implantation of the ISFI implant in a) control (non-treated normal mouse) b) after 4 days of implantation c) after 6 days of implantation and d) after 10 days of implantation..... 166

Figure 7.12: Sonographic representation of tumor growth and response to antibody-bound drug loaded nanomicelle hydrogel composite delivery system (AF(D)NMs). (a) Ascitic fluid development in a nude mouse 5 days post-induction, (b) Tumor growth 10 days post induction with NIH:OVAR-5 cell suspension, (c) Chemotherapeutic implant injected adjacent to tumor growth 11 days post-induction, c) decrease in tumor size and only a small tumor nodule was noticeable 15 days after implementation of the (AF(D) NMs) treatment.....170

Figure 7.13: Nude mouse tumor growth curves illustrating chemotherapeutic efficacy of the three treatment groups vs the control/placebo group, expressed as average tumor sizes in NIH:OVCAR-5 EOC-bearing nude mice. A refers to the methotrexate- and B the cisplatin-loaded nanomicelle implant delivery system in NIH:OVCAR-5 EOC-bearing nude mice. Each point depicts mean (n=10/group); bar, \pm SD.....171

Figure 7.14: (a) An IP-inoculated mouse pre-treatment (red ring), (b) distended abdomen post-treatment (red ring), (c₁,c₂) after necropsy examination, displaying intestinal nodules (white and red arrows), nodules in omentum (black arrow), and (d) illustrates the reduction in tumor size after treatment with the antibody-bound drug loaded nanomicelle hydrogel composite delivery system (AF(D) NMs)..... 172

Figure 7.15: Nude mice average body weight curves illustrating chemotherapeutic efficacy in the 3 treatments and control (placebo) group. Mouse weights in both the comparison (IV cisplatin and methotrexate, respectively) and the 2 experimental treatment groups decreased during the course of this study ($p < 0.05$). Whereas in the placebo group body weights increased slightly and were normalized to baseline weight ($p < 0.05$). A refers to the methotrexate- and B the cisplatin-loaded PNIPAAm-b-PASP nanomicelles delivery system in NIH:OVCAR-5 EOC-bearing nude mice. Each point depicts mean ($n=10/\text{group}$); bar, \pm SD.....173

Figure 7.16: Point-of-euthenasia levels of MUC 16/CA 125 antigens in the plasma and ascitic fluid of mice in the experimental and control groups. (D refers to methotrexate (in graph A) and cisplatin (in graph B)).....175

Figure 7.17: Microscopic view of the liver (a-b) and kidney (b-c) in AF(D)NMs, (D)NMs and IV-drug only treatment groups, stained with H&E. (a) Cystic distension of bile ductule containing bile (dark brown thick arrows), foci of hepatocellular necrosis (dark blue arrow), mild bile ductule proliferation (dark brown thin arrows) and mild lymphocytic infiltration into portal areas (green arrow). (b) Multifocal to coalescing hepatocellular coagulative necrosis with (red thin arrows) or without associated haemorrhage (red thick arrows). (c) Severe nephrosis as evidenced by ragged intraluminal clumps of cell debris (black rings),.HE. (d) Basophilic (calcified), granular intra-tubular cellular detritus (black arrow), multifocal (segmental) karyolysis in some tubular epithelial cells, and multifocal mild distension of proximal convoluted tubular lumens (lined by slightly attenuated epithelium) HE.....178

Figure 7.18: MUC16/CA125-positive labeling of EOC cells in mouse tissues and tumor foci in IP-inoculated nude mice 4 weeks post-inoculation.....179

Figure 7.19: ROI (regions of interest) measurement of IHC images on the stained slides for each treatment group, and the MUC 16 density in each image was calculated as percentage of MUC16-positive labeling per square centimeter of each selected EOC tissue section (one per mouse). (D refers to methotrexate (in graph A) and cisplatin (in graph B)).....181

Figure 7.20: Kaplan–Meier mouse survival curves, showing the three chemo-treatment groups ($n = 10$) including nude mice injected with AF(D)NM's, (D)NM's and IV chemotherapeutic drugs and a control placebo implant treatment group. The survival rate of mice in the AF(D)NM's test group was significantly improved compared with the other groups ($p < 0.05$).....182

Figure 7.21: Typical chromatogram obtained for methotrexate (retention time=1.408min) and internal standard, pyrazinamide (retention time=0.932min)....183

Figure 7.22: Calibration curve of Methotrexate obtained in blank plasma.....183

Figure 7.23: Blood methotrexate levels in experimental nude mice ($SD < 0.044$).....185

Figure 7.24: a) Calibration graph of MTX in PBS
b) calibration curve of MTX in methanol c) drug in the surrounding tissue after 4 or 10 days.....185

Figure 7.25: (a)-Antibody functionalized drug loaded nanomicelles AF(D)NMs/nanomicelle. (b)-AF(D)NMs encapsulated in an optimized implantable composite C-P-N delivery system (ISFI). (c₁,c₂)-ISFI injected and release nanomicelles into the peritoneal cavity. (d₁,d₂)-Specific antibody-muc16 interaction or binding. (e₁,e₂)- Fluorescence images of targeted chemotherapy of human ovarian carcinoma cells. (f)-Intraperitoneal targeted chemotherapeutic mechanism congruently depicted.....186

LIST OF TABLES

Table 2.1: Outline of the distinguishable nanotherapeutic tools designed for ovarian cancer treatment.....	17
Table 2.2: Building block sections of copolymers employed in micelle drug transport nanosystems (adapted from Sutton et al., 2007).....	23
Table 2.3: Polymeric Nanomicellar systems employed for treatment and diagnosis purposes (adapted from Kedar et al., 2001; Chen et al., 2014).....	28
Table 2.4: Polymeric micelle-based formulations containing chemotherapeutic drugs in Clinical trials.....	36
Table 2.5: Nanomicellar patents issued in the area of cancer drug delivery (Adapted from Shared report NanoCarrier Co, 2014).....	38
Table 3.1: Drug release kinetics results for various models of methotrexate-loaded nanomicelles for site-specific targeted therapeutic delivery.....	63
Table 4.1: Nano-formulation variables and responses employed in design.....	70
Table 4.2: Depiction of the 3 ² factor Box Behnken design for micelle formulation.....	71
Table 4.3: Responses data obtained for the 3 factor Box Behnken experimental design micelle formulations.....	75
Table 4.4: Coefficients for equations, r^2 -value for several dependent variables of methotrexate loaded PNIPAAm-b-ASP micelles.....	79
Table 4.5: Model S-values and the coefficient of determination (R2) data acquired for the linear regression equations.....	79
Table 4.6: Summary of the obtained values for each of the responses and the predicted Values and desirability.....	80
Table 4.7: Probabilities of the effects of the variables on the outcomes.....	80
Table 4.8: Drug release kinetics results for various models of methotrexate -loaded nanomicelles for site-specific targeted therapeutic delivery.....	92
Table 5.1: The physicochemical analysis of MTX-loaded polymeric nanomicelles with and without antibody (n=triplicate).....	102
Table 6.1: Textural parameters employed for determination of C-P-N hydrogel matrix hardness, deformation energy and matrix resilience.....	116

Table 6.2: Evacuation and Heating Phase Parameters used for Porositometric Evaluation of the C-P-N hydrogel.	118
Table 6.3: Textural profile of the unhydrated and hydrated cross-linked C-P-N hydrogel.....	127
Table 7.1: Details of the optimal mouse model for human ovarian carcinoma research used in this study.....	144
Table 7.2: Details of the anaesthetics, analgesics and drugs used together with the doses and routes of administration.....	153
Table 7.3: UPLC method for the elution of methotrexate and internal standard pyrazinamide.....	162
Table 7.4: Procedures conducted in nude mice model used for induction of ovarian cancer.....	168
Table 7.5: Inter- and intra- day precision and accuracy of the method were determined (only one set of interday data is shown).....	184

LIST OF EQUATIONS

Equation 3.1: Determination of the viscosity mean molecular weight (M) employing the partially-proportional Mark-Houwink formula, which correlates the inherent/intrinsic viscosity $[\eta]$ with the molar mass (M).....	43
Equation 3.2: Determination of drug entrapment efficiency (DEE) utilizing linearity graph, $r^2 = 0.99$ with Cecil 3021 UV spectrophotometer.....	45
Equation 3.3: Relationship describing the drug content (% w/w) employing weight of the drug loaded in the nanomicelles versus weight of the nanomicelles.....	45
Equation 3.4: The Zero-order model representing a stable release process	47
Equation 3.5: The first-order rate model describes incorporation and/or dispersion of the drug in a permeable matrix with drug release rate independent of its concentration.....	47
Equation 3.6: Higuchi's square root of time reliant model established from the Fickian law of diffusion for therapeutic release from a matrix structure.....	47
Equation 3.7: Korsmeyer-Peppas model is utilized for validation of the process of therapeutic release.....	47
Equation 3.8: Hixson-Crowell law is employed to determine the release reliant on transformation in the surface region and size of the nanoparticle.....	48
Equation 3.9: Mark-Houwink formula in its logarithmic nature permits a quick evaluation of viscosity mean molecular weight	51
Equation 4.1: Polynomial regression equations produced for size, DEE, MDT and cumulative release.....	78
Equation 4.2: The Mean Dissolution Time (MDT) was calculated for each of the formulations and a maximum MDT is the fastest drug release rate achievable.....	79
Equation 6.1: The swelling ratio (S_r , %) were calculated according hydrogel system.....	118
Equation 6.2: The percentage matrix erosion (E, %) at time, t of the hydrogel system.....	118
Equation 6.3: DEE of the device was calculated from the actual drug amount and the theoretical loading amount in 10mg of nanomiceller system, respectively.....	119

Equation 7.1: The percentage of viable cells calculated as functions of number of cells counted per number of quadrants counted. This was a 1:3 ratio which produced a dilution factor of.....146

Equation 7.2: Accuracy and precision of drug concentrations was determined by means of relative standard deviation (%RSD).....162

LIST OF ABBREVIATIONS

AET-HCl	2-Amino ethanethiol hydrochloride
AF(MTX)NM's	Anti MUC 16 MTX-loaded Nanomicelles
AIBN	2, 2'-Azobisisobutyronitrile
APDCNm	Antibody-attached Peptide-bound Drug-conjugated copolymer Nanomicelle
APS	Ammonium persulfate
AC	Anticancer Activity
Asp	Aspartate
AUC	Area under the Curve
BJH	Barrett-Joyner-Halenda
CA	Cancer Antigen
CANSA	Cancer Association of South Africa
CDCl ₃	Deteriorated Chloroform
CMC	Critical Micelle Concentration
COO ⁻	Carboxylic
C-P-N	Chitosan Poly vinyl pyrrolidone Poly N- isopropyl acrylamide
CT	Conventional X-ray Computed Tomography
D _∞	Loading Dose
D _t	Percentage of Dose Released in time
DAB	3,3'-diaminobenzidine
DCC	N, N'-dicyclohexylcarbodiimide
DE:	Deformation energy
DEE	Drug Entrapment Efficiency
Delta Y=	Percentage weight loss from onset point until end point
DLS	Dynamic Light Scattering
DMF	N, N-dimethylformamide
DMSO	Dimethylsulfoxide Dimethylsulfoxide
DNA	Deoxyribose nucleic acid
DoE	Design of Experiments
DOX	Doxorubicin

DSC	Differential Scanning Calorimetric
DT	Decomposition temperature
DTPA	Diethylenetriaminepentaacetic acid
EDC	1-ethyl-3-(3-dimethylaminopropyl)-carbodiimide
EDTA	Ethylenediaminetetraacetic acid
ELISAs	Enzyme-Linked Immunosorbent Assays
EPR	Enhanced Permeability and Retention effect
EOC	Epithelial Ovarian Cancer
FA	Folic Acid
FDA	USA Food and Drug Administration
FBS	Fetal Bovine Serum
FCS	Fetal Calf Serum
FITC	Fluorescein isothiocyanate
FFPE	Paraffin-Embedded
FTIR	Fourier Transform Infra-Red
γ	Shear Strain
G'	storage modulus
G''	loss modulus
GA	Glutaraldehyde
Genexol-PM	Paclitaxel-incorporated PEG-PLA Nanomicelle
Gd	Gold
H&E	Haematoxylin and Eosin
Hyd-Adr	Hydrazone Adriamycin
IHC	Immunohistochemistry
ISFI	<i>in situ</i> forming implant
IP	Intraperitoneal
IPNs	interpenetrating networks
IV	Intravenous
L-Asp-NCA	Aspartic acid-N-carboxyanhydride
LCST	Lower Critical Solution Temperature
LOQ	Limit of Quantification
Mab	Monoconal antibody

MH	Matrix hardness
MR	Matrix resilience
MRI	Magnetic Resonance Imaging
MTD	Mean Dissolution Time
MUC	Mucin
MTT	3-(4,5-dimethyl-thiazol-2-yl)-2,5-diphenyl-tetrazolium bromide
MTX	Methotrexate
(MTX)NM's	MTX-loaded Nanomicelles
η	Intrinsic viscosity
NC-6004	Nanoplatin®
NC-4016	DACH-Platin Micelle
NHS	N-hydroxysulfosuccinimide
NMR	Nuclear Magnetic Resonance
OC	Ovarian Cancer
-OH	Hydroxyl
OVCAR	Ovarian Cancer Cell Line
PAsp	Poly aspartic acid
PBS	Phosphate Buffer Solution
PCCNs	Polycharged Complex Nanomicelles
PCL	Poly (ϵ -caprolactone)
PdI	Polydispersity Index
PDLLA	Poly-DL-lactide
PEG	Poly Ethylene Glycol
PEO	Poly Ethylene Oxide
pHPMAm	Poly (N-(2-hydroxypropyl methacryamide)
PGlu	Polyglutamate
PLA	Poly (L-lactide)
PLGA	Poly (lactide-co -glycolide)
Plys	Polylysine
PNIPAAM	Poly (N-isopropylacrylamide)
PNIPAAm-b-PAsp	Poly N isopropylacrylamide-block-poly aspartic acid
PNIPAAm-NH ₂	Amino poly N- isopropylacrylamide
PPO	Poly-(propylene oxide)

PTX	Paclitaxel
PVA	Poly (N-vinyl alcohol)
PVP	Poly (N-vinyl pyrrolidone)
PYZ	Pyrazinamide
RAFT	Reversible Addition-Fragmentation Chain Transfer
RSD	Relative Standard Deviation
SD	Standard Deviation
SEM	Scanning Electron Microscopy
SLN	Solid Lipids Nanoparticles
SN-38	7-ethyl-10-hydroxy-camptothecin
SOP's	Standard Operational Procedures
SPECT	Single-Photon Emission Computed Tomography
SRN	Stimuli Responsive Nanomicelles
STE	Simulated Tumor Environment
RES	Reticular Endothelial Retention Scheme (RES)
TBA	Tert-butanol
TEA	Triethanolamine
TEM	Transmission Electron Microscopy
TEMED	N, N, N', N'-Tetramethylethylenediamine
TGA	Thermogravimetric Analysis
T _p	First derivative peak temperature associated with highest rate of change on the weight loss.
CH ₃	Methane
THF	Tetrahydrofuran
τ/Torque	Shear Stress
TRC	Thermal Ring-cleavage Polymerization
UPLC	Ultra Performance Liquid Chromatography
WHO	World Health Organization

CHAPTER 1
INTRODUCTION
BACKGROUND AND RATIONALE FOR THIS RESEARCH

1.2. Introduction and Background on Ovarian Cancer

Ovarian cancer (a highly metastatic and lethal gynaecologic malignancy) is a challenging disease to treat and since it presents with few early symptoms, it is usually diagnosed late when in advanced stages, stage III and stage IV (Auersperg et al., 2001; Seiden, 2001; Whitehouse and Solomons, 2003). The disease is classified as early-stage (stages I and II) when confined within the pelvis, and as advanced-stage (stage III and stage IV) when in the upper abdomen and/or lymph nodes or distant sites (pleural space, hepatic or splenic parenchyma). Most patients with early-stage epithelial ovarian cancer are asymptomatic or present vague symptoms, including abdominal fullness, dyspepsia, bloating, pelvic pain, ascites, pleural effusions and early satiety (Auersperg et al., 2002; Chauhan et al., 2006). Most ovarian cancers (90%) are epithelial in origin and, hence, are referred to as epithelial ovarian cancers. Epithelial ovarian cancer is the fifth leading cause of cancer deaths and the most lethal gynaecologic cancer in the United States (Jemal et al., 2005). Ovarian tumors exhibit diverse and altered cell surface antigens such as, HE4, CA 72-4, EGFR, SMRP and mucin (MUC16) that discriminate them from normal ovary cells and other normal cells lining the peritoneum (Stohlbach et al., 1979; Moore et al., 2007). Mucins are heavily glycosylated proteins found in the mucus layer or at the cell surface of many epitheliums (Desseyn et al., 2008). There are two structurally distinct families of mucins, secreted and membrane-bound forms.

The ovarian surface epithelium has a mixed epithelial mesenchyma phenotype and is the only region in the ovaries that expresses mucins (Auersperg et al., 1998; 2001). Normal ovaries do not consist of any glandular tissue or goblet cells; therefore, no secreted mucins are expected to be synthesized by the parenchyma of the ovary. Non-malignant ovarian epithelial cell lines express MUC1 and MUC5AC (Giuntoli et al., 1998) while epithelial ovarian cancers express more mucins (MUC1, MUC2, MUC3, MUC4, MUC5AC, and MUC16) than normal ovarian surface epithelium (Giuntoli et al., 1998; Auersperg et al., 2001; Chauhan et al., 2006). The aberrant changes in mucin expression (mucin switching) during the transformation of normal ovarian surface epithelium to cancer are important in disease progression as they change

adhesive and anti-adhesive properties of tumor cells, thereby promoting the dissemination of tumor cells during metastasis (Rump et al., 2004; Gubbels et al., 2006; Tamada et al., 2007). The role of MUC1, MUC2, MUC3, MUC4 and MUC5AC has not been extensively studied in epithelial ovarian cancer development compared to MUC16.

MUC16 (also known as CA125) is employed as a biomarker in ovarian cancer due to its high expression in ovarian carcinomas and that it is shed into the serum (Bast et al., 1981; Jacobs et al., 1992; Fritsche and Bast, 1998; Yin et al., 2002; Menon and Jacobs, 2002). It is a very large cell surface mucin and was first identified in 1981 by a monoclonal antibody (OC125) that was developed from mice immunized with human ovarian cancer cells (Bast et al., 1981). Serum MUC16 levels are used to identify ovarian cancer patients and those with residual disease following primary therapy to monitor the clinical course of disease. Changes in serum MUC16 levels reflect progression or regression of ovarian cancer more than 90% of the time (Niloff et al., 1986; Mogensen et al., 1990; Buller et al., 1991).

The current treatment for ovarian cancer makes use of aggressive cytoreductive surgery, systemic chemotherapy and external beam radiotherapy (Hoskins et al., 1994; MacGibbon et al., 1999). Paclitaxel and cisplatin are standard chemotherapeutic drugs used for the treatment of ovarian cancer, with methotrexate also used as an option (Khayat et al., 2000; du Bois et al., 2003). The efficacy of intravenous chemotherapy for epithelial ovarian cancer (EOC) is limited mainly by myelotoxicity and frequently impaired by the rapid appearance of resistance to chemotherapeutic drugs. While many patients initially respond to surgery and chemotherapy, the long-term prognosis is generally unfavorable. Since the peritoneal cavity is the principal site of disease in ovarian cancer (Cannistra, 2004), our proposed drug delivery device is aimed at administering drugs directly into the peritoneal cavity to target the MUC16 antigen expressed on the surface of ovarian cancer cells (Figure 1.1).

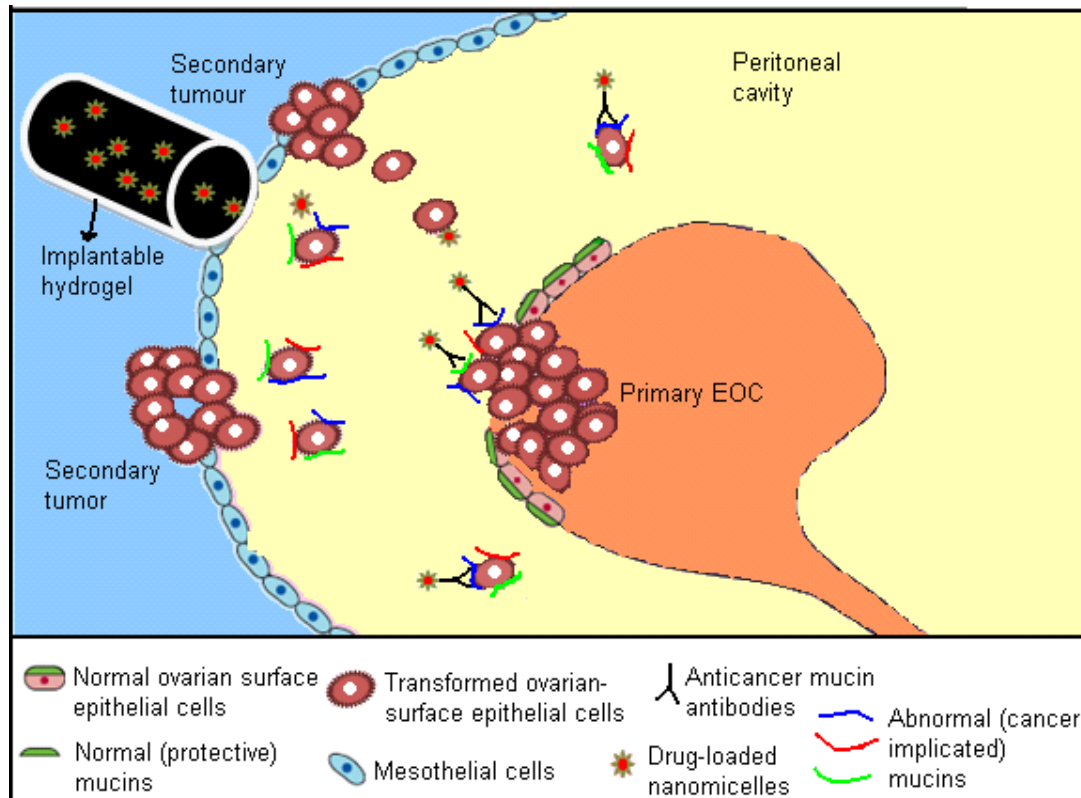


Figure 1.1: A diagrammatic illustration showing the expression of cancer-associated mucins accompanying the development of ovarian cancer and the intraperitoneal implant providing targeted therapy within the peritoneal cavity.

Primary ovarian tumors disseminate cancer cells via the peritoneum resulting in a major cause of recurrent metastatic disease which accounts for the majority of cancer deaths (Tanya et al., 2004). For direct targeting of epithelial ovarian cancer cells, cancer-associated mucin (MUC16) on the surface of epithelial ovarian cancer cells that distinguish them from normal cells will be targeted for the delivery of drugs with minimal side-effects (Moore et al., 2007). The antibody-bound-nanomicelles will be encapsulated in a temperature (body temperature) and pH (peritoneal fluid pH~7) sensitive hydrogel which will be implanted via injection into the peritoneal cavity. Following the release of antibody-bound nanomicelles from the hydrogel, the nanomicelles (formulated to circulate for a long time in the peritoneal fluid) will target specific mucin antigens significantly over-expressed on ovarian cancer cells at the primary tumor site (tumor confined to the ovary in stage I and stage II), those circulating in the peritoneal fluid during stage III and stage IV (when patients are usually diagnosed) and lastly, cancer cells forming nodules at distant sites in the peritoneal cavity (Figure 1.1). This targeting system will help reduce the tumor load responsible for adhesion at the sites of secondary metastasis (peritoneal and abdominal surfaces) (Niloff et al., 1986; Mogensen et al., 1990). The anti-MUC16 antibodies conjugated to nanomicelles has a potential to improve the tumor selectivity of drug-loaded nanomicelles. This approach is likely to overcome the non-specific

destruction of healthy tissue associated with conventional strategies and also reduce the particularly problematic multidrug-resistant tumors to improve disease prognosis in ovarian cancer patients. The success of this method might make IP chemotherapy an appealing treatment option for patients with ovarian cancer.

As there is a critical need to identify new therapeutic drug delivery systems for improving the life of ovarian cancer patients, the proposed intraperitoneal implantable drug delivery system has the significant pharmacologic advantage of delivering antitumor agents directly into the accessible but confined space of the peritoneal cavity, the sole location of disseminated ovarian cancer cells. The development of this novel implantable drug delivery system may circumvent the treatment flaws experienced with conventional systemic therapies, effectively manage recurrent disease and ultimately prolong disease-free intervals in ovarian cancer patients.

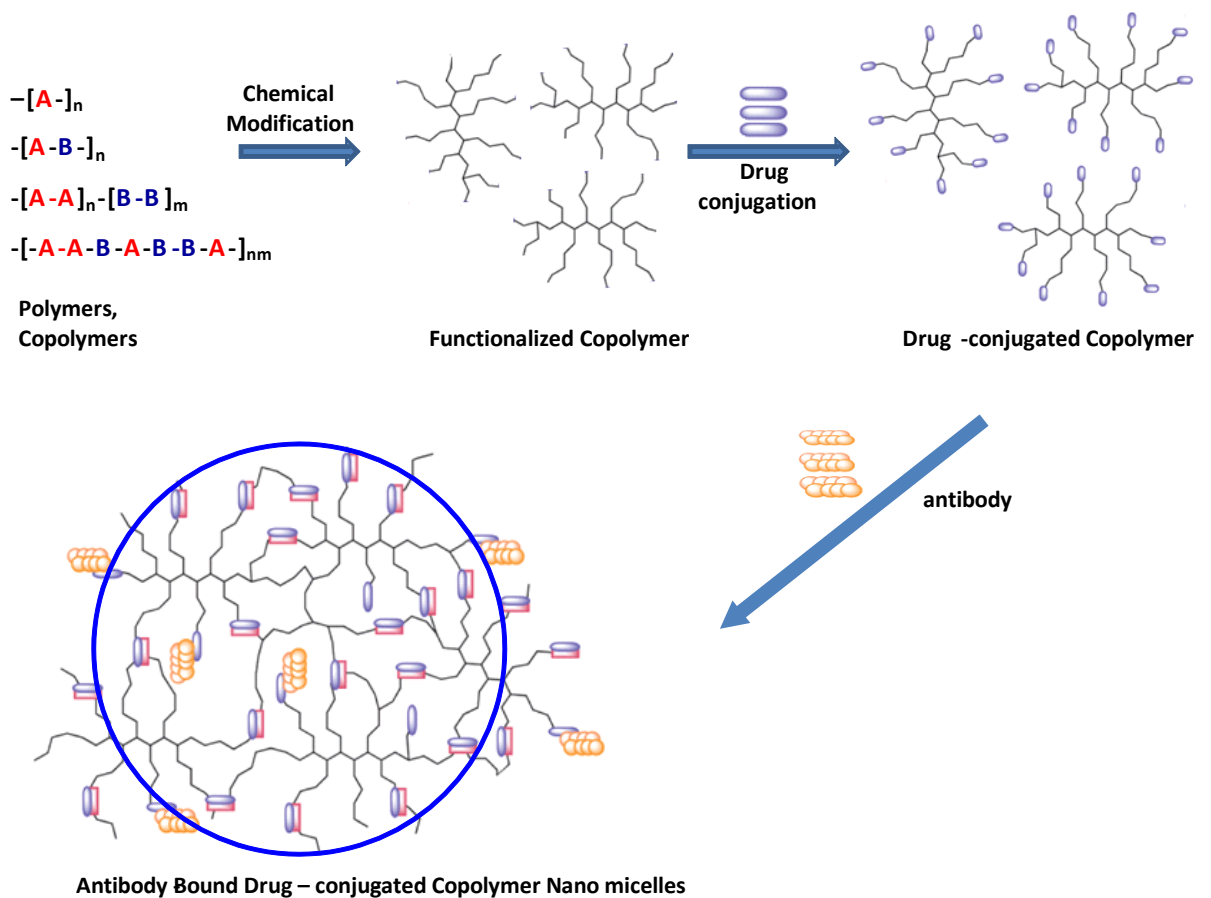
1.2. Rationale and Motivation for this Research

Ovarian cancer is the most commonly fatal gynaecologic malignancy in which many patients are diagnosed at an advanced stage when the disease has spread beyond the ovary. While many patients initially respond to surgery and chemotherapy, the long-term prognosis is generally unfavorable, with recurrence and development of chemo-resistant disease. There is a critical need to identify novel drug delivery strategies that prolong disease-free intervals and effectively manage recurrent disease (Auersperg et al., 2001; Seiden, 2001; American Cancer Society et al., 2010). Mice xenograft models of ovarian cancer using ovarian cancer cell lines (OVCAR-3) have been used as models to study tumor biology in the search for new treatments for ovarian cancer. The spreading of ovarian cancer cells can occur by direct contact and invasion into adjacent tissues, such as the uterus, fallopian tubes, bladder, sigmoid colon, or rectum. The exfoliated tumor cells float in the peritoneal fluid and adhere to the mesothelial cells that line the inner wall of the peritoneum and the outer surface of various pelvic and abdominal organs. Haematogenous metastasis of ovarian cancer cells is a rare phenomenon, and can lead to involvement of other organs, including the brain (Wang et al., 2011). The prognosis of women with advanced stage ovarian cancer remains poor despite extensive research into systemic therapies. The introduction of chemotherapy (paclitaxel and cisplatin) has resulted in longer progression free (15-22 months) and overall (31-44 months) survivals, yet at least 50-75% of these women have persistent or recurrent disease with long-term survival (>5 years) achieved in only 25%. In the majority of patients recurrence is seen within the peritoneal cavity, and in approximately 12% it occurs in the retroperitoneal lymph nodes. Three randomized trials in ovarian cancer patients affirmed this assumption by demonstrating

improved survival with intraperitoneal chemotherapy compared to similar or identical agents delivered systemically. The National Cancer Institute has thus recently proposed to make intraperitoneal chemotherapy part of the standard treatment in ovarian cancer. The concentration of MUC16 is raised in only a few patients with early disease and this limitation results in the majority of patients being diagnosed in advanced disease stages (Seiden, et al., 2001). Some evidence supports the use of radiotherapy, particularly for chemo-resistant ovarian cancer. However, radiotherapy remains controversial for advanced ovarian cancer because of toxicity. Several studies that are in advanced stages of development and in various phases of clinical trials also attempt to provide monoclonal antibody-mediated chemotherapeutics by utilizing various conjugates and antibodies linked directly to drug molecules (Yap et al., 2009). However, none of these strategies utilize the concept of linking antibodies to nanomicelles. Therefore, this study strategically focuses on attaching the anti-MUC16 antibody to a nanomicelle structure due to its potential pharmaceutical stability of the resultant targeting complex and also the fact that anti-MUC16 is extensively used in ovarian cancer as a biomarker. Thus, the proposed strategy would merge the concepts of pharmaceutical nanotechnology and mucin biomarkers for the design of an effective strategy to treat OC via the intraperitoneal route.

The rationale for the proposed injectable intraperitoneal drug delivery strategy to provide therapy in ovarian cancer is based on the fact that ovarian cancer is largely confined to the peritoneal cavity and as ovarian cancer cells spread within the peritoneal cavity, they form secondary nodules by seeding to mesothelium-lined structures. Although the therapeutic approach for ovarian cancer is surgical removal followed by intravenous chemotherapy, malignant cells that might have survived the surgery are often missed (Harries et al., 2001). Animal models such as ovarian tumor-bearing BALB/c mice have been used successfully by researchers to evaluate the potential of drugs via intraperitoneal injection (Vanderhyden et al., 2003). The approach in this study is to inject an in situ forming hydrogel-based implant loaded with anti-MUC16 conjugated nanomicelles in the peritoneum of ovarian tumor bearing mice with the aim to reduce the rate of recurrence, seen in the majority of ovarian cancer patients, and improve the long-term survival rate. This strategy will not only enable specificity, but will also increase the residence time of the drug-loaded nanomicelles at the tumor site and within the peritoneal cavity, enhance tumor uptake of chemotherapeutic drugs and finally aid in preventing metastases, recurrence and chemo-resistance. The significant pharmacologic advantage of delivering drugs directly into the accessible but confined space of the peritoneal cavity will greatly reduce recurrence. Having an intraperitoneal implant (as opposed to conventional intravenous chemotherapy) will be more logical as the peritoneum is the

predominant site of the tumor and will therefore receive sustained exposure to higher concentrations of drugs while normal tissues, such as the bone marrow and others, are largely spared from the toxic side-effects of conventional intravenous chemotherapy. For the first time, this study will demonstrate the application of a an injectable *in situ* forming hydrogel-based intraperitoneal implant using the concept of targeted therapy (anti-MUC16 antibodies) for the delivery of high doses of drug-loaded nanomicelles to ovarian cancer patients who, unfortunately, relapse and die of their disease, indicating that benefits of surgery and chemotherapy, whether these may be new drugs or a new combinations of old drugs, have reached a plateau (Jemal et al., 2008).



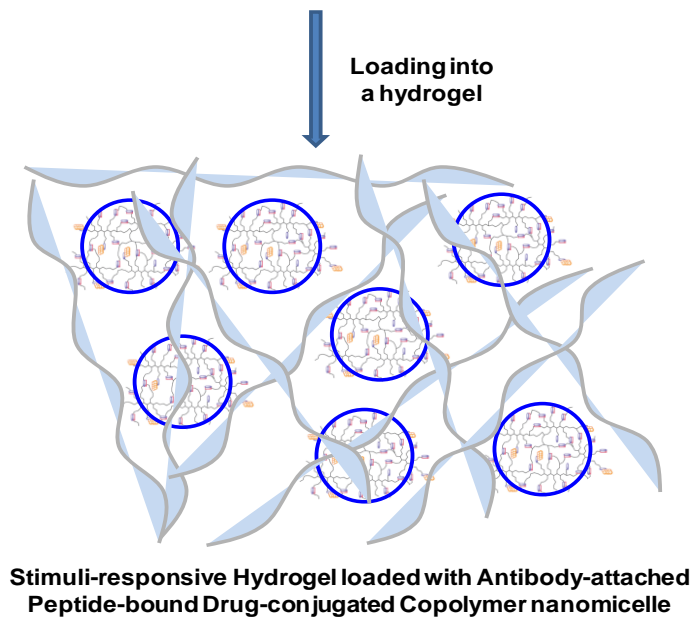


Figure 1.2: A schematic showing the monoclonal antibody-mediated intraperitoneal drug delivery system.

Thus having an implantable targeted drug delivery system for sustained and prolonged drug release will offer an alternative and improved treatment to patients suffering from recurrent ovarian cancer. This will provide effective targeted chemotherapy for ovarian cancer and is likely to overcome the non-specific destruction of healthy tissue associated with conventional intravenous chemotherapy. The potential for reducing multidrug-resistant tumors will also improve disease prognosis in ovarian cancer patients and may make this strategy of intraperitoneal chemotherapy appealing for patients with ovarian cancer since it would offer cancer cell-targeting and significantly reduce side-effects (Menon and Jacobs, 2002). The use of antibody-bound nanomicelles represents an innovative way to deliver drugs to ovarian tumor cells in a targeted manner via the peritoneal cavity.

Additionally, the nanomicelle system will be formulated following a unique step-by-step procedure where the copolymer system will be conjugated with another polymer or small organic molecule (for membrane localisation), drug agent (for therapeutic effect), peptide (for cell penetration), and an antibody (for tumor targeting) either individually or in various combinations as to form antibody-attached peptide-bound drug-conjugated copolymer nanomicelle (APDCNm) (Figure 1.2).

1.3. Novelty of this Research

Since the peritoneal cavity is the principal site of disease in ovarian cancer, this study is aimed at targeting the administration of drugs directly into the peritoneal cavity to target the MUC16 antigen expressed on the surface of ovarian cancer cells. Primary ovarian tumors disseminate cancer cells via the peritoneum resulting in a major cause of recurrent metastatic disease which accounts for the majority of cancer deaths (Chauhan et al., 2006). For direct targeting of epithelial ovarian cancer cells, cancer-associated mucin (MUC16) on the surface of epithelial ovarian cancer cells that distinguish them from normal cells will be targeted for the delivery of drugs with minimal side-effects. The antibody-bound-nanomicelles will be encapsulated in a temperature and pH sensitive hydrogel that will be injected into the peritoneal cavity to form an in situ hydrogel-based implant. Following the release of antibody-bound nanomicelles from the hydrogel, long-circulating nanomicelles will target specific mucin antigens significantly over-expressed on ovarian cancer cells at the primary tumor site (confined to the ovary in stage I and II), those circulating in the peritoneal fluid during stage III and IV (when patients are usually diagnosed) and lastly, ovarian cancer cells forming nodules at distant sites in the peritoneal cavity (Cannistra, 2004).

This strategy will help reduce the tumor load responsible for adhesion at sites of secondary metastasis. The anti-MUC16 antibodies conjugated to drug-loaded nanomicelles will improve tumor selectivity. This will also overcome the non-specific destruction of healthy tissue associated with conventional chemotherapy and reduce multidrug-resistant tumors to improve disease prognosis in ovarian cancer patients. The success of this study will make intraperitoneal chemotherapy an appealing treatment option for patients with ovarian cancer. Biocompatible and biodegradable polymers will be used to design functionalized anti-MUC 16 drug-loaded nanomicelles fixated within an in situ forming hydrogel implant. The implant will be evaluated for its potential to release drugs such as paclitaxel, cisplatin and methotrexate in a targeted manner within the peritoneal cavity with the ability to prevent ovarian cancer cells from using MUC16 to disseminate to other healthy organs from the ovaries. As there is a critical need to identify new therapeutic strategies for improving the current therapy of ovarian cancer, our proposed system has the significant pharmacologic advantage of delivering drugs directly into the accessible but confined space of the peritoneal cavity, the sole location of disseminated ovarian cancer cells. This strategy may circumvent the treatment flaws experienced with conventional intravenous chemotherapy, effectively manage recurrent disease and prolong disease-free intervals in ovarian cancer patients (Menon and Jacobs, 2002). Below is a detailed sequence of the methods to be employed in this project in order to achieve the aim and specific objectives of the project from a pharmaceutical formulation and

pre-clinical evaluation viewpoint. In addition, the project will also involve preclinical testing of the system in BALB/c female mice that have been used as suitable animal models to study ovarian cancer.

1.4. Aim and Objectives of this Research

The aim of this study was to design and develop a novel drug delivery system employing peptide/protein ligand conjugated to drug-loaded nanomicelles encapsulated with Chitosan(C)-poly(N-vinylpyrrolidone) (PVP)-N-isopropylacrylamide (NIPAAm) (C-P-N) hydrogel to form an In Situ Forming Implant (ISFI) for cancer cell-targeting following intraperitoneal implantation to increase the residence time of the nanomicelles at tumor sites, enhancing tumor uptake of drugs and prevent recurrence and chemo-resistance. To achieve this aim, the following objectives are outlined:

1. To design, develop and validate a nanomicelle based system using biodegradable and biocompatible polymers via molecular simulations
2. To undertake encapsulation of chemotherapeutic drugs in polymer nanomicelles in the form of drug copolymer conjugates
3. To assess the feasibility of using targeted ligands to bind to specific receptors and selection of potent peptide sequences from phage display library as co-targeting ligands
4. Formulation and characterization of *in vitro* performance (targeting) of the drug-loaded biodegradable peptide nanomicelles
5. Functionalization kinetics of nanomicelles with peptide/protein for specific targeting of cancer cells
6. Analysis/control of release (physicochemical) properties and targeting functionalities to develop new nano-drugs
7. To perform preliminary *ex vivo* pharmacological studies to determine the effectiveness of multi-ligand nanomicelles using mice as the animal model
8. To undertake *in vivo* biodistribution and biocompatibility evaluation
9. To conduct *in vivo* pharmaceutical evaluation of the drug targeted system

1.5. Overview of this Thesis

Chapter One: serves as the introduction of the thesis and describes the pathophysiology of epithelial ovarian cancer (EOC) in order to highlight the problems preventing the successful treatment of EOC. The novelty of the work and the aims and objectives of this work are also discussed.

Chapter Two: presents a comprehensive literature review focusing on the current work that has been conducted by other researchers in the development of nanomicelle in ovarian cancer chemotherapeutics. It also provides insight into the use of stimuli responsive materials as nanomicelle-forming systems.

Chapter Three: Comprehensively describes the synthesis and development of a novel super-viscosity amphiphilic copolymer for human ovarian carcinoma chemotherapeutics. The micellization process employing thermal ring-opening polymerization by which the copolymer is fabricated is evaluated by conducting tests to determine its yield as well as validating the occurrence of copolymerization in addition to numerous tests conducted to fully characterize the nanomicelles. Utilizing this information, variables for an experimental design were obtained.

Chapter Four: describes the utilization of a Face-Centered Central Composite Design in the determination of an optimum nanomicelle formulation. Amount of copolymer (mg) and homogenizer speed (rpm) were the two selected variables; and size, drug entrapment efficacy (DEE), mean dissolution time (MDT) and cumulative release were selected as the responses limits.

Chapter Five: describes the development and characterization of Anti-muc 16 functionalized PNIPAAm-b-PASP nanomicelles for the targeted delivery of methotrexate to human ovarian carcinoma cells. Mechanism of synthesis of anti-MUC 16 functionalized MTX-Loaded nanomicelle (AF(MTX)NM's) for improved intracellular uptake is also discussed. Drug release was conducted using dissolution, whilst microscopy is used to confirm nanomicelle morphology, formation and distribution of AF(MTX)NM's complex.

Chapter Six: describes *in-vitro* synthesis, characterization and evaluation of a bio-responsive IPN nanomicelle/hydrogel composite based implant for ovarian carcinoma treatment. The

combination of ISFI and nanomicelles was also investigated for rheological properties, mechanical strength, swelling and drug release and are reported on. *In vitro* testing of the implant on NIH:OVCAR-5 cancer cell line is discussed. The use of MTT assays is described and the results obtained from this method of viability testing of cells are evaluated.

Chapter Seven: reports *in vivo* work conducted on the optimal Athymic nude mouse model. Intraperitoneal and subcutaneous induction of human ovarian carcinoma of the said optimal mouse mode was also conducted. Chemotherapeutic Efficacy of various treatment protocols in EOC-inoculated Nude (NU/NU) Mice was validated. Ultra Performance Liquid Chromatography quantification of the amount of drug in the plasma is described and the results evaluated. The biocompatibility of the implant is also discussed.

Chapter Eight: provides the overall the conclusive remarks on the smart ISFI and insight into future outlooks and recommendations in which the study can be enhanced.

CHAPTER 2

A REVIEW OF NANOMICELLAR TECHNOLOGIES FOR TARGETED DRUG DELIVERY IN OVARIAN CANCER CHEMOTHERAPEUTICS

2.1. Introduction

Globally, epithelial ovarian carcinoma (OC) is the most fatal gynaecological disease that accounts for millions of deaths annually in the female population, making this malignancy a major health concern (Bae et al 2014; Davis et al., 2014; Rodríguez-Ayala et al., 2014; Smolle et al., 2014; WHO, 2014). Approximately 21,9 million new patients of OC have been diagnosed with approximately 14,270 deaths predicted in the United States in 2014 (Ovarian Cancer Research Fund Report, 2014). According to the World Health Organization (WHO) 2014, “in developing countries OC is one of the most lethal genital malignancies in females and this asymptomatic disease is exacerbated by the lack of early diagnostic strategies and access to expensive chemotherapeutic drugs. In South Africa, (CANSA, 2014) confirmed more than 500 cases of ovarian carcinoma in 2014 (CANSA, 2014). Worldwide, the five-year survival rate is only between 15–20 % for people who are sick with clinically late stage ovarian malignancy in spite of surgery and platinum treatment (Prat, 2014).

The current treatment for OC makes use of aggressive cytoreductive surgery to remove the infected ovaries, uterus, fallopian tubes, cervix and lymph nodules in the peritoneum abdomen. The surgical approach is then followed by external beam radiotherapy or systemic chemotherapy or both, depending on the stage at which the OC disease is identified. Paclitaxel and cisplatin are standard chemotherapeutic drugs used for the treatment of OC, with methotrexate also considered as an option. However, conventional treatment has its drawbacks such as drug toxicity and subsequent disease relapse, due to the development of multidrug resistance. In addition, the chemotherapeutic drugs are not site-specific for OC cell targeting and hence display dose-dependent side effects (Mishra, 2010; Yallapu et al., 2010; Bae et al., 2013). Furthermore; the long-term prognosis is commonly adverse, with manifestation and progression of chemo-defiant cancer. Patients that survive continue to suffer from various undesirable side-effects such as excessive vomiting, hair loss and a decline in blood cell numbers associated with the administration of non-targeted antineoplastic drugs for OC therapy (Chan et al., 2005). To circumvent these treatment flaws of conventional drugs, several targeted drug delivery platforms have been developed to direct anti-neoplastic drugs to specific tumor sites.

New advances in polymeric nanotechnology with particular emphasis on micelles provide feasible alternatives for targeted treatment of metastatic OC and minimize systemic-toxicity associated with

administration of chemotherapeutic drugs. These therapeutic polymeric systems serve as new drug carriers for antineoplastic drugs and include nanoparticles, micelles, polymer-conjugates and dendrimers. The limitations of these nano-enabled formulations (polymeric systems) include potential inaccuracies in direct drug targeting of tumors, potential toxicity to healthy cells, instability in the circulatory system, rapid degradation and clearance by the immune system and a lack of controlled drug release over prolonged periods of time (Wang et al., 2012; Babu et al., 2013; Díaz and Vivas-Meji, 2013).

In order to overcome these limitations for clinical applications to be feasible, current research focuses on preparation of nanoparticulate delivery systems (including micelles) functionalized with ligands such as antibodies to facilitate preferential specific targeting of tumors, release of the drug payload at a controlled rate and ultimately increase the therapeutic effect. Hence, prolonged circulation in the bloodstream, *in-vivo* stability, biodegradability and polymer-drug compatibility with sufficient retention of the drug within the carrier system are prerequisites to successful design and preparation of drug targeting delivery system. Furthermore, the potential synthetic building blocks for the carrier systems should be nontoxic, not inducing inflammatory responses or severe-toxicity. Other significant properties of polymeric carrier systems are the ability to be (biodegraded and) cleared/excreted by renal pathway after the drug is completely released and the prospect to further track and trace the polymeric system co-encapsulated with molecular imaging agent (Wang et al., 2013).

Therefore this chapter aims to present a comprehensive evaluation of the current advances and nanotherapeutic modalities employed for the chemotherapy of OC. A particular focus has been placed on micelle technologies as one of the most researched nano-archtypes of late for targeted OC treatment. The current status on OC biomarkers is also summarized, with an intergration of work undertaken on mucins and their possible application in early diagnosis and management of OC. These approaches are defined with specific intention to potentially identify the disease at an early stage, halt the disease progression and promote recovery.

2.2. Current Nano-based Drug Delivery Approaches for Ovarian Cancer (OC) Therapy

In response to the clear need for the development of efficient and selective drug transport systems to primary tumors and their metastases, many circulating nano-formulation delivery strategies have been designed including polymer-drug conjugates, dendrimers, liposomes, solid lipid nanoparticles and polymer micelles (Table 2.1 and Figure 2.1) (Alexisa et al., 2008; Wang et al., 2013). All these delivery systems offer advantages but they have their own individual limitations; hence a therapeutic delivery system (including polymeric micelles) needs to achieve several (biopharmaceutical)

prerequisites such as a marked increase in therapeutic impact compared to the free-drug, good biodegradability and biocompatibility, non-toxic and non-inflammatory propensity, prospect to large scale-up its manufacture (Katz, 2012; Sanna et al., 2014). Preferably, a nano-formulation delivery system must have high drug-loading capacity; ability to dissolve the partially water soluble drugs within the inner core, and selective accumulation in tumor tissue through permeability and retention influence (passive or active targeting); thus significantly increasing treatment bioavailability, reducing toxic side effects of chemotherapeutic drugs in healthy tissues, and resulting in improvement in patient condition (Alexis et al., 2010). Therefore, advances in targeted nano-formulation delivery systems improve the survival of ovarian cancer patients compared to conventional chemotherapeutics (Li et al., 2014). In this context, this gives emphasis to the need to invent consistent molecular or clinical indicators for early detection via evaluation of possible novel molecular targets and new approaches in chemotherapeutic modalities (Díaz and Vivas-Mejia, 2013). Several prospective biomarkers of ovarian carcinoma have been currently reported. Ovarian tumors exhibit diverse and altered cell surface antigens such as, HE4, CA 72-4, EGFR, SMRP, mesothelin, osteopontin, AFP, CTLA4, IFN α , KLK6, PLA2G2A, ErbB2, IL-10 and mucins (MUC1-16) that differentiate cancerous cells from normal ovarian cells and other normal cells lining the peritoneum (Niloff et al., 1986; Mogensen et al., 1990; Yin et al., 2002; Whitehouse and Solomon, 2003; Rump et al., 2004; Chauhan et al., 2006; Moore et al., 2007; Felder et al., 2014). Mucins (especially MUC16) display potential as indicators of ovarian malignancy and micelles with surface-attached specific antibodies (immuno-micelles) offer a wide-range of prospects for preferential targeting of ovarian tumor tissue (Miller, 2009). The mortality rate from ovarian disease may possibly be greatly reduced by engineering this innovative tool for early identification and therapy of this lethal illness.

Micelles are uniquely assembled nano-delivery vehicles with flexible characteristics that can be synthesized to dissolve partially water-soluble drugs, for passive/active delivery mechanisms, and enable accumulation of these drugs in tumor tissue (Rapoport, 2007; Akao et al., 2010; Liang et al., 2010; Preetham and Satish, 2011). Micelles and micelles surface-attached with specific antibodies offer important advantages for treatment delivery purposes. Micelles have been established as valuable tools in numerous medical arenas including nanomedicine, environmental science, toxicology, biochemistry, material science, oncology, engineering. These nano-carrier delivery systems are anticipated to result in major advances to tackle many unresolved challenges in clinical diagnosis, prevention, and treatment of various diseases, in particular ovarian cancer. These unique features of polymeric micelles account for their qualities as efficient drug delivery systems. For instance, their small size range (10–100 nanometers) ensures safe endocytotic uptake by target OC cells preventing nonselective destruction of healthy cells (Thassu et al., 2007). Micelles can penetrate and accumulate in areas with permeable vasculatures such as cancer; swollen and

infected regions (Rösler et al., 2001; Thassu et al. 2007; Song et al., 2009). In conclusion, polymer micelles are rapidly becoming valuable tools for diagnostic purposes and OC chemotherapy owing to micelle nano-range (ten-hundred nanometers), excellent biocompatibility, *in-vivo* stability, capabilities to incorporate a wide range of water insoluble anticancer drugs in their micelle core, and prolonged blood circulation times (Arimura et al., 2005; Karel, 2012).

2.3. Critical Comparison of Nanosystems to Micelles for OC Treatment

Nanosystems (nanoparticles) including polymer-drug conjugates are discussed with specific intentions to compare them with currently presented micellar technologies (which are the main focus of this paper) for targeted treatment of metastatic OC. Polymer-drug conjugates are nano-sized macromolecular architectural particles with low molecular weight and a highly versatile functionalized terminal surface, which allows covalent bonding of drugs (Sawant et al., 2006; Song, 2010). Defined physico-chemical parameters (including, pH, enzymatic modification, acid-catalyzed reactions) are essential for the release of treatment at the tumor site. Polymer-drug conjugates have been widely considered for prolonging the chemotherapeutic drug effect in the cancer, tumor accumulation, reduction of non-target toxicity, and improvement of anti-tumor activity (Sumer, 2008; Zhang et al., 2008; Guo and Huang, 2014). Therapeutics in ovarian cancer also employ dendrimers, synthesized from various polymers and genes; however acrylamide dendrimers are commonly employed. Dendrimers are composed of three important engineered subdivisions: (i) Exterior, with multiple prospective attachment locations, (ii) the central portion (i.e., where distinct dendrons delineate the separated unit stratum) coating the matrix, and (iii) the matrix for dendrons conjugation. The three sections of dendrimers can be modified for various applications including, nanodrug and DNA transport, or intrinsically performing as treatments (Parveen, 2012). Both polymer-drug conjugates and dendrimer nanosystems require the covalent binding of drug entities to the polymer carriers. This consecutively would necessitate the presence of functionalizable biochemical groups on the drug units, restraining the generality of this strategy. In light of the marked chemical stability of covalent conjugations, specific biochemical processes (such as *in vivo* enzymatic degradation, acid-catalyzed hydrolysis reaction) are required to release the drug at peritoneal tumor sites (Sinha et al., 2010; Kim et al., 2011; Lu and Park, 2012). Furthermore, due to the minute-size of these nanosystems (normally, 10 nm), they are able to simply pass through cellular membranes in the glomeruli filtration parts of kidneys and be rapidly cleared/excreted, resulting in shortened survival (half-lives) in the bloodstream (Wang et al., 2013). Vital structures and differentiating characteristics of nanocarrier systems are shown in Table 2.1 and in Figure 2.1 (Blanco et al., 2009).

Liposomes are microscopic spherical vesicles consisting of lipid bilayers enclosing an aqueous compartment, making biological membranes more accessible and offering a flexible platform to encapsulate both lipophilic and hydrophilic chemotherapeutic drugs. Lipophilic drugs are incorporated within the lipid bilayer while hydrophilic drugs reside in the vesicle cavity. Encapsulation of antineoplastic drugs in liposomes causes a change in pharmacokinetic and pharmacodynamic properties, resulting in potential reduction of therapeutic degradation and also limiting dose-limiting side effects (Sapra and Allen, 2003; Chang et al., 2009). Liposomes can be used for specific, selective targeting of cancer tissues, but they are rapidly cleared by immune system response unless special modifications via attachment of ligands are applied to the phospholipids' surface to improve cellular uptake by tumor tissues, thus, enabling a pronounced therapeutic effect (Nobs et al., 2004; El Bayoumi and Torchilin, 2009). Solid lipid nanoparticles (SLN) also have similar properties to liposomes but can be well-produced on a large scale. In contrast, the major problems associated with liposomes are their instability and difficulty in large-scale manufacture of sterile liposomes. Poorly water-soluble therapeutics are captured inside the hydrophobic inner core, however the delivery ability is tapered by membrane subverting sources. However, most liposomal and SLN particles are above 90 nm in size, due to intrinsic structural parameters, which may significantly limit their delivery in ovarian tumor tissues. To surmount the setbacks associated with liposomes and solid lipid nanoparticles, other nanoparticles including solvent emulsions, polymeric nanomolecules and polymeric micelles are employed (Blanco et al., 2009).

Table 2.1: Outline of the distinguishable nanotherapeutic tools designed for ovarian cancer treatment.

Nano-systems	Polymer-drug conjugates	Dendrimers	Polymer micelles	Liposomes	Solid Lipid Nanoparticle (SLN)
Size	≤ 10 nm	2-10 nm	10-100nm	100-200nm	50-1000 nm
Structural characteristics	Macromolecular structure	Macromolecular Tree-like structure	Spherical Supramolecular Core shell structure	Spherical bilayer vesicle structure	Spherical, bilayer nanocapsular structure
Carrier composition	Water-soluble polymer	Hyperbranched polymer chains	Amphiphilic di and tri-block copolymers	Phospholipids , cholesterol membrane lipids	solid lipid emulsifier water
Drug incorporation strategy	Covalent conjugation requiring functional groups on drug and polymer	Covalent conjugation requiring functional groups on drug and polymer	Non-covalent encapsulation/ compatible with hydrophobic drugs	Non-covalent encapsulation/ compatible with hydrophilic drugs	Non-covalent encapsulation/ compatible with hydrophilic drugs
Clinical status	PEG-paclitaxel & HPMA copolymer-doxorubicin – phase II trials	Dendrimer-docetaxel & Viva gel- phase II & III trials	CRLX-101&NKTR-102- phase II/III clinical trials	SGT53-01& MCC- 46 phase I clinical trials	SLNs with [Gd-DTPA(H ₂ O)] ²⁻ and [Gd-DOTA(H ₂ O)]- compounds- preclinical trials
	SMANCS &CDP870 (Cimza)- Approved	PSMA-targeted dendrimers & Avidimer-dendrimers- Approved	Genexol- PM- Approved	Doxil, Ambisome & DaunoXome- Approved	Diazemuls & Diprivan- Approved

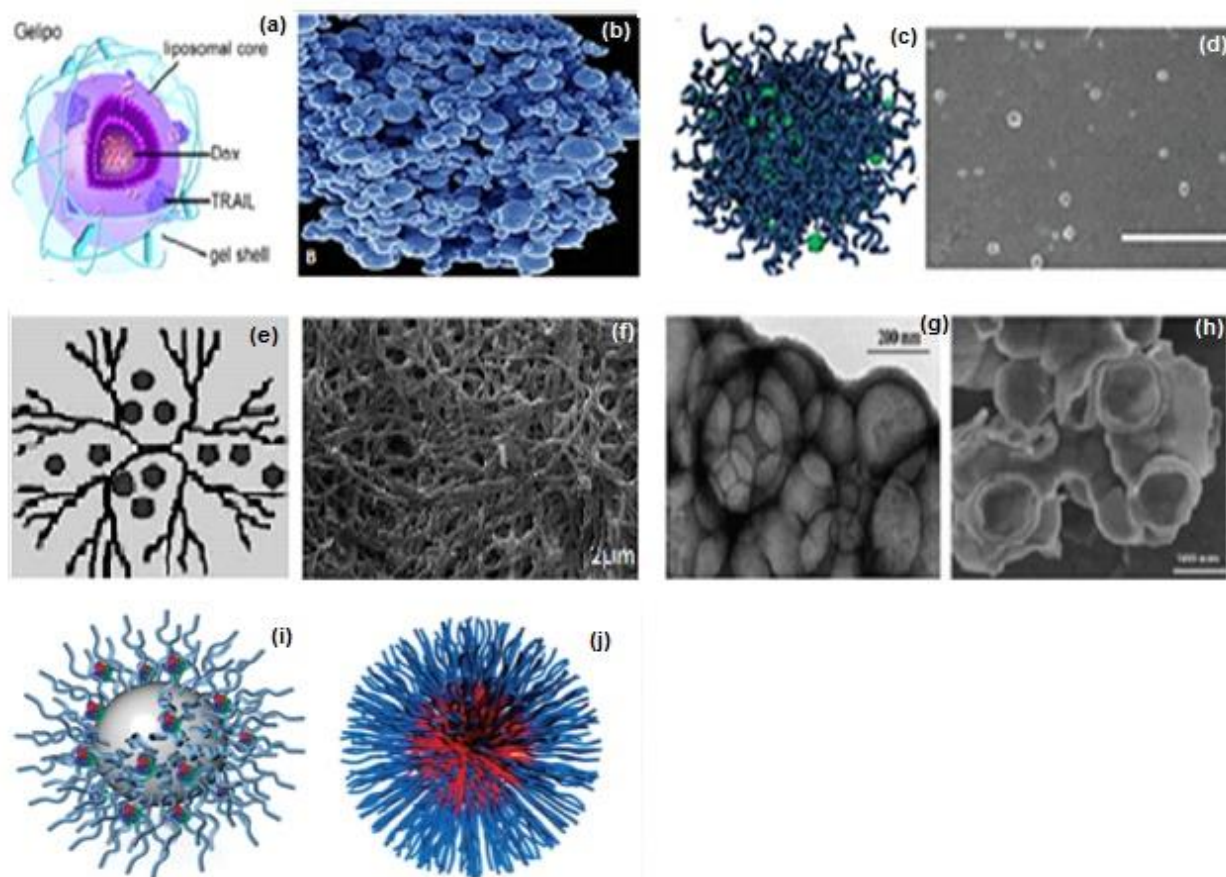


Figure 2.1: Schematic depicting examples of nano-sized delivery systems; liposomes (a-b), polymer drug conjugates (c-d), dendrimers (e-f) and solid lipid nanoparticles (g-h) and polymeric micelles (i-j) currently being exploited for transport of chemotherapeutic agents [(adapted from (a-b) (Jiang et al., 2014), (c-d) (Tong et al., 2010), (e-f) Santos et al., 2010, (g-h) Pasc et al., 2011, (i) Palivan et al., 2012; (j) Ding et al., 2015).

2.4. Micellar Morphology, Composition, and Mechanism of Formation

Micelles are spontaneously self-assembled or aggregated versatile nanoparticles formed in water at certain physico-chemical parameters including concentration (above CMC - critical micelle concentration), temperature and conductivity employing amphiphilic surfactants (hydrophilic-hydrophobic polymers) with opposite-affinities toward a particular solvent (Güney et al., 2011). The morphology of resultant micelles is produced by hydrophilic and hydrophobic constituent interaction. The copolymer chain length determines the structure of the formed micelles, with rod shaped micelles produced when the hydrophobic segment is longer than the hydrophilic segment. Spherical micelles are normally a result of a lengthier hydrophilic segment with a shorter hydrophobic segment or when these segments are of the same length (Soliman et al., 2011). Compositions of the formed polymeric micelles are normally di or tri block, or a fixed copolymer (Figure 2.2).

Poly ethylene oxide (PEO) polymers form a barrier to micelle degradation and ensuring micelle dissolvability in an aqueous medium (Wu, 2005; Rapport, 2007). The hydrophobic core usually has a biodistortable polymaterial including poly ethers, poly-(propylene oxide) (PPO) and poly-esters (β -amino ester), which can be used as reservoirs to dissolve poorly water soluble pharmaceuticals, thus protect the drugs from the aqueous environment, increasing their bioavailability and *in vivo* stability (Adams; 2003; Zana, 2005; Mourya et al., 2011).

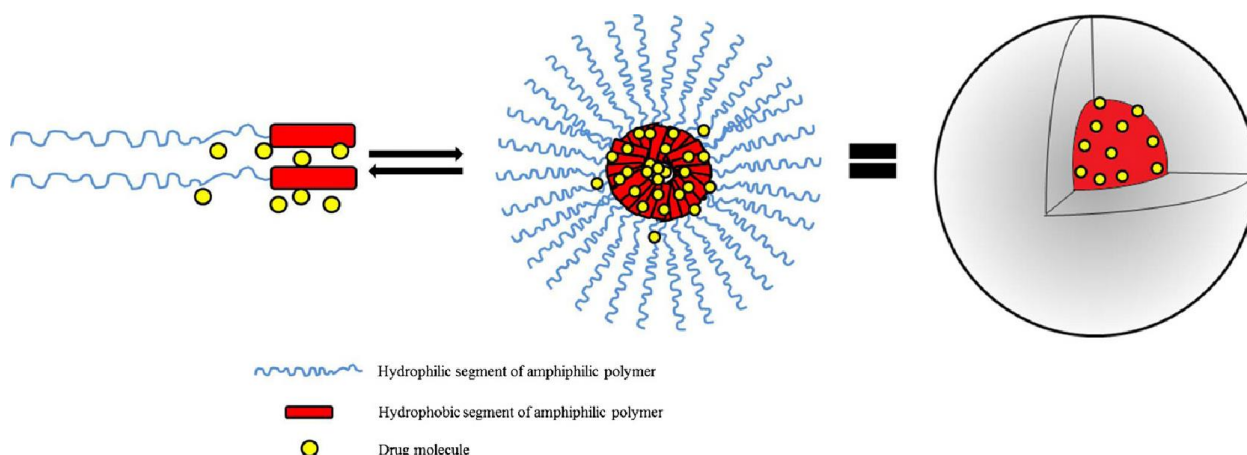


Fig 2.2: Schematic representation of the supramolecular structure of polymeric micelles (adapted from Lu and Park, 2012).

At low concentrations in aqueous media, these copolymers exist individually, but, when their molar ratio is elevated, flocculation occurs in a relatively narrow concentration range (Horacio, 2009). Flocculates are called micelles, comprised of many copolymers in a spherical configuration. The amount of copolymer required for micelle formation is termed the critical micelle concentration (CMC) and defines the thermodynamic balance of micelle; whereas the degree beneath which hydrophilic-hydrophobic nanomolecules subsist as single units and beyond as confluences is known as the decisive micellization degree (Torchiin, 2004; Wang et al., 2001). When conjugation in polymer moieties is expected, compounds such as carboxylic (COO^-) and amines (NH) are conjugated as the chain terminating groups to activate the hydroxyl ($-\text{OH}$) groups (Rapport, 2007).

2.5. Classification of Micelles

Micelles can be classified into three main distinguishable classes namely, micelles prepared from aggregation of polar and non-polar molecules in aqueous medium (amphiphilic aggregates), polyionic micelles originating from oppositely charged polymers forming an agglomeration due to electrostatic interaction, and micelles originating from metal complexation (Wang et al., 2001; Oberoi, 2012; Gaucher, 2005; Sutton, 2011).

2.5.1. Amphiphilic Micelles

Amphiphilic micelles are produced by hydrophobic interactions involving the inner matrix and the outer surface of the surfactant molecules in the dissolving medium (Adams et al., 20013). A surfactant molecule possesses an amphiphilic structure and is composed of a hydrophobic moiety and a hydrophilic moiety (Sutton, 2011). The hydrophilic groups that constitute the polar head groups are based on functional groups such as carboxyl, sulfonate, ammonium, hydroxyl and amide. Hydrophobic groups are nonpolar tails, such as hydrocarbon chains with eight or more carbon atoms, and can be linear or branched structures. Both lipophilic and hydrophilic polymers are soluble to some degree in aqueous suspension, but assemble into micelles when sufficient surfactant concentration is attained. This concentration of surfactant at which micelles are formed is called the critical micelle concentration (CMC). Figure 2.3 illustrates the situation where surfactant molecules are aligned at the air/water interface, and form micelles when submerged in a particular solvent due to the different charge attractions. The polar head forms the exterior hydrophilic surface of the micelles with the nonpolar tail forming the inner hydrophobic core.

The quantity of drug incorporated into copolymeric micelles is affected by physicochemical factors including electrostatic exchanges, and complexation between block copolymers and charged chemotherapeutic drugs. Thus, a deeper consideration of the physicochemical trends could be an invaluable tool in the synthesis of drug loaded copolymeric micelles. The basic amphiphilic segment copolymer, Pluronic®, produces micelles in response to electrostatic exchanges (Bronstein et al., 2000; Wang et al., 2012).

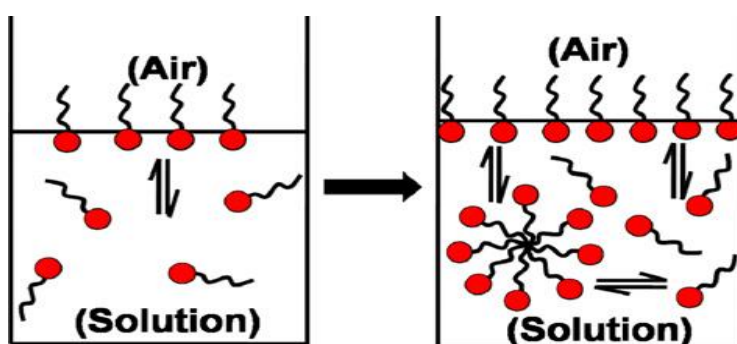


Figure 2.3: Scheme of surfactant molecules aligning on water/air interface at pre and post 'CMC' point (adapted from Mukherjee et al., 2013).

2.5.2. Polycharged Composite Micelles

Polycharged complex micelles (PCCMs) originate from assembly of charged polymers of opposite polarity to form an aggregate that is distributed in aqueous suspension by a nonionic hydrophilic head group, commonly poly (ethylene glycol) (PEG), covalently attached on one of the two charged polymers. Electrostatic interactions are the intermolecular cohesive force of the assembled composite; with both electrostatic and hydrophobic interactions utilized in the formed micelle complexes. PCCMs have some peculiar procedures such as simple synthetic method, spontaneous self-assembly or aggregation in aqueous milieu, physical stability, elevated treatment entrapment efficiency, and extended flow in the blood stream. PCCMs are formed by segment copolymers in water exclusive of any organic solutions, hence avoiding the related toxicity produced by the remaining organic solution. These micelles are very constant, having low decisive micelle intensity values compared with amphiphilic micelles, as low as 10^{-6} M. The central portion of the PCCMs can encapsulate several therapeutics including water soluble and insoluble drugs employing intermolecular cohesive force and hydrogen linkage interactions. Therapeutics such as cisplatin and ionic large-scale drugs are released from PCCMs following inducement by appropriate stimuli (Bayó-Puxan et al., 2011).

2.5.3. Non-covalently Connected Polymeric Micelles

These micelles are prepared without using a segment-copolymer approach employing homo polymeric material, co-polymers, or monomer units with covalent bonding used as the cohesive force of micelle agglomeration. The inner and the outer surface are bonded at the polymer edges via precise intermolecular interactions including hydrogen-linkages or metal-binding group interactions in the assembly, and for this reason these are known as noncovalently linked micelles. Poly (4-vinylpyridine) functionalized with carboxyl terminated polybutadiene has been used as the mainstay of intermolecular interaction owing to hydrogen linkages forming in a common organic solvent such as chloroform (Wang et al., 2001).

2.6. Polymers Used in Micelle Targeted Drug Delivery for Ovarian Cancer

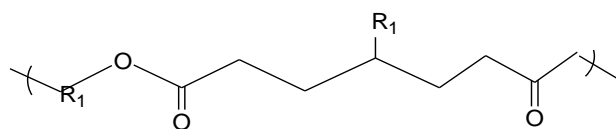
Surfactant polymers utilized for therapeutic delivery have either an ester or amino acid moiety serving as an interior core for dissolving hydrophobic chemotherapeutic drugs (Table 2.2). Furthermore, poly(lactic acid) (PLA), poly(ϵ -caprolactone) (PCL), and poly(glycolic acid) (PLGA) are all biocompatible, non toxic and biodegradable polyesters which form hydrophobic tails of micelles and are commercially approved by the FDA for biopharmaceutical applications in humans. Conversely, the soluble hydrophilic portion of the micelle generally exploited in drug release kinetics is comprised of poly (N-

isopropylacrylamide) PNIPAAm, poly (vinyl pyrrolidone) and poly (ethylene glycol). In this context, these two polymers self-arrange into surfactant micelles in aqueous suspension, with the amino or ester section molecularly uncharged or linked to inner portion groups. In addition, protein building fragment copolymers (including drug-peptide-copolymers) are now considered for improved chemotherapeutic delivery due to their enhanced accumulation at pathological sites and enhanced endocytotic uptake into the tumor cells. Modification of a specific section of the amino acid sequence alters their enzymatic distortion and level of immune response. Furthermore, ether moieties such as segment copolymer of pluronics represent a new group of biomaterials that can be exploited in synthesis of micelles for chemotherapeutic delivery (Gaucher et al., 2005).

Table 2.2: Building block sections of copolymers employed in micelle drug transport nanosystems (adapted from Sutton et al., 2007).

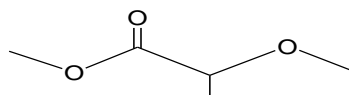
Copolymers	Abbreviation	Repeating Unit Structure
Corona segment		
Poly (ethylene glycol)	PEG, PEO	
Poly (N-vinyl pyrrolidone)	PVP	
Poly (N-isopropylacrylamide)	PNIPAAM, NIPAM	
Poly (N-vinyl alcohol)	PVA	
Poly (N-(2-hydroxypropyl methacryamide)	pHPMAm	
Core segment		
Polyesters		
Poly (propylene oxide)	PPO	
Poly esters		
Poly(L-lactide)		
Poly (D,L- lactide)	PLA,PDLLA*	
Poly (lactide-co -glycolide)	PLGA	
Poly (ε-caprolactone)	PCL	

Poly (β -amino ester)



Poly (lactic acid)

PLA



2.7. Preparation of Drug-loaded Micelles in Ovarian Cancer

Preparation of therapeutic-loaded micelles involves two major categories of therapeutic loading reliant on physicochemical characteristics of segment copolymer (Figure 2.3) (Kedar et al., 2010). The first method, dissolution, entails suspension of the segment copolymer together with the drug in aqueous medium. This method is commonly used for comparatively hydrophobic polymers, including poloxamers, and may necessitate heating of the aqueous medium for micelle aggregation to occur utilizing dehydrated core profiling portion. This dissolution technique is also employed in the preparation of PCCMs, with therapeutic and polymer suspended separately in aqueous solution. Micelle aggregation is impelled by mixing the two suspensions to balance therapeutic–polymer ionic proportions (Torchilin, 2001; Tyrrell, 2012). The drawback of this technique is that low drug quantities are loaded in the formed micelles, and this has been shown by surfactant segment polymers with drug that aggregate in aqueous suspension producing micelles with low drug quantities (Jones, 1999; Adams, 2003).

The second method of therapeutic loading involves surfactant polymers which are partially water-soluble and for which an organic suspension communal to both the polymer and the therapeutic (including tert-butanol, methanol, ethyl acetic acid, toluene, dichloromethane (DCM), diethyl ether, chloroform) is required (Goa et al., 2013). The manner by which micelle aggregation is triggered is reliant on the solvent-extraction technique. For water-miscible organic solutions, copolymer preparations can be extracted with water via dialysis exchange method, whereby sluggish extraction of the organic portion activates micelle aggregation. The drawback of the dialysis exchange method is that drug-polymer emulsification involving usage of chlorinated solution is toxic and the dialysis exchange method frequently needs extra time (< 36 hrs) for proficient packaging of the drugs into the micelles. Alternatively, the solvent-evaporation technique can be utilized and this involves removal of organic solution by air diffusion to produce a polymeric thin layer composed of polymer and a drug. Addition of water

to the thin layer with heating of the aqueous suspension facilitates the production of drug-loaded micelles. Micelles formed from solution-removal technique have enhanced potential to dissolve greater quantities of partially water-soluble therapeutics. In addition, therapeutic-loaded micelles may also be formed by oil-in-water (O/W) suspension technique exploiting a non-aqueous miscible organic solution (viz., diethyl ether, chloroform, N, N-dimethylformamide (DMF), acetonitrile, THF). The aforementioned methods all necessitate sterilization and freeze-drying stabilization processes for preservation of the prepared injectable (parenteral) formulations. Fig. 2.4 below depicts the drug loading techniques that may be employed.

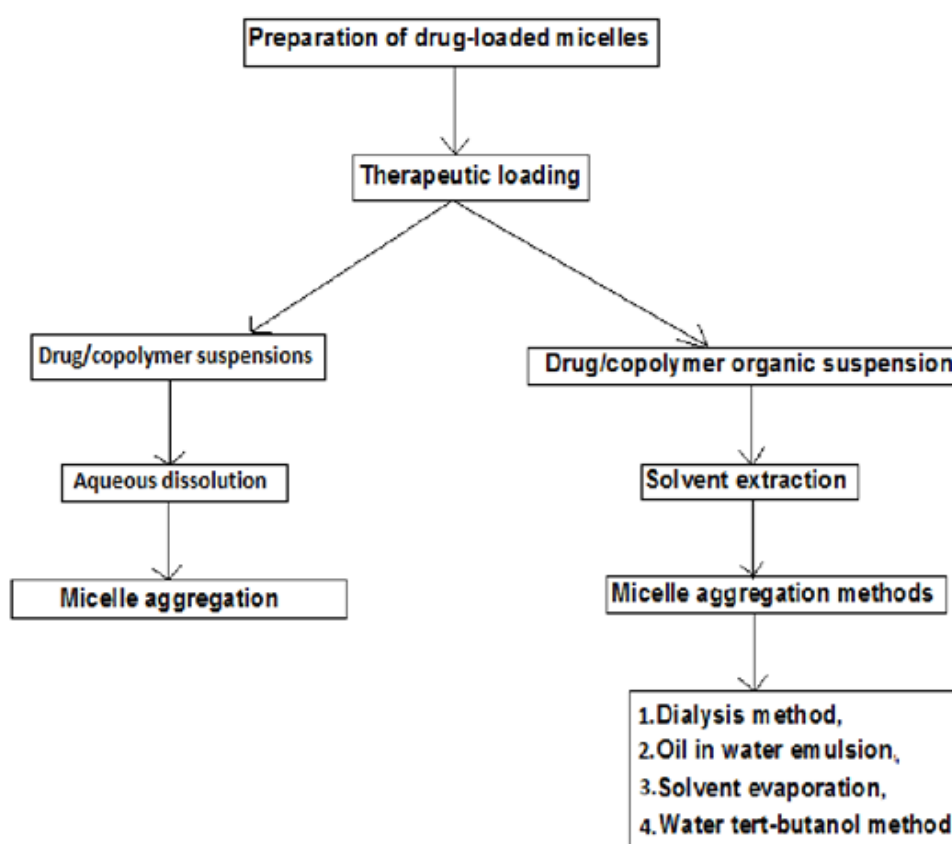


Figure 2.4: Main methods of drug loaded micelle preparation from copolymers.

The above stated confines in preparations of therapeutic-loaded micelles can be surmounted by exploitation of improved strategies including single-step method which involves the suspension of both the copolymer and the therapeutic in a water/tert-butanol (TBA) medium with lyophilization to produce a lyophilized powdered cake. Stable drug-loaded micelles spontaneously self-aggregate upon reorganization of the lyophilized powdered polymer–therapeutic cake in aqueous medium (Fournier et al., 2004; Le Garrec et al., 2004; Gaucher et al., 2005).

2.8. Applications of Micelles in Ovarian Cancer

Micelles are considered as prospective drug carriers for chemotherapeutics due to their prolonged blood circulation times, retained drug stability, and specific targeting of proliferating tumor tissue. Micelles can be employed as multifunctional nanocarriers of molecular imaging probes for identification (diagnosis), noninvasive screening and treatment of early ovarian cancer (Jones, 1999).

2.8.1. Diagnosis of Ovarian Cancer Employing Micelles

Ovarian carcinoma is usually detected in advanced stages (International Federation of Gynecology and Obstetrics (FIGO) stage III–IV) due to the comparative lack of sure recognition and indicative medical symptoms in initial periods, shared with absence of early diagnostic methods (Zhang et al., 2008). The transport and management of the release of drug for site-specific chemotherapy and imaging indicative tools for early cancer detection are of great pertinence (Cheng et al., 2010; Chithrani et al., 2010). Imaging entails visualization of ovarian cancer disease progression, determination of the activity and biodistribution of a drug to tumor tissue or determination of molecular bio-indicators of the disease (Liu et al., 2008). Disease monitoring and screening of therapeutic efficacy can be accomplished by using modern clinical imaging modalities including basic radiography, anatomical scanning probes (CT scanning), ultrasound and magnetic resonance imaging (MRI) (Torchilin, 1999). These imaging techniques can be categorized according to the energy utilized to develop visual images (heterogeneous X-ray beams, positron emissions, photon emissions), spatial specific resolution accomplished (macroscopic-, meso-scale, microscopic), or the nature of the captured information (anatomical, physiological or molecular/cellular imaging) (Torchilin, 2000; Zhang et al., 2008). However, these imaging techniques rely on diagnosis of cancer when tumors have developed to approximately 1 cm³ size and at this stage the malignancy has around 1 billion metastatic tumor cells (Choi et al., 2010). Furthermore, their low signal transmission, instability, imprecise interactions, and rapid degradation from the circulatory system have resulted in the invention of advanced molecular imaging probes (Stimpf, 1999).

Nanotherapeutic applications incorporating non-invasive tumor molecular imaging have the prospect to achieve early diagnosis, increasing the accuracy, efficiency of chemotherapy, and enabling improved disease outcomes (Zhang et al., 2008). If distinguishing imaging modalities are used to visualize tumors; improved tumor resolution can be obtained with contrast agent nanocarrier systems than with conventional image diagnosis of tumors. Nanoparticles have methods for molecular targeted deposition, drug triggering, or improvement of pathological

areal imaging. Polymeric nanoparticles such as poly(ethylene glycol)-b-poly(Lysine) copolymer micelles have great potential in diagnostic molecular imaging and monitoring of cancer development or regression (Zhang et al., 2008). Tiny particles within the nanometer range, for instance gold-based particles and functionalized metallic quantum particles are the most commonly utilized, however additional nanomaterials for exploitation at nanometer level plus bio-indicators also display potential as powerful tools for possible transmission improvement and medicinal involvement in nanodiagnosis of diseased locations.⁴³ Various one-off administered micelle-based therapeutic delivery systems for tracking and targeting of ovarian cancer are concisely outlined in Table 2.3.

Table 2.3: Polymeric Nanomicellar systems employed for treatment and diagnosis purposes (adapted from (Kedar et al., 2001; Chen et al., 2014).

Polymer structural formula	Method of synthesis	Method of micellization	Delivered Agent	Mode of delivery
PLGA-b-PPO-b-PLGA and PEG-b-PPO	Ring-opening polymerization	Dialysis method	Doxorubicin (DD)	P
Poly(ϵ -caprolactone)-b-PEO	Anionic ring opening polymerization	Dialysis method	Pyrene (hydrophobic fluorescent probe) (DA)	P
Poly(lactic acid)-polyurethane	Step condensation	Microphase separation method	Gliclazide (DD)	P
PMP C-b-PBMA	RAFT technology	Self-emulsion evaporation method	Paclitaxel (DD)	P
Poly(ethylene glycol-b-lactide)	Anionic ring opening polymerization	Oil-in-water emulsion method	Taxol (DD)	P
Poly(lactide-b-PEG)	Solvent polymerization	Self-emulsion solvent evaporation method	Paclitaxel (DD)	P
mPEG-b-p(HEMAM-Lac _n)	Free-radical polymerization	Rapid heating procedure	Pyrene (DA)	P
?-Benzyl L-glutamate N-Carboxyanhydride	Polymerization	Dialysis	Adriamycin (DD)	P
Acetal-PEG-b-PLA	Ring-opening polymerization	Dialysis method	Docetaxel, I (DD), (DA)	Tyrosine-A, tyrosyl-glutamic acid-A
COOH-PEG-b-PLGA	Polymerization	Dialysis method	Docetaxel, paclitaxel (DD)	RNA aptamer-A DNA aptamer - A
PEG-b-PCL	Free-radical polymerization	Dialysis method	Paclitaxel, rapamycin (DD)	Folate- A
PEG-b-PLLA and P(HEMA)-b-p(His)	Solvent polymerization	Dialysis method	Doxorubicin (DD)	-
P(HEMA)-b-p(His)	Solvent polymerization	Dialysis method	Doxorubicin(DD)	Folate- A
PEG-b-PLA and HEMA-co-his-g-PLA	Anionic ring opening polymerization	Oil-in-water emulsion method	Doxorubicin, Cy 5.5 (DD), (DA)	Folate- A
PEG-b-PLA and P(NVI-co-NVP)-g-PLA	Anionic ring opening polymerization	Oil-in-water emulsion method	Doxorubicin, I (DD), DA	Folate- A
mPEG-b-PLA and P(NIPAAm-co-MAAc)-g-	Solvent polymerization	Self-emulsion solvent evaporation method	Doxorubicin, FITC (DD), DA	Galactosamine- A

Abbreviations: DD (Drug Delivered), DA (Diagnostic Agent), P (Passive targeting), A (Active targeting), mPEG-b- p (HEMAM-Lac_n), methoxy poly (ethylene glycol)-b-poly (N-(2 hydroxyethyl) methacrylamide)-oligolactates: PMPC, poly (2-methacryloxyethyl) phosphorylcholine; ?-Y, RAFT, reversible addition-fragmentation chain transfer.

A number of nanomicellar designs have been developed and are presently undergoing extensive preclinical and clinical trials for application in chemotherapeutics and diagnostic imaging of ovarian cancer. Hydrophilic-hydrophobic segment copolymers that self-aggregate to produce double-coated micelles are prospective transporters of partial dissolving treatments and diagnostic tools. Partially water-soluble therapeutics or diagnostic tools can

be incorporated into the interior matrix or hydrophilic exterior of micelles to generate a balanced distribution in aqueous medium. Micelles can be used as transporters for the distribution and slow release of imaging agents and drugs (Chithrani et al., 2010).

Diagnostic modalities for three main imaging probes are ring clustered radioactive metals for example indium-111 (^{111}In) or technetium-99m ($^{99\text{m}}\text{Tc}$), used for scintigraphy; clustered/chelated magnetic metals including Gold for magnetic resonance imaging (MRI); and iodine for conventional X-ray computed tomography (CT). The conventional contrast agents employed in medical therapeutics are low-molecular weight complexes composed of these chemical probes. Several diagnostically significant amphiphilic composites have been effectively integrated into micelles including diethylenetriaminepentaacetic acid (DTPA) moieties, which are the most accepted chelating media for diagnostic imaging. Various nanomicellar platforms have been developed for utilization in MR diagnostic imaging. Polymeric micelle systems including iodine-containing PLL-PEG micelles are employed for cancer diagnostic imaging utilizing conventional computed tomography (CT) and single-photon emission computed tomography (SPECT). Furthermore, to monitor micelles formulations and exchanges with the cancer disease, micelle co-encapsulated with imaging clustered/chelated metallic group have been employed, for example gold compounds, manganese oxide loaded nanoparticles have been utilized with ultrasound (US) and magnetic resonance imaging (MRI) (Parveen, 2012). Currently, gadolinium (Gd)-contrast medium including Magnevist®) are medically employed where visual contrast is elevated by limiting the T1 reduction period (period of high longitudinal magnetization with brighter image) of aqueous protons. Integration of Gd compound on the micelles' surface can successfully upsurge the T1 reductivity and reactivity of diagnosis. The reactivity is further improved by utilization of various iron oxide nanoparticles (Superparamagnetic iron oxide nanoparticles-SPIONS) that congregate in micelle inner core and display MRI reactivity at nanomolar rate. Micellar transport of both treatment and imaging agents including Rhodamine and FITC is of valuable significance as it permits imaging of the precise area of the treatment release inside the tumor tissue with distinctive structural visualization. Therefore, polymeric micelles are favorable as a carrier for combined diagnosis and therapeutic systems (Shaw., 2004; Feki et al., 2009; Fritsche and Bast, 1998).

2.8.2. Treatment of Ovarian Cancer using Micelles

2.8.2.1 Delivery Routes of Micelles

Commonly, micelles have been formulated for intravenous (IV) systemic application of chemotherapeutics but face many challenges of the blood circulatory system resulting in exposure of normal cells to drug before reaching their specific site of action in the peritoneal cavity (Torchilin, 2010). The peritoneal cavity is the principal site of disease in ovarian cancer (Gabizon, 1995). Primary ovarian tumors disseminate malignant cells throughout the peritoneum resulting in a focal origin of recurrent metastatic disease, which is responsible for high mortality rate from ovarian carcinoma (Mahmud et al., 2007). Therefore, intraperitoneal (IP) chemotherapy employing micelles can also be used to treat ovarian carcinoma. This inventive chemotherapeutic approach transports the chemotherapeutic loads directly to the peritoneal region, destroying malignant cells and also reducing drug interaction with normal cells. Clinical research findings have proven that IP chemo-treatment improves the health of women suffering from ovarian disease in contrast to intravenous (IV) chemo-treatment (Dayananda et al., 2007; Xiong et al., 2007; Madaswamy, 2009).

2.8.3. Targeting strategies for micelles

Selective delivery of nanosize sustained release polymeric micelles loaded with drugs is a prospective significant chemotherapeutic approach with distinct treatment advantages that are also applicable for advanced therapeutic extended systemic drug delivery (Musacchio et al., 2009). Targeting is commonly attained as a result of two transport mechanisms as shown in Figure 2.5; (i) passive reactive targeting using the improved porosity and absorbency influence (Roesler, 2001) (ii) active targeting by attachment of precise moieties to the micelle periphery including linking individual antibodies to the micelle exterior surface, i.e. dynamic/active treatment by means of antibody-bonded micelles (Wang et al., 2001).

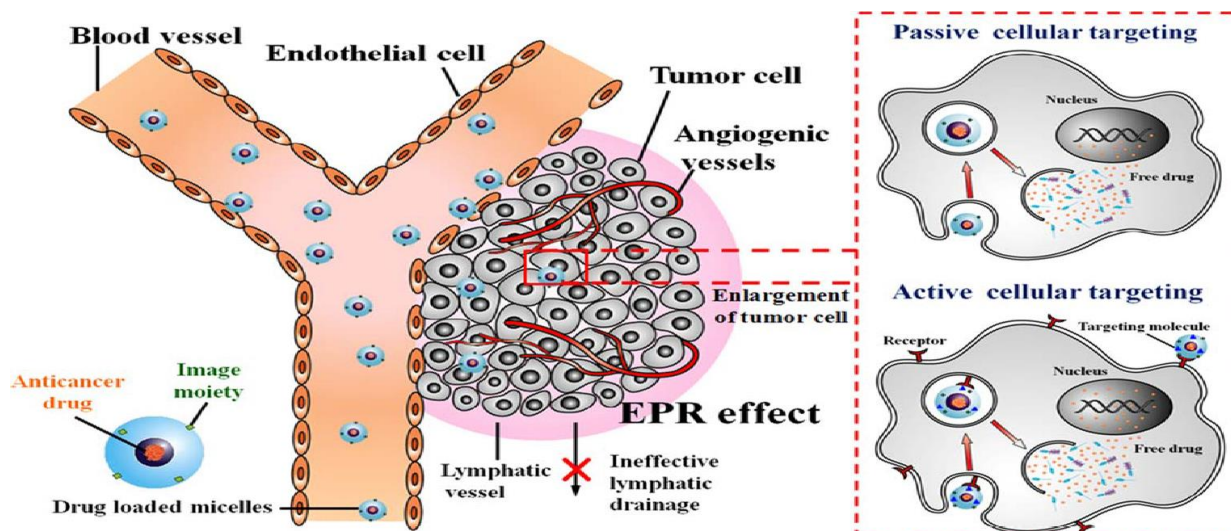


Figure 2.5: Schematic illustration of drug loaded micelles (spheres) with imaging agent delivery from injection location to tumor tissue. After administration, micelles (10–200 nm) display specific targeting of tumor growth and the nanomaterial collects at the solid cancer site due to the tumor vessels and passage through reticular endothelial system. Passive targeting is attained by cellular endocytotic uptake from exterior fluid to the cancer cells. Active targeting can be attained by attachment of antibody ligand molecule to the exterior of micelles that encourage site-precise detection and attachment (Adapted from Chen et al., 2014).

2.8.3.1. Passive/Reactive targeting via improved permeability of tumor blood vessels

When micelles without ligand functionalization have a significant continual blood circulation period, and successfully accumulate in tumors through the enhanced permeability retention (EPR) effect, this phenomenon is known as passive targeting (Parveen, 2012). The therapeutic payload is exposed into the tumor extracellular matrix and distributed through the tumor cells and tissue. Passive targeting is also attributed to pathophysiological characteristics of solid tumors that are not observed in normal tissue. These characteristics include defective tumor blood vessel architecture (often termed “leaky vasculature”), defective lymphatic drainage system, and increased production of permeability mediators (Kabanov and Alakhov, 1997; Jule et al., 2003; Mall, 2008; Solaro et al., 2010). Several passive/reactive targeting nanocarriers have a PEG coating for stealth and “concealment” properties. These include among others Genexol-PM, SP1049C, NK911, Opaxio™ (formerly Xyotax™), CRLX101, ProLindac™, SPI-77 and CPT-11 (Parveen, 2012).

2.8.3.2. Active targeting with ligand/antigen pairs

The active targeting approach involves the attachment of functional ligands to the micelle shell that identify tumor-specific receptors over-expressed on the cancer cell plasma membranes, resulting in increased uptake and increased internalization into tumor tissue via the receptor-mediated endocytosis process (Dash et al., 2000; Kaneko, 2003; Park et al., 2005). Commonly

utilized affinity ligands are classified into the following categories: small unrefined molecules, nucleotides (RGD sequence), oligopeptides, sugar groups, proteins, folates, monoclonal antibodies (mAb), and nucleic DNA/RNA aptamers (Kobayashi, 1993). Targeting the polymer micelles to a tumor cell is necessary in drug delivery in order to kill the cancerous cells without damaging normal cells. There are many technologies that are being used to target molecules to tumor cells. The application of a functionalizing group is a dynamic approach that is dependent on accurate connections at attachment location; these exchanges incorporate immunoglobins (antibody), antigens and functionalizing group connections (Figure 2.6). The “magic bullet” Ehrlich hypothesized of antibody-functionalized nanocarriers has advanced into a system with three components: a drug, a copolymer and functionalizing group connected as one formulation. This targeting treatment approach offer noticeable rewards for example high target specificity for the pathological/infected area and minimal toxicity to the healthy cells. The afore-mentioned approach also increases malignancy treatment, particularly for the treatment of metastatic carcinoma or premature carcinoma, when the papillary tubes are still immature. Targeting ligands should have a high specific affinity for the target antigen, have declined immunogenicity *in vivo*, and be efficiently cellular uptaken/internalized after attaching to specific antigen. The transport of treatment via dynamically accurate prolonged circulating micelles shows potential as an approach to advance its site specific action (Dash et al., 2000; Kaneko, 2003; Park et al., 2005).

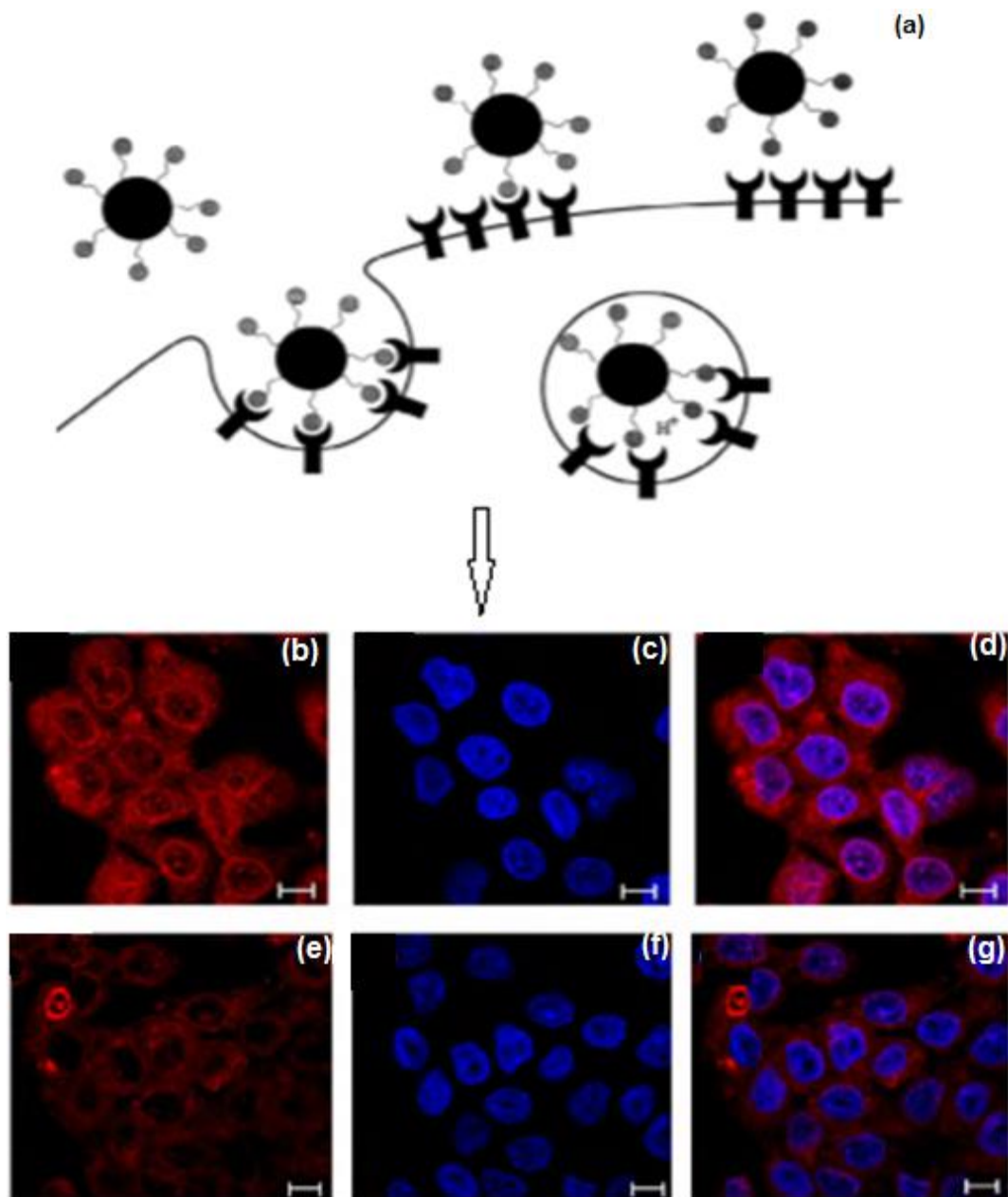


Figure 2.6: Schematic depicting (a) active targeting, (b-g) confocal images of A431 cellular uptake incubated with cetuximab encapsulated micelles and lysotracker. The fluorescence intensity of A431 cells (b-d) treated with targeting micelles was 1.45 times higher than in cells incubated with antibody-free micelles (e-g) (Adapted from (Zhou et al., 2013; Zhu et al., 2013).

2.9. Mucins as Targets for Antibodies in Cancer Chemotherapeutics

Most ovarian carcinomas are of epithelial origin and express mucins, which may be utilized as prospective diagnostic/indicative and treatment targets. Mucins are large extracellular, heavily glycosylated proteins found in the mucus layer and their unusual production has been associated with pathology of different types of malignant diseases, such as ovarian carcinoma. Presently, there are 20 identified mucins which have two classifications: discharged epithelial mucins (gelating: MUC2, MUC5AC, MUC5B, MUC6, and non-gelating: MUC7, MUC8, and

MUC11); and film attached mucins (MUC1, MUC3, MUC4, MUC9, MUC10, MUC12, MUC13, MUC16, MUC17, MUC18 and MUC20) (Bast et al., 1983; Kobayashi, 1993; Mura et al., 2013). Various research studies on the production of mucin antigen in ovarian cancer have identified overproduction of film attached mucins especially MUC4, MUC5AC, and MUC16 but their biological applications are not evidently defined. The role of MUC1, MUC2, MUC3, MUC4 and MUC5AC and MUC13 has not been extensively studied in epithelial ovarian cancer development compared to MUC16. MUC16 (also known as CA125) is employed as a clinical biomarker in ovarian cancer due to its high expression in ovarian carcinomas and that it is shed into the serum (Oerlemans et al., 2010; Preetham and Satish, 2011; Chen et al., 2011). It is a very large cell surface mucin and was first identified in 1981 by Robert Knapp, who detected this glycoprotein using monoclonal antibody (OC125) (Biswas et al., 2013). Serum levels of CA125 are utilized to clinically diagnose OC patients and those with residual infection following primary chemotherapy to evaluate the clinical progression of the infection. Alterations in blood plasma MUC16 quantities are indicative of advancing or declining cancer carcinoma in above 90% of cases (Cho et al., 2013). Additionally, unusual mucin production can cause an immune response and possibly activate strong antibody reaction. The antibody reaction is indicative of disease manifestation. Antibodies aligned with mucins can have prospective use in advancing the identification and treatment of ovarian malignancy, but there is little existing literature addressing this subject matter, thus further research is necessary. The latest research findings confirmed the existence of MUC1 antibodies in extracted blood plasma analysis that showed reverse correlation with the possibility of ovarian carcinoma (Rivory, 1995).

2.10. Stimulus-responsive Micelles

Stimuli responsive micelles (SRN) are smart nanoparticles mechanically engineered to react to internal intrinsic or external extrinsic stimuli of bodily, chemical or bio-compound origin to accomplish curtailed and sequential release of drug payloads at the precise site and duration. SRN deliver drug payloads by going through structural alterations in reaction to the triggering stimulus. The reaction may lead to degradation/disruption, polymerization or assembly of micelles. The common internal stimuli in a cancer microenvironment comprise of an acidic pH, the electrochemical redox potentials of the unit cell, and the availability of certain over-produced matrix enzymes; whereas the external stimuli comprise of temperature, attraction via magnetic field, light illumination (UV, infrared or visible) and ultrasound waves (Mall, 2008). In this context, the preparation of micelle susceptible to external or internal stimuli may symbolize an alternative approach to targeted therapeutic release. However, even though *in vitro* models have provided evidence of success for a number of stimuli-responsive

approaches, only a small proportion have been confirmed in animal preclinical prototypes, and also few (thermosensitive liposomes and iron oxide nanoparticles) are at the clinical stage of investigation (Xuan, 2006).

2.11. Micelles in Clinical Evaluation

A number of drug-incorporated polymeric micelles intended for chemotherapeutic treatment are under evaluation in preclinical research for evaluation of their toxicity and bioavailability (Chen et al., 2014). Some examples of polymeric micelles quoted are for other type of cancers but can also be utilized for OC treatment. Preclinical evaluations and findings have discovered many positive results of employing micelles as therapeutic delivery means for transport of hydrophobic cancer drugs (Sumer and Gao, 2008). Numerous micellar nanoformulations are under clinical evaluations, all being stealth micelle preparations, specifically, they have an exterior PEG coating for stabilization to ensure a dense conformational cloud on the exterior and protection against opsonization by plasma proteins (Table 2.4) (Chen et al., 2014). Genexol-PM is a paclitaxel-incorporated PEG-PLA micelle formulation (Sutton et al., 2007). NK012 is a synthetic micellar nanoformulation also composed of a PEG polymer coating with polyglutamate (PGlu) coupled with 7-ethyl-10-hydroxy-camptothecin (SN-38) (Chen et al., 2014). The PGlu portion is core-hydrophobically dissolved to induce micelle aggregation. Preclinical animal trials with NK012 formulations proved potent anticancer performance in mice. Recently, the success and suitability of NK012 formulations were investigated in phase II trials in breast tumor cases (Chen et al., 2014). Innovative PTX clinical formulations are being evaluated, including the NK105 nanomicellar formulation that is composed of PEG and transformed polyaspartate as the hydrophobic portion (Chen et al., 2014). PTX is indeed encapsulated in the central core segment by hydrophobic associations with the hydrophobic portion. Furthermore, a major decline in toxicity, originating from Cremophor EL plus ethanol following standard PTX dosage, was observed with NK105 formulations. During phase I trials with NK105, slight allergic responses were observed in cases with pancreatic, bile duct, gastric, and colonic carcinomas in contrast to standard PTX therapy (Chen et al., 2014).

Table 2.4: Polymeric micelle-based formulations containing chemotherapeutic drugs in clinical trials.

Formulation Trade name	Incorporated Drug	Purpose	Polymer	Particle size(nm)	Drug loading (%)	Phase
Genexol-PM	Paclitaxel	Solubilization	Mpeg-PDLLA	< 50	16.7	III,IV
NK-105	Paclitaxel	Targeting	PEG-P(Asp)	85	23.0	II,III
SP-1049C	Doxorubicin	Anti-MDR effect	Pluronic L61,F127	30	8.2	I,II,III
DTXL-TNP	Doxorubicin	Targeting	PLA-PEG, PLA-PEG-ACUPA	100	10	I
NC-6004	Cisplatin	Targeting	PEG-P(Glu)-Cisplatin	30	39	I,II
NC-4016	DACH-platin	Targeting	PEG-P(Glu)-DACH-platin	20-100	25	I
NK 012	SN-38	Targeting	PEG-P(Glu)-SN38	20	20.0	II
NK911	Doxorubicin	Targeting	PEG-(Asp)-Dox	40	n.a	II

A phase II trial in patients with highly advanced stomach carcinoma is in progress (Chen et al., 2014). SP1049C nanoformulation has been prepared as doxorubicin (DOX)-incorporated Pluronic micelles. In these phase II cancer pharmaceutical studies, it was also discovered that SP1049C formulations displayed superior effectiveness compared to doxorubicin in treatment of different types of cancer (Chen et al., 2014). SP1049C formulations displayed greater anticancer performance, effectiveness and an elevated AUC in cancer tissue in many *in vivo* cancer models and in doxorubicin defiant malignancies in contrast to conventional doxorubicin (Chen et al., 2014). SP1049C formulations are now evaluated in phase III in cases with spreading adenocancer of the gastrointestinal track. To decrease toxicity and increase the efficiency of cisplatin, the nanomicellar clinical formulation NC-6004 (Nanoplatin™) was invented. The NC-6004 formulation consists of PEG with poly(γ - benzyl L-glutamate)/CDDP composite. A minor phase I trial, revealed that NC-6004 formulations were accepted by cancer patients that are affected by colorectal cancer, upper esophageal carcinoma, lung cancer, (Chen et al., 2014). Genexol-PM is a nanomicellar paclitaxel nanoformulation prepared from poly ethylene glycol with polymerized lactic acid (Rhyner, 2011). Preclinical animal trials with Genexol-PM displayed a 3-fold elevation in the mean dissolution time (MTD) and a considerably amplified anticancer efficiency contrast with unconventional PTX (Chen et al., 2014).

2.12. Patents in Nanomicellar Technologies for Targeted Drug Delivery

In a patent by Kwon and colleagues (2012) the solubilization of gossypol (a yellow natural phenolic aldehyde plant pigment for inhibition of various dehydrogenase enzymes) with micelles was evaluated and the discovery presents suitable micelles packed with single or second lively bioactive. Micelles can incorporate chemotherapeutics including gossypol, and a mixture of nanodrugs. The micelle composition enable successful incorporation of insoluble drugs exclusive of a supplementary dissolving medium (Rhyner, 2011; Mukherjee et al., 2013). Thus; the invention provides stable and biocompatible drug formulations that improve bioavailability without causing toxicity. In another invention, micelles encapsulating SN-38 for the treatment of various cancers including OC are presented. According to one depiction, this invention provides a micelle comprising a multiblock copolymer having a SN-38 derivative of camptothecin encapsulated (Sudimack and Lee, 2000). This SN-38 has a competitive edge over its camptothecin derivatives in that it is not reliant on activation by the liver in animals (Table 2.5) (Sudimack and Lee, 2000; NanoCarrier Co, 2014). Yu Alakhov *et al.* (2012) presented the use of the block copolymer micelle of poly (oxyethylene)-poly(oxypropylene) in administrating an anti-neoplastic agent, providing non-covalent solubilization, which reduces water-instability. A number of these copolymers are commercially available under the generic names of "poloxamers" and "pluronic". The innovation by Perumal *et al.* (2012) includes micelle aggregates, composites having self-aggregated/assembled micelles, and techniques for synthesizing micelle aggregates and composites thereof. The nanoformulation also includes a prolamine proteins attached to a polyethylene glycol (PEG)-coated micelle. The innovation additionally includes techniques for incorporation of drugs utilizing the conjugates of the polymer protein micelle invention. In a patent by Rhyner (2008) micellar structures, methods of making micellar structures, methods of imaging, methods of delivering therapeutic agents and/or biological compounds, and the like, are provided (Pasc et al., 2011). This patent provided a therapeutic method using water-soluble, high molecular weight block polymer to enable an intraperitoneally administered anti-cancer agent to maintain long-term retention in the abdominal cavity to sufficiently exert the effect of the anti-cancer agent and reduce adverse side-effects thereof. The patent further describes a therapeutic agent-loaded micelle preparation, comprising a copolymer having an exterior hydrophilic moiety and a polycarboxylic acid derivative moiety; and an anti-cancer agent bonded to or encapsulated in the micelle, wherein the micelle preparation may have controlled drug release, and enables an extension of retention time period of the anti-cancer agent in an abdominal cavity. A superior life-prolonging effect was found in an intraperitoneal administration mouse model compared with intravenous administration.

Table 2.5: Nanomicellar patents issued in the area of cancer drug delivery (Adapted from Shared report NanoCarrier Co, 2014.

Patent type	Title	Patent no	Structural formula	Action of treatment	YEAR	Inventor/Assignee
Micelles	C6-c18-acylated derivative of hyaluronic acid	WO2014082609 A1	(HA)-[O(C=O)NH-M] _p	AC	2014	Contipro Biotech S.R.O.
Micelles	Polymer conjugated protein micelles	EP 2678001 A2	PEG-Prolamine	AC	2014	South Dakota State University
Paclitaxel Micelle (NK105)	Micellar Preparation Containing Sparingly Water-Soluble Anticancer Agent And Novel Block Copolymer	09705599.0	(poly(ethylene glycol)-copoly (L-aspartic acid))	AC	2013	Nanocarrier Co. Ltd. Nippon Kayaku Co., Ltd.
Nanoplatin® (NC-6004)	Pharmaceutical Composition and Combined Agent	098101554	(poly(ethylene glycol)-copoly (amino acid))	AC	2013	TOUDAI TLO Ltd.
DACH-Platin Micelle (NC-4016)	Coordination Compound Composed Of Diaminocyclohexane Platinum (II) And Block Copolymer And Anti-Cancer Agent Comprising The Same	2007-520209	(poly(ethylene glycol)-copoly (amino acid))	AC	2013	The University of Tokyo
Protein Micelle	Electrostatic Bonding Type Macromolecular Micelle Drug Carrier And Drug Carried Thereon	EP2583563 A1	polyethylene glycol and poly(α,β -aspartic acid)	AC	2013	TOUDAI TLO Ltd.
siRNA Micelle	Polyethylene Glycol/Polycation Block Copolymer	EP2087912 A1	PEG-PLys	AC	2013	The University of Tokyo
Sensor Linked Micelle	Active Targeting Polymer Micelle Encapsulating Drug, And Pharmaceutical Composition	2008-539901	poly(ethylene glycol)-b-poly(2-aminoethyl methacrylate)-b-poly(styrene)	AC	2013	Nanocarrier Co. Ltd.
pH-Sensitive Micelle	Novel Block Copolymer Used For Preparing Ph-Responsive Polymer Micelle, And Method For Producing Same	2009-7007877	[PEG-p(Asp-Hyd-Adr)]	AC	2013	The University of Tokyo
Docetaxel Micelle	Docetaxel Polymer Derivative, Method For Producing Same And Use Of Same	2009250393	(mPEG-PDLLA)	AC	2013	Nanocarrier Co. Ltd.
Bortezomib Micelle	Pharmaceutical composition that includes block copolymer	EP 2692777 A1	polyethylene glycol-polyglutamic acid	AC	2013	Nanocarrier Co. Ltd.

Micelles	containing boronic acid compound Micelles for the solubilization of gossypol	20120321715	Poloxamer or PEG-PCL	AC	2012	Wisconsin Alumni Research Foundation., US
----------	---	-------------	----------------------	----	------	---

Abbreviations: AC (Anticancer activity including ovarian cancer and various cancers such as lung and prostate cancer), MA Microaggregates), PEG/PEG 2000 (poly (ethylene glycol-2000), Hyaluronic acid A (hyaluric acid), C=O (carbonyl group), -Plys (polylysine), Asp (Aspartate), Hyd-Adr (hydrazone Adriamycin, poly-DL-lactide (PDLLA), PCL (polycaprolatone).

2.13. Future Recommendations

Whether micelles are employed as drug carrier nano-systems, treatment agents, or image contrast agents, will require being extensively differentiated physiochemically, nanopharmacologically, and classic immunologically prior to their approval for application in humans. Drug efficacy of most nanoformulations for anti-cancer chemotherapy has not advanced to an appropriate level to evolve the prepared nanomedicine into clinical application. Thus, great research endeavors should be dedicated at optimization of the physicochemical profile of micelles. Therapeutic combination with synergistic response against ovarian cancer will be another approach to enhance the drug efficacy. Toxicity studies will also need to be conducted in both *in-vitro* and *in-vivo* models before they can attain FDA approval for clinical evaluations.

The prime challenge is now linked with the interpretation of diverse successfully confirmed experimental inventions into clinical application. The performance of the therapeutics is restricted by their degradation, exchanges with unit cells, and incapability to permeate tissues due to their chemical character. Numerous challenges must be considered before application of micelle formulations into clinical application, including intricacies in accomplishing the optimal combination of physicochemical parameters for direct tumor targeting, effective clearance from the physiological environment, preferential therapeutic release and least/no toxicity to unit cells of organisms. Co-incorporation of two or more therapeutics in one nanocarrier system can be challenging due to different solubility of the optimal drug combination. Therapeutics activated by a positive detection of an ovarian cancer disease are in the near future.

2.14. Concluding Remarks

The novel micellar technologies developed to date are focused on enhancing the pharmacodynamics and pharmacokinetic profiles of the incorporated therapeutic agent, along with enhancing the safety and comfort of the delivery mechanism to improve the survival rate

of ovarian cancer patients. Micelles have developed as a significant therapeutic delivery system due to their smart design formulated by self-assembly or regulated accumulation in a solvent medium. Micelles can be simply loaded with a broad range of partially soluble nanomedicines, hence ensuring improved bio-availability of these drugs, including those neglected due to insolubility and toxicity challenges. Micelles' capability to incorporate a second or more additional agents including drugs and imaging modalities introduces a dual detection and delivery strategy to the fields of oncology. Polymeric multipurpose micelles have superior attributes as drug delivery nanosystems, and have shown considerable accomplishment in the scope of clinical diagnosis and chemotherapeutics. Polymeric micelles functionalized with antibody ligands facilitate specific active targeting of tumor proliferation than other nanocarrier therapeutic delivery systems, and therefore improve therapeutic outcomes in ovarian chemotherapy.

CHAPTER 3

SYNTHESIS OF NOVEL AMPHIPHILIC POLY(N-ISOPROPYLACRYLAMIDE)-B-POLY(ASPARTIC ACID) NANOMICELLES FOR POTENTIAL TARGETED CHEMOTHERAPY IN OVARIAN CANCER

3.1. Introduction

Amphiphilic copolymers have versatile properties that make them suitable for the delivery of hydrophilic and hydrophobic chemotherapeutic drugs (Qiao et al., 2010; Jin et al., 2012; Zhang et al., 2009). These copolymers may be synthesized from aqueous miscible and partially soluble polymers that agglomerate to form a myriad of structures including nanomicelles, tubular cylinders or vesicles. The inner core can be equilibrated by an outer shell-like surface that is dependent on the copolymer block size, polymer ratios, vehicle composition or external stimuli such as pH, temperature or ionic strength within the aqueous medium during synthesis (Nakayama et al., 2006; Frank et al., 2010; Topp et al., 1997). Recently, significant interest has been placed on the synthesis of stimuli-responsive polymers to form nanomicelles with modified physicochemical parameters. The most commonly used stimuli are temperature and pH that induce polymer transitions when prepared from amphiphilic surfactant copolymers for application in clinical nano-enabled chemotherapeutics (Lee et al., 1999).

Poly(N-isopropylacrylamide) (PNIPAAm) is categorized as a thermo-responsive polymer with a LCST of 32°C. Furthermore, it is aqueous-miscible at physiological temperatures lower than the LCST value. However, when the LCST is exceeded it transforms into impenetrable hydrophobic agglomerates (Eeckman et al., 2001; Zhang et al., 2001; Chung et al., 1998; Bergbreiter et al., 1998). Polyaspartic acid (PAsp) is another synthetic polymer that is of pharmaceutical significance to deliver partially soluble drugs and has been used for numerous biomedical applications such as dialysis membranes, artificial skin and orthopedic implants (Rao et al., 1993; Nita et al., 2011; Nakato et al., 1998; Wang et al., 2010; Liu et al., 2010). In particular, PAsp nanomicelles with hydrophilic segments have been explored previously as a potential drug delivery vehicle for sparingly soluble chemotherapeutic drugs commonly entrapped in hydrophobic domains (Soppimath et al., 2005; Veronese et al., 1991; Kohori et al., 1998). Combination of PNIPAAm and PAsp as an amphiphilic copolymeric nanomicelle structure may potentially enhance the bioavailability, stability, physicochemical parameters

and targeted release of chemotherapeutic drugs (Bertrand et al., 2009; Wei et al., 2006; Cheng et al., 2006).

To our knowledge, stimuli-responsive nanomicelles of PNIPAAm-b-PAsp prepared via thermal ring-cleavage polymerization for potential application as a targeted form of chemotherapy in Ovarian Cancer (OC) has not yet been explored. This is despite the fact that PNIPAAm has been widely used with other polyamino acids as a blend to produce inter-incisive polymeric networks (Malonnea et al., 2005; Bonina et al., 2004; Chung et al., 1997). Therefore this study provides an innovative approach to firstly synthesize PNIPAAm-b-PAsp employing PNIPAAm-NH₂ for copolymerization onto PAsp. This novel copolymer was subsequently used as a framework for the preparation of drug-loaded nanomicelles as a targeted form of chemotherapy in OC. Special interest was placed on the nanomicelle properties as well as their drug encapsulation efficiency and pharmaceutical stability.

3.2. Materials and Methods

3.2.1 Materials

Poly(N-isopropylacrylamide) (PNIPAAm) was purchased from Sigma Aldrich (St. Louis, MO, USA) that was hexane recrystallized, vacuum dried at 20°C and the 2,2'-azoisobutyronitrile (AIBN) initiator agent was ethanol-recrystallized prior to use. Aspartic acid, 2-amino ethanethiol hydrochloride (AET-HCl) and triphosgene were procured from Sigma Aldrich (St. Louis, MO, USA) and vacuum dried at 20°C. N,N'-dimethylformamide (DMF) (98%), tetrahydrofuran (THF), ethyl ether and petroleum ether (30-60°C) was purchased from Merck Chemicals Co. (Pty) Ltd. (Darmstadt, Germany) and were used as received. All other reagents and organic solvents were of analytical grade and vacuum dried prior to use.

3.2.2. Synthesis of amino poly (N- isopropylacrylamide) (PNIPAAm-NH₂)

PNIPAAm-NH₂ was synthesized by radical polymerization employing a chain transfer agent 2-amino ethanethiol HCl (AET-HCl) and an initiating agent AIBN. N-isopropylacrylamide (4×10^{-3} mol), AIBN (0.8×10^{-5} mol) and AET-HCl (0.6×10^{-4} mol) were dissolved in 10 mL DMF. The mixture was degassed by purging with N₂ for 1 hour and then refluxed at 70°C for 10 hours. Following the polymerization reaction, the solution was concentrated by condensed pressure distillation to evaporate the DMF. The yield was precipitated by introduction of diethyl ether followed by vacuum drying. Excess triethanolamine (TEA) in THF was added drop-wise to this polymer mixture at 20°C to convert PNIPAAm-NH₂-HCl into PNIPAAm-NH₂. The

resultant polymer was further purified by precipitation in excess diethyl ether followed by filtration with a 0.22 μ m filter membrane and finally the yield was vacuum dried at 30°C.

3.2.3. Synthesis of L-aspartic acid-N-carboxyanhydride using a triphosgene approach

A triphosgene approach was employed to synthesize L-Asp-NCA. Briefly, 11g of excess triphosgene was introduced into a 7% aspartic acid tetrahydrofuran solution at 50°C. In order to remove the phosgene gas, the solution was bubbled with N₂ for 30 minutes until the solution increased in clarity. L-Asp-NCA precipitated after the introduction of the solution into excess petroleum ether (30-60°C) and finally the yield was vacuum dried at 30°C.

3.2.4. Synthesis of the amphiphilic poly-N-isopropylacrylamide-b-polyaspartic acid copolymer

The 8.9mg PNIPAAm-b-PAsp copolymer was synthesized by ring-cleavage polymerization of L-Asp-NCA. The reaction scheme is shown in Scheme 1(A-D). PNIPAAm-NH₂ was suspended in DMF and the reaction mixture was degassed by purging with N₂ for 30 minutes followed by introduction of L-Asp-NCA. All reactions were conducted at 20°C for 72 hours. The resultant copolymer was purified by precipitation of excess diethyl and finally the yield was vacuum dried at 30°C.

3.2.5. Establishment of the copolymer molecular mass

The mean molecular mass of the synthesized copolymer in aqueous solution was determined utilizing the partially-proportional Mark-Houwink relationship (Equation 3.1) that correlated the inherent/intrinsic viscosity [η] with the molar mass (M).

$$[\eta] = KM^a \quad (3.1)$$

Where, 'a' is a specific solvent-polymer interaction parameter and 'K' is an empirical proportionality constant. Solvents with value of 'a'=0.5 is suggestive of a theta solvent. A value of 'a'=0.8 represents an ideal solvent. Flexible polymers have values between 0.5 \leq a \leq 0.8 and partially-flexible polymers the value of 'a' \geq 0.8. In this study, water was utilized as the preferred solvent which interacted with the biopolymer sequence hence displaying an elastically expandable molecular arrangement with an 'a' value of 0.8 and an empirical proportionality 'K' value of 6.31 \times 10⁻⁵. Viscosity evaluation of 0.01%, 0.001% and 0.0001% concentrations of aqueous suspensions of the synthesized copolymer were undertaken on a Haake Modular

Advanced Rheometer System (MARS) with the mean viscosity of the dilutions evaluated and used to compute the mean molecular mass of the copolymer.

3.2.6. Establishment of the nanomicellization process

MTX-loaded nanomicelles were synthesized by a dialysis tubing technique (Qiao et al., 2010). Briefly, 10mg of PNIPAAm-b-PAsp and 7mg MTX were suspended in 4mL DMF and added into a dialysis membrane (molecular weight cut-off: 3500kDa) and dialyzed against 2L of deionized water that was altered every 3 hours in a 24 hour cycle. The solution was then filtered through a 0.45 μ m filter to remove any agglomerates and subsequently lyophilized at -80°C on a lyophilizer machine (FreeZone[®] 2.5, Labconco[®], Kansas City, MS, USA) to yield a powder.

3.2.7. Micelle size and stability determination

Micelle size, zeta-potential and polydispersity index (PDI) were determined by initial dispersion of 2mg of the lyophilized nanomicelles in deionized water. Results were acquired by active dynamic beam scattering (DLS) on a Zeta-sizer Nano-ZS machine (Malvern Instruments, Worcestershire, United Kingdom).

3.2.8. Determination of the MTX loading efficiency within the nanomicelles

15mg of Lyophilized nanomicelle samples were weighed and suspended in 10mL phosphate buffered saline (PBS) (pH 7; 37°C) and centrifuged at 10,000rpm for 60 minutes. The supernatant was filtered through a 0.22 μ m filter (Millipore Corp., Bedford, MA, USA) in order to remove any insoluble copolymer residue. The drug entrapment efficiency (DEE) was measured from the calibration curve Figure 3.1 at 306 nm utilizing a linearity profile ($r^2 = 0.99$) with a Cecil 3021 UV Spectrophotometer and using Equation 3.2.

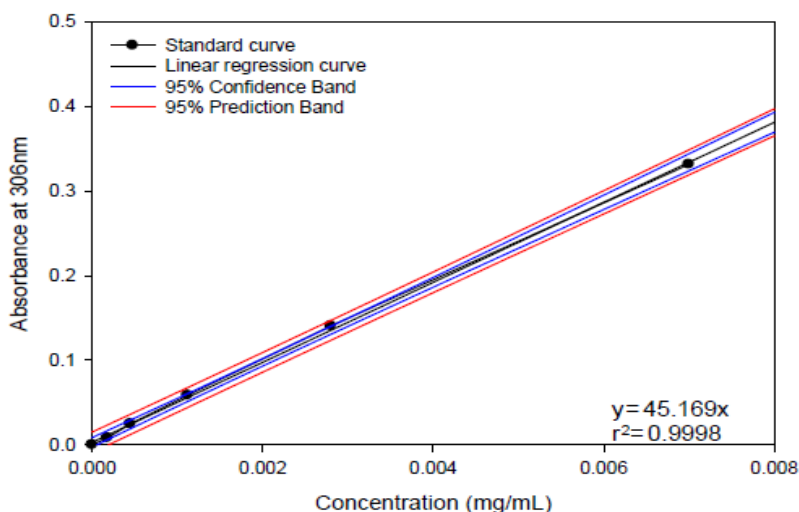


Figure 3.1: Calibration curve of the absorbance of Methotrexate in PBS (pH 7) using Cecil 3021 UV spectroscopy at 306 nm (in all cases n=3 and SD<0.025).

The MTX-loading capacity (%w/w) was computed using Equation 3.3. All measurements were performed in triplicate.

$$\text{DEE \%} = \frac{\text{Mass of MTX in Nanomicelles}}{\text{Mass of Nanomicelles}} \times 100 \quad (3.2)$$

$$\text{MTX Loading (\%w/w)} = \frac{\text{Mass of MTX in Nanomicelles}}{\text{Mass of Nanomicelle Yield}} \times 100 \quad (3.3)$$

3.2.9. Determination of the Critical Micelle Concentration of the PNIPAAm-b-PAsp nanomicelles

Firstly, preliminary formulations of PNIPAAm-b-PAsp nanomicelle solutions with a series of concentrations ranging from 0.05-1mg/mL were prepared according to the dialysis tubing technique as previously discussed in this chapter, section 3.2.6. Aliquots of FITC stock solution (10^{-6} - 10^{-7} M in methanol, 50 μ L) were introduced into glass test tubes and methanol was air evaporated. The nanomicelle solutions (5mL) with varying concentrations were then transferred to the glass test tubes with FITC residue to produce a final FITC concentration of 6×10^{-5} M. The combined solutions of FITC and the nanomicelles were maintained in the dark at room temperature under gradual agitation for 24 hours prior to evaluation. Thereafter, the fluorescence spectrum of each sample was recorded using a Fluorescence Spectrophotometer (Cecil 9000 series, England). Emission spectra were determined at 390nm (I_1) and 310nm (I_3), whereas the excitation emission wavelength was set at 400nm. The CMC

value was calculated by obtaining the midpoint of the block copolymer ratio at which the relative intensity ratio (I_1/I_3) changed.

3.2.10. Investigation of the chemical structure integrity of the PNIPAAm-b-PAsp copolymer

Overall vibrational spectroscopy investigations were undertaken on the originally synthesized polymers (PNIPAAm-NH₂ and PAsp) and the block copolymer PNIPAAm-b-PAsp to evaluate, determine and correlate the structural modifications that occurred. Vibrational spectroscopy studies were undertaken on a Perkin Elmer Spectra 2000 Vibrational Spectrometer with a MIRTGS Sensor (PerkinElmer spectroscopy 100, Lantrisant, Wales, UK) using a vibrational unit with a diamond gemstone interior indicator component. Analysis was performed between 650-4000cm⁻¹ wavenumber series with a 4cm⁻¹ resolution and 64 scans per spectrum.

3.2.11. Thermodynamic stability analysis of the PNIPAAm-b-PAsp copolymer

Relative Differential Scanning Calorimetry (DSC) scans were generated on PNIPAAm, PAsp-NCA and the block copolymer PNIPAAm-b-PAsp employing a Mettler Toledo, DSC1, STARe Instrument (Schwerzenback, Switzerland) at a temperature ramp of 10°C/min from -10-325°C in a stable stream of N₂ gas. Precisely weighed samples (10-15±0.1mg) of each test material were introduced into enclosed aluminium pans. Indium steel (99.99%) was utilized to standardize the DSC modulus scans. A blank sample pan was utilized as a point of reference and investigational scans were generated by warming the weighed samples from -10-125°C with a stable isotherm for 15 minutes. DSC thermograms were then evaluated for changes in thermal episodes.

3.2.12. Thermogravimetric (TGA) analysis of the PNIPAAm-b-PAsp copolymer

TGA facilitated rapid degradation analysis by approximating the deformation speed (dependent on the time of collection) and the specific heat. TGA was carried out by connecting the TGA software (PerkinElmer STA 6000, Beaconsfield, United Kingdom) to a FTIR instrument (PerkinElmer Spectrum 100, Beaconsfield, United Kingdom) to elucidate the thermal characteristics of PNIPAAm-b-PASP copolymer and its constituents. Heating was undertaken from 30-600°C at a rate of 10°C/min. Duration dependent software was utilized for vibrational spectroscopic data elucidation and plotting of a Gram-Schmidt profile. The copolymer sample that displayed constancy was assessed by pulverizing the sample into a fine powder. TGA analysis was performed in triplicate for each sample (N=3). Each sample comprised fine particles of 10-20mg in mass.

3.2.13. *In vitro* MTX release studies from the PNIPAAm-b-PAsp nanomicelles

In vitro release of MTX from the nanomicelles was investigated at 37°C in PBS of pH 6.75 to represent a simulated tumor micro-environment as well as at pH 7.4 (normal physiological conditions). To open the pores, the dialysis tubing (Mw=3500kDa) was first soaked in warm water. Nanomicelles were then introduced into the dialysis tubing and immersed into 200ml dissolution medium in an orbital shaking incubator set at 25rpm at 37°C. At predetermined time intervals 3mL samples were removed in order to determine MTX concentration by UV spectroscopy (Cecil 3021 UV Spectrophotometer) at 306nm and 3mL of drug-free PBS was added to preserve sink conditions. This approach was sufficiently sensitive for investigating rapid release of drug from nanomicelles with release intervals >1 hour (Lin et al., 2005; Saadat., et al., 2014).

3.2.14. *In vitro* Kinetic evaluation of drug release from the MTX-loaded Nanomicelles

Modelling of drug release kinetics was determined by substituting drug release data in Equations 3.4-3.8, being Zero Order, First Order, Higuchi model, Hixson-Crowell and Korsmeyer-Peppas kinetics release equations. Sigma Design 12 software (Systat program, Inc., California, USA) was utilized for arithmetical and statistical investigations. The zero-order model (Equation 3.4) represents a stable release process.

$$Y = a_0 + K_0t \quad (3.4)$$

The first-order rate model (Equation 3.5) describes incorporation and/or dispersion of the drug in a permeable matrix with drug release rate independent of its concentration.

$$\text{Log } Y = \text{log } a_0 + K_1t \quad (3.5)$$

Higuchi's square root of time reliant model was established from the Fickian law of diffusion (Equation 3.6) for therapeutic release from a matrix structure.

$$Y = Kt^{1/2} \quad (3.6)$$

For validation of the process of therapeutic release, the initial 60% of released therapeutic was substituted in Korsmeyer-Peppas model (Equation 3.7).

$$F = \frac{M_t}{M_\infty} = Kt^n \quad (3.7)$$

Where M_t/M_∞ is the quantity of released ratio at time t , M_t is the quantity of therapeutic released at any specific period of time, M_∞ is the greatest quantity (weight/load) accessible for release, t is the release period of time, k is the kinetic constant, and n is a characteristic release power. Owing to the distended nanoparticle magnitude after incorporation of therapeutics, the Hixson-Crowell law (Equation 3.8) was employed to determine the release reliant on transformation in surface region and size of the nanoparticle.

$$\sqrt[3]{Q_a} - \sqrt[3]{Q_m} = K_k t \quad (3.8)$$

The kinetic model with the greatest R^2 value was regarded as the best fitting model for validating the release of MTX from the nanomicelles. The n release power value for Korsmeyer-Peppas law was utilized for determining the type of release (Fickian or non-Fickian diffusion, anomalous diffusion, or erosion).

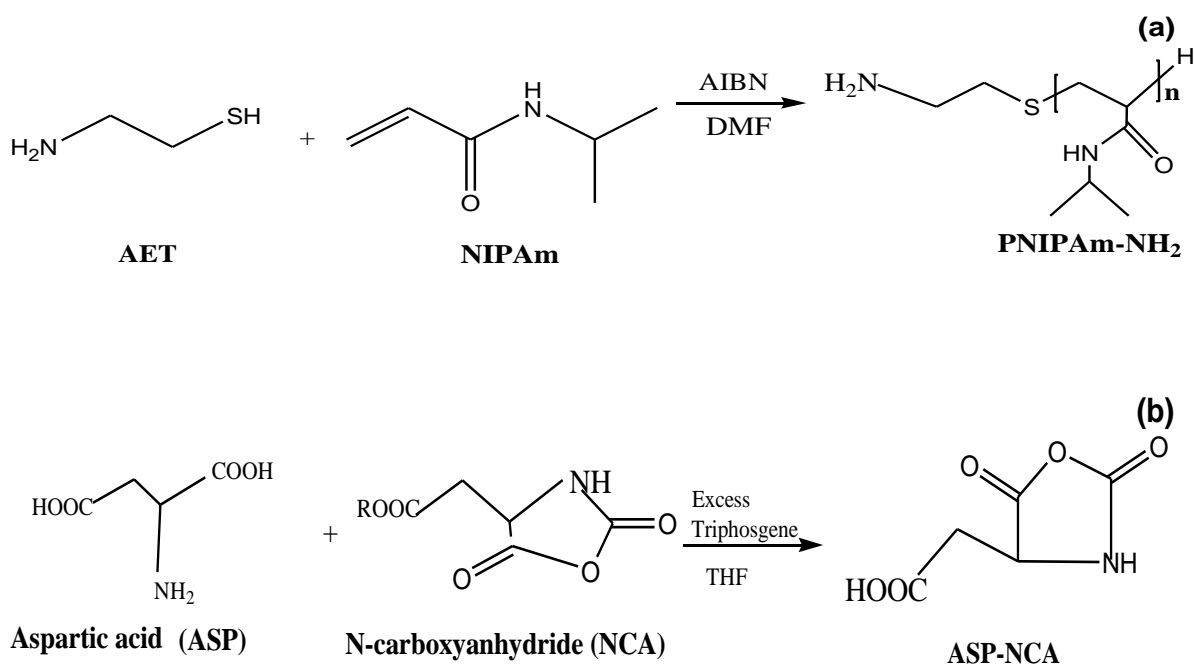
3.3. Results and Discussion

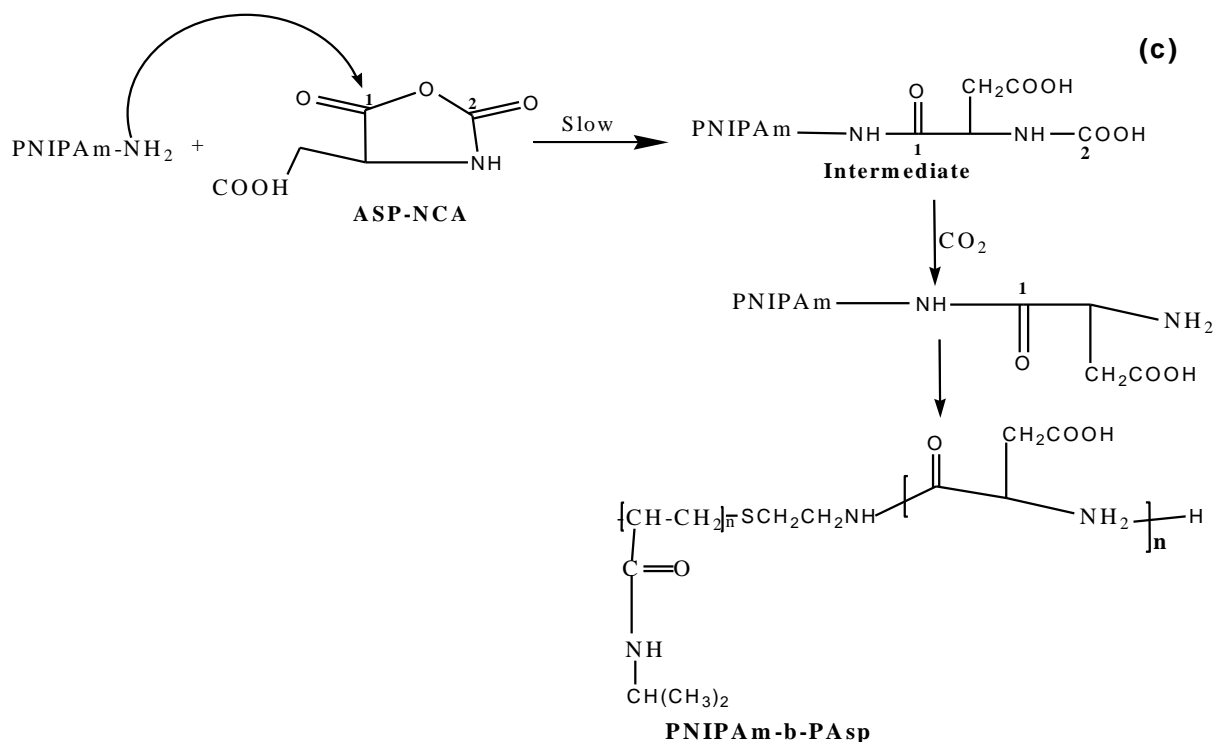
3.3.1. Assessment of the copolymerization strategy and nanomicelle synthesis

In this study Thermal Ring-Cleavage polymerization (TRC) was used to synthesize the novel blocks copolymer PNIPAAm-b-PAsp. This is a type of chain-expanding polymerization with the polymer chain terminals acting as a reactive-site where additional cyclic polymers can respond by slicing the ring structure in order to produce an extended polymer sequence. The propagating site can be a free radical that is positively or negatively charged (Kumar et al 2012; Bawa et al 2011; Fernandes et al 2005). A few norbornene or cyclo-octadiene ring forming monomers can be co-polymerized into high molecular mass polymers via metal catalysts. However, in this study a non-metallic catalyst (triphosgene) was employed. TRC is the most flexible technique for assembling key biopolymer groups especially when needed in larger quantities (Lin et al 2005; Yoksan et al 2004). The initiator for ring-cleavage of cyclic polymers is via the split in attachment-angle tension (steric-repulsions) between particles at the inner-core of the ring. Hence, as in other polymerization approaches, the enthalpy transition in TRC polymerization is negative (Gao et al 1998).

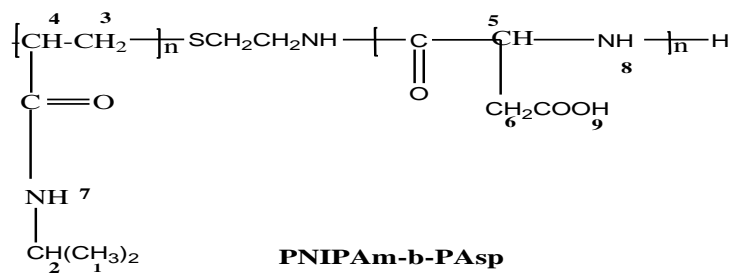
The current study was based on amphiphilic copolymers synthesized from a group of hydrophobic and hydrophilic polymers using TRC. Results demonstrated the exceptionality of preparing PNIPAAm-b-PAsp inclusive of monomer utilization that can be explained by a copolymerization mechanism. A copolymerization reaction mechanism was used to determine the synthesis process parameters. Briefly, radical polymerization of NIPAm produced an amino terminated PNIPAAm using AET-HCl as a chain-transfer agent to introduce amino ions

and AIBN used as an activating agent as shown in Scheme 1(a). This was also used in aspartic acid carboxylation via the triphosgene approach followed by thermal ring opening of L-Asp-NCA with the amino terminated PNIPAAm shown in Scheme 1(b-c). Interestingly, the amino terminated PNIPAAm played a binary role by primarily splitting the polymers and in so doing facilitated the production of free radicals that resulted in assembly of the high molecular mass block copolymer PNIPAAm-b-PASP. Therefore, the attachment of amino ions to PNIPAAm was influential for the bonding of PNIPAAm directly onto N-carboxylate functionalized PAsp chains that finalized the ring cleavage copolymerization process. In agreement with the aforementioned discussion, the likelihood of generating single homopolymer material was very low with strong bond interferences, atomic rigidity abridged via N-carboxyanhydride cleavage with an amine charge. The synthesized amphiphilic block copolymer PNIPAAm-b-PASP was further confirmed with correlation from chemical structural formula and NMR peak assignments (Figure 3.2).





Scheme 1: Synthesis of amino terminated poly (N-isopropylacrylamide) by free-radical polymerization of NIPAm (a), carboxylation of aspartic acid (Asp) using triphosgene method (b) and thermal ring opening polymerization of Aspartic acid-N-carboxyanhydride using amino-terminated NIPAM to form the PNIPAAm-b-PASP amphiphilic copolymer product (c).



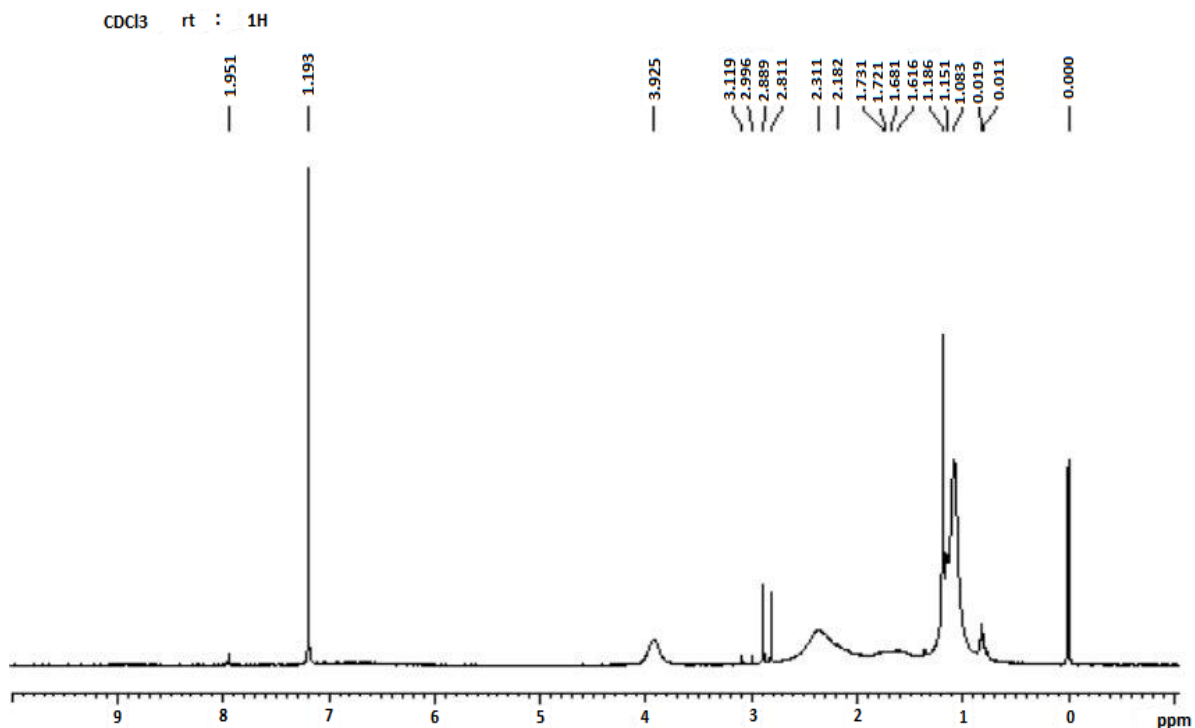


Fig 3.2: ^1H NMR spectra of PNIPAAm-b-PASP in CDCl_3 and peak assignment confirming the structure of the synthesized amphiphilic copolymer.

3.3.2. Establishment of the molecular mass of the synthesized PNIPAAm-b-PASP copolymer

The copolymer sample that demonstrated stable rheological properties (a viscoelastic profile with increased structural recovery after distortion) (Venugopal et al. 2010), mechanical robustness (ability to endure high shear stress $>70\text{dynes/cm}^2$) and ideal swelling dynamics (reduced swelling in order to diminish the potential shear effects when used in OC) was confirmed. This optimized copolymer was used for nanomicelle preparation. The viscosity of the 0.01%, 0.001% and 0.0001% concentrations of the synthesized copolymer was measured and the mean inherent viscosity at each concentration ($IV=494.527\text{mPas}$) was calculated from the profiles shown in Figure 3.3. The mean viscosity-based molecular mass of the synthesized copolymer in aqueous solution was then determined utilizing the partially-proportional Mark-Houwink formula (Equation 3.1), which correlated the inherent viscosity $[\eta]$ with the molar mass (M). In the logarithmic form the Mark-Houwink formula permitted rapid evaluation of the parameters used by simple substitution in the linear Equation 3.9.

$$\text{Log } [\eta] = \text{logK} + a \text{ log M} \quad (3.9)$$

Thus, the mean viscosity-based molecular mass was calculated to be $2.217 \times 10^6 \text{kDa}$.

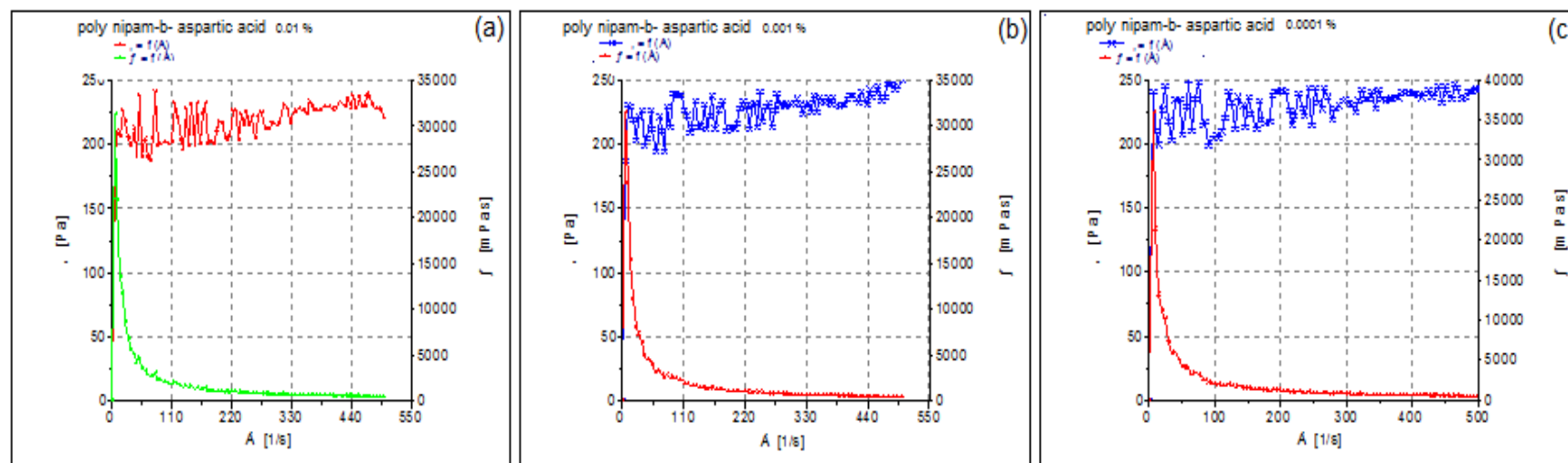


Figure 3.3: Flow curves shear stress (τ), Viscosity (η) versus shear strain (γ) at various concentrations of amphiphilic copolymer synthesized (a-c).

3.3.3. Quantitative image assessment of PNIPAAm-b-PASP copolymer morphology

The PNIPAAm-b-PASP copolymer topology is a significant factor that influences their physical properties and potential applications. To regulate copolymer topology, a specific architecture is now a focal theme in polymer nanotechnology with the purpose of producing macromolecules with innovative properties (Santos et al 2010). SEM images were used to demonstrate a broad-spectrum analysis of the copolymer microstructure and to confirm the morphological variations of the different forms of the synthesized PNIPAAm-b-PASP amphiphilic copolymer. Initially, the copolymer in powdered form (Figure 3.4a-b) was compared with thin-films (Figure 3.4c-d) that were non-porous followed by lyophilized samples (Figure 3.4e-h) with a high degree of pore distribution. In di-block and tri-block copolymers, two modal peaks are commonly examined if the blocks are of similar size. Indeed in this study the PNIPAAm-b-PASP copolymer displayed two thermal transitions as confirmed by DSC thermograms in Figure 3.8.

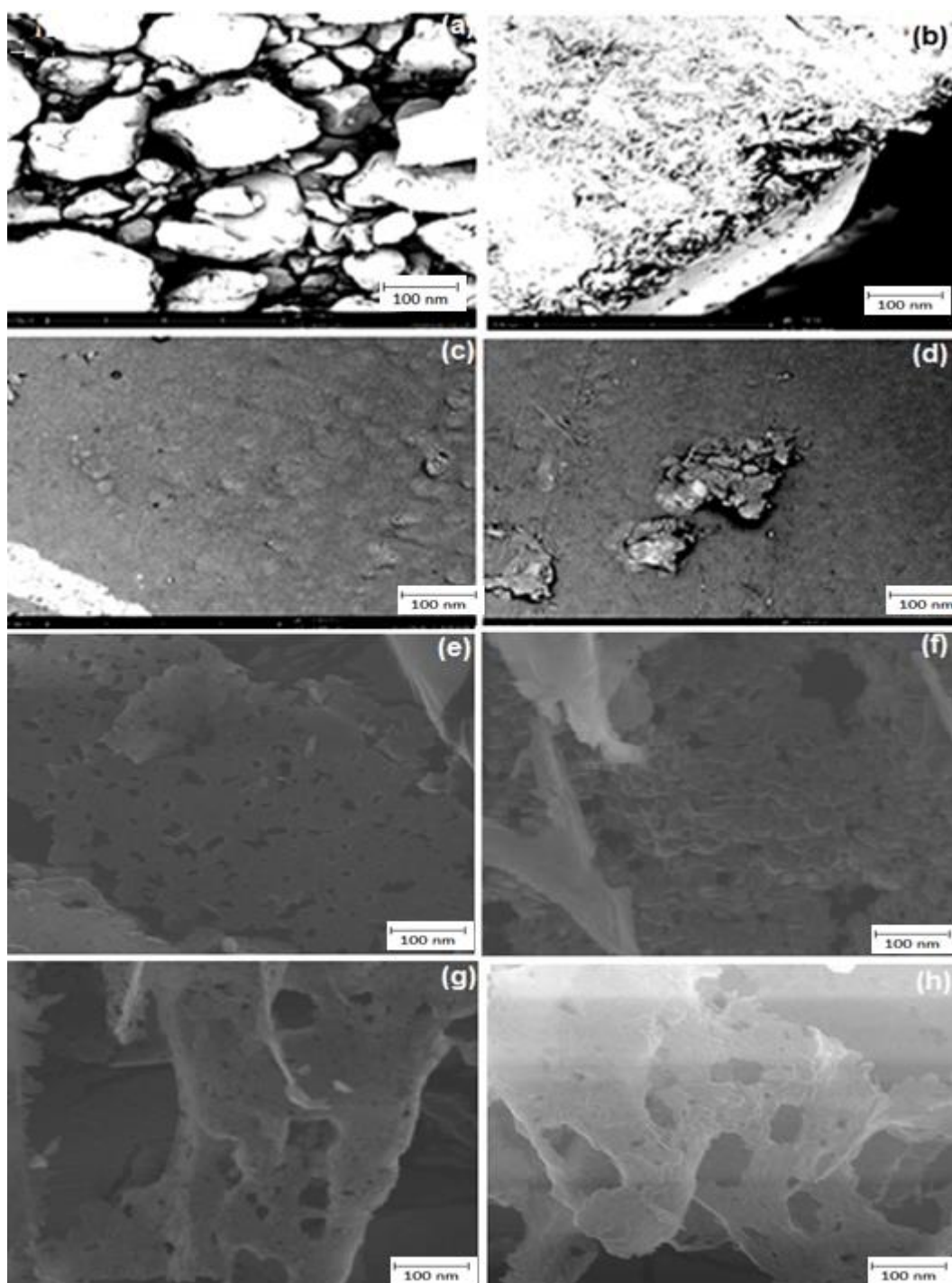
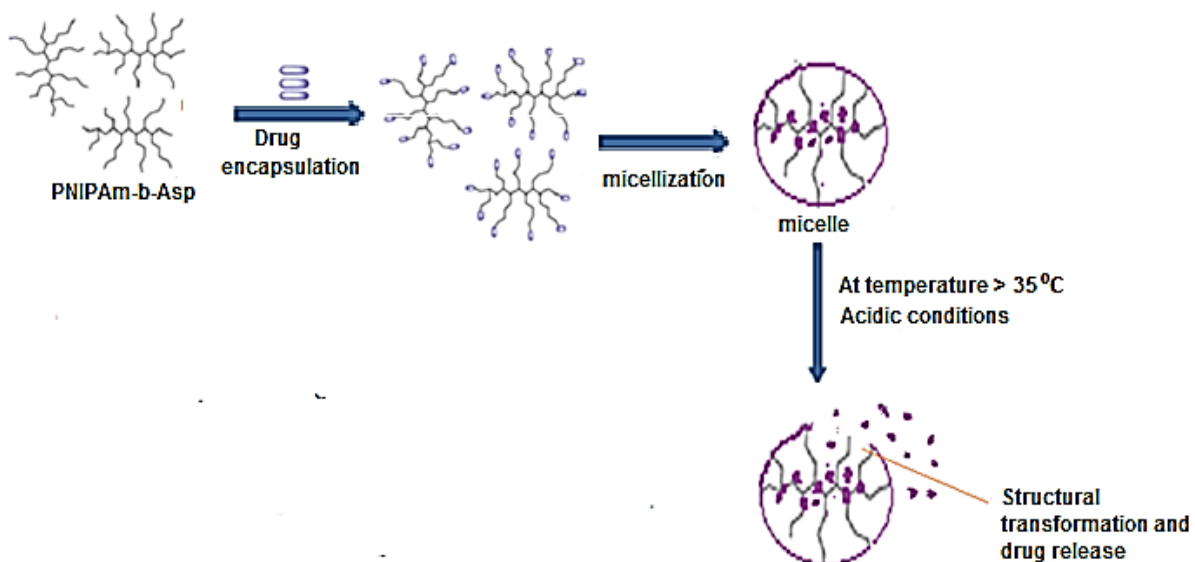


Figure 3.4: Scanning electron microscopy (SEM) images of synthesized copolymer in powder form (a-b), Surface of copolymer in film form (c-d), lyophilized copolymer displaying pore distribution and pore diameter variation (e-h).

3.3.4. Assessment of the nanomicellization process and MTX entrapment efficiency

The new PNIPAAm-b-PAsp copolymer synthesized was used to formulate a nanomicelle carrier system by the dialysis technique for direct MTX delivery in OC treatment (Scheme 2). The structure of the nanomicelles was observed with SEM and TEM (Figure 3.5) and was confirmed to be of spherical shape and 90nm in size. This also validated that dispersion occurred in the interior of the nanomicelles demonstrating hydrophobic copolymeric self-aggregation into a phase-separated interior region owing to the hydrophobic influence. The water-soluble exterior shield separated the assembled hydrophobic interior region of the nanomicelle from the aqueous medium. The nanomicelle size is a significant factor to ensure controlled loading and release of MTX for targeted delivery to an OC tumor environment. Nanomicelles displayed a mean particle size of 90nm, a zeta-potential value of -0.539mV and polydispersity index (PDI) of <0.5 which was indicative of a homogenous nanomicelle size distribution. The zeta-potential value suggested that the MTX-loaded PNIPAAm-b-PASP nanomicelles were electrostatically controlled although they had the propensity for reversible flocculation. The results of this study demonstrated stable MTX loading into the partially water soluble inner core of the PNIPAAm-b-PASP nanomicelles with a DEE of >77%. The loading of hydrophobic drugs in the inner core (PAsp region) of the nanomicelles resulted in improved solubility, metabolic stability and prolonged distribution time of MTX. The copolymer showed improved solubility in a broad-spectrum of organic solvents including DMF, dioxane as the concentration of PAsp increased. The DEE value relied on the electrostatic exchange between MTX and the interior core of the nanomicelles. MTX-copolymer exchange indicated that the largest quantity of MTX loading per nanomicelle was attained when the inner-core of the nanomicelles was appropriately coordinated with the MTX. Thus, in order to improve the DEE value of MTX coupling between MTX and the copolymer should be elevated.



Scheme 2: Incorporation of methotrexate with copolymer employing micellization process to form micelles which have potential application in cancer treatment as antineoplastic drug delivery systems, also included is the structural transformation due to changes in temperature and pH resulting in drug release.

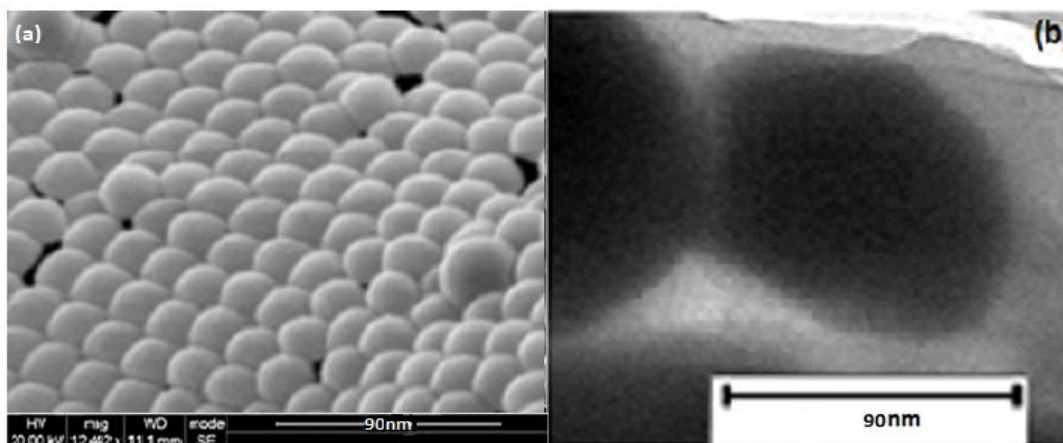


Figure 3.5: SEM (a) and TEM (b) images depicting self-assembled PNIPAAm-b-PASP copolymeric nanomicellar formulation. The scale for all images is 90 nm.

3.3.5. Analysis of the Critical Micelle Concentration value of the nanomicelles

The self-aggregation of amphiphilic polymers is initiated as the concentration of the copolymer reaches the CMC. Therefore, the CMC value is a significant parameter displaying the self-aggregation capability of polymers to form nanomicelles. The CMC value of the PNIPAAm-b-PASP copolymer was determined by using the FITC fluorescence probe technique. FITC is a molecular fluorescent probe with the intensity ratio of the first crest (390nm) and the third crest (290 nm) I_1/I_3 in its emission spectrum that is highly responsive to the ionic charge of the

solution. Thus, the fluorescence intensity ratio- (I_1/I_3) displayed a noticeable change. The typical fluorescence spectra of PNIPAAm-b-PASP copolymers with increased concentrations are shown in Figure 3.6a. Figure 3.6b displays the intensity ratio (I_3/I_{333}) of the FITC excitation spectra versus concentrations of PNIPAAm-b-PASP copolymer. The CMC was computed as the midpoint of the PNIPAAm-b-PASP copolymer concentration at which the I_1/I_3 intensity ratio considerably decreased and was determined to be at a value of 0.09mg/mL.

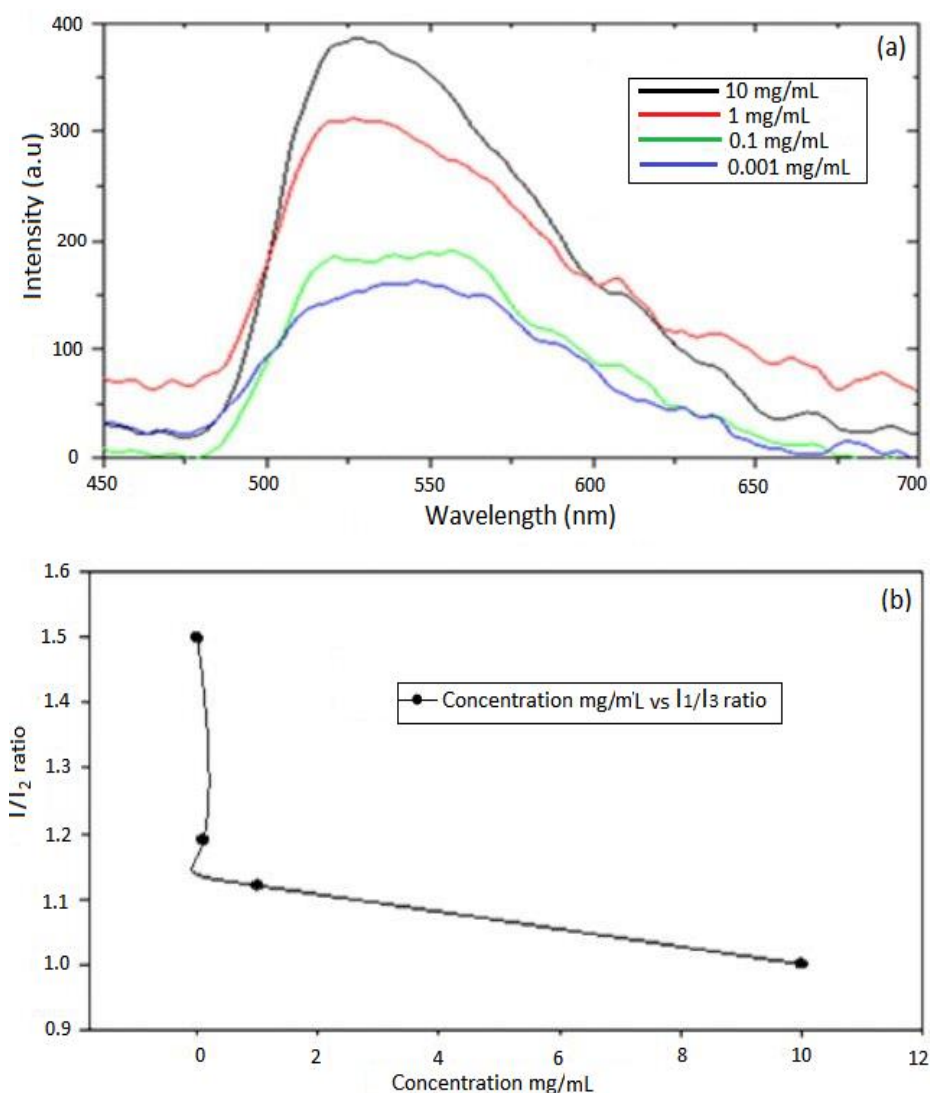


Figure 3.6: (a) FITC emission spectra of PNIPAAm-b-PASP solutions. (b) I_{390}/I_{290} intensity ratio for FITC as a function of the concentration of PNIPAAm-b-PASP copolymer in deionized water. The CMC was obtained as the midpoint value of copolymer concentration at which the I_1/I_3 intensity ratio considerably decreases.

3.3.6. Influence of nanomicelle size

Micelle size is a prime factor since it influences the MTX encapsulation, therapeutic release, and ultimately site-specific release of methotrexate across the reticular endothelial system (RES). The micelle size obtained from the nanomicelles was 90 nm and remained the same upon utilization of solvent evaporation method to further enhance the MTX entrapment efficacy (Figure 3.7). For intraperitoneal chemotherapeutic interventions, the size of the nanomicelles would be favorable for dissemination into the tumor-cellular structure with pore size of 100nm or less at the site of treatment. The RES penetration also has to be taken into consideration as nanomicelle with a size greater than 100nm may not be able to escape through the RES.

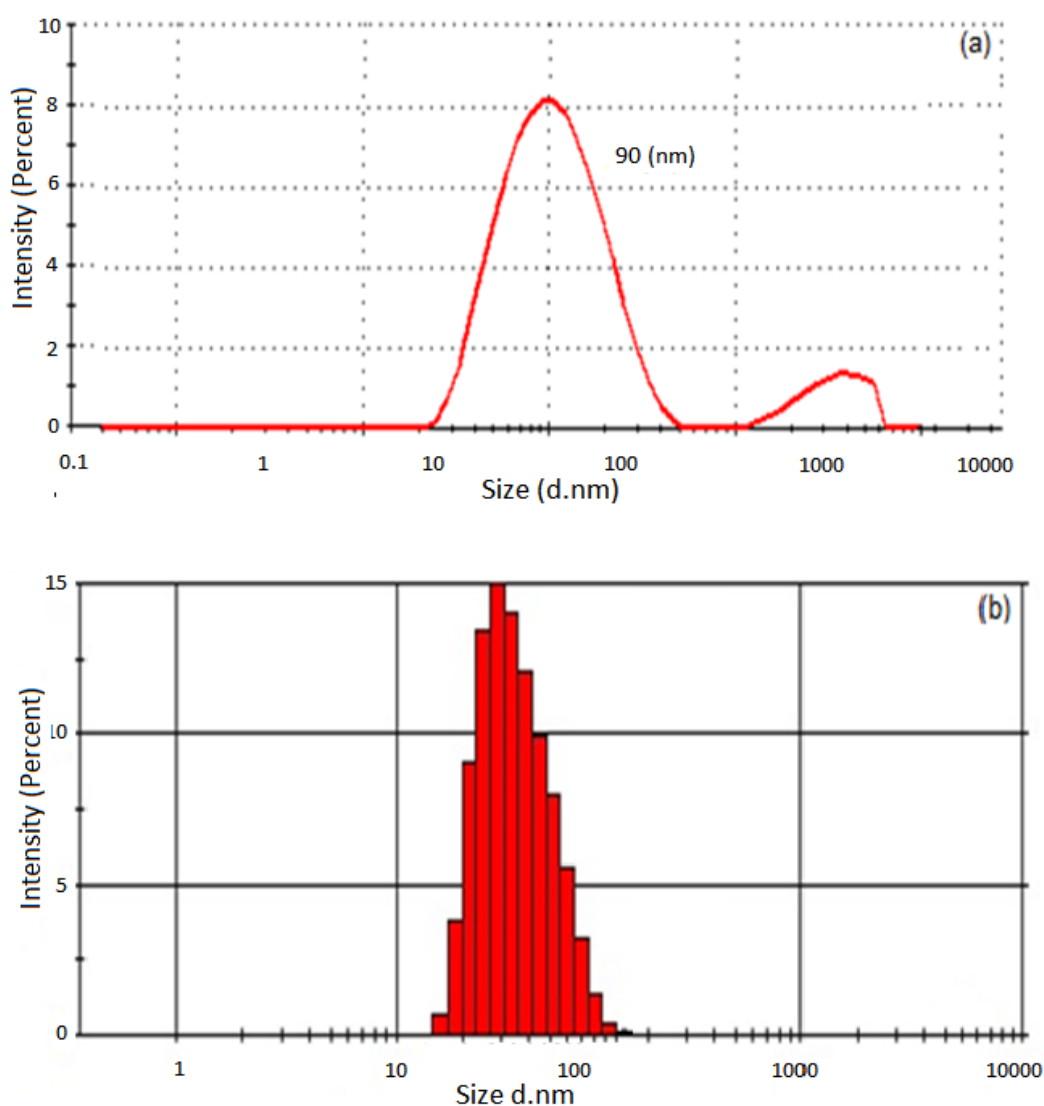


Figure 3.7: (a) Zeta size graphs illustrating the hydrodynamic size of PNIPAm-b-PAsp nanomicelle formulation, (b) size intensity distribution for the optimized monotype PNIPAm-b-PAsp nanomicelle.

The mean zeta-potential values of the experimental MTX-loaded nanomicelles did not vary greatly and ranged from -0.02383mV to -1.89mV . These zeta potential values showed that the MTX-encapsulated PNIPAAm-*b*-PAsp nanomicelles were only partially stabilized by electrostatic forces but may have high propensity of aggregation outside the designated parameters. Design of a nano-encapsulating neurodeformable polymeric carrier could be employed for stabilization and delivery of the nanomicelles to the tumor site.

3.3.7. Analysis of the copolymer chemical structure integrity and transformation

Figure 3.8 displays the vibrational spectroscopy profiles of the homopolymers PNIPAAm-NH₂ and L-Asp-NCA with the resultant porous PNIPAAm-*b*-PAsp copolymer also shown. In the spectrum of PNIPAAm-NH₂, the peaks at 3286cm^{-1} and 1635cm^{-1} were indicative of N-H pulsation. Furthermore, a noticeable peak at 1638cm^{-1} was attributed to an amide carbonyl functional set. In the FTIR spectrum of L-ASP-NCA the peak at 2945cm^{-1} was allocated to a regular elongating pulsation of the amide attachment. The vibrational spectrum also displays the C=O broadening group of NCA at 1746cm^{-1} and 1704cm^{-1} and CH₃ vibrations were allocated to peaks at 1386cm^{-1} and 1283cm^{-1} .

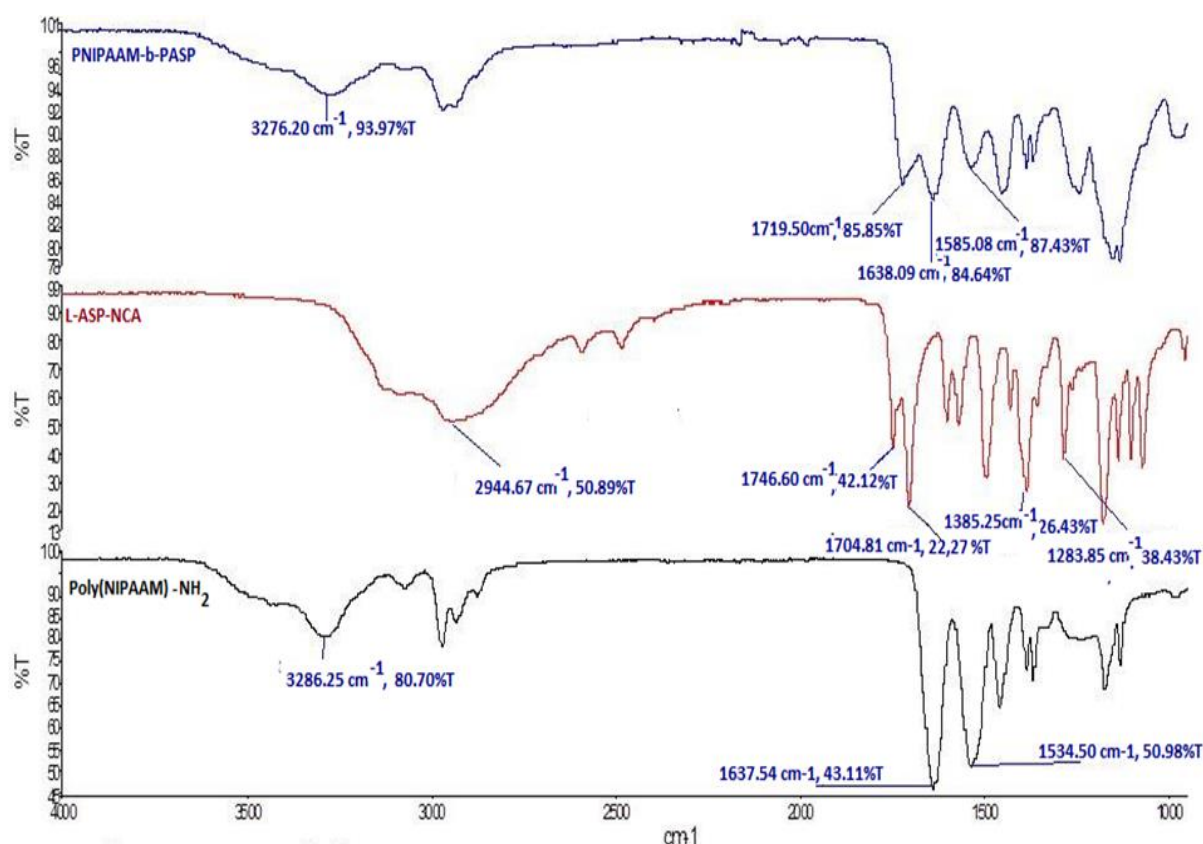


Figure 3.8: Overall Vibrational-Spectroscopy of Poly-N-isopropylacrylamide-block-poly aspartic acid (PNIPAAm-*b*-PAsp), L-Asp-NCA, Poly NIPAAm-NH₂ (descending order).

As for the PNIPAAm-b-PAsp, peaks at 1746cm^{-1} and 1704cm^{-1} were displaced and signified that the acid anhydride structure was destructed. A peaks at 1638cm^{-1} was allocated to the C=O group. The peak at 1535cm^{-1} was the absorption peak of the amide group coupled with the slanting vibration of the amide attachment and elongating vibration of the cyanide attachment. Episodes of copolymerization were confirmed with ^1H NMR for differentiating the arrangement of the formed amphiphilic copolymer. The methine proton in PNIPAAm was allocated at the 4.1ppm peak and the PAsp methine proton peak was at 4.2ppm. All ^1H NMR vibrations were ascribed to PNIPAAm-NH₂ and PAsp components shown in Figure 3.2. These results are consistent with previous studies on thermal ring opening copolymerization of PNIPAAm-NH₂ onto polyamino acids (Kang et al. 1997; Wei et al. 2009; Huang et al. 2008; Rimmer et al. 2007).

3.3.8. Assessment of the thermodynamic stability of the PNIPAAm-b-PAsp copolymer

Figure 3.9 shows the DSC scans for the thermal events of L-ASP-NCA, PNIPAAm-NH₂ and PNIPAAm-b-PAsp, respectively. The onset to melting and the end of melting points are shown with a shift to the left of the melting temperature peak for the combinational PNIPAAm-b-PAsp shown in Figure 3.9. For the PNIPAAm-b-PAsp, the heat transition emerged at 160°C despite the fact that the thermal peaks varied in terms of the range and depth of the final peaks for confirmation of the structural properties of the combinational PNIPAAm-b-PAsp copolymer as supported by the FTIR results.

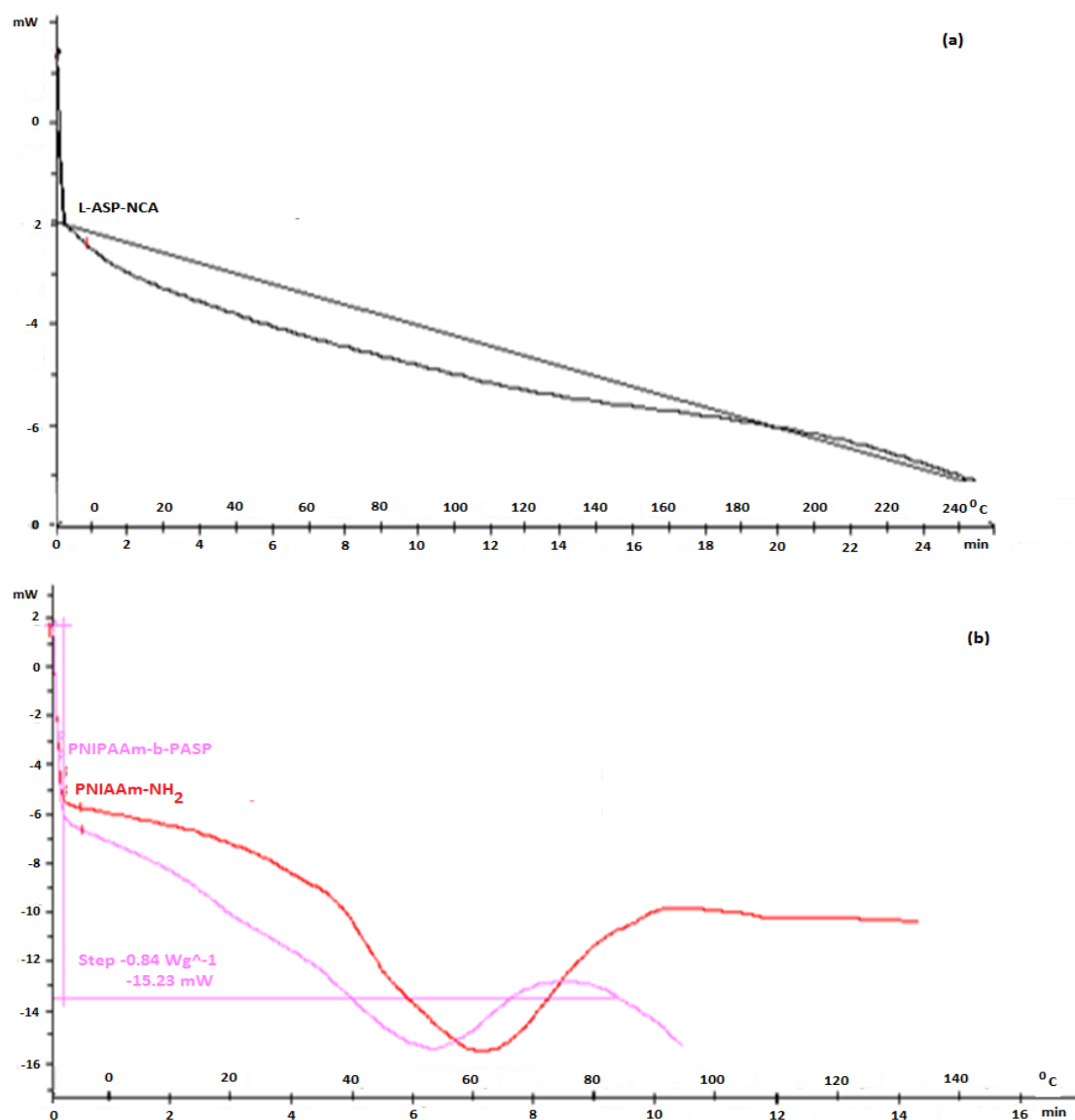


Figure 3.9: (a) DSC scan of (a) L-ASP-NCA (b) PNIPAAm-NH₂, PNIPAAm-b-PAsp copolymer formed from the combination of PNIPAAm-NH₂ and L-ASP-NCA via ring opening polymerization.

3.3.9. Thermal degradation analysis of the PNIPAAm-b-PASP copolymer

Figure 3.10 shows the TGA profiles acquired and revealed the rate of mass variation that is useful in defining the temperature of the first onset of breakdown for each mass loss incidence. The peak at 210°C indicated the evaporation of the residual DMF from the PNIPAAm-b-PASP copolymer that was not removed via lyophilization. This was followed by degradation of PNIPAAm and PAsp between 300-500°C. Within this region CO₂ and residual bound water was released which resulted in mass variation due to oxidation. Elevating the heating rate (6-10°C/min) increased the degradation rate and activation energy as displayed

in the Figure 3.10. Three heating rates are shown in Figure 3.10 as they were used to determine the decomposition kinetics. The heating rates became comparable after 450°C due to decomposition of all carbon based materials.

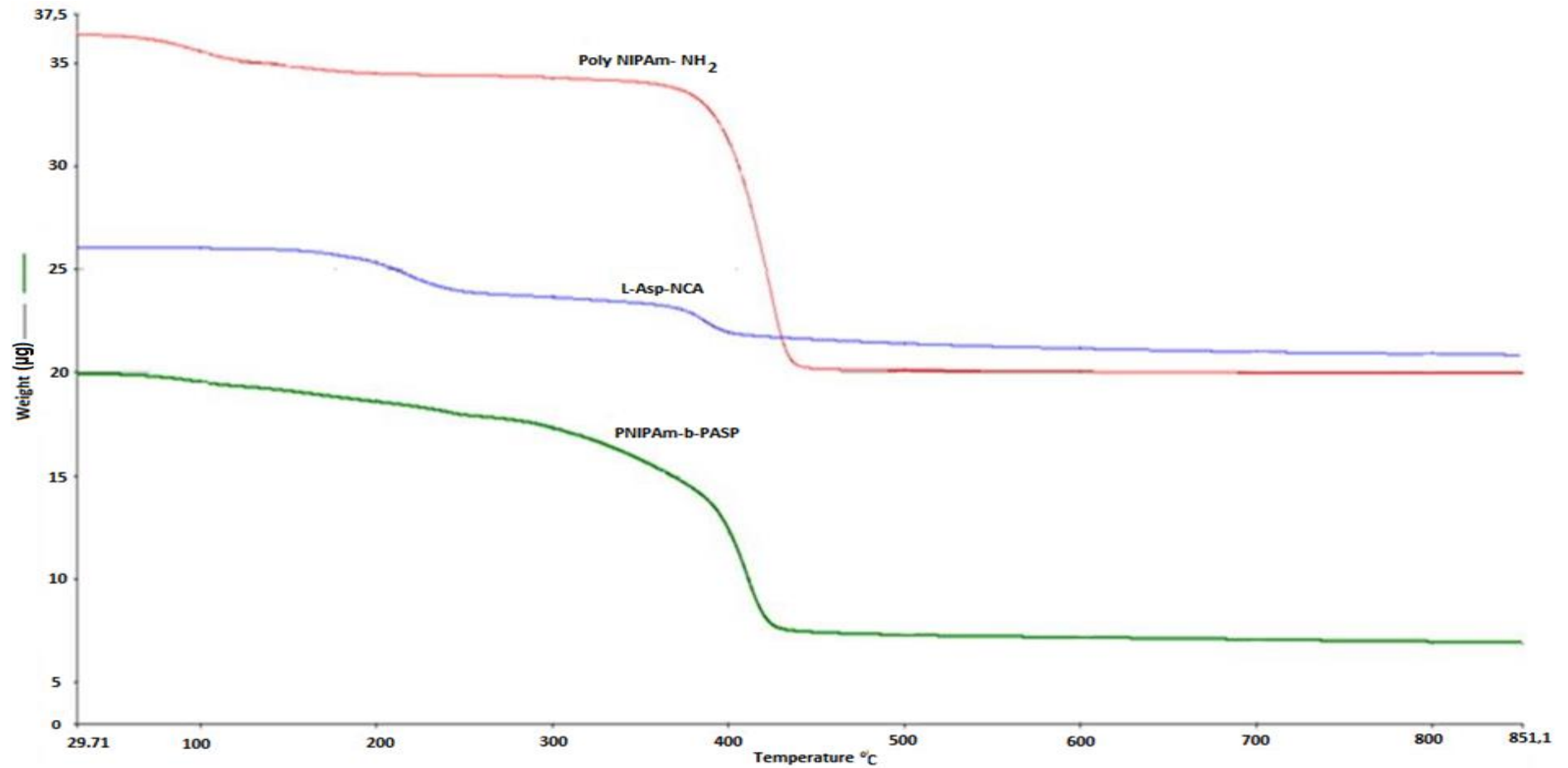


Figure 3.10: TGA properties of PNIPAAm-NH₂ (A), L-ASP-NCA (B) and PNIPAAm-b-PASP (C) depicting various melting points.

3.3.10. *In vitro* analysis of MTX release from the PNIPAAm-b-PASP nanomicelles

Figure 3.11 demonstrates the MTX release profile from thermosensitive polymeric micelles in ultra-pure distilled water, which is a stable pH/thermosensitive controlled release behavior. Below lower critical solution temperature (LCST) at 25 °C, only small quantity (40%) of MTX was released from polymeric micelles during the 72 h study. One of the smart features of PNIPAAm micelles as drug nano-carriers is their intellectual property to external temperature variations. However, when the temperature was increased to 37°C (exceeding LCST), the complete MTX release increased to 70% due to the temperature-impelled structural modifications of the micelles. Above LCST the PNIPAAm surface became hydrophobic, which led to the exterior shell degradation. The degradation of the amphiphilic nanoparticles triggered the release of the encapsulated MTX. Figure 3.11 illustrates that the MTX release does not reach 100%; this might be due to the fact that fractional drugs were entrapped in the deformed micelles for the interactions between nano-carriers and MTX.

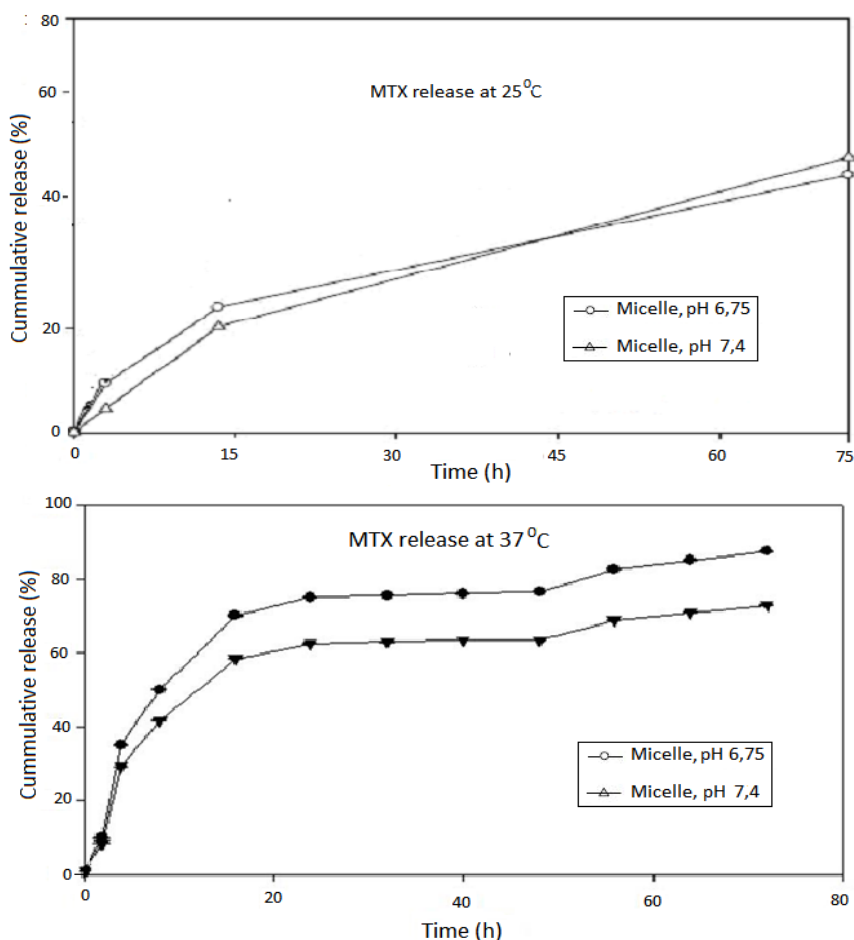


Figure 3.11: Methotrexate release from PNIPAAm-b-PASP copolymeric nanomicelles in acidic (pH 6.75) at 38 degrees and normal physiological conditions (pH 7.4) at 37 degrees. Each point depicts mean \pm SD (n=3).

3.3.11. *In vitro* kinetic evaluation of drug release from the MTX-loaded Nanomicelles

The experimental release profile of PNIPAAm-b-PASP micelle displayed continual drug release in the MTX-loaded nanomicelles (Figure 3.11). Modeling of drug release kinetics was undertaken by fitting drug release data to equations of Zero Order kinetics, First Order, Higuchi model, Hixson Crowell and Korsmeyer Peppas (Table 3.1). Prolonged release up to 72 h was attained due to the degradation of the biopolymer material and slowed dispersion of the therapeutic from the micelle interior core. MTX release from the nanomicelle was best described by the Higuchi model ($R^2=0.8459$), which in this case describes the release of MTX through the collapsed outer hydrophobic PNIPAAm as a square root of time dependent process based on Fickian diffusion. For the Korsmeyer-Peppas law, the fit was only average ($R^2=0.6626$). According to this law, if the release power coefficient (n value) is greater than 0.45 and smaller than 0.89, it implies that the therapeutic release is due to anomalous transport behavior (Non-Fickian diffusion), while $n<0.45$ implies that the drug release was due to Fickian diffusion law. For release from the MTX-loaded nanomicelle, the 'n value' which was established to be 0.1552, implying that the drug release was due to Fickian diffusion of the MTX from the inner core through the collapsed PNIPAAm, which is congruent with the fit with Higuchi's square root law. The rate of diffusion/dispersion was also confirmed by the aforementioned amorphous state established for MTX and slackening of the micelle hydrophobic core. This suggests that MTX-loaded PNIPAAm-PASP amphiphilic nanomicelles are significant for encapsulation of hydrophobic drugs (Zhang et al. 2005; Jeong et al. 2009; Lin et al. 2015).

Table 3.1: Drug release kinetics results for various models of methotrexate-loaded nanomicelles for site-specific targeted therapeutic delivery.

Model	Equation	R-squared	R-squared adjusted	n-value
(a) Zero-order	$Y = a_0 + K_0t$	0.6368	0.5964	Not relevant
(b) First-order rate model	$\text{Log } Y = \text{log } a_0 - K_1t$	0.8037	0.7710	Not relevant
(c) Higuchi's square root law	$Y = Kt^{1/2}$	0.8459	0.8202	Not relevant
(d) Korsmeyer-Peppas law	$F = M_t/M_\infty = Kt^n$	0.6626	0.6251	0.1552
(e) Hixson-Crowell law	$\sqrt[3]{Q_a} - \sqrt[3]{Q_m} = k_1t$	0.5089	0.4543	Not relevant

Furthermore, the pharmaceutical applicability of the uniquely merged amphiphilic PNIPAm-b-PAsp copolymeric nanomicelles for the targeted delivery of MTX was evaluated by incubation with OC cells (NIH:OVAR-5) and the treated cells were analyzed by the use of a MTT assay, confocal microscope for evaluation of the cytotoxic and uptake ability of the MTX-loaded nanomicelles as described later in Chapter 5, section 5.2.6.

3.3.12. Conclusions

A new PNIPAAm-b-PAsp amphiphilic copolymer with high molecular mass was synthesized by free radical polymerization and self-aggregated in aqueous solution to form nanomicelles of 90nm in size. Vibrational spectroscopy and DSC results validated the assembly of PNIPAAm-NH₂, L-Asp-NCA into the PNIPAAm-b-PAsp nanomicelles. The results further confirmed stable MTX entrapment into the partially-water soluble inner core of the PNIPAAm-b-PASP nanomicelles with a DEE value of >77%. The premise that this amphiphilic copolymer self-assembled into nanomicelles in aqueous solution was further validated by the relatively low CMC value (0.09mg/mL). MTX release from the nanomicelles was controlled by the pH and temperature of the release medium. This was favourable for the potential application of the nanosystem for targeted chemotherapy in OC as a new stimuli-responsive chemotherapeutic nanocarrier system.

CHAPTER 4
**OPTIMIZED DESIGN OF COMBINATIONAL (POLY N-ISOPROPYLACRYLAMIDE)-
BLOCK-POLY (ASPARTIC ACID) NANOMICELLES FOR TUMOR-SPECIFIC
MICROENVIRONMENTAL RELEASE OF METHOTREXATE DELIVERY**

4.1. Introduction

Drug carrier approaches, which are intended for transporting chemotherapeutics at preferred rate and to a specific location for optimal treatment at the targeted infected area of the body, are utilized to surmount the drawbacks of clinical systemic administrations (Liu et al., 2005; Hu et al., 2008; Mukherjee et al., 2008). A range of therapeutic delivery approaches, including polymeric nanoparticles, micelles, polymer-conjugates, dendrimers, liposomes and lipids/mineral nanomolecules, have attained technological advancement in terms of preferred release rate and site-specific therapeutic delivery (Gupta et al., 2000; Pignatello et al., 2002; Hou et al., 2003). Thus far, bio-compatible and bio-degradable nanomicelles are a highly favoured nanosystem for therapeutic transport (Veronese et al., 1991, Soppimath et al., 2001; Soppimath et al., 2005). Core shell polymeric nanomicelles have been widely explored for drug delivery purposes, and recently for the transport of anti-neoplastic drugs. Nanomicelles have a hydrophobic interior and hydrophilic outer surface, offering important advantages. The hydrophobic interior specifically serves as a nano-reservoir for partially water soluble drugs and the hydrophilic surface serves as a protective coating against the reticular endothelial retention system (RES). The findings of Thunemann *et al.* (Thünemann et al., 2000) revealed that ion intricate nanomicelles involving poly (ethylene oxide)-b-poly (L-lysine)s (PEO-PLL) with all-trans retinoic acid displayed the assemblage of core-shell nanomicelles (Thünemann et al., 2000).

Methotrexate (MTX) was the model antineoplastic drug utilized in this study for chemotherapeutic treatment of intraperitoneal ovarian cancer, chemical structure is illustrated in Figure 4.1. MTX is an antagonistic metabolic analogue of folic acid that acts by impeding the malignant cell division and multiplication, by restraining the dihydrofolate reductase enzyme activity. This reductase enzyme usually transforms folic acid into tetrahydrofolic acid metabolites, which are vital for the preparation of nucleic acid (DNA) inside the unit cell. Cell units are incapable of mitosis, proliferation and resurgence without tetrahydrofolic acid producing new genetic material (DNA). Since MTX digests cell units of this metabolic nutrient, it destroys malignant cells and impedes the tumor growth. Unfortunately, MTX has its own share of detrimental toxic side-effects including toxicity to normal mitotic cells, therapeutic

resistance, renal toxicity, bone marrow repression, severe persistent hepanoxious, and persistent interstitial disruptive pulmonary infection (Zhang et al., 2005).

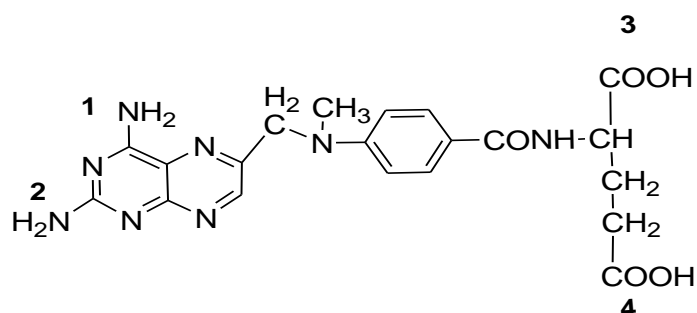


Figure 4.1: Methotrexate structure with IUPAC name (S)-2-(4-(((2,4-diaminopteridin-6-yl)methylamino) benzamido) pentanedioic acid, molar mass 454,46 g/mol, chemical formula C₂₀H₂₂N₈O₅ with all possible binding sites also depicted.

A range of MTX-loaded micelle carrier nanosystems with small sizes (up to 100 nm) enabling cellular uptake including cellular permeation have been developed to surmount the described toxicity challenges. The exterior ionic charge of the micelle is also a significant factor in facilitating escape of nanomicelles from endocytotic attack and enabling delivery of chemotherapeutic drugs directly to tumor intracellular locations (Jeong et al., 2009). Kang et al. (Kang et al., 2002) findings revealed that MTX/copolymer composite comprised of poly ethylene glycol /poly (2-hydroxyethyl L-aspartamide) in aqueous solution self-aggregated into nanomicelles for continuous release of MTX at 37°C, pH 7.4 (Kang et al., 2002). MTX was encapsulated into self-agglomerates of poly (2-hydroxyethyl aspartamide) complex by attachment. Tri A-B-A block multifunctional copolymers were also assembled to encapsulate MTX, however entrapment efficacy was only between 7-30 % w/w of the biopolymer material. Low drug entrapment efficacy has been a major drawback of the fabricated drug encapsulated nanomicelles (Zhang and Zhuo, 2005).

Several micellization methods have been employed to enhance drug entrapment efficacy including solvent evaporation, dialysis, microphase separation, self-emulsion evaporation, oil-in-water emulsion approach and rapid heating procedures (Alexisa et al., 2008; Katz et al., 2012; Wang et al., 2013; Sanna et al., 2014). Drug incorporation into the nanomicelles can be accomplished by integration of the drug during micelle preparation (Vyas et al., 2008). Poly aspartic acid (PAsp) is one of the mainly frequently utilized polyanionic, hydrophobic and biodegradable poly (amino acids). As PAsp contains pendant carboxylic groups, it is pH-sensitive (pKa = 3.9) exhibiting minimal swelling at acidic pH and increased swelling at neutral pH. It is therefore an ideal pH sensitive material for localized delivery of drugs. Several nanomicelles prepared from PAsp-based surfactant copolymers have been evaluated for

various clinical nano-chemotherapeutic platforms (Skarda et al., 1993; Tsubokawa et al., 1994; Giammona., 1996; Giammona et al., 1998; lwata et al., 1998; Li et al., 2008). Poly(*N*-isopropylacrylamide)(PNIPAAm) is a popular hydrophilic thermoresponsive polymer demonstrating a sharp phase transition at temperatures exceeding its lower critical solution temperature (LCST). Previous investigations have utilized poly(*N*-isopropylacrylamide) with polyamino acids as a mixture to formulate inter-penetrating polymer networks (Cammass and Kataoka, 1995; Bonina et al., 2004; Malonnea et al; 2005). In this investigation, the combination of poly(*N*-isopropylacrylamide)-*b*-(polyaspartic acid) (PNIPAAm-*b*-PAsp) was formulated as nanomicelles via dialysis and solvent evaporation techniques for exploitation of their temperature- and pH-responsive capabilities as a tumor-specific controlled delivery system.

The purpose of this work was to enhance the incorporation efficiency of MTX and properties for cancer targeting (i.e. size and drug release capabilities), which could lead to minimization of cytotoxicity of MTX and enhanced therapeutic outcomes, by inclusion of MTX in the nanomicelles utilizing the PNIPAAm-*b*-PASP copolymeric composite to generate a superior antineoplastic chemotherapeutic nanosystem. The PNIPAAm-*b*-PASP nanomicellar formulations were extensively characterized and experimentally optimized for appropriate size, drug incorporation, and controlled MTX release capability. Both PAsp and PNIPAAm have ionic features in aqueous media resulting in polyion compound development involving anionic (negatively charged) MTX, with cationic (positively charged) PAsp forming the inner core of the designed polymeric nanomicelle.

4.2. Materials and Methods

4.2.1. Materials

N-isopropylacrylamide polymer (Sigma Aldrich, St. Louis, MO, USA) was hexane recrystallized, vacuum dried at 20°C and 2, 2'-azoisobutyronitrile was ethanol recrystallized prior to its usage. Aspartic acid, 2-Amino ethanethiol hydrochloride (AET-HCl) and triphosgene were procured from (Sigma Aldrich, St. Louis, MO, USA), vacuum dried at 20°C; and methotrexate (MTX) was also procured from Sigma Aldrich (St Louis, MO, United States of America). 98% *N,N'*- dimethylformamide (DMF), Tetrahydrofuran (THF), ethyl ether and petroleum ether (30–60 °C) were obtained from Merck SA. All other reagents and organic solvents were of analytical grade prior to their usage.

4.2.2. Determination of Critical Micelle Concentration of PNIPAAm-*b*-PASP

The optimized PNIPAAm-*b*-PASP copolymer formulation was utilized for the synthesis of micelles. Formation of the micelle employing PNIPAAm-*b*-PASP copolymer was studied by fluorescence spectroscopy. Here, FITC was used as an extrinsic fluorescent hydrophobic probe molecule, and the CMC was determined from the fluorescence emission wavelength and excitation spectra as FITC partitions between the aqueous and micellar milieus. Briefly, FITC (10^{-6} - 10^{-7} M) in methanol was introduced to a series of glass test tubes and the methanol was air evaporated. Deionized water (10ml) with different concentrations of the block copolymer from 0.05 to 1 g/mL was introduced to each test tube and the solutions were incubated for 24 hours at room temperature under mild mixing. Subsequently, the fluorescence of each sample was measured utilizing a fluorescence spectrophotometer (Cecil 9000 series, Cambridge, England, UK). Emission spectra were determined at 390 nm (I_1) and 310 nm (I_3), whereas the excitation wavelength was set at 400 nm. The FITC fluorescence intensity ratios of I_3/I_1 as a function of the copolymer concentration in the FITC emission spectra are shown in Figure 4.2. The critical micelle concentration (CMC) was calculated by obtaining the midpoint of the block copolymer ratio at which the relative intensity ratio (I_1/I_3) changed (Figure 4.2).

4.2.3. Formulation of the Methotrexate-encapsulated PNIPAAm-*b*-PASP nanomicelles

Nanomicelle formation with MTX incorporation into the nanomicelles was achieved employing a solvent evaporation method – this approach yielded enhanced drug entrapment compared to the dialysis approach employed in preliminary investigations. In dialysis tubing method, MTX (7mg) and 10-125mg PNIPAAm-*b*-PASP copolymer were dissolved in 4mL *N,N'*-dimethylformamide (DMF) with mild magnetic stirring at 25°C for 30 min (Figure 4.1). Deionized water (6 ml) was added dropwise to the solution with homogenization at various speeds (300-2000rpm) on a homogenizer machine ((Virtis Tempest I.Q. 2 Homogenizer, Sentry Microprocessor, Kent City, MI) for 5 minutes at room temperature. Thereafter the solutions were introduced into a dialysis tubing (molecular weight cut-off: 3500kDa) and dialyzed with two litres of deionised water at 10 °C for 6 hours. During dialysis tubing procedure, deionised water was replaced every two hours to get rid of DMF (Figure 4.1). The nanomicellar suspension was filtered to eliminate agglomerates (0.45µm Millipore filter, Billerica, United States of America) and lyophilized to yield a powder (FreeZone® 2.5, Labconco®, Kansas City, MS, USA). Furthermore, solvent evaporation method was fabricated in the same manner as the dialysis tubing method except that the solvent was removed by a rotary vacuum evaporator.

A Face-Centered Central Composite design (CCD) approach was developed for optimization of the effect of pertinent MTX-encapsulated nanomicelle formulation variables on selected response. CCDs are highly systematic and flexible, providing considerably information on experimental variable influence and overall investigational error in a least number of significant runs. The accuracy of various varieties of CCDs supports their use under varied experimental settings of focus and operability. CCDs consists of an embedded factorial or fractional factorial design with central points augmented with clusters of star points (axial points) that allow evaluation of curvature of the response of the formulation variables to the outcome hence providing an idea of the response surface and allowing evaluation of interactions (Hu et al., 2008). In the present study, the amount of copolymer (mg) and homogenizer speed (rpm) were the two selected variables; and size, drug entrapment efficacy (DEE), mean dissolution time (MDT) and cumulative release were selected as responses (Table 4.1), central points were run 6 times for generation of the 13 experimental design nanoformulations employing Minitab V15 software (Minitab® Incorporation, PA, USA) (Table 4.2).

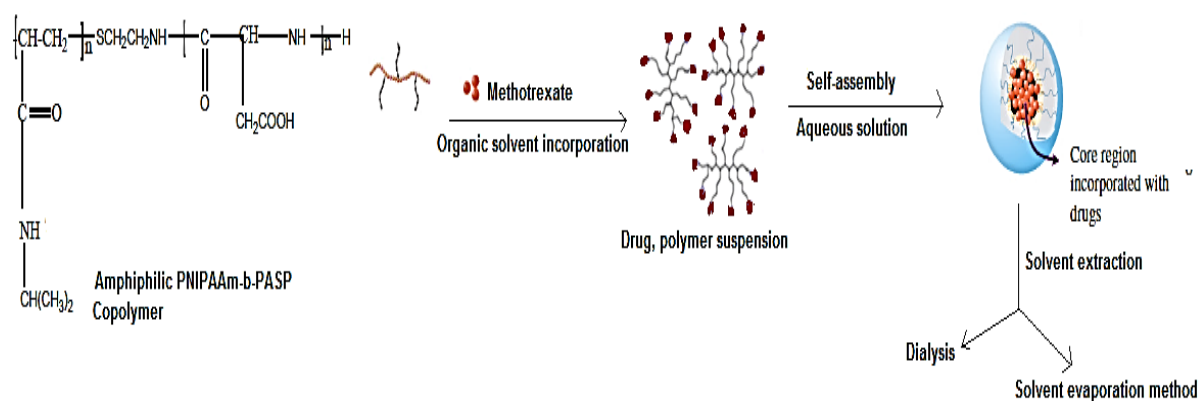


Figure 4.2: Schematic of amphiphilic PNIPAAm-b-Pasp copolymer assemblage in aqueous media to form spherical nanomicelles.

Table 4.1: Nano-formulation variables and responses employed in design

	Levels		Objective
	Upper	Lower	
Parameters			
Copolymer amount (mg)	125	10	
Homogenizer speed (rpm)	2000	300	
Responses			
Size			Minimize
DEE			Maximize
*MDT			Minimize

* MDT: Mean Dissolution time

Table 4.2: Depiction of the 3² factor central composite design for micelle formulation

Formulation number	Copolymer amount (mg)	Homogenizer speed (rpm)
1	67.5	1150
2	67.5	1150
3	67.5	1150
4	125	1150
5	67.5	1150
6	10	2000
7	125	2000
8	67.5	1150
9	10	300
10	67.5	2000
11	67.5	300
12	125	300
13	10	1150

4.2.4 Characterization of Nanomicelles

Micelle size, zeta-potential and polydispersity index (Pdl) were determined as previously described in Chapter 3, Section 3.2.7 employing active dynamic beam scattering (DLS) on a Zetasizer NanoZS instrument (Malvern Instruments (Pty) Ltd., Worcestershire, UK). The drug entrapment efficiency (DEE) and *in vitro* release of MTX from the nanomicelles were also measured as previously described in Chapter 3, section 3.2.8. and 3.2.13.

4.2.5. Optimization of the Nanomicelle Formulation

Following generation of the polynomial equations relating the dependent and independent variables, the formulation process was optimized under constrained conditions for the responses. Simultaneous equation solving for optimization of the formulation process was performed to obtain the levels of independent variables for enhancing the performance of the nanomicelle system employing Minitab® V15.

4.2.6. Characterization of the Optimum Nanomicelle Formulation

4.2.7. *In vitro* Kinetic evaluation of drug release from the optimum nanoformulation

Modeling of drug release kinetics was determined by substituting drug release data in Equations 3.4-3.8, being Zero Order, First Order, Higuchi model, Hixson Crowell and Korsmeyer Peppas kinetics release equations as previously described in Chapter 3, section 3.2.14.

4.2.8. Fourier Transform Infrared spectroscopic characterization of the Nanomicelle Molecular Arrangement

Methotrexate-loaded and blank nanomicelles formulations were investigated and compared via Fourier Transform Infrared spectroscopic analysis employing a PerkinElmer® Spectrum 100 Series fitted with a universal ATR Polarization Accessory (PerkinElmer Ltd., Beaconsfield, UK). Spectra were recorded over the range $4000-625\text{cm}^{-1}$, with a resolution of 4cm^{-1} and 32 accumulations.

4.2.9. Nanomicelle morphological characterization

The morphology of the nanomicelles was investigated utilizing scanning electron microscope (SEM; Joel JSM-840, Japan) and transmission electron microscopy (TEM, JEM-100S, JOEL Pty Ltd, Tokyo, Japan). Samples for TEM were prepared by placing one drop of the micelle suspension onto a film coated carbon copper grid. Excess suspension was wiped-away with the filter paper, and the copper grid was air dried for a day. The sample on the grid was not stained. Sample analysis was conducted utilizing TEM instrument (JEM-100S, JOEL Pty Ltd, Tokyo, Japan) at an accelerating voltage of 100 kilovolts (kV). Prior to SEM analysis, a drop of micelle suspension were fixed on a sticky carbon tape on aluminium stumps and were gold-platinum sputter coated for seven minutes. The micelle specimen was observed via SEM at accelerating voltage of 20 kV at several magnifications.

4.2.10. Differential scanning calorimetry for elucidation of thermal events of the methotrexate-loaded nanomicelles

Differential Scanning Calorimetry (DSC) studies were conducted employing a Mettler-Toledo advanced DSC 1 STARe instrument (Ohio, USA). The Mettler-STARe software program (version-9.x), was utilized for DSC results acquisition and interpretation. A blank specimen pan was used as point of reference and investigational scans were conducted by warming the weighed samples from -10°C - 125°C with a stable isotherm for fifteen minutes. The lyophilized powder specimens (10mg) were placed into a DSC aluminium-pan and compressed sealed. Relative DSC scans were conducted on blank micelles, optimized MTX-loaded micelles and pure MTX at a heating rate of $10^{\circ}\text{C}/\text{minute}$ from -10 - 325°C in a stable stream of nitrogen gas. Fresh sample analysis was conducted in triplicate for method development and validation purposes. DSC thermograms were then evaluated for changes in thermal episodes. The phase changes of the drug-free micelle and MTX were correlated with the phase changes of the optimized MTX-loaded PNIPAAm-*b*-PASP nanomicelles.

4.3. Results and Discussion

4.3.1 Critical Micelle Concentration Determination

As for a surfactant, the self-aggregation of amphiphilic polymer is initiated as the concentration of the copolymer reaches the verge/threshold concentration (CMC); therefore, the CMC is a significant parameter in displaying the self-aggregation capability. The CMC values of the optimized PNIPAAm-*b*-PASP micelles were determined by using the FITC fluorescence probe technique. FITC is a molecular fluorescent probe with the intensity ratio of the first crest (390 nm) and the third crest (290 nm) I_1/I_3 in its emission spectrum very responsive to the ionic charge of the solution. Thus, the fluorescence intensity ratio- (I_1/I_3) would reveal a noticeable change. The typical fluorescence spectra of PNIPAAm-*b*-PASP micelle with intensifying micelle concentration are depicted in Figure 4.2a. Figure 4.2b displays the intensity ratio (I_1/I_3) of the FITC excitation spectra versus concentrations of PNIPAAm-*b*-PASP copolymer. The CMC is the midpoint of PNIPAAm-*b*-PASP micelle concentration at which the I_1/I_3 intensity ratio considerably decreases and was determined to be 0.09mg/mL.

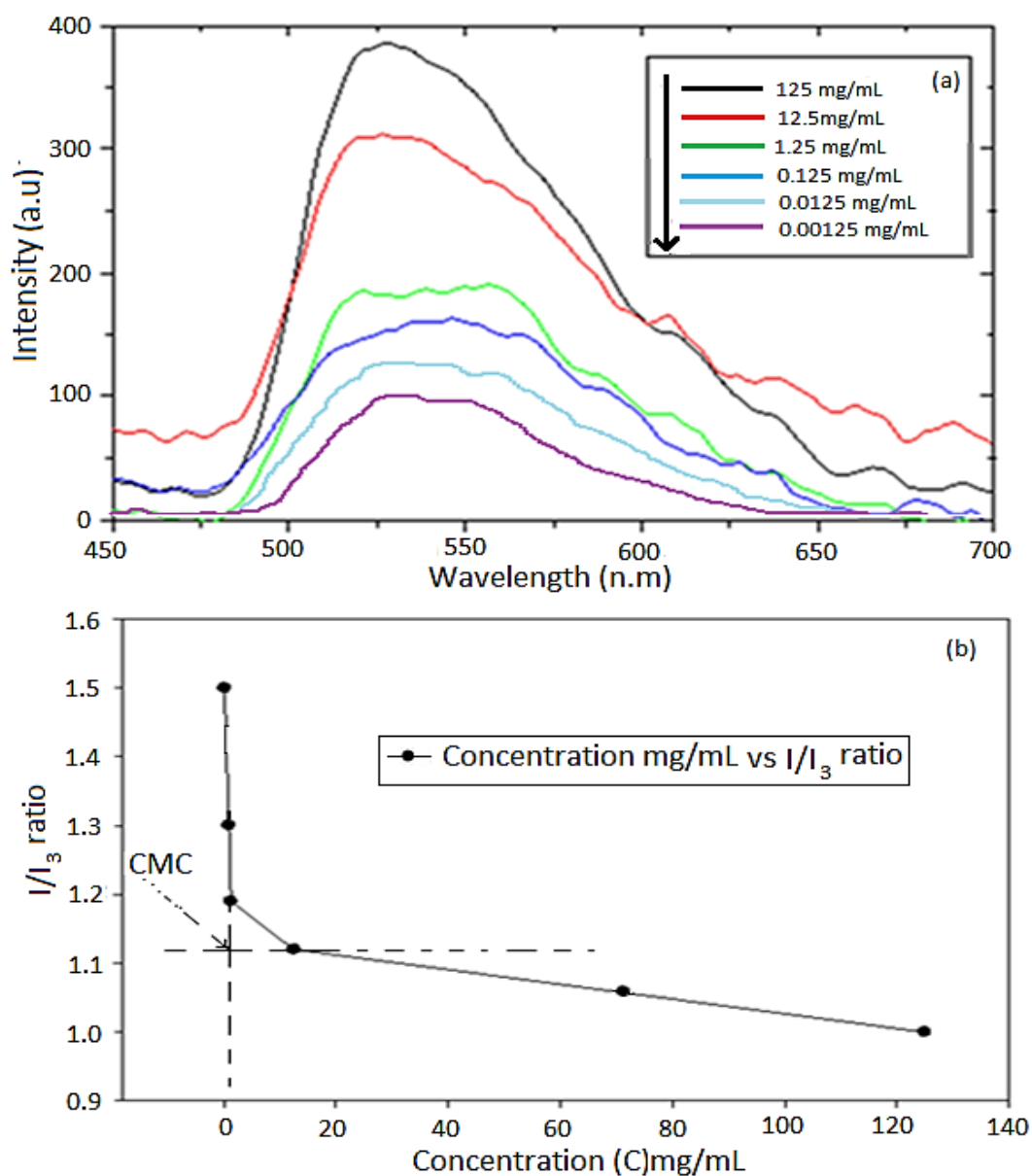


Figure 4.3: (a) FITC emission spectra of PNIPAAm-*b*-PASP solutions. (b) I_{1390}/I_{290} intensity ratio for FITC as a function of the concentration of PNIPAAm-*b*-PASP copolymer in deionized water. The CMC was obtained as the midpoint value of copolymer concentration at which the $I_{1/13}$ intensity ratio considerably decreases.

4.3.2. Analysis of the Experimental Design Formulations and Statistical Optimization of the PNIPAAm-*b*-PASP Nanomicelles

The purpose of this study was to synthesize MTX-loaded nanomicelles by solvent evaporation method, and to optimize the influence of independent variables on formulation responses. The solubility and partitioning features of MTX in the PNIPAAm-PASP copolymer were highly influential in the selection of the organic solution employed. Formulation of therapeutic-loaded nanomicelles involved two major methods of therapeutic loading reliant on physicochemical features of segment copolymer. The dialysis tubing technique was initially employed to

prepare the experimental design PNIPAAm-*b*-PASP polymeric micelles and exhibited satisfactory encapsulation of MTX into the copolymer (Optimised). The exchange flow of water and organic solvent into the composite MTX-PNIPAAm-*b*-PASP system determined the development of the nanomicelles. From the resultant responses for the various dialysis methods nano-formulations, the target-particle size, MTX-entrapment efficiency, and the MDT were utilized for the optimization procedure (Table 4.3). The optimized nano-emulsion was generated as per the variable levels in Figure 4.4 and possessed a size of 65nm, MDT of 40.867, and a DEE of 80.6%.

Table 4.3: Responses data obtained for the 3² factor central composite experimental design micelle formulations.

Formulation number	Size (nm)	DEE (%)	MDT	Cumulative release at 72 hrs (%)
1	76.45	73.2	40.609	0.277
2	57.66	72.9	41.276	0.289
3	66.64	73.1	40.776	0.278
4	66.33	84.8	39.031	0.259
5	63.23	82.6	41.943	0.283
6	78.63	70.7	37.489	0.238
7	66.35	89.8	25.214	0.242
8	68.11	73.8	39.276	0.281
9	63.21	76.4	40.393	0.266
10	60.13	77.5	39.014	0.249
11	52.46	86.7	38.727	0.249
12	57.8	73.6	40.251	0.258
13	51.67	86.7	41.503	0.263
Optimized (O)	65	65.3	40.867	0.261
Optimized 1 (O1)	65.0	80.6	40.000	0.264

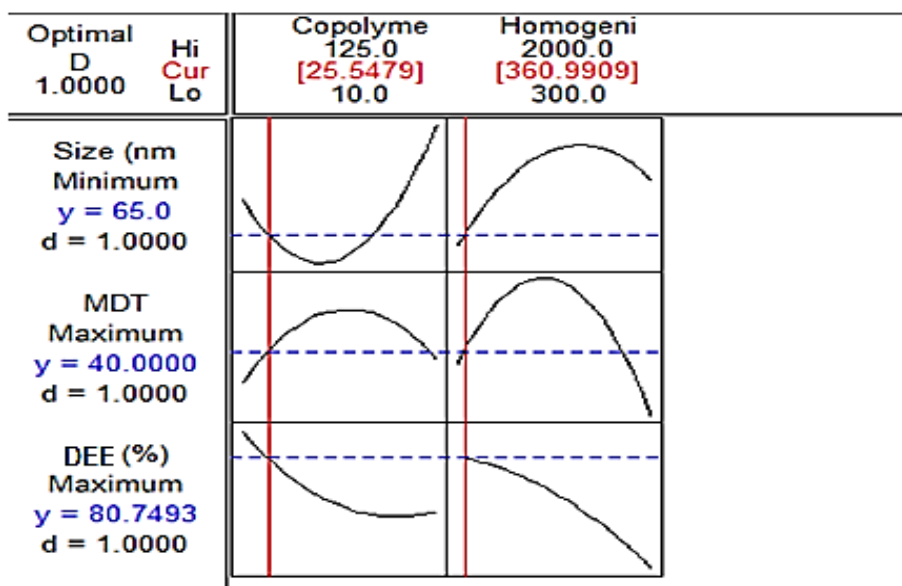


Figure 4.4: Desirability graphs for optimized showing the crucial variables for generating PNIPAAm-PAsp micelles with the desired targeted responses.

4.3.3. Influence of independent variables nanomicelle size, incorporation efficiency and drug release

Micelle size is a prime factor since it influences the MTX encapsulation, therapeutic release, and ultimately site-specific release of methotrexate across the reticular endothelial system (RES) as previously discussed in Chapter 3, section 3.3.6. The micelle size obtained from the optimized nanomicelles was 65 nm and remained the same upon utilization of solvent evaporation method to further enhance the MTX entrapment efficacy (Figure 4.5& 4.6). For intraperitoneal chemotherapeutic interventions, the size of the optimized nanomicelles would be favorable for dissemination into the tumor-cellular structure with pore size of 100nm or less at the site of treatment. The RES penetration also has to be taken into consideration as nanomicelle with a size greater than 100nm may not be able to escape through the RES. Response surface analysis as visualized via the surface plots highlighted that nanomicelle size was lowest at median copolymer amounts; these levels being optimal for formation of small and compact micellar structures (Figure 4.6).

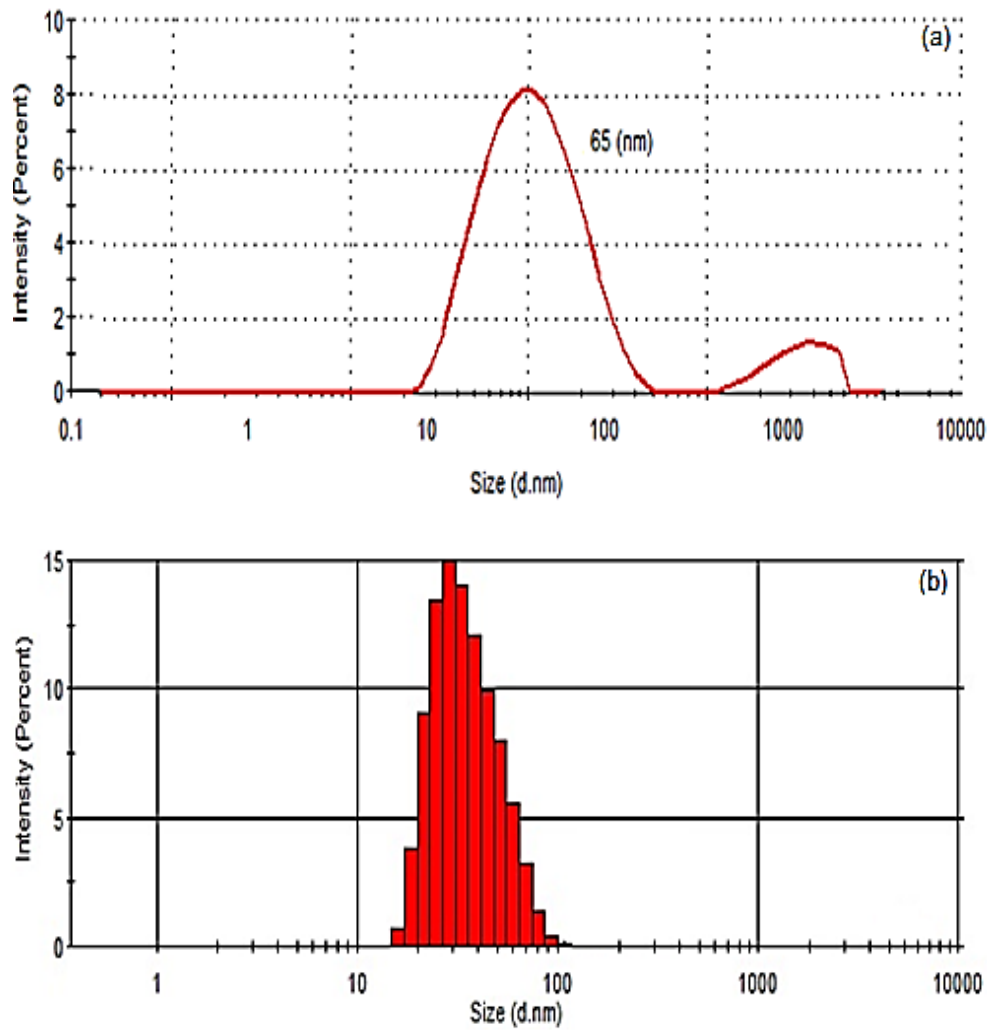


Figure 4.5: (a) Zeta size graphs illustrating the hydrodynamic size of PNIPAAm-b-PASP nanomicelle formulation, (b) size intensity distribution for the optimized monotype PNIPAAm-b-PASP nanomicelle.

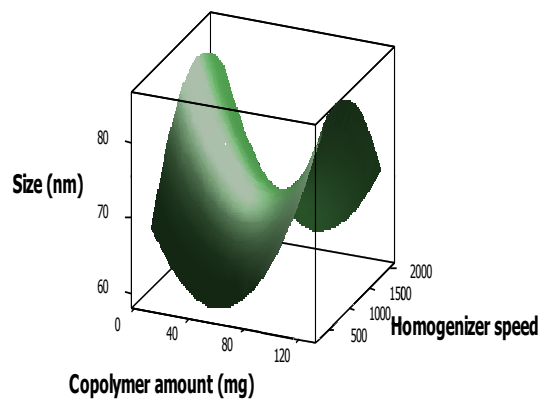


Figure 4.6: Three dimensional surface graphs produced by the 3^2 factor central composite experimental design approach investigating the influence of copolymer amount and homogenizer speed on size of the synthesized nanomicelles.

The mean zeta-potential values of the experimental design nanomicellar formulations did not vary greatly and ranged from -0.02383mV to -1.89mV . These zeta potential values showed that the MTX-encapsulated PNIPAAm-*b*-PAsp nanomicelles were only partially stabilized by electrostatic forces but may have high propensity of aggregation outside the designated parameters as previously discussed in Chapter 3, section 3.3.6. Design of a nano-enclathrating neurodeformable polymeric carrier could be employed for stabilization and delivery of the nanomicelles to the tumor site.

Nanomicelle formulations from the experimental design exhibited good MTX encapsulation efficiency (Table 4.4) due to the amphiphilic PNIPAAm-*b*-PAsp copolymer self-assembly in water effectively forming micelles while incorporating chemotherapeutic drug (MTX) in their interior core (Chung et al., 1997). The encapsulation was greatest when a greater amount of copolymer was used in combination with a high homogenizer speed during nanomicelle formation. Slower drug release (a lower MDT) was achieved when high levels of copolymer were employed and a high homogenizer speed was used, which correlated with the variable settings for attaining enhanced MTX incorporation. The interaction between these formulatory variables had a significant effect on the MDT ($p = 0.042$). An increased amount of copolymer better entrapped the drug within the core, while providing a more compact micellar structure, following contraction of the PNIPAAm component of the nanomicelle in response to temperature, for controlling MTX release to a greater extent.

4.3.4. Statistical optimization of the Face-Centred Central Composite Design

Statistical regression (average least squares) was utilized to fit the results by predicting the influences of the independent variables [Copolymer amount (mg) and Homogenizer speed (rpm)] on responses (size, DEE and MDT) such that the sum of squared variations between estimated and experimental responses was reduced by optimization Eq 4.1 and Table 4.4. The standard inaccuracy of the model (S) and the R^2 coefficient value of the proposed model showed the goodness of fit the mathematical model outlined in Table 4.5. Polynomial regression equations produced for size, DEE, MDT and cumulative release are as depicted by polynomial Equation 4.1, Table 4.4 and Table 4.5. Output response

$$Y = c + fX_1 + gX_2 + hX_1 X_2 + iX_1^2 + jX_2^2 \quad (4.1)$$

Table 4.4: Coefficients for equations, r² value for several dependent variables of methotrexate loaded PNIPAAm-b-ASP micelles

Coefficients	Coefficient data for dependent variables			
	Size	MDT	DEE	Cumulative Release
c	62.4211	35.1010	85.2222	0.246508
f	-0.4456	0.0988	-0.1811	0.000256
g	0.0385	0.0107	-0.0030	0.000046
h	0.0043	-0.0005	0.0007	-0.000003
i	-0.0000	-0.0000	-0.0000	0.000000
j	-0.0001	-0.0001	0.0001	0.000000
r²	62.2	81.3	33.0	82.3

Table 4.5: Model S-values and the coefficient of determination (R²) data acquired for the linear regression equations

	Size	MDT*	DEE	Cumulative Release
S	7.979	2.435	7.027	0.008557
R²	62.2	81.3	33.0	82.3

Mean Dissolution Time = , MDT* = Average/Mean Dissolution Time

The Mean Dissolution Time (MDT) was calculated for each of the formulations using Equation 4.2 and a maximum MDT is the fastest drug release rate achievable (Govender et al., 2005).

$$MDT = \sum_{i=1}^n t_i \frac{M_t}{M_{\infty}} \dots \dots \dots 4.2$$

Where M_t is the fraction of dose released in time (t_i = t_i + t_{i-1})/2 and M_∞ corresponds with the loading dose.

Following generation of the polynomial equations (Eq 4.1) relating the dependent and independent variables, the formulation process was optimized under constrained conditions for the responses (as previously discussed in section 4.2.5 of this chapter). Simultaneous

equation solving for optimization of the formulation process was performed to obtain the optimal levels of independent variables for enhancing the performance of the nanomicelle system employing Minitab® V15 as summarized in Table 4.1. Table 4.6 presented the obtained values for the responses with the optimized formulation as well as the predicted values and desirability.

Table 4.6: Summary of the obtained values for each of the responses and the predicted values and desirability.

Response	Obtained	Predicted	Desirability
Size	65	65.5	1.0000
MDT	40	42.4	40.0000
DEE	80.7493	84.622	1.0000

The lower model S-value implies the improved combination/fit of the model. The model S-value for size is relatively small and the model-R² coefficient value also indicates the good fit of this mathematical model (Table 4.5). MDT has a lower fit with a smaller R² coefficients, and DEE values were also combination. A significant p value ≤0.05 indicated that the expected influence of the independent variable can be regarded to be of significance (Table 4.7).

Table 4.7: Probabilities of the effects of the variables on the outcomes

Term	p-value			
	Size	MDT	DIE	Cumulative Release
Copolymer Amount (mg)	0.088	0.193	0.390	0.232
Homogenizer speed (rpm)	0.055	0.074	0.843	0.039
Copolymer Amount (mg) *				0.078
Copolymer Amount (mg)	0.021	0.277	0.603	
Homogenizer speed (rpm)*				0.009
Homogenizer speed (rpm)	0.091	0.070	0.759	
Copolymer Amount (mg) *				0.304
Homogenizer speed (rpm)	0.213	0.042	0.163	

4.3.5. Statistical analysis of the residual error in the experimental design

Analysis of the residual error is of significant consideration in the establishment of the cumulative release, size, mean dissolution time (MDT) and drug entrapment efficacy (DEE) of an investigational design. Figure 4.7 display a variety of residual graphs that necessitate evaluation. The standard probability graphs (a-d) for all the responses demonstrated fairly accurate straight lines indicative of normal residuals dispersion. The normal residuals against fitted distributed graphs (e-h) exhibited arbitrary dispersion of the residuals around 0 as

anticipated. This graph offers detection of non-stable variation, with absence of upper order terms and outer parameters. None of these observations were encountered in the fitted plots. Residual graphs against the data order are utilized to establish the time reliance of the residuals. The plotted graphs (i-l) showed no lucid pattern indicative of a lack of reliance. Histograms, fitting residuals versus frequency (m-p) were inconsistent; some were bell-shaped curves (m-n), but others were not bell-shaped (o-p) and seemed to be indicative of existence of outliers (i.e. big residuals data points). Since the specimen size is diminutive (<65) a histogram is not regarded as the premium option in the assessment of normality and the normal probability graphs is highly responsive.

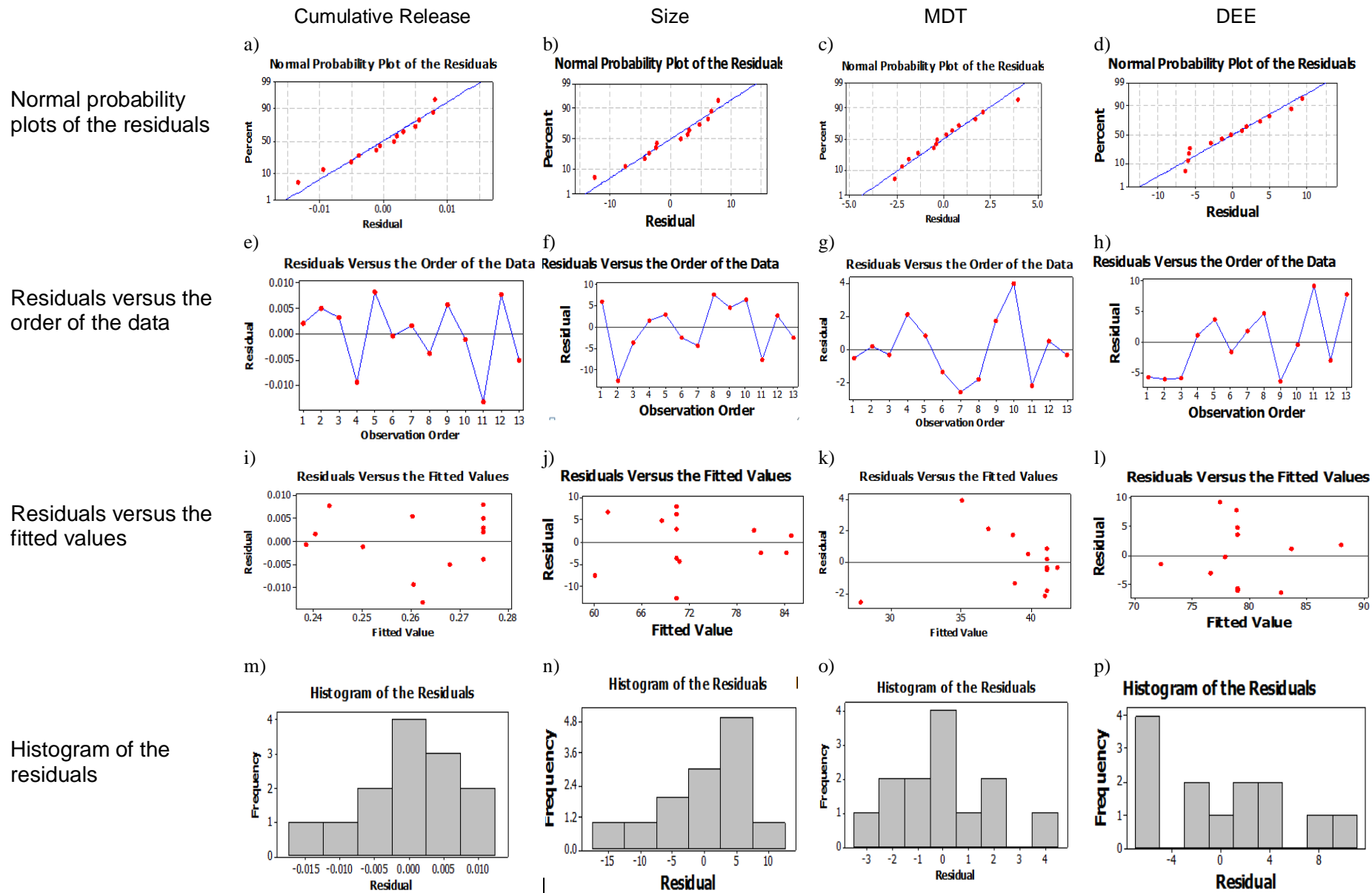


Figure 4.7: Residual graphs of the data for cumulative release, size, MDT and DEE for the micelle nano-emulsions.

4.3.6. Characterization of the Optimized Nanomicelle Formulation

4.3.7. Molecular transitions of the PNIPAAm-*b*-PAsp nanomicelles

The FTIR spectra of the MTX, blank micelles and MTX-loaded optimized nanomicelle formulation were compared. Variations were noticeable in FTIR spectra involving the blank micelles and MTX-loaded micelle nanoformulations (Figure 4.8). The additional peaks that were noted in the MTX-loaded nanoformulations compared to the drug-free micelles were due to the existence of a 1,3 replacement composite ($1516.53\text{--}1451.23\text{cm}^{-1}$) and a phenyl amino compound ($1647.22\text{--}1451\text{cm}^{-1}$). This indicated that MTX was entrapped in the nanomicelle hydrophobic interior core either by weak electrostatic H-bonds involving the COO-assemblage of MTX and the OH-grouping of aspartic acid, or by charged ionic attachments involving the NH_2 bonds of MTX and the COO-bonds existing in PNIPAAm-*b*-PAsp. This enabled effective MTX incorporation and controlled diffusion from the PNIPAAm-*b*-PAsp matrix (potentially in the amorphous form).

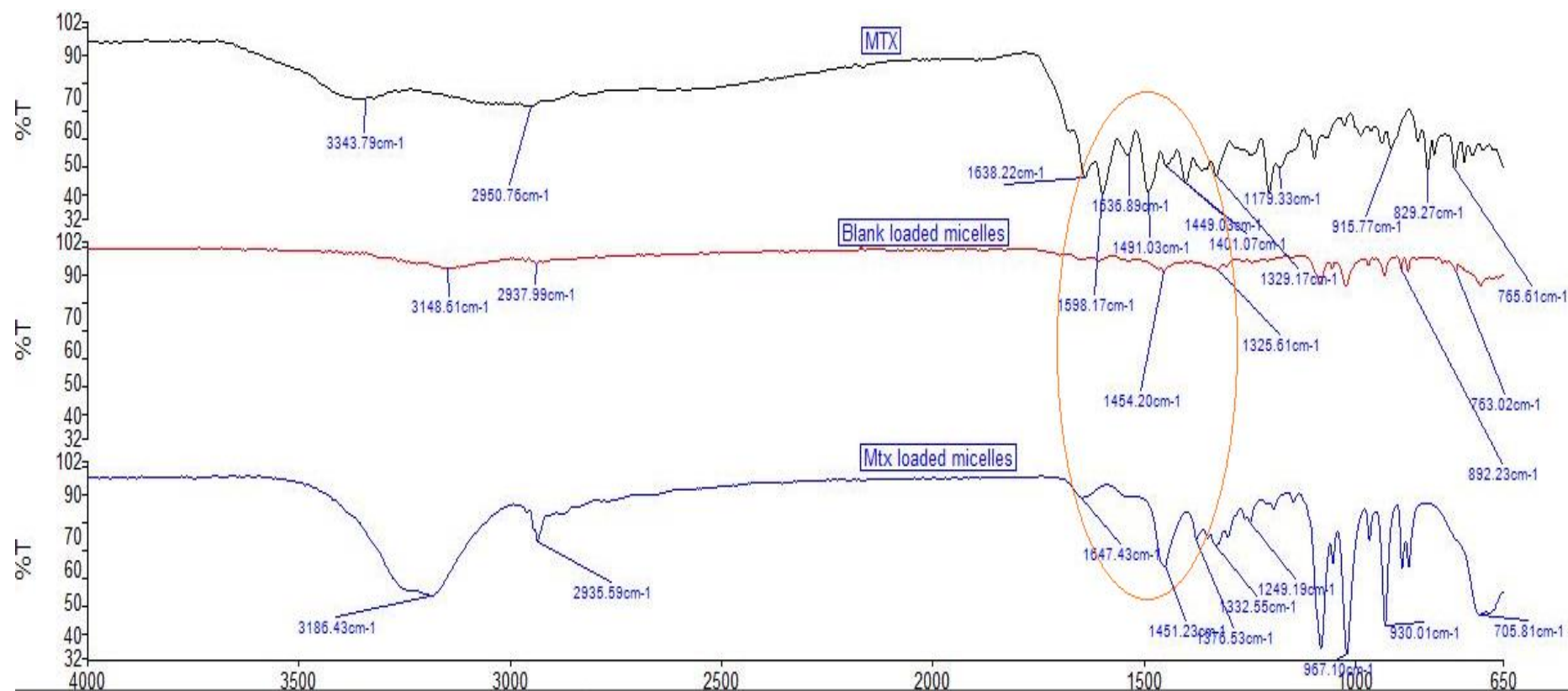


Figure 4.8: FTIR spectrum of MTX, blank micelles and MTX- loaded PNIPAAm-b-PAsp nanomicelles depicting the variations in the spectra.

4.3.8. PNIPAAm-*b*-PAsp micelle morphological characterization

Scanning electron micrographs were utilized to describe the nanomicelle surface morphology (Figure 4.9a). The SEM images also displayed micelle agglomerates that were attached onto an even plane (Figure 4.9a). TEM imagery showed the development of amphiphilic nanomicelles with an outer lighter hydrophilic shell and inner darker (more intense) hydrophobic core structural arrangement (Figure 4.9b). In addition, it was also observed that all specimens were spherical with a smooth outer shell with a size distribution in congruence with the data attained through active-dynamic beam scattering (DLS) measurements. These darker inner portions were ascribed to the PAsp segment of the block-copolymer and the electrostatically-encapsulated MTX and the lighter outer shell represented the hydrophilic groups of PNIPAAm (Figure 4.9b). This type of hydrophobic–hydrophilic arrangement of PNIPAAm-*b*-PAsp nanomicelles has a significant function in offering prolonged blood distribution periods since the PNIPAAm hydrophilic exterior of the nanomicelles creates a barrier to impede the identification of the nanomicelles the by immune system which consequently diminish their uptake in the RES (Qiao et al., 2010; Owens III & Peppas, 2006).

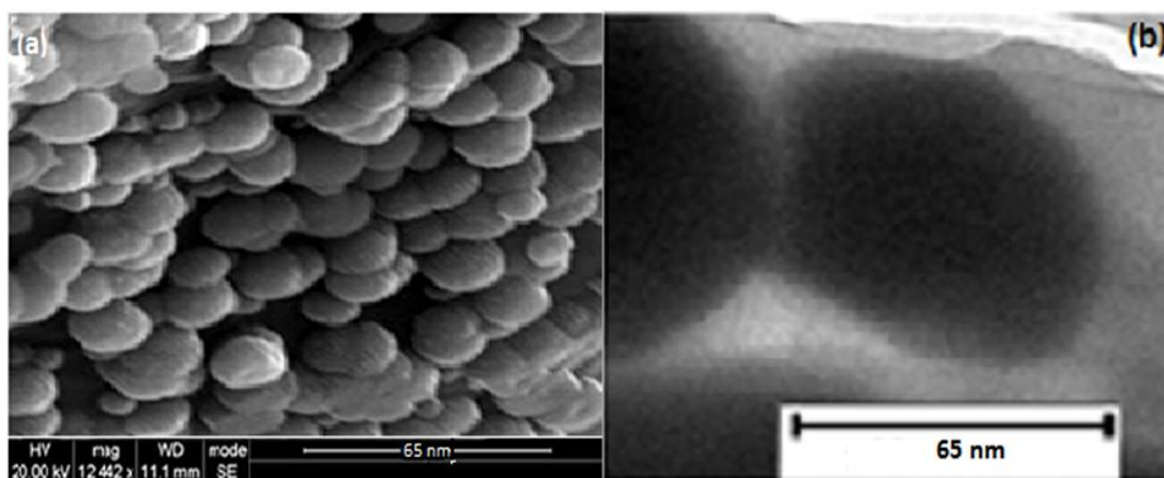
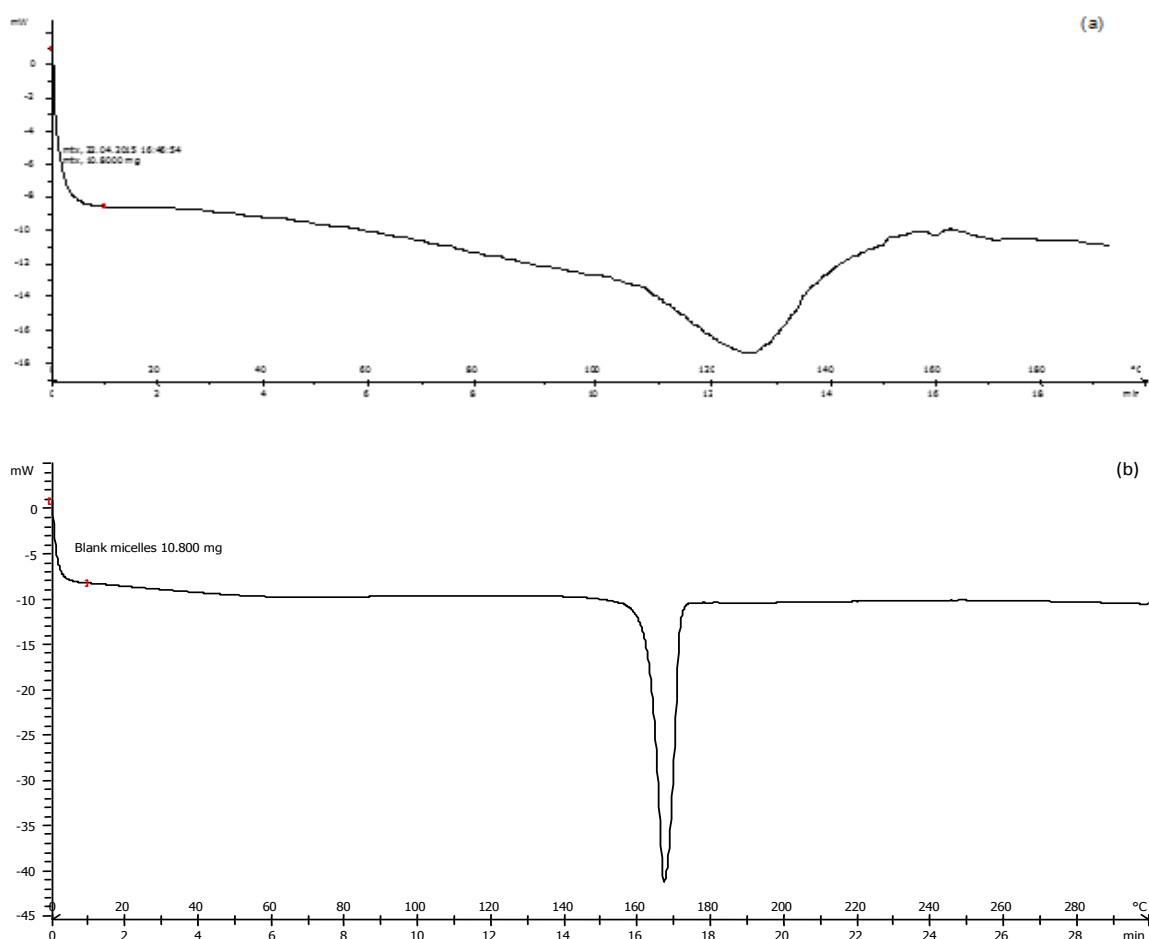


Figure 4.9:(a) Scanning electron microscopy (SEM) image showing the shell morphology of the optimized PNIPAAm-*b*-PAsp nanomicelle formulation with average size of 65nm and (b) TEM images depicting of the optimized spherical MTX-loaded PNIPAAm-*b*-PAsp nanomicelle formulation, also with average size of 65nm.

4.3.9. Analysis of the thermal features of the drug-free and MTX-loaded PNIPAAm-*b*-PAsp nanomicelles

Differential scanning calorimetric investigations were conducted to observe the drug's physical form in the nanomicelle, since this could affect the drug release from the delivery system. DSC thermograms of MTX, blank micelles and MTX-loaded micelles are depicted in Figure 4.10. The DSC curve of the MTX displayed a critical melting peak at 125°C. MTX-loaded micelles displayed the melting peak for the drug at 145°C. Incorporation of MTX within the nanomicelle thus elevated the melting point indicative of enhanced thermal stability of the drug as previously observed (Vadia and Rajput, 2012). This would suggest that on incorporation of the partially soluble crystalline MTX within the hydrophobic core it was converted to a less crystalline form and resulting in improved MTX entrapment efficacy of $80.6 \pm 0.3\%$. The glass transition temperature (T_g) of the copolymeric nanomicelles is also evident at $\sim 150^\circ\text{C}$, correlating with previous findings (Liu et al., 2012).



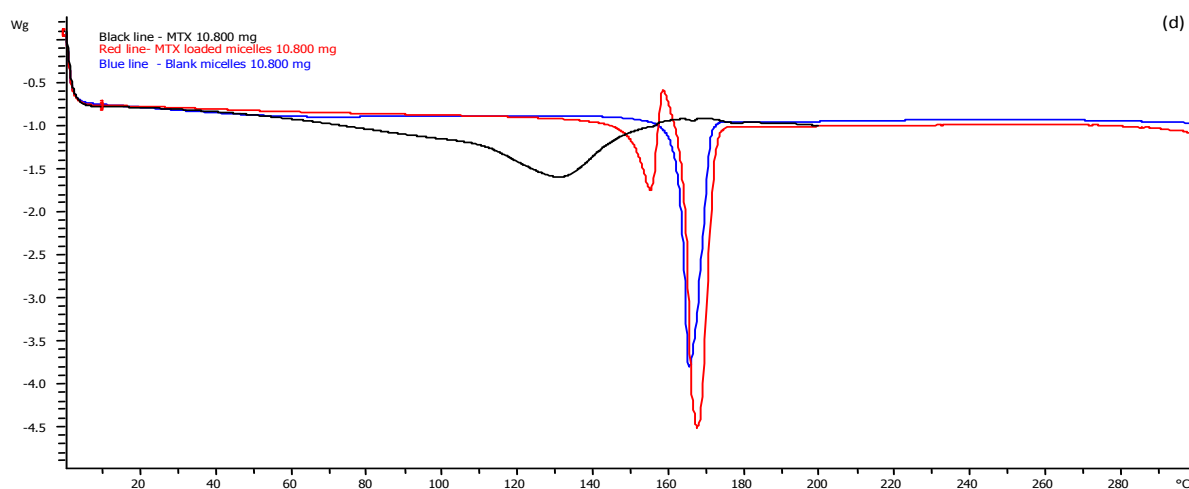
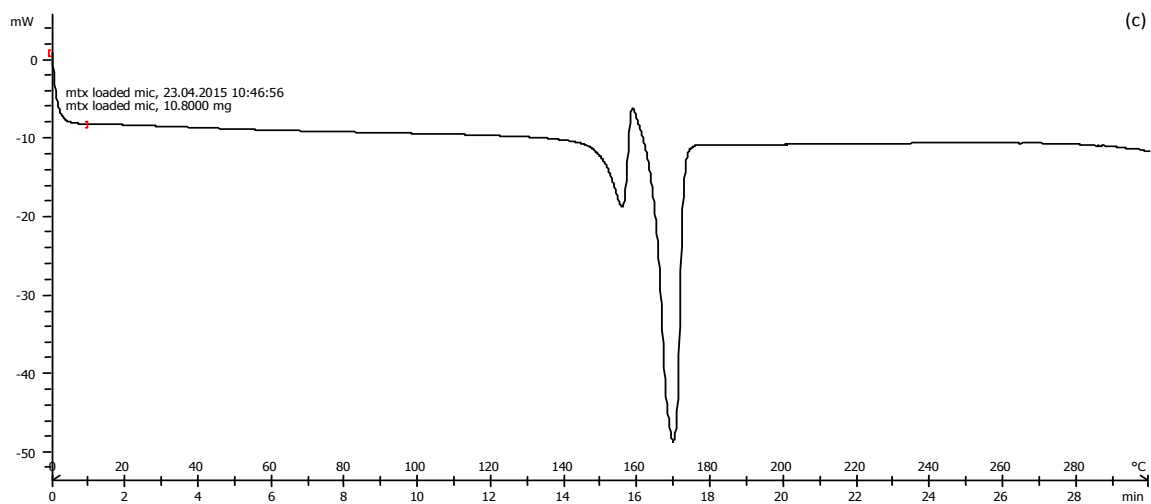


Figure 4.10: DSC thermograms of (a) pure MTX (b) blank micelle nanoformulation (c) MTX-loaded micelle formulation and (d) temperature variations and shifts in the curves of MTX, blank micelles and MTX-loaded micelles.

4.3.10. Methotrexate release behavior from the optimized nanomicelle under normal and tumoral conditions

MTX release from the optimized nanomicelles was performed at physiological pH (7.4) and tumoral pH (6.75) (Figure 4.11). A pH of 7.4 also represents the intracellular pH of tumor cells and release behavior at this pH would thus also be demonstrative of release from the nanomicelle following tumor cell uptake. The size of the nanomicelles as well as responsiveness to the tumoral microenvironment is pertinent for achieving targeted delivery to the tumor site. Release profiles revealed controlled release of MTX from the optimized micelle nano-formulation. The basis of MTX release was to a certain level regulated by the distinctive performance of the essential constituent amphiphilic polymers in the release medium. One of the smartest attributes of PNIPAAm synthesized micelles as therapeutic nano-carriers is their thermosensitivity to surface temperature transitions. The nanomicelle

release results displayed that temperature transitions of the release medium served to control and prolong therapeutic release. PNIPAAm is water soluble at room temperature; however, LCST of PNIPAAm (32°C), it is more likely to gel with a transition temperature very similar to the body temperature, with predominance of the hydrophobic interactions. Further, the presence of the hydrophobic aspartic acid monomer results in a potential LCST decrease. Thus, at temperatures below LCST, the hydrogen bonds predominate between the polymer amide groups. At temperatures exceeding the LCST of PNIPAAm the hydrogen bonds could dissociate with the nanomicelles expelling water, dehydrating and becoming more hydrophobic, thus contracting or shrinking (shielding effect) to allow the MTX from the core through the outer PNIPAAm cloud, while controlling the release rate at the same time (Almeida et al., 2012). The release of MTX was controlled over the 72 hours period of observation (Figure 4.11).

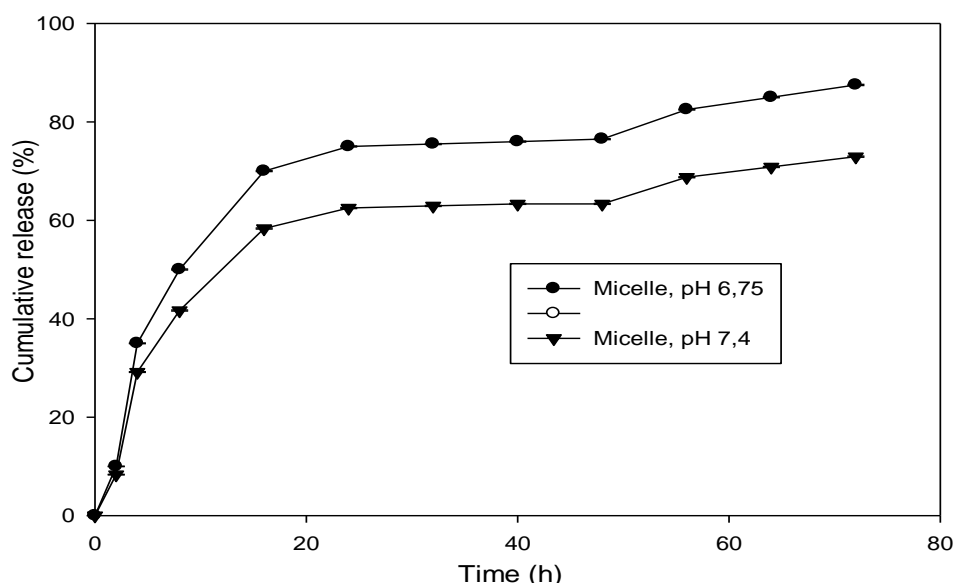


Figure 4.11: Methotrexate release from the optimized PNIPAAm-*b*-PASP copolymeric nanomicelles in acidic (pH 6.75, ie tumor simulated micro-environment) at 38 °C and normal physiological conditions (pH 7.4) at 37 °C. Each point depicts mean \pm SD (n=3).

In the pH 6.75 tumor milieu, approximately 40% of MTX release was observed from nanomicelles in the initial first 10 hours at 37°C due some swelling of the PAsp core of the PNIPAAm-*b*-PAsp nanomicelle in concert with contraction of the PNIPAAm, compared to at pH 7.4 when ~50% MTX release has occurred due to further swelling of the PAsp component of the micelle. Several therapeutic nanocarrier systems have been formed to regulate the MTX release, however in PNIPAAm-synthesized micelles, sustained release for prolonged periods is still a challenge. Notably, the new PNIPAAm-*b*-PAsp as a therapeutic nanocarrier extends the release period to 72 h with the released quantity limited by temperature and pH transitions.

As established, temperature-sensitive polymers such as PNIPAAm are not easily degraded, and this is one of the hurdles in employing these polymers in nanomedicine. The peptide-connection of the poly(L-aspartic) sequence can be deformed to safe monomer chains by enzymatic degradation. Thus, the bio-adjustability and deformability of the PAsp has potential to enhance the degradation of the biopolymer material.

The design of a controlled/sustained-release nanoparticulate system as demonstrated from the release profile achieved from the nanomicelle is proffered as an effective and efficient therapeutic tool for spatio-temporal local drug delivery, for a few major reasons. Firstly, nanosized systems can enhance drug uptake into the tumor, thus reducing systemic toxicity by avoiding drug delivery to non-malignant tissue. Secondly, the nanomicelle can provide controlled and sustained drug release into the tumor cells for a long period of time, leading to increased drug effectiveness and decreased dosing frequency. Ultimately, this nanomicellar system can circumvent drug resistance (Lin et al. 2015). Hence, the PNIPAAm-*b*-PASP copolymeric micelles show potential as degradable therapeutic transport system for regulated release at the tumor site.

4.3.11. *In vitro* kinetic evaluation of drug release from the optimum nanoformulation

The experimental release profile of PNIPAAm-*b*-PASP micelle displayed continual drug release in the optimized nanoformulation (Figure 11). Modeling of drug release kinetics was determined by fitting drug release data to equations of Zero Order kinetics, First Order, Higuchi model, Hixson Crowell and Korsmeyer Peppas (Table 4.8 and Figure 4.12). Prolonged release up to 72 h was attained due to the degradation of the biopolymer material and slowed dispersion of the therapeutic from the micelle interior core. MTX release from the nanomicelle was best described by the Higuchi model ($R^2=0.8459$), which in this case describes the release of MTX through the collapsed outer hydrophobic PNIPAAm as a square root of time dependent process based on Fickian diffusion. For the Korsmeyer-Peppas law, the fit was only average ($R^2=0.6626$). According to this law, if the release power coefficient (n value) is greater than 0.45 and smaller than 0.89, it implies that the therapeutic release is due to anomalous transport behavior (Non-Fickian diffusion), while $n<0.45$ implies that the drug release was due to Fickian diffusion law. For release from the optimized nanomicelle, the ' n value' which was established to be 0.1552, implying that the drug release was due to Fickian diffusion of the MTX from the inner core through the collapsed PNIPAAm, which is congruent with the fit with Higuchi's square root law. The rate of diffusion/dispersion was also confirmed by the aforementioned amorphous state established for MTX and slackening of the micelle hydrophobic core. This suggests that MTX-loaded PNIPAAm-PASP amphiphilic nanomicelles

are significant for encapsulation of hydrophobic drugs (Chung et al., 2004; Zhang et al., 2005; Jeong, et al., 2009).

Table 4.8: Drug release kinetics results for various models of optimized methotrexate-loaded nanomicelles for site-specific targeted therapeutic delivery.

Model	Equation	R-squared	R-squared adjusted	n-value
(a) Zero-order	$Y = a_0 + K_0t$	0.6368	0.5964	Not relevant
(b) First-order rate model	$\text{Log } Y = \text{log } a_0 - K_1t$	0.8037	0.7710	Not relevant
(c) Higuchi's square root law	$Y = Kt^{1/2}$	0.8459	0.8202	Not relevant
(d) Korsmeyer-Peppas law	$F = M_t/M_\infty = Kt^n$	0.6626	0.6251	0.1552
(e) Hixson-Crowell law	$\sqrt[3]{Q_a} - \sqrt[3]{Q_m} = kkt$	0.5089	0.4543	Not relevant

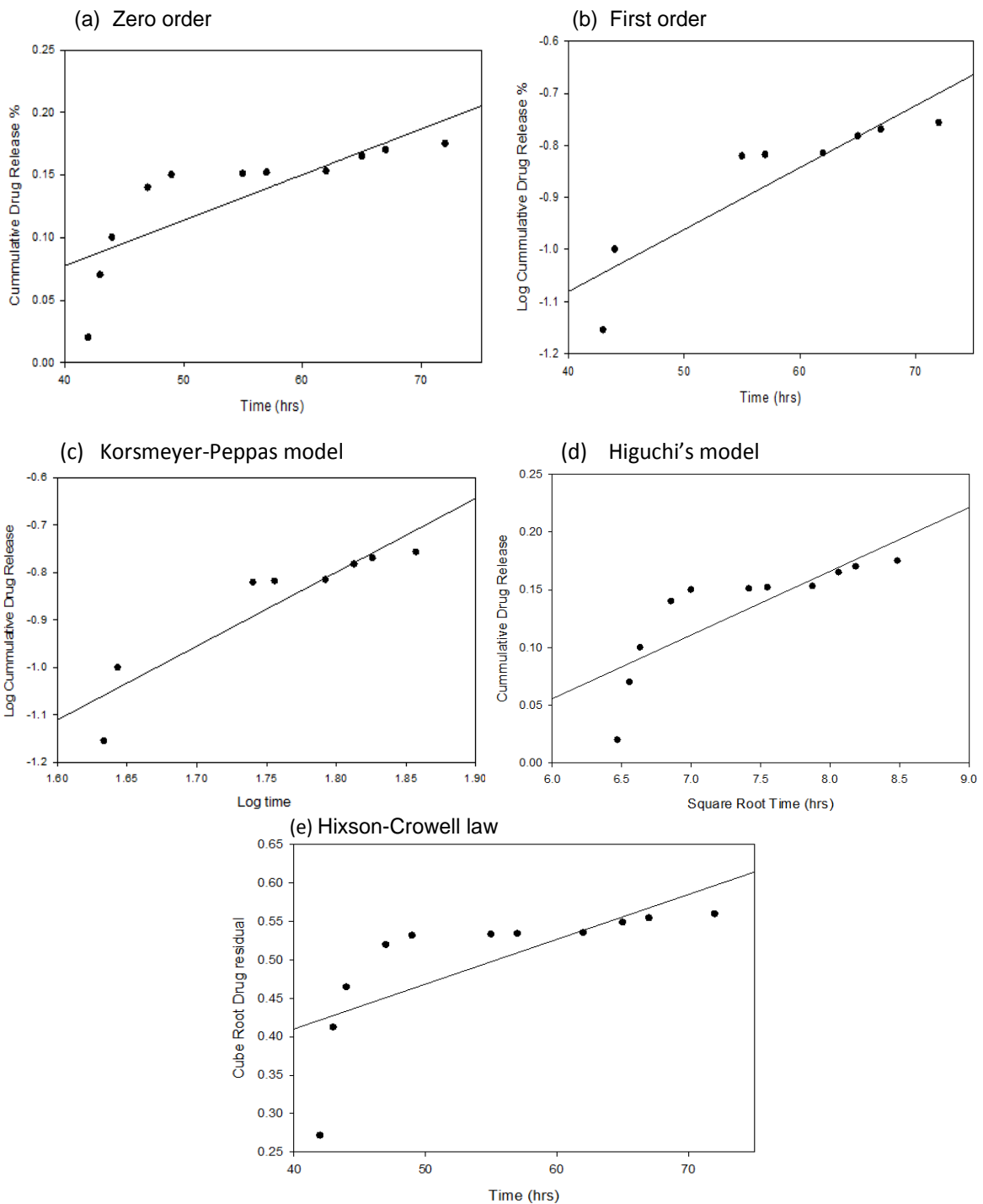


Figure 4.12: *In vitro* Kinetic analysis of drug release, Zero Order kinetics, First Order release, Higuchi Hixson law and Crowell Korsmeyer law.

Furthermore, the pharmaceutical applicability of the optimized MTX-loaded nanomicelles for the targeted delivery of MTX was evaluated by incubation with OC cells (NIH:OVAR-5) and the treated cells were analyzed by the use of a MTT assay, confocal microscope for evaluation of the cytotoxic and uptake ability of the optimized MTX-loaded nanomicelles as described later in Chapter 5, section 5.2.6.

4.4. Concluding Remarks

MTX-loaded PNIPAAm-*b*-PASP nanomicelles were optimized utilizing a Face-Centred Central Composite Design. Nanoformulations of PNIPAAm-*b*-PASP nanomicelles were initially synthesized employing a dialysis tubing method, however, the DEE was further enhanced by employing a solvent evaporation method. Design optimization investigations revealed the notable influence of the variables, namely amount of copolymer and homogenizer speed, on the dependent variables (size, MDT, DIE, cumulative release). These variables interacted significantly to affect the MDT ($p=0.042$). The MTX-entrapment efficacy was considerably enhanced through MTX encapsulation onto the inner hydrophobic core of the amphiphilic PNIPAAm-*b*-PASP nanomicelle. The development of amphiphilic core-shell nanomicelles with adequately small size was verified utilizing scanning electron microscope and transmission electron microscope imagery. The MTX release kinetics of the optimized formulation was best described by the Higuchi square root model with an R^2 value of 0.8459 indicative of drug release from the nanomicelles as a square-root of time-reliant mechanism confirmed by Fickian diffusion law. The MTX-loaded nanomicelles also noticeably minimized the cytotoxic side-effects of MTX and enhanced therapeutic efficiency to tumor cells, by inclusion of MTX in the nanomicelles utilizing the PNIPAAm-*b*-PASP copolymeric composite to generate a superior antineoplastic chemotherapeutic nanosystem. Owing to the prospective use in targeted treatment, it is anticipated that the PNIPAAm-*b*-PASP micelles are being further evaluated in an ovarian cancer cell line and mouse tumor model.

CHAPTER 5
ANTI-MUC 16 FUNCTIONALIZED PNIPAAm-B-PASP NANOMICELLES FOR THE
TARGETED DELIVERY OF METHOTREXATE TO HUMAN OVARIAN CARCINOMA
CELLS

5.1. Introduction

Ovarian carcinoma (OC) is a challenging disease to treat since it is usually diagnosed in advanced stages (International Federation of Gynecology and Obstetrics (FIGO) stage III–IV) due to the lack of early indicative medical symptoms and the absence of early diagnostic methods. Targeted treatment using biomarkers for OC holds great promise to improve the survival of patients with OC. Actively targeted chemotherapy has considerably advanced to passive-targeting based on the Enhanced Permeability and Retention (EPR) effect. To this end, actively targeted chemotherapeutic drug delivery employing nanotechnology has had a remarkable impact on cancer treatment with the following advantages: 1) able to deliver antineoplastic drugs to treat specific cancer metastatic sites; 2) can reduce the quantity of drug necessary to achieve a required therapeutic dose at the target cancer tissue; and 3) reduces the quantity of drug to healthy cells thus decreases cell cytotoxicity (William et al., 2009; Song et al., 2010; Sawant et al., 2012). In this context, the coating of nanomicelles with specific antibody targeting ligands can assist in conjugation of the nanomicelles to precise biomarkers and antigen receptors over-expressed on OC cells in order to target tumors with improved accuracy (Batrakova et al., 2004; Wang et al., 2007). The flexibility of coated amphiphilic nanomicelles is amenable to modified forms of chemotherapy. Targeting cancer cells at a molecular level using nanocarriers such as nanomicelles may be the ultimate goal for more personalized chemotherapy. Antibodies are the most significant target ligands that have offered a broad-spectrum of possibilities in terms of drug targeting and accuracy of interaction. Antibody-targeted nanomicelles (or immunomicelles) can be engineered by composite conjugation of antibodies (or nanobodies) onto the trigger (exposed free terminal) of a hydrophilic segment of the nanomicelle. This ensures active targeting nanomicelle preparation without any steric-hindrance for the ligand-antibody (Torchilin, 2002; Xie et al., 2010).

A significant consideration when preparing such nanomicelles is to ensure that functionalization with the antibodies do not significantly enlarge their size, since delivery and accumulation at the tumor environment is dependent on the magnitude of particle size limits posed by the compromised tumor blood vessels (Hobbs et al., 1998).

Therefore, this study has innovatively focused on the use of mucins (specifically MUC1, MUC4 and MUC16) for the advanced design of a novel intraperitoneally administered (as opposed to conventional intravenous chemotherapy) OC cell-targeting nanomicelle drug delivery system to significantly improve the chemotherapy of OC. The uniqueness of the delivery system is via the use of antibody-functionalized nanomicelles to specifically target mucin antigens known to be over-expressed on OC cells. To our knowledge this has not been investigated before. Ovarian tumors display diverse and modified cell surface antigens such as HE4, CA 72-4, EGFR, SMRP, mesothelin, osteopontin, AFP, CTLA4, IFN α , KLK6, PLA2G2A, ERBB2, IL-10 and mucins (MUC1-16) that differentiate cancerous cells from normal ovarian cells as well as from other healthy cells lining the peritoneum (Niloff et al., 1986; Mogensen et al., 1990; Yin et al., 2002; Whitehouse and Solomon, 2003; Rump et al., 2004; Chauhan et al., 2006; Moore et al., 2007). MUC16 specifically is an eminent cell surface antigen in OC that is shed into the serum and therefore it is also widely used clinically for the diagnosis and management of epithelial OC (Mogensen et al., 1992; Jaeger et al., 2007; Teicher, 2009; Felder et al., 2014). The non-specific delivery of chemotherapeutics to healthy tissues other than the OC tumors is one of the leading cytotoxicity challenges of chemotherapy. Therefore this study also endeavoured on surmounting this challenge by designing MUC16 antibody-functionalized antineoplastic drug-loaded nanomicelles to specifically target OC cells via the peritoneum. Methotrexate (MTX) was used as a model drug in this study. The amphiphilic MTX-loaded nanomicelles were prepared by self-assembly and thereafter functionalized with anti-mucin16 (anti-MUC 16) antibody, resulting in the nanomicelle antibody-functionalized MTX nanomicelles. The composite was then incubated with OC cells (NIH: OVAR-5) with over-expression of MUC 16 and the treated cells were analyzed by the use of a MTT assay, confocal microscope and cell-Elisa Kit for evaluation of the targeting ability of the nanomicelle.

5.2. Materials and Methods

5.2.1. Materials

Methotrexate (MTX), 3-(4,5-dimethyl-thiazol-2-yl)-2,5-diphenyl-tetrazolium bromide (MTT), 100 IU/mL penicillin/100mg/mL streptomycin, RPMI 1640, 10% heat-inactivated fetal bovine serum (FBS) and 0.25%w/v trypsin 0.03%w/v EDTA solution were purchased from Sigma Aldrich (St. Louis, MO, USA). NIH: OVCAR-5 cells were purchased from Dr. Tom Hamilton (Fox Chase Cancer Institute, PA, USA). RayBio[®] Human CA-125 (MUC16) Elisa Kit for serum, plasma, cell culture supernatants, and urine (96-wells) were purchased from Biocom Biotech (Pty) Ltd. (Centurion, Pretoria, RSA). Anti-MUC16 antibody [OC125] ab693 was procured from

Abcam Inc. (Cambridge, USA). Purified deionized water was prepared by a Milli-Q System (Millipore Co., Billerica, MA, USA). 98% DMSO, N,N'-dimethylformamide (DMF), tetrahydrofuran (THF), ethyl ether and petroleum ether (30-60°C) was obtained from Merck Chemicals Co. (Pty) Ltd. (Darmstadt, Germany) and were of analytical grade. Culture plates were purchased from Corning Inc. (NY, USA). All OC cells were grown in an incubator from RS Biotechnological Galaxy (Irvine, UK) maintained at 37°C in a fully humidified atmosphere of 5% CO₂. All cell experiments were performed in the logarithmic phase of growth.

5.2.2. Preparation of the Anti-MUC 16 Functionalized MTX-Loaded Nanomicelle

5.2.2.1. Synthesis of the amphiphilic PNIPAAm-b-PASP copolymer for the Nanomicelle

Firstly, a copolymer comprising PNIPAAm-b-PASP was synthesized by solvent evaporation as described previously (Lu et al., 2003; Daman et al., 2014). Thereafter the PNIPAAm-b-PASP copolymer (0.125g, 0.0079mmol), anti-MUC 16 antibody (0.2mL, 0.022mmol), NHS (0.60mg, 0.0522mmol) and DCC (10.8mg, 0.0522mmol) were dissolved in 10mL DMF. The solution was mixed under a N₂ atmosphere at room temperature in the dark for 14 hours before dilution with 25mL deionized water followed by centrifugation to extract DCU. The aqueous supernatant was further extracted by membrane dialysis against deionized water for 24 hours with subsequent lyophilization.

5.2.2.2. Preparation of the MTX-loaded Nanomicelle

MTX-loaded nanomicelles were prepared by solvent evaporation as reported previously (Wei et al., 2009). Briefly, 7mg MTX and 25mg of PNIPAAm-b-PASP were dissolved in 5mL DMF with 20mL distilled water added dropwise to the solution under homogenization at 360rpm for 5 minutes at room temperature. This was followed by solvent removal using a rotary vacuum evaporator to obtain a nanomicelle solution that was then filtrated through a 0.2µm filter membrane to remove any residual MTX with subsequent lyophilization. The anti-MUC 16 antibody functionalized MTX-loaded nanomicelles were prepared with modifications by introducing the anti-MUC 16 functionalized block copolymer (Fig. 5.7) (Bae et al., 2007; Wang et al., 2007; Bae et al., 2009). Furthermore, blank FITC-labeled targeted nanomicelles were prepared with modifications of replacement by a FITC-labeled block copolymer. The FITC-labeled block copolymer was prepared as reported previously (Zhang et al., 2010).

5.2.3. Evaluation of the Molecular Structural Integrity of the Functionalized Nanomicelles

Fourier Transform Infrared (FTIR) spectroscopy (Perkin Elmer Life and Analytical Sciences Inc., Shelton, CT, USA) was utilized to differentiate the molecular structure of the block copolymer Nanomicelle following nanomicelle coating with the anti-MUC 16 antibody. Firstly, a background IR spectrum of a native KBr was scanned. Nanomicelle samples of 20mg were triturated with 2g KBr and 8 tons using a 13mm die to produce a compact thin pellet. Pure MTX, blank nanomicelles, MTX-loaded nanomicelles and the MTX-loaded Nanomicelle was characterized by FTIR in the mid-IR region between 650-4000cm⁻¹.

5.2.4. Particle Size, Zeta Potential and Morphological Analysis of the Nanomicelle

The nanomicelle size (with and without anti-MUC 16), the zeta potential and polydispersity index (Pdl) were determined using a ZetaSizer NanoZS instrument (Malvern Instruments, Worcestershire, UK). Briefly, 2mg of nanomicelle samples were initially dispersed in deionized water. The nanomicelle solution was subsequently filtered with a 0.22µm Millipore filter (Billerica, USA) to remove any polymer aggregates. The results were determined utilizing active dynamic light beam scattering (DLS). Transmission Electron Microscopy (TEM) and Scanning Electron Microscopy (SEM) (Jeol 1200 EX, Japan) were also used to determine the morphology of the nanomicelles. The *in vitro* release profiles of MTX from the MTX-loaded nanomicelles and the MTX-loaded Nanomicelle was undertaken in a simulated tumor environment (PBS; pH 6.5; 37°C) by a membrane dialysis method previously reported by (Zhang et al., 2010).

5.2.5. Determination of MTX Encapsulation into the Nanomicelle

Drug encapsulation efficiency (DEE %) was determined using Equations 3.2 and 3.3. The quantity of MTX encapsulated within the nanomicelles was measured by introducing a weighed quantity of nanomicelles into 10mL PBS (pH 7.4; 37°C) followed by centrifugation at 5000rpm for 60 minutes and the supernatant was sampled. The DEE% value was measured at λ_{306nm} utilizing a linearity profile $r^2=0.99$ with a Cecil 3021 UV spectrophotometer and instituting Equation 3.2 and MTX-encapsulation (%w/w) using Equation 3.3. Equation 3.2 and 3.3 are described in Chapter 3, section 3.2.8. All measurements were performed in triplicate.

5.2.6. *In vitro* cytotoxicity assay

The *in vitro* cytotoxicity of the Nanomicelle was investigated by a Methylthiazole Tetrazolium salt (MTT) Assay of NIH: OVCAR-5 cells. In order to determine the cytotoxicity of the MTX-loaded nanomicelles and the effectiveness of anti-MUC 16 Nanomicelle for cellular internalization, NIH: OVCAR-5 ovarian cells that over-expressed the MUC 16 antigen on the cell surface were cultured in 96-well plates at the confluence/density of 10000 cells per well. After 1 day of incubation at 37°C with a 5% CO₂ atmosphere the medium was removed and the cells were resuspended for 48 hours in fresh culture media comprising the MTX-loaded Nanomicelle, MTX-loaded nanomicelles, blank nanomicelles and pure MTX at various concentrations ranging from 0.01-10µg/mL. After 48 hours of cell incubation with the various treatments, the cell survival rate was measured using a tetrazolium salt MTT assay. At predetermined time intervals, 180µL of fresh RPMI growth medium and 20µL of MTT (5mg/mL) solution were added to each well. The plates were incubated for further 6 hours, and then 200µL of DMSO (for cell lysis) was introduced to each well to suspend any purple formazan crystals formed. The microplates were vigorously agitated before evaluating the relative color intensity. The purple formazan absorbance at 570nm of each well was measured by a Thermo Labsystems Multiskan Mk3 microplate reader.

5.2.7. Confocal Microscopic Analysis of the Nanomicelle on NIH: OVCAR-5

Cell mounting media was prepared by dissolving 2-4g paraformaldehyde and 2-0.4g NaOH in 100mL of PBS. The PBS solution was prepared by adding NaH₂PO₄ (1.68g) and the pH was adjusted in the range of 7.5-8.0 by adding NaOH. Fluorescence specimen mounting media containing 20mM Tris (pH 8.0), 0.5% *N*-propyl gallate and 50-90% glycerol was also prepared.

Intrinsic fluorescence of MTX was undertaken to investigate the permeation and internalization of the MTX loaded into the nanomicelles. NIH:OVCAR-5 cells were cultured on microscope glass coverslips (1cm) at a confluence/density of 1600 cells/slip placed in petri dishes and incubated for 24 hours at 37°C in FBS-free RPMI 1640 medium. The growth medium was replaced with 0.1% FITC-labeled MTX-loaded Nanomicelle samples in FBS-free RPMI 1640 medium and incubated for 2.5 hours at 37°C. Following incubation the loading solution was removed, the cells were washed thrice with PBS to remove non-internalized MTX, then exposed to 4% buffered paraformaldehyde for 20 minutes at 48°C, rinsed thrice with PBS, and mounted on microscope glass slides using a mounting gel. The slides were observed under a confocal laser fluorescence scanning microscope (Leica TCS SP2, Germany). A sequence of images were obtained in the z-axis (0.5mm apart) with an Olympus FV300 confocal laser

fluorescence scanning unit coupled to an Olympus BX61 upright microscope. Images were developed by Fluoview™ software.

5.3. Results and Discussion

5.3.1. Analysis of the Molecular Structure Integrity of the Functionalized Nanomicelle

FTIR spectral analysis is one of the most robust analytical techniques to evaluate the molecular structure block copolymer functional groups (Weers and Scheuing, 1991). FTIR spectra were analyzed to describe the interactions of the MTX-loaded nanomicelles and anti-MUC 16. Data on the FTIR spectra for pure MTX, blank nanomicelles, MTX-loaded Nanomicelle and MTX-loaded nanomicelles are shown in Figure 1. As demonstrated, there were distinct chemical structure transitions for the functionalized MTX-loaded nanomicelles compared with the non-functionalized MTX-loaded nanomicelles. The FTIR spectra of the blank nanomicelles and MTX-loaded Nanomicelle were congruent with those of the native polymers PNIPAAm and ASP (Rimmer et al., 2007). This result showed that the polymer transformation occurred with minor chemical modification during the polymerization process. Hence, it was the nanomicelles revealed elemental chemical features that were representative of the native polymers. In addition, variations were also noted in the FTIR spectrum of the blank nanomicelles and MTX-loaded nanomicelles in Figure 5.1. The other peaks that were recorded in the MTX-loaded nanomicelles were due to the 1, 3 replacement composite ($1516.53\text{--}1451.23\text{cm}^{-1}$) and a phenyl amino compound ($1647.22\text{--}1451.13\text{cm}^{-1}$). This indicated that MTX was entrapped within the hydrophobic interior of the nanomicelle structure by weak electrostatic H-bonds involving the COO- moiety of MTX and the OH-group of aspartic acid or by the charged ionic groups involving the NH₂ bonds of MTX and the COO-bonds existing in PNIPAAm-b-PASP. MTX was diffused within the PNIPAAm-b-PASP matrix in the amorphous form exclusive of any polymorphic transformation or alteration in the aqueous form. The anti-MUC 16 amine groups (N-H) were observed by the 1660.20cm^{-1} peak as well as the derived amine groups induced by the broad range O-H group and the C-H group observed between $1090.30\text{--}1310.11\text{cm}^{-1}$ that also overlapped the $1000.12\text{--}1200.22\text{cm}^{-1}$ describing C-O groups that were attributed to the PNIPAAm-b-PASP copolymer. These transitions indicated that there was intensity of interaction with prominent interactions between the MTX-loaded nanomicelles and the anti-MUC 16 antibody that confirmed the surface coated functionalization of the MTX-loaded Nanomicelle.

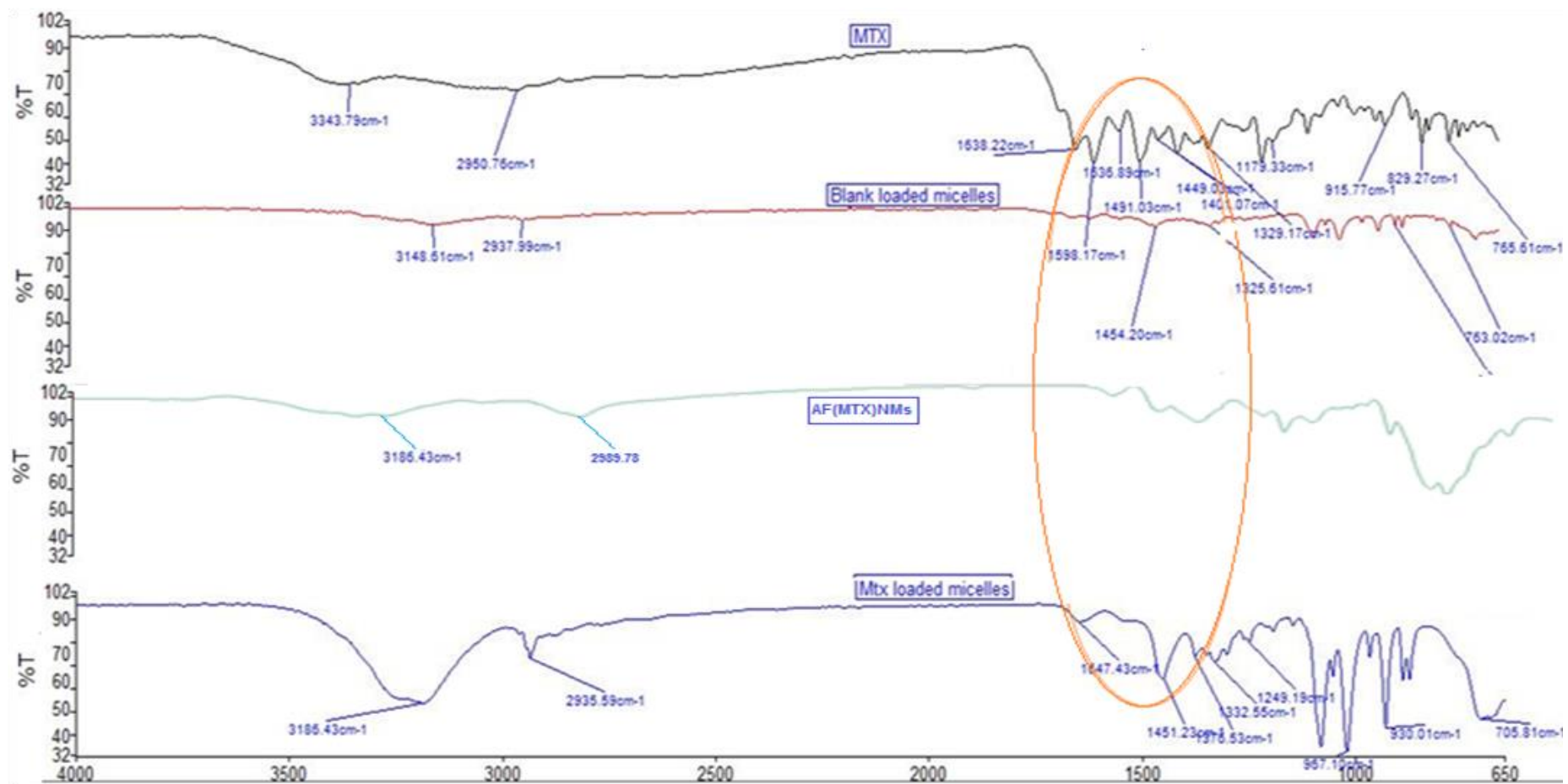


Figure 5.1: FTIR spectra illustrating the molecular structural transitions of MTX, blank micelles, AF(MTX)NM's and (MTX)NM's.

5.3.2. Assessment of Particle Size, Zeta Potential and Morphology of the Nanomicelle

The physicochemical analysis and MTX-loading limits of the nanomicelles were evaluated as shown in Table 5.1. Nanomicelle size is a key factor due to its influence in MTX entrapment, release and passive targeting ability via the Reticular Endothelial System (RES). The particle sizes recorded for the MTX-loaded nanomicelles and the MTX-loaded Nanomicelle were 65nm and 75nm respectively with desirable PDI values of ≤ 0.5 (Figure 5.2). The MTX-loaded nanomicelles and MTX-loaded Nanomicelle displayed similar negative surface charges. The mean zeta potential values varied between -3.132mV for the MTX-loaded nanomicelles to -4.712mV for the MTX-loaded Nanomicelle. These zeta potential values indicated that the MTX-loaded nanomicelles were balanced by electrostatic forces with potential aggregation outside the recorded limits. The nanomicelle aggregation can be overcome by decreasing or diluting the quantity of copolymer (PNIPAAm-b-PASP) used to prepare the MTX-loaded nanomicelles.

Table 5.1: The physicochemical analysis of MTX-loaded polymeric nanomicelles with and without antibody (n=triplicate).

Formulation	Micelle size (nm)	Zeta potential (mV)	PDI	DEE%
MTX(NM's	65	-3.132	0.104	80.6
AF(MTX)NM's	75	-4.712	0.078	78.6

It can be seen from Table 5.1 that functionalization of the nanomicelle surface with anti-MUC 16 has a slight influence on MTX DEE%. However, the DEE% of the MTX-loaded Nanomicelle remained as high as 78%. As shown in Table 5.1, the *in vitro* release behavior of the MTX-loaded nanomicelles and the MTX-loaded Nanomicelle had similar release patterns with 80% of MTX released within 72 hours. The results also indicated that the controlled attachment of anti-MUC 16 did not significantly impact the *in vitro* release profile of the nanomicelles (Figure 5.3).

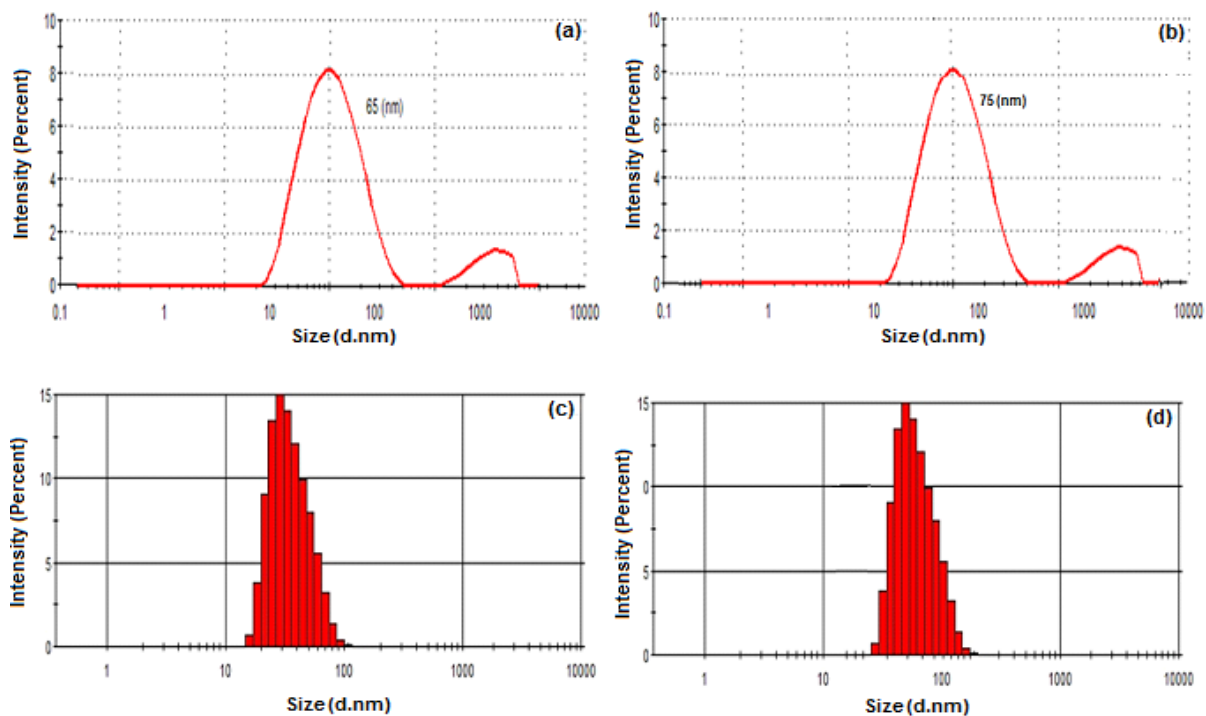


Figure 5.2: Dynamic light scattering (DLS) plots of (MTX)NMs without (a) and (b) with anti-mucin 16 antibody modified including PNIPAAm-b-PASP micelle hydrodynamic size and monotype size distribution (c) (MTX)NMs (65 nm), AF(MTX)NMs (75 nm).

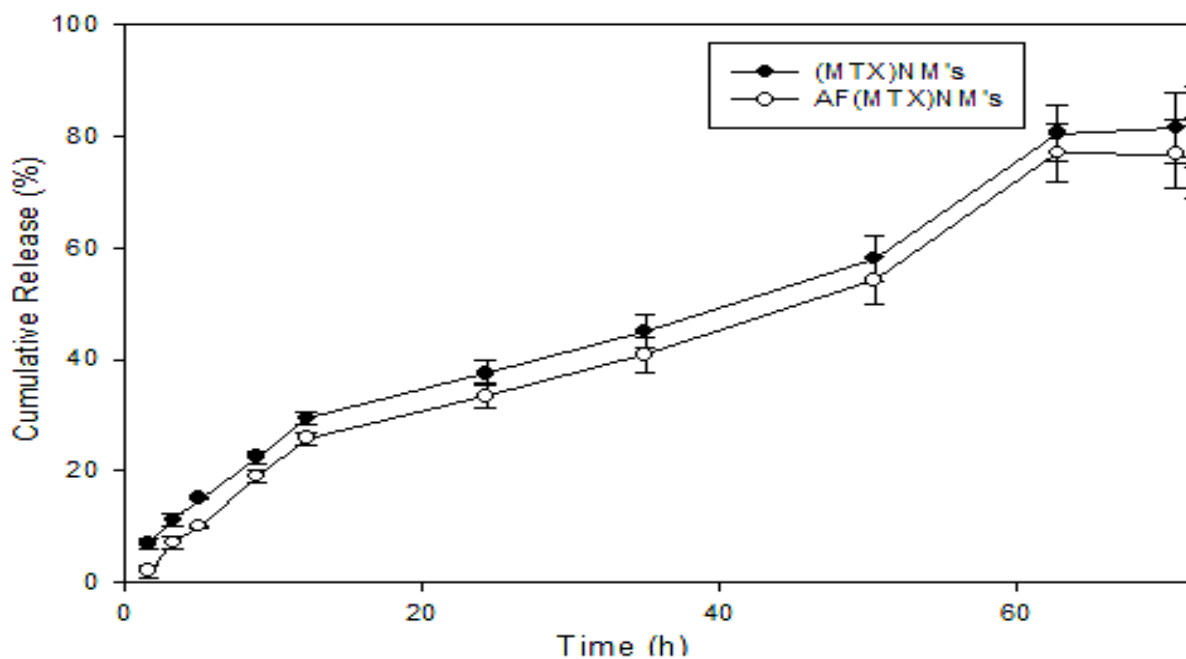


Figure 5.3: Methotrexate release from (MTX)NM's and AF(MTX)NM's in PBS (pH 7.4) at 37 degrees. Each point depicts mean \pm SD (n=3).

5.3.3. Morphological Characterization of the Nanomicelle

TEM images revealed homogeneity and uniformity in the non-functionalized and functionalized nanomicelle formulations (Figure 5.4a and 5.4 b). These TEM images also showed that the non-functionalized and functionalized nanomicelles produced were at the nanoscale and spherical in shape. SEM images of the functionalized nanomicelles also displayed uniformity in surface morphology. These results further validated that the anti-MUC16 ligands were coated onto the surface of the nanomicelles by covalent or non-covalent bonding and contributed to the surface morphology (Figure 5.4c and 5.4 d).

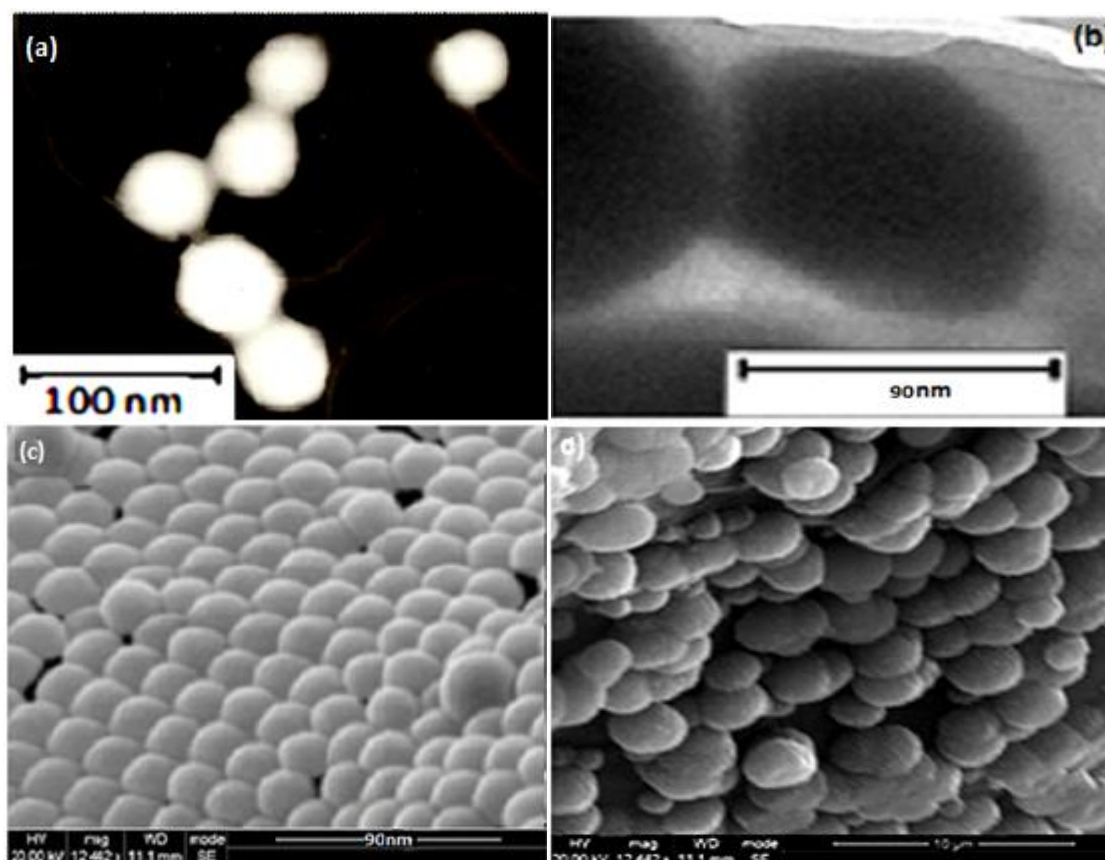


Figure 5.4: TEM (a and b) and SEM images (c and d) of native NMs (a and c) and antibody-functionalized NMs (b and d) for interaction with mucin 16 particles.

5.3.4. Cell Culture and *In Vitro* Cytotoxicity Assay

In order to fully understand the potential of using the PNIPAAm-b-PASP nanomicelles for intracellular chemotherapeutics, the first factor that had to be observed was the cytotoxicity. The MTT assay as depicted in Figure 5.5 generated for pure MTX, the MTX-loaded nanomicelles, the MTX-loaded Nanomicelle and the blank nanomicelles showed increasing cytotoxicity with regression in cell viability after incubation for 72 hours as the formulation

concentration increased. While PNIPAAm-b-PASP displayed superior biocompatibility *in vitro* even at the highest concentration of 0.01mg/mL a value of 86% cell viability was recorded. This high cell survival rate for PNIPAAm-b-PASP confirmed that the hydrophobic and Asp inner core offers excellent biocompatibility for intracellular biomedical applications. Although the cytotoxicity of the blank nanomicelles against NIH:OVAR 5 cells was insignificant (86% and 82% cell viability, respectively), increasing the concentration of MTX or the MTX-loaded nanomicelles (1-10 mg/mL) after 72 hours of incubation displayed a pronounced anti-proliferation effect (45% and 40% cell viability). The results also showed that all MTX concentrations of 0.01µg/mL, 0.1µg/mL, 1µg/mL and 10µg/mL exhibited lower cytotoxicity than those of the MTX-loaded nanomicelles at the same concentration of MTX [cell viability of 86±1% vs. 80±1% (0.01µg/mL MTX), 82±1% vs. 76±1% (0.1µg/mL MTX), 40±1% vs. 35±1% (10µg/mL MTX)]. This was also observed in all the MTX-loaded Nanomicelle formulations with concentrations of 0.01µg/mL, 0.1µg/mL, 1µg/mL and 10µg/mL that exhibited higher cytotoxicity compared with the MTX-loaded nanomicelles at the same concentration of MTX [cell viability of 80±1% vs. 76±1% (0.01µg/mL MTX), 76±1% vs. 70±1% (0.1µg/mL MTX), 45±1% vs. 43±1% (1µg/mL MTX), 39±1% vs. 35±1% (10µg/mL), respectively]. The cellular anti-proliferation effect due to MTX increased with encapsulation and further increased with the addition of the targeting ligand anti-MUC 16 to the encapsulating nanomicelles. The *in vitro* cytotoxicity caused by the MTX-loaded nanomicelles was due to the passive EPR influence whilst the enhanced cytotoxicity resulting from the MTX-loaded Nanomicelle was attributed to active MUC 16 receptor targeting and functionalization with anti-MUC 16 onto the PNIPAAm-b-PASP amphiphilic copolymeric nanomicelles. Thus, the enhanced cytotoxicity of the MTX-loaded Nanomicelle was due to the synergistic influence of MUC 16 mediated receptor targeting and modulation of OC cells by PNIPAAm-b-PASP copolymeric nanomicelles.

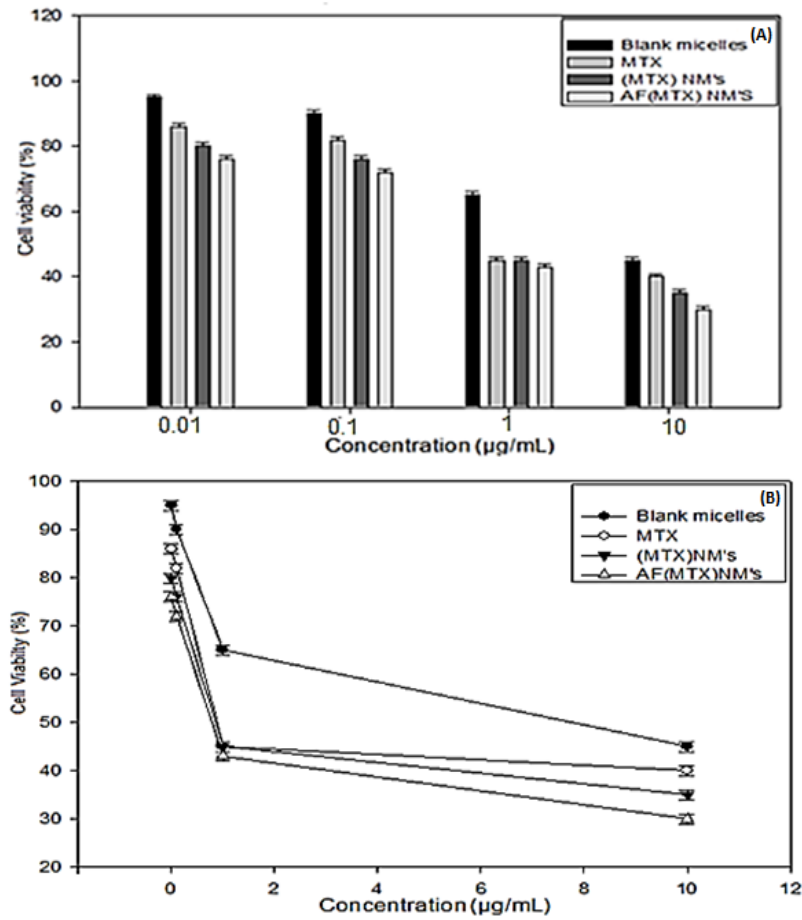


Figure 5.5: Tetrazolium salt MTT assay to evaluate the effect of MTX, (MTX)NM's and AF(MTX)NM's formulations on percentage viability of NIH:OVCAR-5 cells, blank micelles were utilized as control, invitro cytotoxicity of MTX-incorporated polymeric micelles with and without antibody including control against NIH:OVCAR-5 cells (a,b). All NM's were incubated with ovarian cells for 72 hours prior to cell viability evaluation in each treatment group. Each point depicts average \pm SD (n =3).

5.3.5. Confocal Microscopy Analysis of the Nanomicelle

In order to confirm the intracellular distribution of the nanomicelles with and without anti-MUC 16 functionalization, samples were labeled with FITC and observed under a fluorescence microscope. The intracellular distribution of FITC-labeled MTX-loaded nanomicelles and the MTX-loaded Nanomicelle was investigated to prove the targeted delivery of the MTX-loaded Nanomicelle into NIH: OVCAR-5 cells. Fluorescence microscopy analysis confirmed that the OC cells incubated with the MTX-loaded nanomicelles fluoresced (green) and was indicative of the MTX-loaded nanomicelle attachment to the surface of the NIH:OVCAR-5 cells and were not removed with PBS or aqueous medium (Figures 5.6b-c). On the other hand, OC cells incubated with the MTX-loaded Nanomicelle exhibited stronger fluorescent signals (bright green) and were also not removed with PBS or medium. This implied that the MTX-loaded Nanomicelle specifically targeted the NIH: OVCAR-5 cancer cells that over-expressed MUC

16 on the cell surface (Figures 6e-f). Surface engineering of the nanomicelles with anti-MUC 16 was therefore a useful strategy to increase the cellular uptake of the MTX-loaded NnaoComposite.

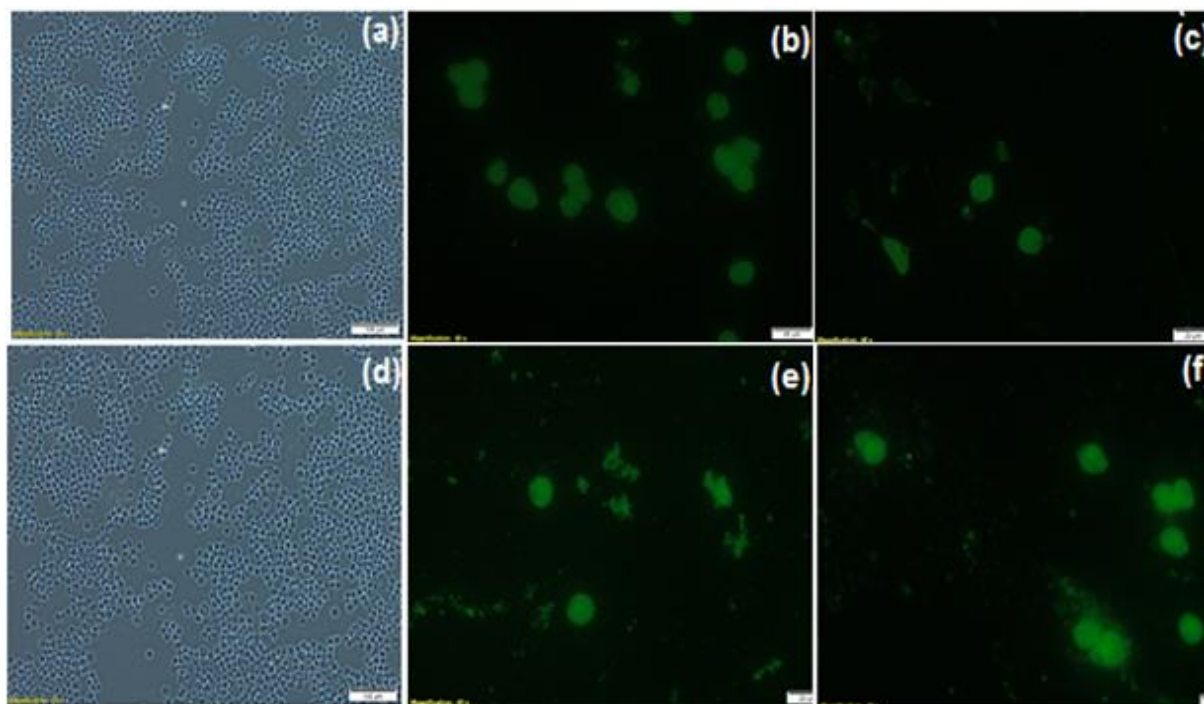


Figure 5.6: Confocal fluorescence microscopy for determination and analysis of cell uptake with antibody binding on the surface of micelles [(a-b) control micelle transmission images, (b-f) fluorescence overlay images of NIH:OVCAR-5 cells treated with (MTX)NMs (b-c) and AF(MTX)NMs (e-f) formulations showing selective enhanced uptake following 24 hour incubation.

5.3.6. Mechanism of Synthesis of the Anti-MUC 16 MTX-Loaded Nanomicelle

Amphiphilic block copolymers are expected to offer improved applications in chemotherapeutics owing to nanomicelles used as nanocarriers for ionic and non-ionic drug loading (Qiao 2010; Abolmaali et al., 2013; Bastakoti et al., 2013). Ionic complexes/composites involving anionic antineoplastic drugs and aspartic acid can be produced and nanomicelles further synthesized by self-assembly of the drug and amphiphilic copolymer in an aqueous medium. In this amphiphilic structure, the hydrophilic surface shields the hydrophobic interior from the interaction of the inner core with the surrounding aqueous environment that confers the nanomicelles to be used as a vehicle for targeted drug delivery. The limitations of nanomicelles include the inaccuracy in directly targeting tumor tissue, its potential toxicity, relative instability in the circulatory system, rapid degradation and clearance by the immune system and the lack of controlled drug release over prolonged periods of time (Jeong et al., 2009; Wang et al., 2012; Díaz and Vivas-Mejia, 2013). In order to overcome these limitations, this work focused on preparing functionalized nanomicelles with anti-MUC

16 ligands to facilitate specific targeting of OC cells and. To date, a wide range of active targeting approaches including the use of folates, antibodies, peptides, aptamers transferring and oligosaccharides have been utilized to achieve site-specific targeting of nanomicelles to cancer cells (Duncan, 2006; Sun et al., 2008; Prabakaran et al., 2009).

In this study, a more efficient strategy (under moderate formulation conditions) was utilized to ensure superior targeting of the functionalized core-shell nanomicelles using a simplified synthetic approach outlined in Figure 3.1 and Figure 5.7. The physical synthesis comprised two synthetic steps: 1) the block copolymer constituted an aspartic backbone and PNIPAAm outer surface in order to self-assemble the MTX-loaded core-shell nanomicelles by solvent evaporation in an aqueous medium. The polycationic backbone formed between PASP and MTX generated the inner core of the nanomicelle while the non-ionic PNIPAAm formed the outer hydrophilic shell. PASP was used to conjugate the MTX (a carboxylic drug) to its amine groups to form an amide (CO-NH) linkage. Furthermore, the anti-MUC16 antibody was surface coated to the nanomicelles via carbodiimide-sulpho-NHS mediated conjugation through carboxylic (COOH) linkage of PNIPAAm-b-PASP copolymer. This linkage was also significant for the elucidation of the orientation of the anti-MUC 16 to ensure binding affinity and stability. In this case, the MTX-loaded nanomicelles were incubated with 1-ethyl-3-(3-dimethylaminopropyl)-carbodiimide and N-hydroxysuccinimide for 15 minutes at room temperature. The resulting activated nanomicelles were then covalently linked to the anti-MUC16 antibody (1% weight compared with the polymer concentration) (Figure 5.7). The resultant anti-MUC16 antibody-functionalized MTX-loaded nanomicelles (the Nanomicelle) were then lyophilized (Freezone 6, Model 79340, Labconco, MO, USA). Furthermore, the prepared Nanomicelle was directly targeted and interacted with the NIH: OVAR 5 cancer cells for intracellular uptake into the cytoplasm via receptor-mediated endocytosis through amide-carboxyl linkage (Figure 5.8). MTX was then released from the Nanomicelle and inhibited malignant cell division and multiplication in their late G2 or M phases by restraining the dihydrofolate reductase enzyme activity and reduced/eliminated OC cells.

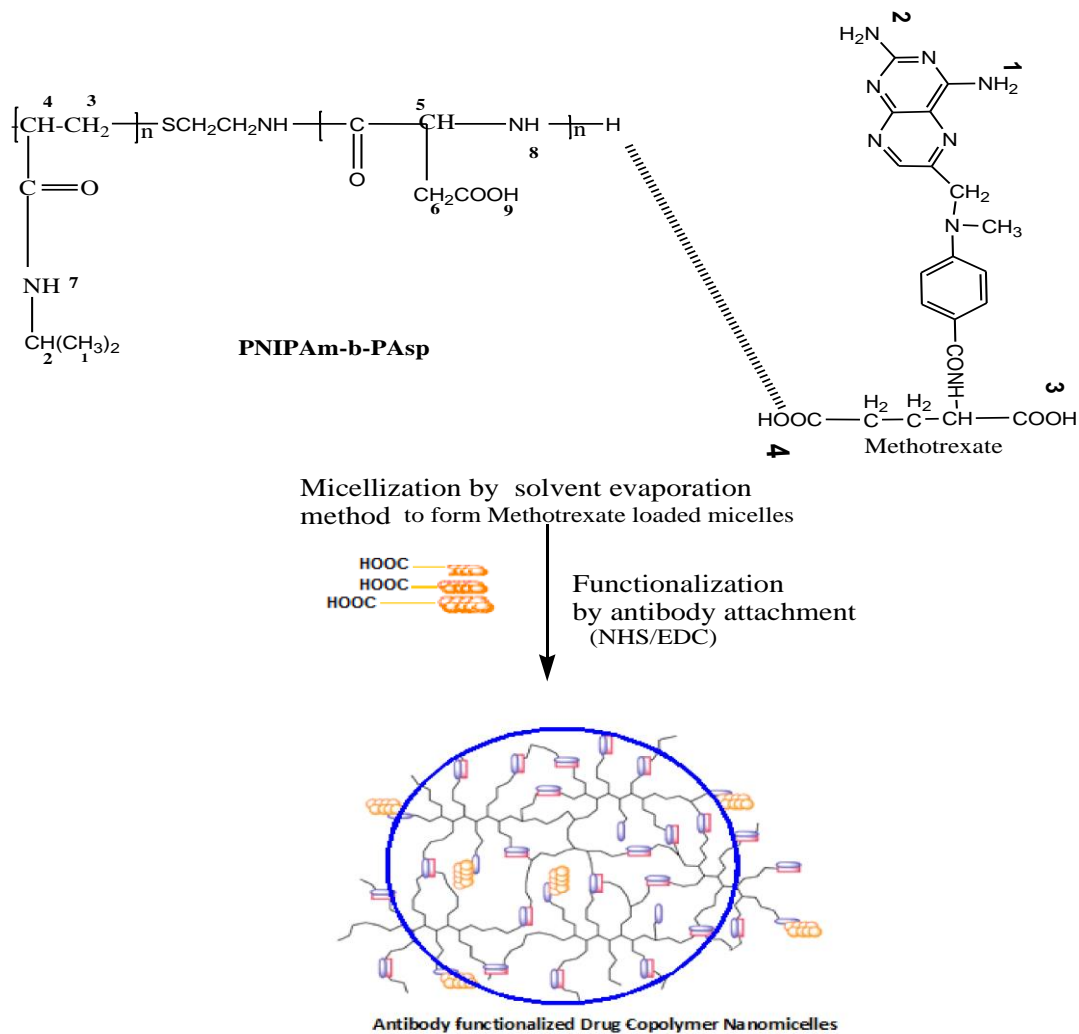


Figure 5.7: A schematic illustration of monoclonal antibody-mediated methotrexate loaded nanomicelle drug delivery system.

The results of this study confirmed that MTX can be loaded into the inner core of the PNIPAAm-b-PAsp nanomicelles and the carboxyl-amine-groups of the nanomicelles were amenable to surface coating with the anti-MUC 16 antibody. The resultant functionalized MTX-loaded nanomicelles directly targeted OC cells while leaving healthy cells without expression of the MUC 16 antigen untouched.

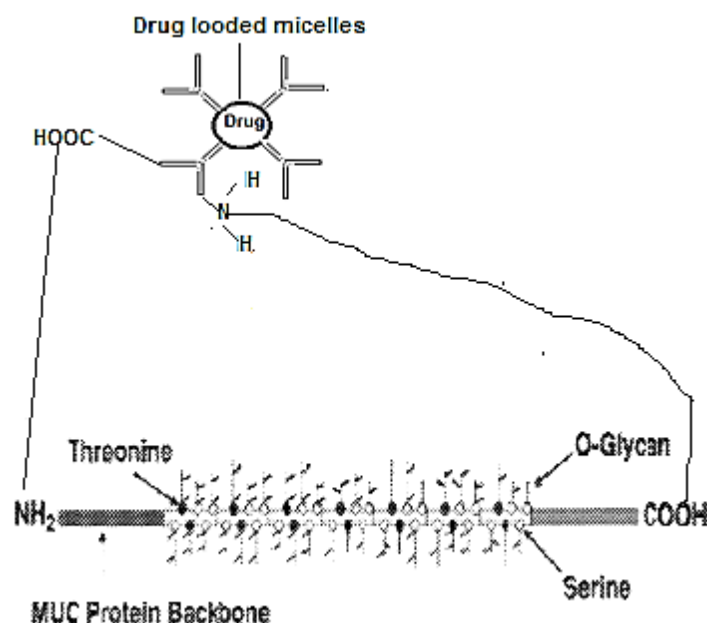


Figure 5.8: Schematic illustration of (antibody-antigen interaction) the anti-mucin 16 methotrexate loaded micelle interaction with mucin 16 (as known as CA 125) receptor.

It is well known that MUC 16 is highly expressed on malignant cells and not on healthy cells and therefore the Nanomicelle can impede tumor growth and even stem metastasis based on the binding to MUC 16. In addition, it is important to note that OC cells also use MUC 16 as a mechanism for metastasis via mucoadhesion to other organs within the peritoneum. Thus the developed Nanomicelle has far-reaching potential for the targeted treatment and management of OC using advanced nanochemotherapeutics.

5.4. Concluding Remarks

In this study, biodegradable copolymeric PNIPAAm-b-PAsp nanomicelles functionalized with anti-MUC 16 was developed and evaluated for the ability to provide targeted receptor-mediated endocytotic delivery of MTX to OC cells. Characterization studies confirmed that the Nanomicelle was pharmaceutically stable and cellular uptake studies showed that the MTX-loaded Nanomicelle exhibited improved intracellular uptake compared with the MTX-loaded nanomicelles when exposed to NIH: OVARY5 cells that over-express MUC 16 receptors. The Nanomicelle also noticeably minimized the cytotoxic side-effects of MTX. In conclusion, the Nanomicelle can directly target and specifically reduce or eliminate OC cells in a targeted manner and thus shows great promise for application in clinical OC detection, targeting and chemotherapy.

CHAPTER 6

***IN-VITRO* SYNTHESIS, CHARACTERIZATION AND EVALUATION OF A BIO-RESPONSIVE IPN NANOMICELLE/HYDROGEL COMPOSITE BASED IMPLANT FOR HUMAN OVARIAN CARCINOMA TREATMENT**

6.1. Introduction

While the advancements in novel chemotherapeutic drugs continue, focus has been stirred to improve targeted drug delivery platforms (Weinberg et al., 2008). Recently, there has been great deal of interest in hydrogel matrix development for the controlled delivery of various chemotherapeutic agents (Ma et al., 2012). Hydrogels are hydrophilic three-dimensional network systems fabricated from synthetic and/or natural biomaterials which can strongly absorb and hold large quantities of water. The molecular structure of the hydrogel is formed by the hydrophilic monomers or functional domains in biopolymeric system upon the gel hydration in aqueous solution (Rosiak & Yoshii, 1999). Hydrogels are classified as permanent chemical gels when they are stable covalently cross-linked systems and reach equilibrium swelling rate depending on the polymer-water interaction and crosslink network density (Rosiak & Yoshii, 1999). Hydrogels are also classified as reversible physical gels when the polymer networks are connected together by molecular bonds, and/or secondary intermolecular forces including covalent hydrogen bonding or hydrophobic and ionic interactions. In physically cross-linked network hydrogels, dissolution is hindered by physical intermolecular interactions between various polymer structures (Hennink & Nostrum, 2002). All these interactions are flexible, and are disrupted by modifications in physical settings or the utilization of strain (Rosiak & Yoshii, 1999).

The water absorption capacity and porosity are the most significant properties of a cross-linked hydrogel. The hydrophilic segments are foremostly hydrated upon interaction with aqueous solution which results in the development of primary bound aqueous solution. Thus, the network system swells exposing hydrophobic segments that are also water miscible. The network system also absorbs free water, due to the osmotic active force of the network system towards increased dilution. The further swelling is balanced by the covalent or physical networks, resulting in an elastic network negation force. As a result the hydrogel system will reach an equilibrium swelling rate that is dependent on the nature and constituents of the hydrogel network. The next phase is the degradation and/or disintegration if the network structure or cross-interfaces are dissolvable. Due to their increased water absorption and

biocompatibility, disintegratable hydrogels comprising of labile-bonds have been utilized in many applications (Rosiak & Yoshii, 1999; Hoffman, 2002; Nho et al., 2005; Benamer et al., 2006).

Generally, hydrogel systems have excellent compatibility since their hydrophilic exterior has a low intermolecular free energy when subjected to biological fluids, which leads to a low propensity for cells, peptides and proteins to attach to these exterior surfaces. Furthermore, the soft and rubbery form of hydrogels diminishes irritation to the local tissue (Anderson & Langone, 1999; Smetana, 1993). The networks between various polymer interchains lead to viscoelasticity and sometimes good elastic behavior while contributing to the gel structure (hardness) and stickiness. It is possible to modify the chemistry of hydrogels by controlling their polarization, surface functionality, mechanical strength and swelling kinetics (Syed et al., 2011).

The various modification techniques include adopted include reversible physical cross-linking, permanent chemical cross-linking, grafting copolymerization and direct or indirect radiation cross-linking (Hennink & Nostrum, 2002; Barbucci et al., 2004; Said et al., 2004; Fei et al., 2000; Liu et al., 2002b). Such transformations can enhance the mechanical strength and viscoelasticity of hydrogels for biomedical and biopharmaceutical applications (Barbucci et al., 2004; Nho & Lee, 2005; Rosiak et al., 1995; Rosiak & Yoshii, 1999). Various cross-linking agents including formaldehyde, epichlorohydrin, glutaraldehyde (GA), genipin and N,N-methylenebisacrylamide have been employed to improve stability and applicability of hydrogels in drug delivery platforms. The mechanical or rheological properties of Poly(Vinyl Alcohol)-Chitosan-Poly(Acrylic acid) hydrogels have been validated to be controlled by thermal susceptibility, pH, cross-linkers and polymers used during preparation (Wang et al., 2007).

Implantable hydrogels for solid intratumors can be fabricated to release chemotherapeutic drugs over prolonged periods of weeks, or even months, thus diminishing the dire-need for daily administration of systemic chemotherapy. The intraperitoneal conditions that surround the tumor tissue including pH, temperature and electric charge vary quite considerably compared to surrounding conditions of health body cells. This facilitates stimuli-responsive drug delivery. The small chemotherapeutic delivery through implantable gels may not be an effective solution due to prolonged stable gel formation and may result in an initial burst release (Jain, 1999; Krupka et al., 2006; Shim et al., 2007). However, the use of multifunctional micelles and the distribution of immunomodulators to the specific tumor site have potential for the effective cancer chemotherapy through implantable gels (Ma et al., 2012; Lee et al., 1999).

The implant response parameters are controlled by the molecular mass, constituency and ratio of the polymers utilized in forming the implant.

Therefore the purpose of this phase of the study was to synthesize a cross-linked C-P-N hydrogel for the preparation of an *in situ* forming implant (ISFI) for ovarian carcinoma treatment. ISFI was fabricated by encapsulating a nanomicelle comprising of anti-MUC 16 (antibody) functionalized methotrexate (MTX)-loaded PNIPAAm-b-PASP nanomicelles within non-fluorescence or fluorescence-labeled C-P-N hydrogel. Nanomicelles were fabricated as per protocol described in Chapter 5, Section 5.2.2.2. The C-P-N hydrogels were synthesized by radical polymerization of NIPAAm monomers in presence of glutaraldehyde (G) and N,N-methylenebisacrylamide as crosslinkers as well as chitosan and poly(N-vinylpyrrolidone). The C-P-N hydrogels were characterized of their physicochemical and physicomechanical properties. The *in vitro* stability, morphology and biodistribution of nanomicelles post-encapsulation within the C-P-N hydrogel of the ISFI and fluorescence-labeled nanomicelles were visualized employing real-time fibered fluorescence microscopy and optical Immuno-fluorescence microscopy.

6.2. Materials and Method

6.2.1. Materials

Natural and synthetic biopolymers such as Chitosan (MW=600.000) and Poly(N-vinylpyrrolidone) (MW= 40.000) purchased from Sigma-Aldrich (Steinheim, Germany). N-isopropylacrylamide (MW=113), poly(N-vinylpyrrolidone) (MW=40.000), N,N-methylenebisacrylamide, glutaraldehyde (GA) (25%), ammonium persulfate and methotrexate were purchased from Sigma Aldrich (St. Louis, MO, USA). Hydrochloric acid, potassium chloride, disodium hydrogen phosphate, and potassium dihydrogen phosphate were purchased from Merck Chemicals (Pty) Ltd. (Darmstadt, Germany). Purified deionized water was prepared by a Milli-Q System (Millipore Co., Billerica, MA, USA). All other reagents used were of analytical grade and were employed as purchased.

6.2.2. Synthesis of the Chitosan-PVP-PNIPAAm (C-P-N) hydrogel

IPNs were prepared by free radical polymerization of N-isopropylacrylamide monomers in the presence of chitosan and poly(N-vinylpyrrolidone) (PVP). Poly (N-vinylpyrrolidone), N-isopropylacrylamide (NIPAAm) monomers, N,N-methylenebisacrylamide, and glutaraldehyde crosslinkers were dissolved in aqueous chitosan solution (20 mL, 2% in 1.6% acetic acid), and stirred. Chitosan(C), poly(N-vinylpyrrolidone) (PVP), and N-isopropylacrylamide (NIPAAm)

were employed in 2.0:2.0:45 weight ratio. The ratios (w/w) between glutaraldehyde and chitosan in IPNs were 1%, 2%, and 4%. The weight ratio between N,N-methylenebisacrylamide and NIPAAm was 4%. N,N,N',N'-Tetramethylethylenediamine (TEMED)/ammonium persulfate (APS) solution was utilized as initiator in the cross-linking process of NIPAAm. Thereafter, APS-TEMED solution (24 μ L, 4%) was subsequently added to this reaction mixture. A cross-linked Chitosan-PVP-PNIPAAm (C-P-N) hydrogel formed within 1 hour of polymerization reaction at 25 $^{\circ}$ C. After 24 hours, the IPN hydrogels were washed with deionised water, dried in air/vacuum. The samples prepared were named as F₁= C-P-N/1, F₂= C-P-N/2, and F₃=C-P-N/3 IPNs employing different concentrations of crosslinker.

6.2.3. Physico-chemical characterization of the cross-linked C-P-N hydrogel

6.2.3.1. Nuclear Magnetic Resonance (NMR) Spectroscopic analysis

¹H-NMR measurements were applied to the C-P-N components for the confirmation of the copolymer structure and composition. For ¹H-NMR measurement, 5 mg sample vacuum dried at 50 $^{\circ}$ C for 48 hours was added into a 5mm ϕ NMR test tube, and further vacuum dried at 50 $^{\circ}$ C for 48 hours, to which 500 μ l D₂O solvent was introduced, and lastly the test tube was vortexed to dissolve the polymer in solution. The NMR spectrum was generated using a Bruker DRX400 spectrometer (Bruker, Germany).

6.2.3.2. Determination of Polymeric Structural variations

Molecular structural changes in the polymer backbone may alter the inherent chain stability and therefore affect the physicochemical and physicomechanical properties of the selected polymer type for the intended purpose. The molecular structure of native polymers (CHT, PVP, PNIPAAm) the non-cross-linked, and cross-linked C-P-N hydrogel, blank micelles and drug-loaded micelles were analyzed using FTIR spectroscopy to elucidate any variations in vibrational frequencies and subsequent polymeric structure as a result of drug-co-polymer interaction during nanostructure and hydrogel formation. Samples were analyzed in triplicate at high resolution with scans ranging from 4000 to 400cm⁻¹ on a PerkinElmer Spectrum 100 Series FTIR spectrometer coupled with Spectrum FTIR research grade software (Perkin Elmer Life And Analytical Sciences Inc., USA).

6.2.3.3. Differential Scanning Calorimetry analysis

Thermal analysis of the native CHT, PVP and PNIPAAm, and cross-linked lyophilized C-P-N hydrogel were evaluated using differential scanning calorimetry (DSC) (Mettler Toledo DSC1 STARe System, Switzerland). The samples were weighed (5-8mg) and sealed in perforated aluminum pans. The samples were further scanned at a temperature gradient of 10-260°C, at a rate of 10°C/min under an 8kPa N₂ atmosphere. Indium steel (99.99%) served as a reference for all DSC scans.

6.2.3.4. Thermogravimetric analysis

Thermogravimetric analysis (TGA) of the native CHT, PVP and PNIPAAm and the C-P-N hydrogel was carried out by connecting the TGA software (PerkinElmer STA 6000, Beaconsfield, United Kingdom) to a Fourier transmission infrared (FTIR) spectrophotometer (PerkinElmer Spectrum 100, Beaconsfield, United Kingdom) to elucidate the chemical reactions and/or temperature changes that occurred when native polymeric components were blended together in the presence of GA as a cross-linking agent. The following parameters were employed for the analysis: heat from 30-450/500°C at a rate of 10°C/min and nitrogen gas (N₂). The percentage mass loss was calculated using delta Y software against maximum decomposition temperature-initial decomposition temperature.

6.2.4. Physicomechanical characterization of the fabricated C-P-N hydrogel system

The micromechanical properties of the crosslinked hydrogel may directly influence the ability of the nanomicelles to diffuse out of the polymer matrix. Textural profile analysis was therefore conducted in a 2-fold approach: (a) micro-scale: Texture Analyzer (TA.XT *plus* Stable Microsystems, Surrey, UK) and (b) nano-scale: Hysitron's nanomechanical instrument suite (nanoTensile™ 5000, Hysitron Incorporated, Minneapolis MN, USA), on the hydrated samples of the crosslinked polymer framework to characterize the 3D salient core regions of the crosslinked network in terms of Serial Force–Time/Distance profiles for necessary computations of Matrix Resilience, Energy of Deformation, Work performed in deformation and the Brinell Hardness Number. The parameter settings employed for the analysis are outlined in Table 6.1. Samples were analyzed for variations in MH (N/mm²), DE (J) and MR (%) (Table 6.1).

Table 6.1: Textural parameters employed for determination of C-P-N hydrogel matrix hardness, deformation energy and matrix resilience

Parameters	MH ^a (N/mm ²)	DE ^b (J)	MR ^c (%)
Pre-test speed	1.00 mm/s	1.00 mm/s	1.00 mm/s
Test speed	2.00 mm/s	2.00 mm/s	2.00 mm/s
Post-test speed	10.0 mm/s	10.0 mm/s	10.0 mm/s
Target mode	Force	Force	10 % strain
Target force	0.98067 N	0.98067 N	-
Trigger type	Auto (force)	Auto (force)	Auto (force)
Trigger force	0.04903 N	0.04903 N	0.04903 N
Load cell	5 kg	5 kg	5 kg

^aMH: Matrix hardness, ^bDE: Deformation energy, ^cMR: Matrix resilience

6.3.5.1. Water content of the cross-linked C-P-N hydrogel

The C-P-N hydrogel samples were analyzed for water content determination using the Karl-Fischer Titrator (Mettler Toledo V30 Volumetric KF Titrator, Mettler Toledo Instruments Inc., Greifensee, Switzerland). Different percentage water volumes in the cross-linked C-P-N hydrogel were observed, being 10% water content for F₁, 9% for F₂ and 7% for F₃. In the case of the ISFI, was influenced by cryoprotectant employed to preserve drug-loaded functionalized nanomicelles during the embedding process (Chen et al., 2010).

6.2.4.2. Determination of the gelation temperature of the polymeric formulations utilizing oscillatory rheology

Dynamic rheology is one of the most extensive methods to study rheological properties of polymer hydrogels, and is also the most direct and reliable way for the determination of sol-gel transitions. Viscoelastic properties were measured with a Modular Advanced Rheometer system (ThermoHaake MARS Rheometer, Thermo Fischer Scientific, Karlsruhe, Germany) to indicate the storage modulus (G'), the loss modulus (G''), and tan δ of a aqueous solution of the sol, using cone plate geometry where the G' and G'' were recorded under constant deformation. The study of the flow properties was considered extremely significant to this study as it is central to the mechanisms by which the ISFI functions. At room temperature the implant remains in the liquid state to allow delivery via a 18G needle and at body temperature (37°C) the implant forms a solid-like structure. In order to characterize and analyze the flow

behavior and determine the LCST or gelation temperature of the ISFI formulations, rheology studies were conducted using a Haake Modular Advanced Rheometer System (ThermoFisher Scientific, Germany). As the polymeric material acts as a visco-elastic solid, some background on viscoelastic solids is provided. In order to determine the lower critical solution temperature (LCST) and hence the gelation temperature of the ISFI formulation, the temperature of samples was ramped from 20-50°C at a rate of 0.25°C/min while applying the predetermined stress obtained from the stress sweeps previously described, at the frequency observed in that test. The gelation temperature was determined as the temperature at which the cross-over of G' and G'' occurred i.e., the point at which the formulation was no longer acting as a liquid (G'') but as a solid (G'). In all cases a solvent trap was used to prevent sample evaporation.

6.2.5. Surface morphological characterization of the cross-linked C-P-N hydrogel

Surface morphology, surface area and porosity of the C-P-N hydrogel post-lyophilization was evaluated by employing SEM (JEOL JSM-Japanese Electronic Optical Laboratories, Tokyo, Japan) and a porosimetry analyzer (ASAP 2020 Micrometrics, Georgia, USA). Microscopic analysis of the surface of the nano-enabled structure of the C-P-N hydrogel was undertaken, by first lyophilizing the hydrogel at 25mTorr (Virtis™, Gardiner, New York, USA). The sample was mounted onto double-sided tape attached to a metallic sample stand and sputter-coated with a layer of gold. Each sample was viewed under varying magnifications at an accelerating voltage of 20keV. Surface properties of the C-P-N hydrogel structure were validated using a porosimetry analyzer (ASAP 2020, Micrometrics Georgia, USA).

6.2.5.1. Porositometric analysis

Porosimetry was employed to determine various quantifiable aspects of the hydrogel's porous nature such as total pore volume, surface area and average pore diameter which provides information about the distribution of macro-, meso- and micro-pores existing in the hydrogel illustrated in Table 6.2. These parameters were detected in triplicate using the surface area and porosity analyzer equipped with the ASAP 2020 V3.01 software (Micromeritics, ASAP 2020, Norcross, GA, USA) where the porosimetric evaluations were performed in degassing (to remove air, gases and other adsorbed specimens from the sample surface) and analysis phases.

Table 6.2: Evacuation and Heating Phase Parameters used for Porositometric Evaluation of the C-P-N hydrogel.

Parameter	Rate/target
Evacuation Phase	
Temperature ramp rate	10°C/min
Target temperature	40°C
Evacuation rate	50.0mmHg/s
Unrestricted evacuation from	30mmHg
Vacuum set point	500µmHg
Evacuation rate	60 min
Heating phase	
Temperature ramp rate	10°C/min
Hold temperature	30°C
Hold time	900 min

6.2.5.2 Determination of the swelling and erosion behavior

The hydrogel system was dried by gradual replacement of water by ethanol and then drying in an oven at 60°C until a constant dry mass was reached. Thereafter, they were immersed in PBS and allowed to swell. Samples were collected at selected time intervals using a thin needle, lightly dried with filter paper to remove excess PBS from the gel surface, and weighted. The swelling ratio (S_r , %) were calculated according Equation (6.1):

$$S_r = \frac{m_w - m_d}{m_d} \times 100 \quad \dots (6.1)$$

where, m_d and m_w are the masses of the dry and swollen hydrogels at time t , respectively. The samples were then dried to constant weight (W_i) in an oven at 50°C. The percentage matrix erosion (E , %) at time, t , were calculated using Equation (6.2):

$$E = \left[\frac{(W_i - W_{dp}) - W_t}{W_i - (D + P)} \right] \times 100 \quad \dots (6.2)$$

where, W_{dp} is total weight of drug and polymer lost up to time t , W_t is weight of dried partially eroded matrix at time t and D and P represent initial weight of drug and polymer added to the matrix.

6.2.6. Preparation of bio-responsive IPN nanomicelle/hydrogel composite based implant (ISFI)

The ISFI was fabricated by encapsulating FITC labeled functionalized nanomicelle comprising anti-MUC 16 (antibody) functionalized methotrexate (MTX)-loaded PNIPAAm-b-PASP nanomicelles within the synthesized bio-responsive C-P-N hydrogel followed by freeze drying. Fluorescence-label nanomicelles were fabricated as per protocol described in Chapter 5, Section 5.2.2.2. In brief, non-FITC or FITC-labeled functionalized nanomicelles were loaded into the C-P-N hydrogel at a ratio of 1:5 (functionalized NM's: C-P-N hydrogel). The FITC-labeled functionalized nanomicelles in suspension were added drop-wise to the C-P-N hydrogel, and mixtures were also allowed to agitate until a homogenous mixture was attained under mechanical vortexing at 37°C.

6.2.7. Drug encapsulation efficiency (DEE)

DEE of the device will be calculated using Equation (6.3):

$$E = \left[\frac{(W_i - W_{dp}) - W_t}{W_i - (D + P)} \right] \times 100 \quad \dots (6.3)$$

where, M_{actual} and $M_{\text{theoretical}}$ are the actual drug amount and the theoretical loading amount in 10mg of nanomiceller system, respectively.

6.2.8. Determination of drug release from the ISFI at a simulated tumor site

Drug release studies were conducted in an orbital shaker bath (37±0.5°C, 25rpm). As discussed in Chapter 4, Section 4.2.6 of this thesis a dialysis tubing method similar to that described by Graves et al., (2007) was used. 30mL samples were drawn at the following intervals: 6 hours, 1 day, 3 days, 5 days, 9 days, 13 days and 17 days, 22 days, 27 days, 32 days and 40 days. Pre-warmed buffer (30mL) was replaced at each time interval to maintain sink conditions. Large volumes were extracted to compensate for the poor solubility of the drug. Samples were passed through a 0.22µm pore size filter (Cameo Acetate membrane filter, Millipore Co., Bedford, MA, USA) and analyzed using a UV spectrophotometer (Specord 40, Analytik Jena, AG, Germany) at the wavelength for methotrexate (MTX), 306nm, and the amounts of MTX were quantified using a calibration curve for the drug. Each ISFI formulation was tested in triplicate. The Mean Dissolution Time (MDT) as described by Pillay and Fassih

(1998) at 30 days was calculated for each of the formulations using Equation 4.1 and a maximum MDT is the fastest drug release rate achievable (Govender et al., 2005).

6.2.9 Ex vivo evaluation of the ISFI

6.2.9.1. Cytotoxicity analysis of the polymer framework on cell culture

The *in vitro* cytotoxicity and cytocompatibility of the AF(MTX)NM's, ISFI and C-P-N formulations was investigated by a Methylthiazole Tetrazolium salt (MTT) Assay of NIH: OVCAR-5 cells as discussed in section 5.2.6. Briefly, in order to determine the cytotoxicity of the MTX-loaded nanomicelles and the effectiveness of anti-MUC 16 Nanomicelle for cellular internalization, NIH: OVCAR-5 ovarian cells that over-expressed the MUC 16 antigen on the cell surface were cultured in 96-well plates at the confluence/density of 10000 cells per well. After 1 day of incubation at 37°C with a 5% CO₂ atmosphere the medium was removed and the cells were resuspended for 48 hours in fresh culture media comprising the AF(MTX)NM's, ISFI and C-P-N at various concentrations ranging from 0.01-10µg/mL. After 48 hours of cell incubation with the various treatments, the cell survival rate was measured using a tetrazolium salt MTT assay. At predetermined time intervals, 180µL of fresh RPMI growth medium and 20µL of MTT (5mg/mL) solution were added to each well. The plates were incubated for further 6 hours, and then 200µL of DMSO (for cell lysis) was introduced to each well to suspend any purple formazan crystals formed. The microplates were vigorously agitated before evaluating the relative color intensity. The purple formazan absorbance at 570nm of each well was measured by a Thermo Labsystems Multiskan Mk3 microplate reader.

6.2.10. Optical fluorescence imaging of fluorescence-labeled functionalized nanomicelles embedded within the C-P-N hydrogel framework system

Fluorescence activities of the FITC or rhodamine-labeled functionalized NLPs embedded within the ISFI, C-P-N hydrogel stained with DAPI or trypan blue and double-labeled ISFI were further visualized using Olympus IX71 Immunofluorescence Microscopy (Olympus Co., Tokyo, Japan). All samples were mounted directly on a glass slide and thereafter dried under a fume hood prior to examination. Fluorescence measurements were executed at a different excitation and emission spectrum; 450/525nm for FITC, 540-625nm for rhodamine, 540/585nm for trypan blue stain and 350/470nm for DAPI stain. The images for all samples were viewed at 10X magnifications.

6.3. Results and Discussion

6.3.1 Synthesis of Chitosan-Poly(N-vinylpyrrolidone)-Poly(N-isopropylacrylamide) (C-P-N) hydrogel

Figure 6.1 illustrates the constituent chemical structures and mechanism of synthesis of the C-P-N composite hydrogel structure. Physicochemical characterization via NMR, FTIR, and TGA analysis indicated the formation of chitosan-poly(N-vinylpyrrolidone)-poly(N-isopropylacrylamide) covalent bonds between the protonated amine groups of chitosan (annotated with green circles) and carboxylated groups of poly(N-vinylpyrrolidone) (annotated with blue circles). Both covalent crosslinking and chemical structure moderated the swelling of the IPN hydrogel. The synthesized C-P-N hydrogel was further confirmed with correlation from chemical structural formula and NMR peak assignments (Figure 6.1&6.2).

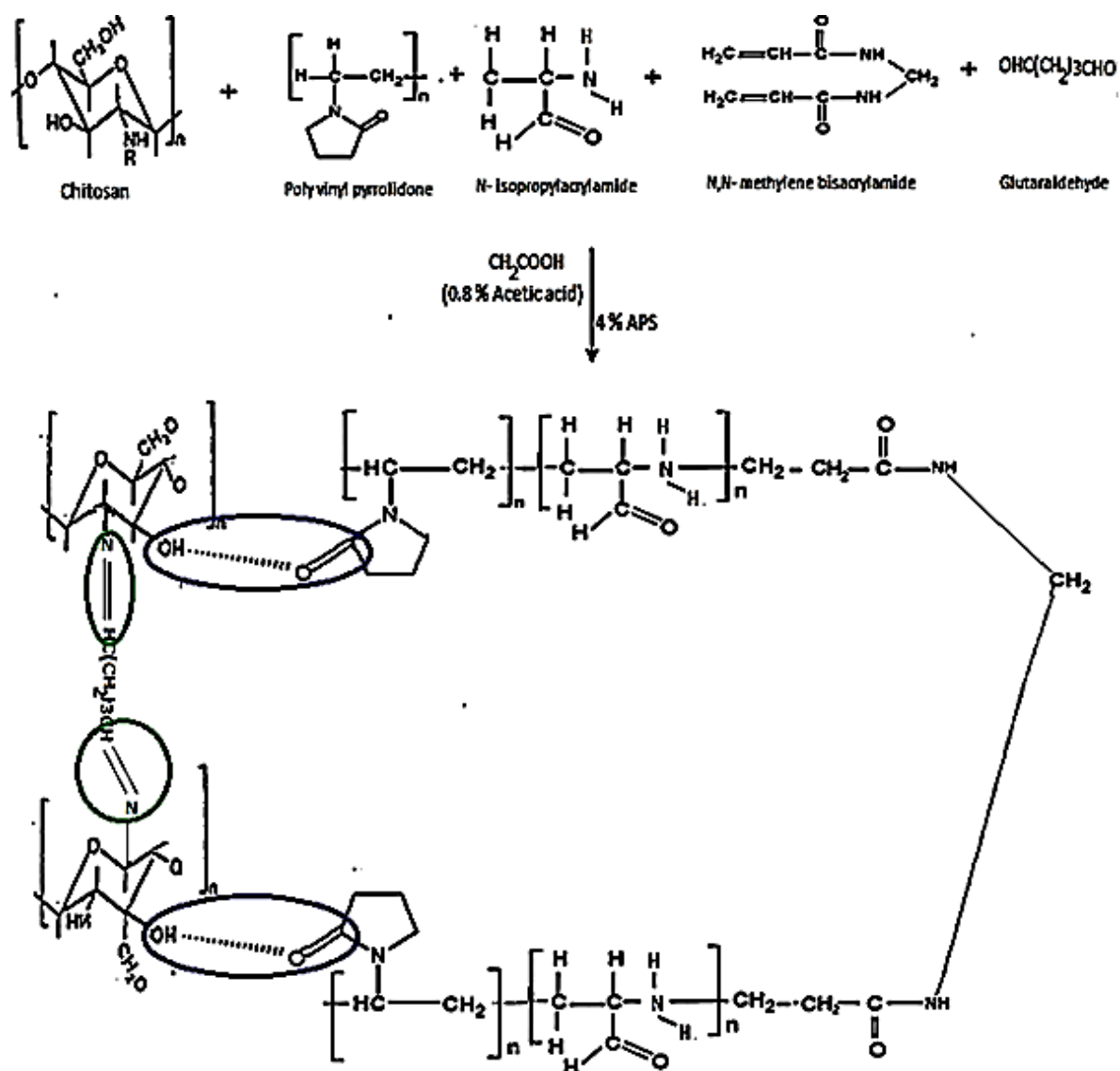


Figure 6.1: Illustration of constituent chemical structures and reaction mechanism forming composite hydrogel structure. Covalent crosslinking and chemical structure moderated the swelling of the IPN hydrogel

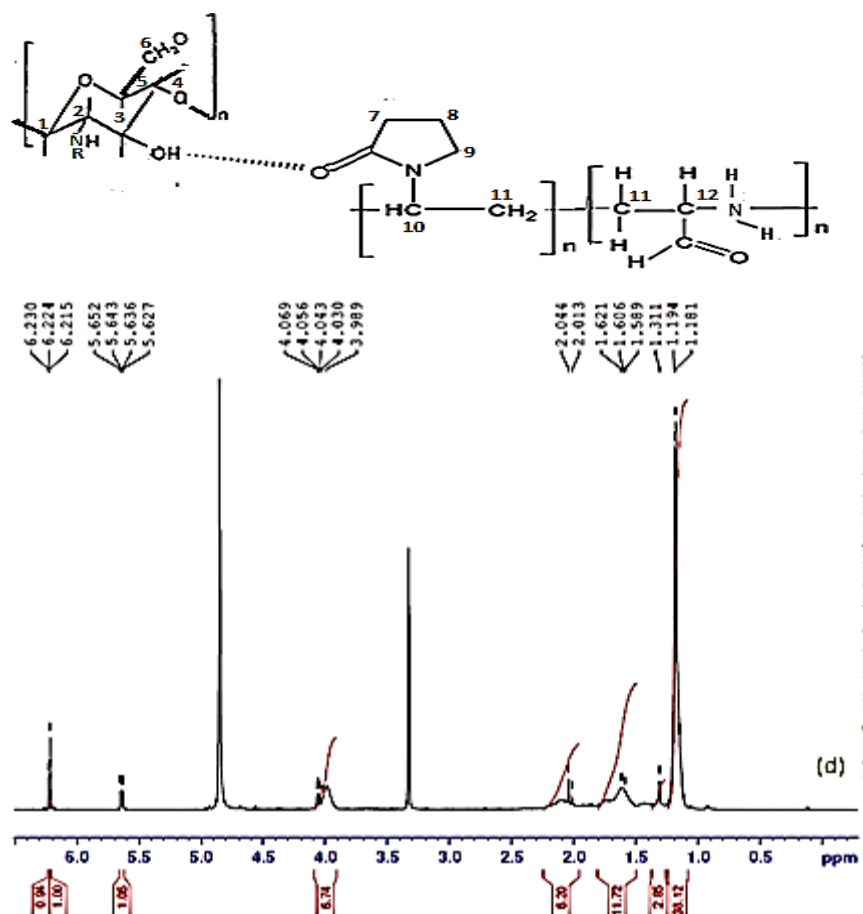


Figure 6.2: ^1H NMR spectra of CHT-PVP-PNIPAAm hydrogel in D_2O and peak assignment confirming the structure of the synthesized composite C-P-N.

6.3.2. Assessment of polymeric structural variations of the cross-linked C-P-N hydrogel

FTIR analysis of the C-P-N hydrogel proved successful radical polymerization of CHT, PVP and PNIPAAm, and interpenetration of GA within the cross-linked network (Figure 6.3). The FTIR spectrum of the C-P-N hydrogel demonstrated peaks at 3428 and 1654cm^{-1} assigned to stretching vibration of $-\text{NH}$ and $-\text{OH}$ as well as CO vibration in the amide group, respectively. The peak at 1720cm^{-1} was attributed to the stretching vibrations of CO in the PVP-PNIPAAm molecule that was the difference between chitosan and the chitosan derivative (CHT-PVP). Figure 6.3 (b), generated from the PNIPAAm hydrogel sample exhibited significant peaks at 1654 , 1551 , 1385 and 1369cm^{-1} , which were assigned to the characteristic peaks of amide I, amide II and the isopropyl group, respectively. For the composite hydrogel, the intensity of absorption peak at 1654cm^{-1} was attributed to increased amide group compared with the CHT-PVP hydrogel due the incorporated NIPAAm. The intensity of the methyl peak and isopropyl peaks decreased when compared with PNIPAAm hydrogel. This indicated successful radical polymerization of CHT-PVP-PNIPAAm and interpenetration by GA and N,N-methylenebisacrylamide.

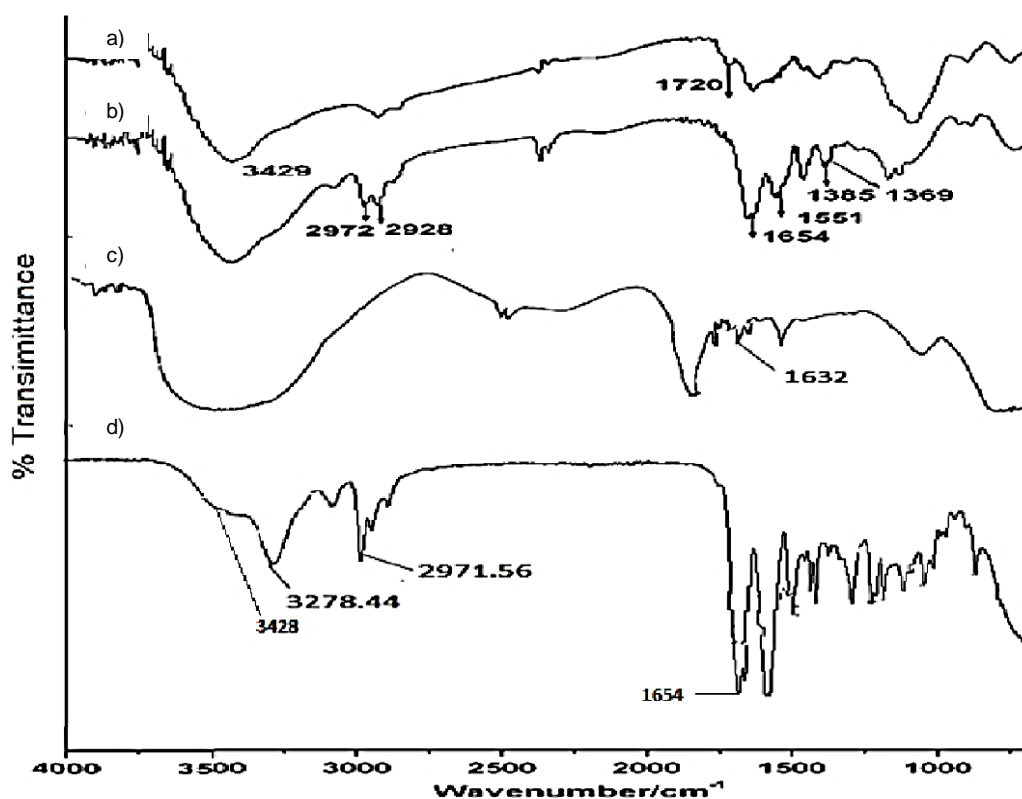


Figure 6.3: Vibrational-Spectroscopy-FTIR of Chitosan (a), PNIPAAm (b), PVP (c) and combinational CHT-PVP-PNIPAAm hydrogel (d).

6.3.4. Assessment of thermal degradation at various heating rates

The stability and decomposition temperatures of the native polymeric components (CHT, PVP and PNIPAAm) and lyophilized cross-linked C-P-N hydrogel were confirmed by TGA (Figure 6.4). Samples were analyzed for both the initial and maximum decomposition temperature at 30-450/500°C at a rate of 10°C/minute under N₂ gas. Figure 6.4a and Appendix A(1) show the highest thermal stability point of the original CHT at 350°C, with less than 2% weight loss. At 279.41°C, the CHT decomposed and its mass deplete as it vaporized with the maximum decomposition at 350°C. Figure 6.4b (Table in Appendix A(1)) represents thermal stability and decomposition of native PVP. Results show the highest thermal stability of PVP at 374.29°C. Initial decomposition temperature of PVP was at about 293.88°C, and the maximum decomposition temperature was 374.29°C. 66.31% of the mass was lost between the onset and offset range temperatures. Figure 6.4c and Appendix A(1) also represent thermal stability and degradation temperature of original PNIPAAm. The results displays the highest mass loss of about 95% at an initial temperature of 281.27°C and maximum temperature of 318.70°C. The quick depletion of mass may have been influenced by loss of water and full decomposition or polymer degradation, which influenced the high evaporation state. Figure 6.4d and

Appendix A(1) depict a thermograph of the post-lyophilized cross-linked C-P-N hydrogel (weight loss graph is the solid line, and its first derivative is the dashed curve). In the case of C-P-N, since the polymer networks are more tightly intertwined together, thermal stability of C-P-N is higher than those of the native polymeric components. This indicates the formation of C-P-N comprising of CHT, PVP, and PNAAm polymers.

The data also demonstrated remarkable stability when native polymeric constituents (CHT, PVP and PNIPAAm) were mixed simultaneously in the presence of GA as a cross-linking agent to form the cross-linked hydrogel. Decomposition and mass depletion only occurred at around 350°C. This may have been influenced by the following:

- amalgamated physicochemical properties of each original polymer,
- strong intermolecular and intramolecular hydrogen bonds occurring between the polymers in the presence of GA as a cross-linking agent.

The data also demonstrated only single (slope)-stage degradation which shows high mass loss when the degradation temperature is reached. The cross-linked C-P-N hydrogel demonstrated a derivative temperature peak (T_p) at around 417.32°C; this observation could be attributed to a decomposition pattern associated with the highest amount of weight loss.

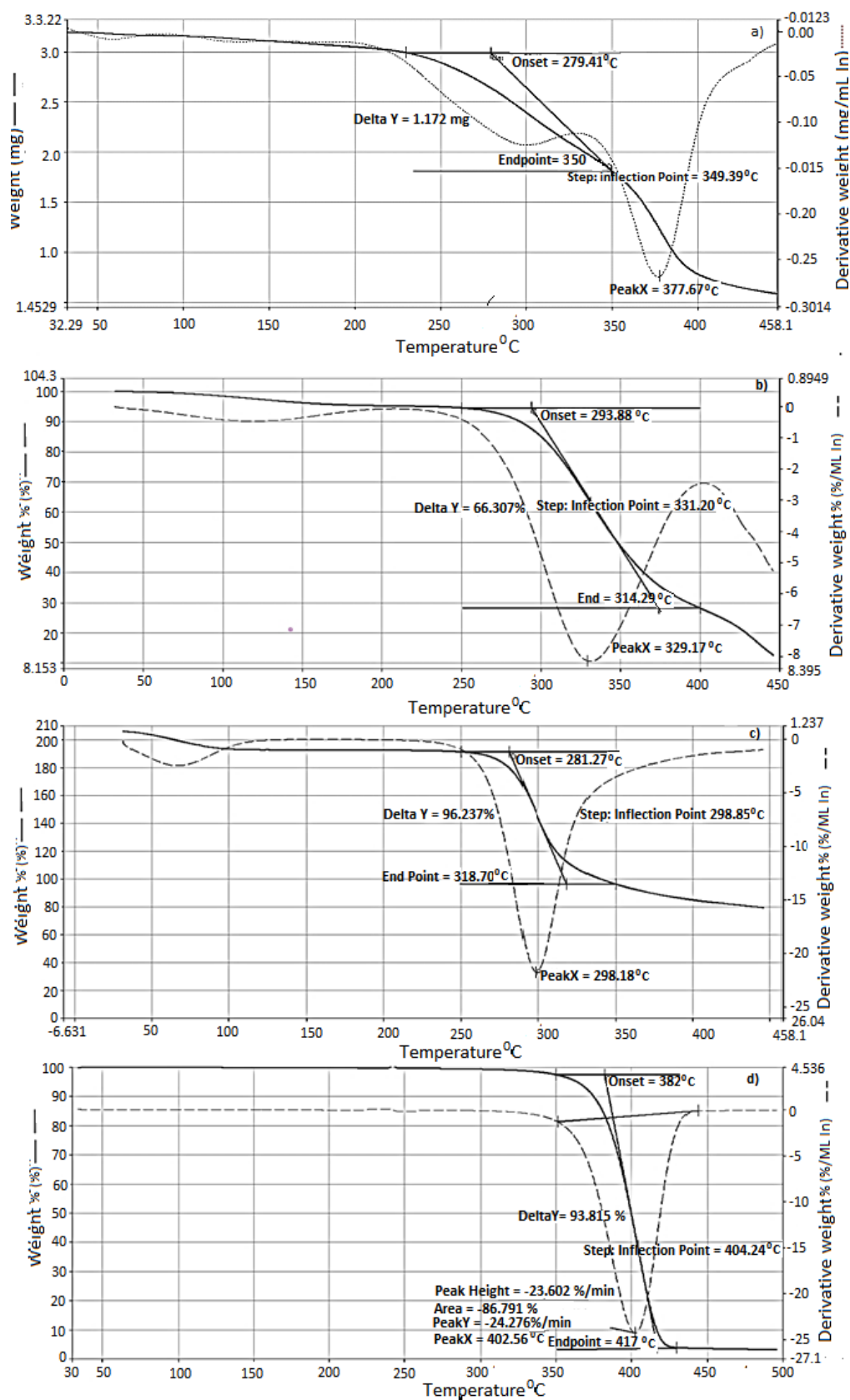


Figure 6.4: TGA thermographs of the cross-linked C-P-N hydrogel; native a) CHT, b) PVP and c) PNIPAAm and d) cross-linked C-P-N hydrogel.

6.3.5. Physicomechanical analysis of C-P-N Hydrogel

The textural properties, water contents, hydration, swelling characteristics and rate of erosion were characterized on the lyophilized cross-linked C-P-N hydrogel samples post-exposure to a simulated tumor environment (STE) (0.1M PBS, pH 6.75; 37°C).

6.3.5.1. Assessment of Textural properties of the cross-linked C-P-N hydrogel

Textural properties of the cross-linked C-P-N hydrogel such as Matrix Hardness (MH), Matrix Resilience (MR) and deformation energy (DE) were measured in the unhydrated and hydrated state in a STE using a calibrated Texture Analyzer. Table 6.3 lists the Force-Time and Force-Distance profiles of the cross-linked C-P-N hydrogel for determining a) DE, b) MR and c) MH. The unhydrated cross-linked C-P-N hydrogel showed high MR at a range of 11.53-14.42%, CPN/1-CP-N/3 respectively. However, when exposed to STE, the MR decreased (8.87-13.37%). In the case of the MH value and deformation energy, the unhydrated samples showed high MH (10.67-12.76N/mm) and deformation energy (0.031-0.049J). However, the hydrated cross-linked C-P-N hydrogel had a slight decline in MH (7.97-9.65N/mm) and deformation energy (0.029-0.049J). These findings were influenced by hydrolysis or the swelling behaviour of the network structure in STE that results in chain relaxation of the C-P-N hydrogel.

Table 6.3: Textural profile of the unhydrated and hydrated cross-linked C-P-N hydrogel

Unhydrated C-P-N hydrogel			
# F	Matrix Hardness MH (N/mm ²)	Matrix Resilience MR (%)	Deformation Energy DE (J)
F ₁	10.67	11.53	0.031
F ₂	12.07	12.81	0.039
F ₃	12.76	14.42	0.049
Hydrated C-P-N hydrogel (% Decrease)			
F ₁	7.97	8.87	0.029
F ₂	8.87	10.38	0.036
F ₃	9.65	13.37	0.040

F₁ = C-P-N/1, F₂ = C-P-N/2, F₃= C-P-N/3, F#: Formulation

*DT= Decomposition temperature, aDelta Y= percentage weight loss from onset point until end point, #Peak Tp = First derivative peak temperature associated with highest rate of change on the weight loss.

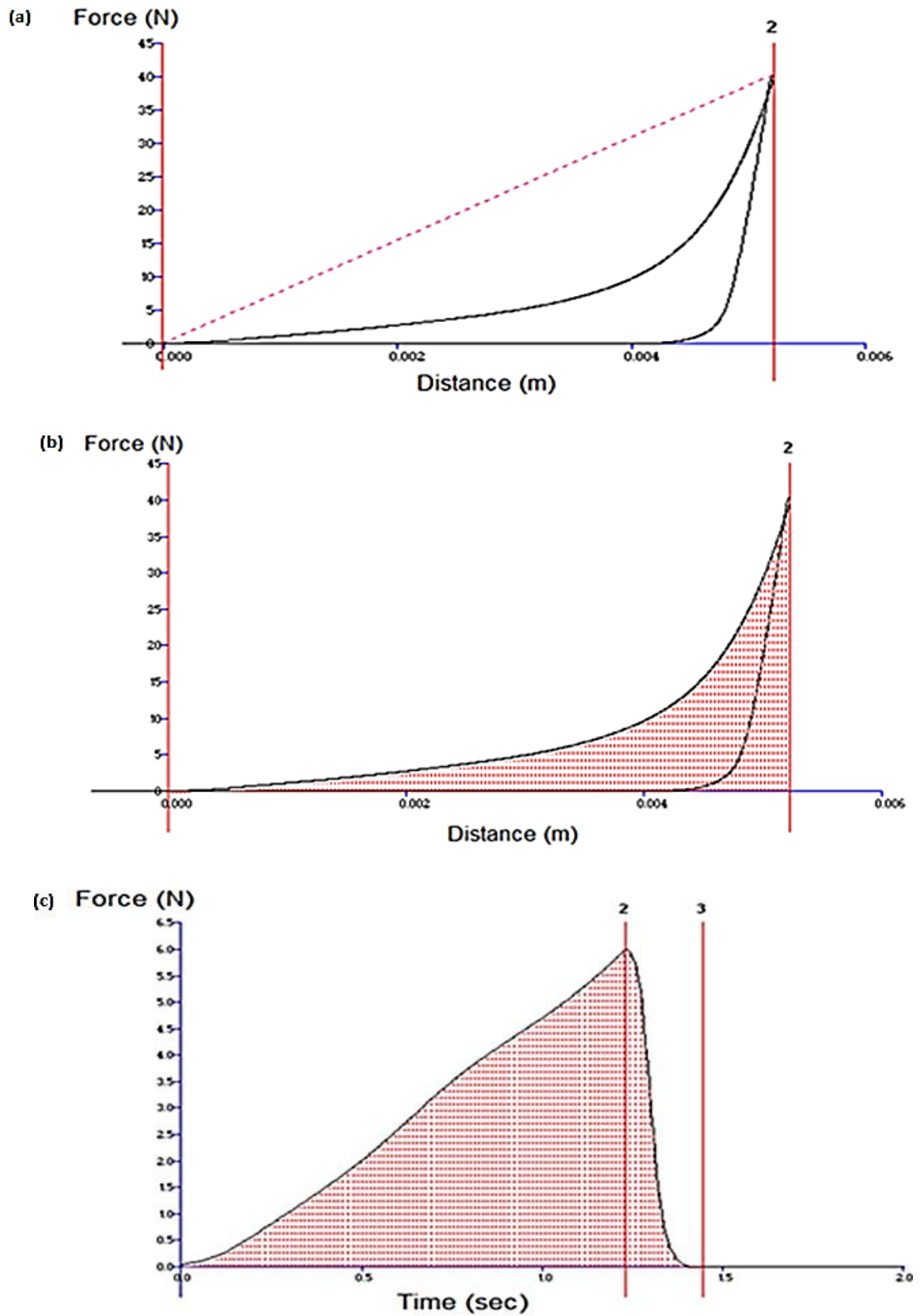


Figure 6.5: Typical textual profiles of the cross-linked C-P-N hydrogel for determining, deformation energy, matrix resilience and matrix hardness.

6.3.6. Assessment of the gelation temperature using oscillatory rheology

The crossover of the storage and loss modulus (G' and G'') indicates the gelation temperature (T^g) for the hydrogel as illustrated in Figure 6.6 b. The storage modulus (G') of a viscoelastic solid is associated with the solid properties or the elastic energy storage properties which indicated that the sample would return to its original state following removal of the deformational energy, while the loss modulus (G'') explains the behavior of the viscoelastic solid when it is acting as a liquid i.e. the viscous properties of the sample representing the dissipation of energy after the application of the deformational stress. Hence at the point at which the storage modulus exceeded the loss modulus, the C-P-N hydrogel was behaving more like a solid than a liquid and hence this was used to determine the thermal gelation temperature. Gelation studies were also conducted on non-crosslinked samples and used as controls (Figure 6.6 a).

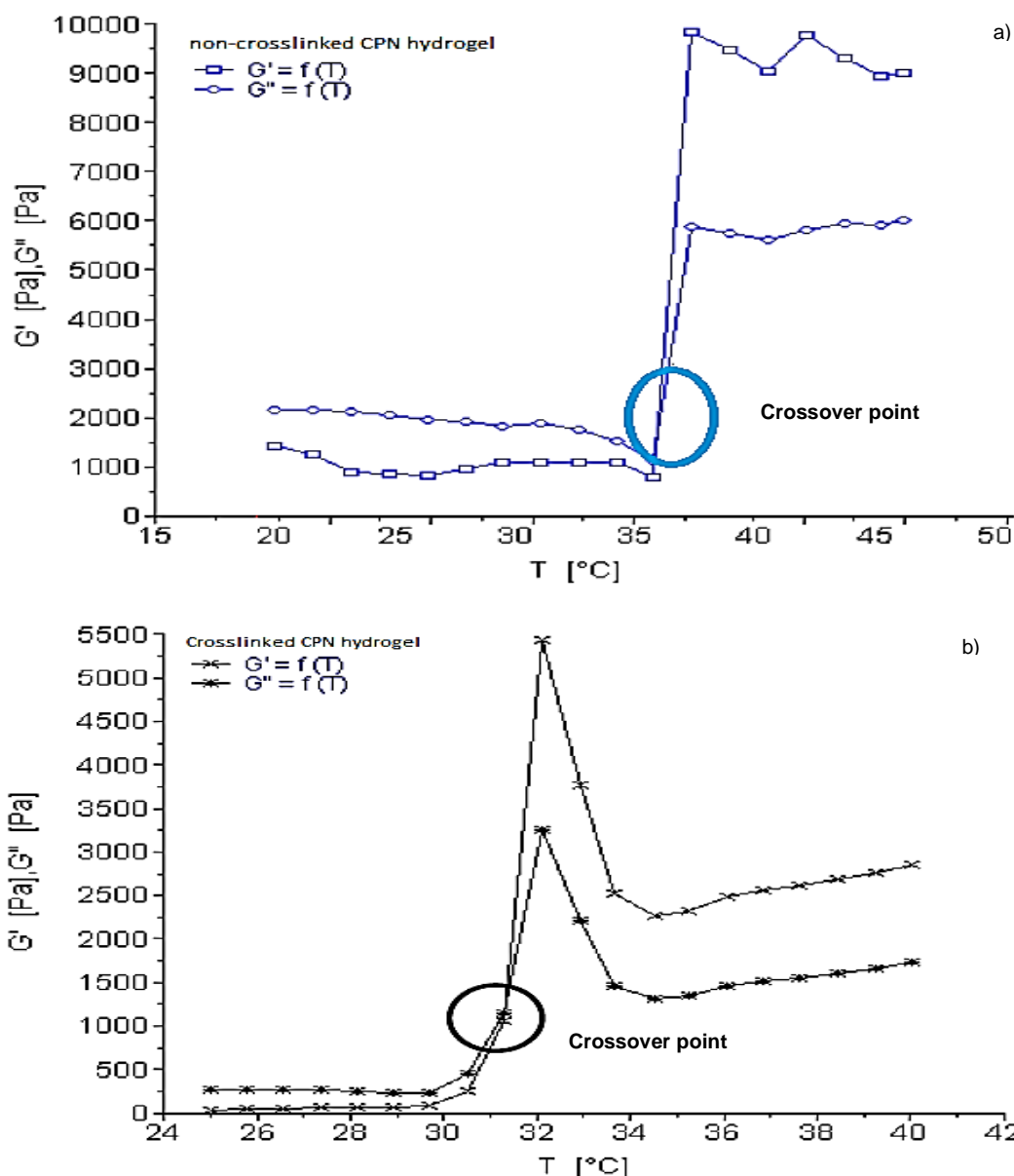


Figure 6.6: Typical profile obtained during oscillatory rheological testing of non crosslinked a) and crosslinked C-P-N hydrogel samples. The black circle demarcates the crossover point storage modulus (G') and the loss modulus (G'').

6.3.7. Assessment of Surface morphological properties

6.3.7.1. Porositometric analysis

The morphology and architecture of the C-P-N hydrogel were observed employing Olympus BX 63 Pictures and SEM (Jeol JSM-120, Tokyo, Japan), Figure 6.7 (a-d) & (e-f) depicts the surface and cross sectional porous morphology of the C-P-N hydrogel respectively. The images reveal that developed structures have spherical interconnected pores with a random size distribution. The pore structures and size were controlled by various parameters including quantities of hydrophilic polymer or cross-linking agents. Furthermore, the pore shape and

size was influenced by the diffusion of water molecules during evaporation or lyophilization processes.

Porosity data accumulated by employing a micrometrics Analyzer displayed linear isothermal adsorption and desorption indicative of highly porous C-P-N hydrogels. Different percentages of porosity were obtained from F₁-F₃. The percentage porosity showed a decrease with increased polymer concentration, being 90% for C-P-N hydrogel (F₁), 85% for CP hydrogel (F₂) and 80% for P-N hydrogel (F₃). Typical C-P-N hydrogel formulation exhibited a type IV isotherm, which indicates microporosity (Figure 6.8). The isotherm was near $P/P_0=1$, which is indicative of the presence of macropores. In addition, SEM micrographs further reveal a pore structure with a spherical shape, an interconnected pore system and random distribution. Porosity distribution of the C-P-N hydrogels may have been controlled by the fabrication procedure, concentration of hydrophilic polymers (PNIPAAm and CHT), freezing temperature (-80°C, 48 hours) and freeze-drying (48 hours). The structure and architecture of developed porous C-P-N hydrogel exhibited essential parameters that may add advantages to prolonged release when drug-loaded functionalized nanomicelles escape through diffusion post-embedded into the ISFI. Furthermore, an interconnecting pore network of the C-P-N hydrogel is even more important for cell culturing and proliferation studies following NIH:OVCAR-5 cells being cultured on the surface of the C-P-N hydrogel.

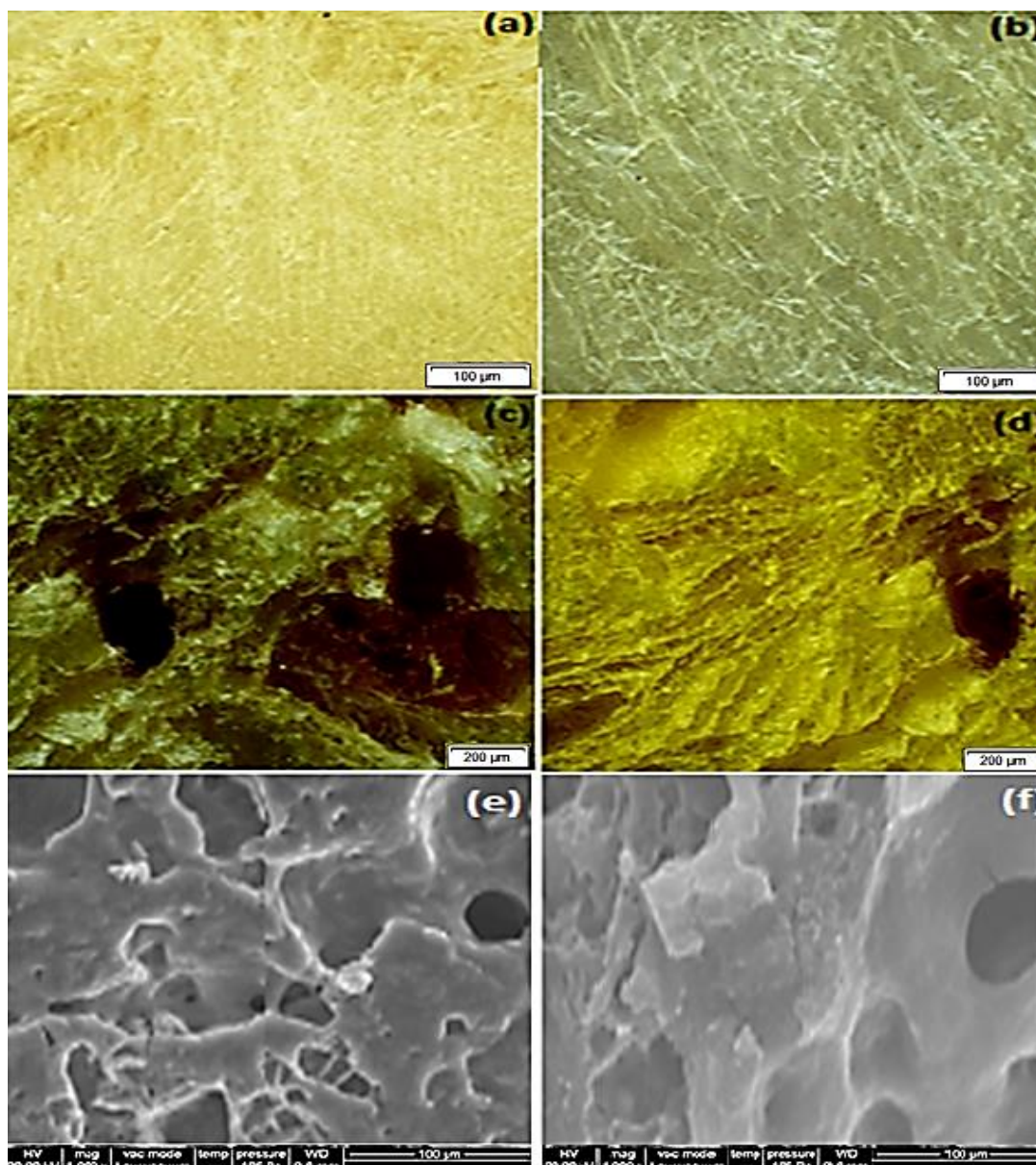


Figure 6.7: Digital images of the surface of the C-P-N hydrogel (a-d) and representative cross sectional area of C-P-N hydrogel observed by scanning electron microscope (SEM) (e-f).

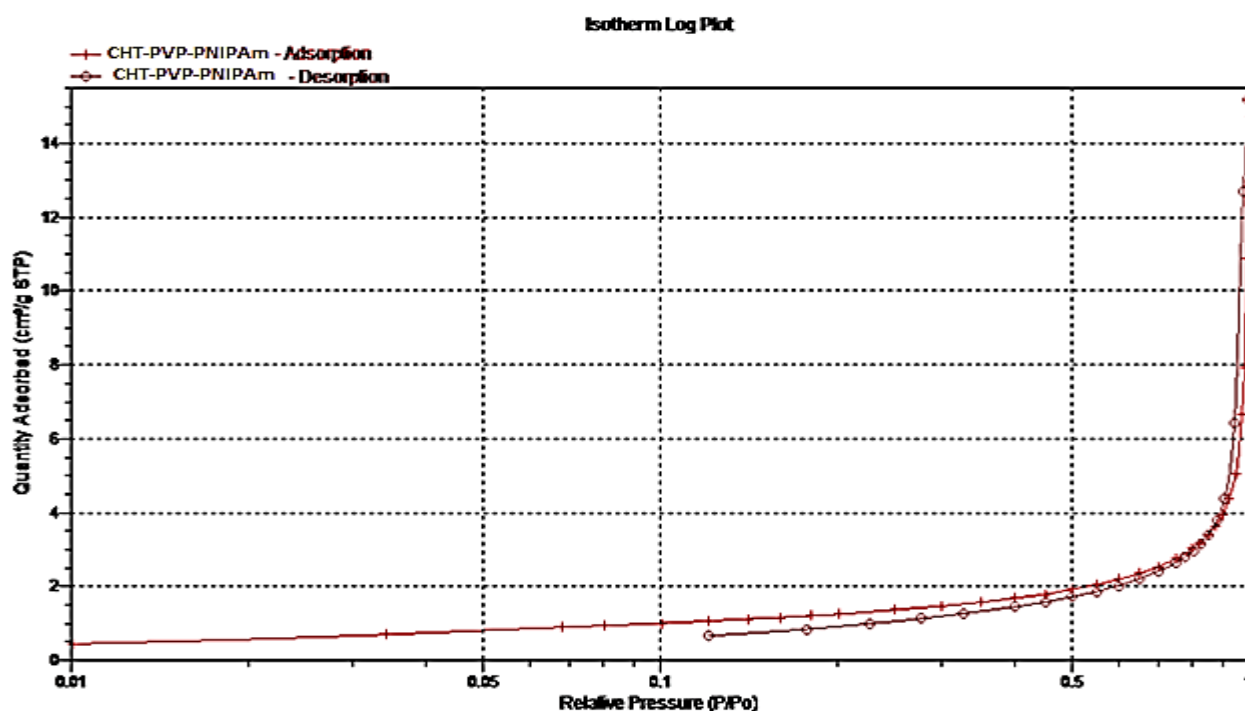


Figure 6.8: Isotherm log plot of the polymerized C-P-N hydrogel.

6.3.7.2. Assessment of the swelling and erosion behavior

Matrix erosion (ME) of the C-P-N hydrogel in a STE was evaluated utilizing an orbital shaking incubator (at 20rpm, 37°C) over 30 days. Figures 6.9 a-b shows the ME of the non-cross-linked and cross-linked C-P-N hydrogel. Figure 6.9a shows high ME on the non-cross-linked C-P-N hydrogel at about 65-79% weight loss over 30 days, for F₁-F₃ respectively. In contrast, Figure 6.9b displays low ME on the cross-linked C-P-N hydrogel at about 42-60% weight loss over 30 days, for F₁-F₃ respectively. The low ME is due to crosslinking decreasing hydrolytic cleavage. Furthermore, the presence of the biodegradable polymers such as CHT and PNIPAAm as building constituents of the C-P-N hydrogel may have added significant impact in erosion behaviors (Kean and Thanou, 2010).

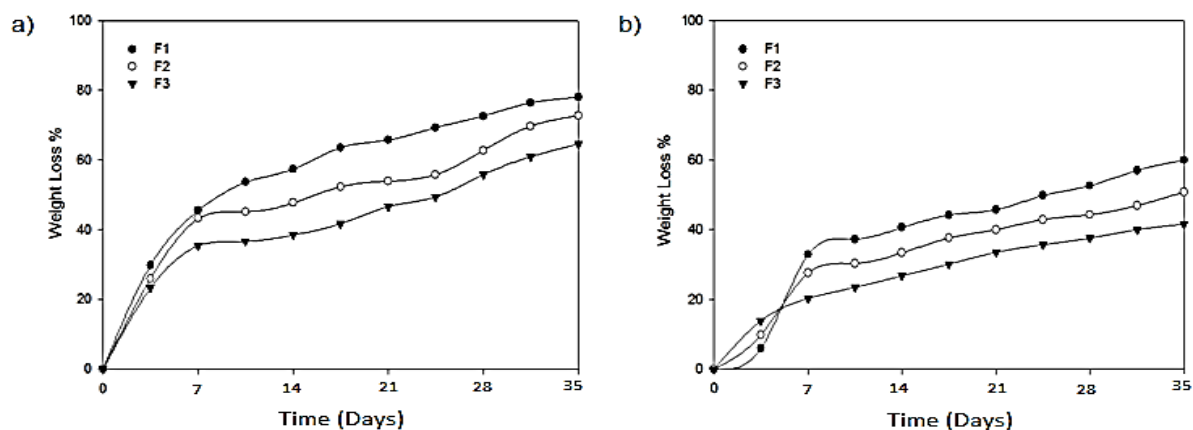


Figure 6.9: Weight loss profiles of the C-P-N hydrogels (F₁-F₃) in simulated tumor condition over 30 days; a) non-cross-linked C-P-N hydrogel and b) cross-linked C-P-N hydrogel.

6.3.8. Morphological characterization of the ISFI

Morphology of the ISFI was characterized by confocal microscopy and SEM. Figure 6.10 evidently depicts the morphology of the drug-loaded functionalized nanomicelles post-encapsulated into the C-P-N hydrogel of the ISFI. Figures 6.10 a-c shows the surface morphology of the ISFI with intact drug-loaded functionalized nanomicelles. Drug-loaded functionalized nanomicelles evidently possessed a uniform spherical shape previously demonstrated in Chapter 5, section 5.3.3 and Figure 5.4. Confocal microscopy further validates distribution of the labeled functionalized nanomicelles in the temporal polymeric-based depot systems as previously discussed in Chapter 5, Section 5.3.5. Control native or unlabeled C-P-N hydrogel depicts no rhodamine activities. The overall results substantiate that drug-loaded functionalized nanomicelles remain intact post-lyophilization for 48 hours.

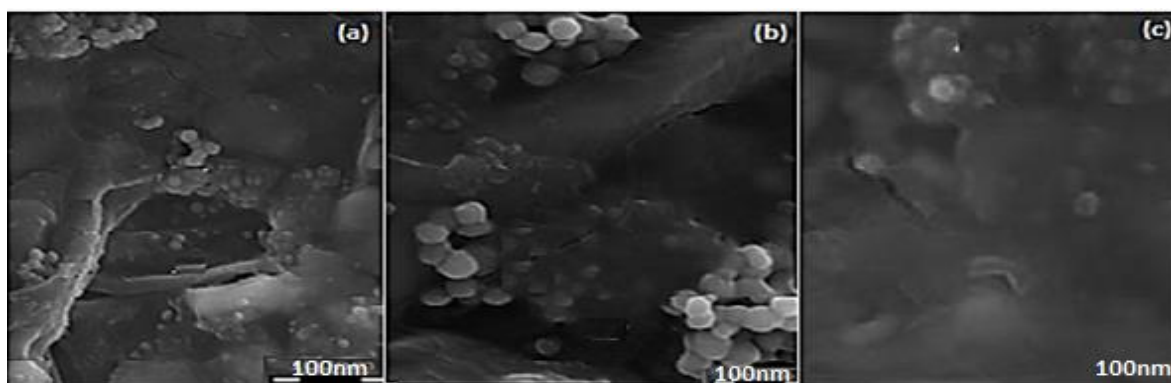


Figure 6.10: Typical SEM micrographs of the drug-loaded functionalized nanomicelles post-encapsulated within the C-P-N at 50x magnification (a & c), b) high magnification 100x of the ISFI.

6.3.9. Assessment of drug release from the ISFI at a simulated tumor site

Studies conducted thus far had been completed employing the drug, folic acid due to its similarity with the chemotherapeutic drug methotrexate. With the determination of an optimized formulation, the release of MTX from the formulation had to be determined. To date, a calibration curve of MTX was prepared in order to quantify the amount of drug that had been released using standard UV spectroscopy. A stock solution of methotrexate in phosphate-buffered saline was prepared at a concentration ratio of 0.4%w/v. Serial dilutions were then made to yield a concentration range of (0.00034-0.012 mg/mL). The solutions were then assayed using a UV Spectrophotometer (Specord 40, Analytik Jena, AG, Germany) using a wavelength of 306nm. The optimized formulation loaded with methotrexate (7mg/mL) was utilized as presented in Figure 6.11. Release studies as per Chapter 3, Section 3.2.13 of this chapter were conducted at 37°C in 0,1 M PBS of pH 6.75 to represent a simulated tumor micro-environment. The release profiles of MTX from the hydrogel drug delivery system (Figure 6.12) was established to exceed 30 days, with almost 20 % of the drug being released after this time.

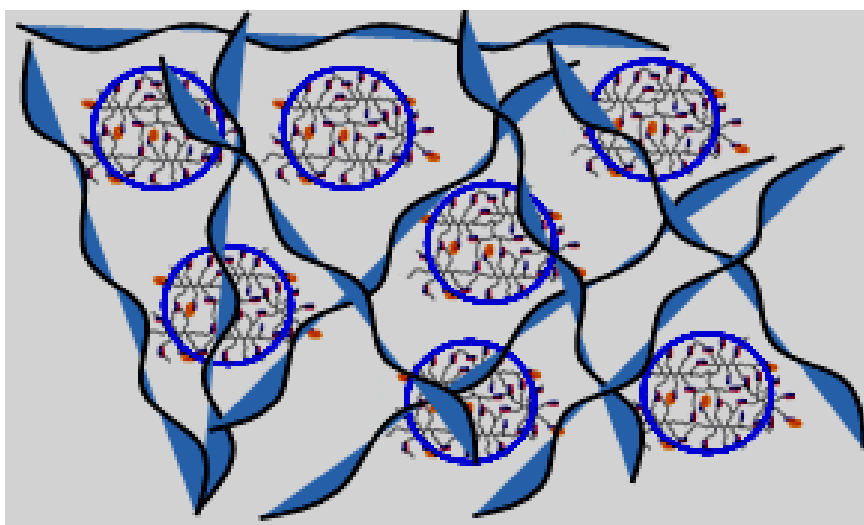


Figure 6.11: An optimized implantable antibody functionalized methotrexate loaded nanomicelles hydrogel composite delivery system.

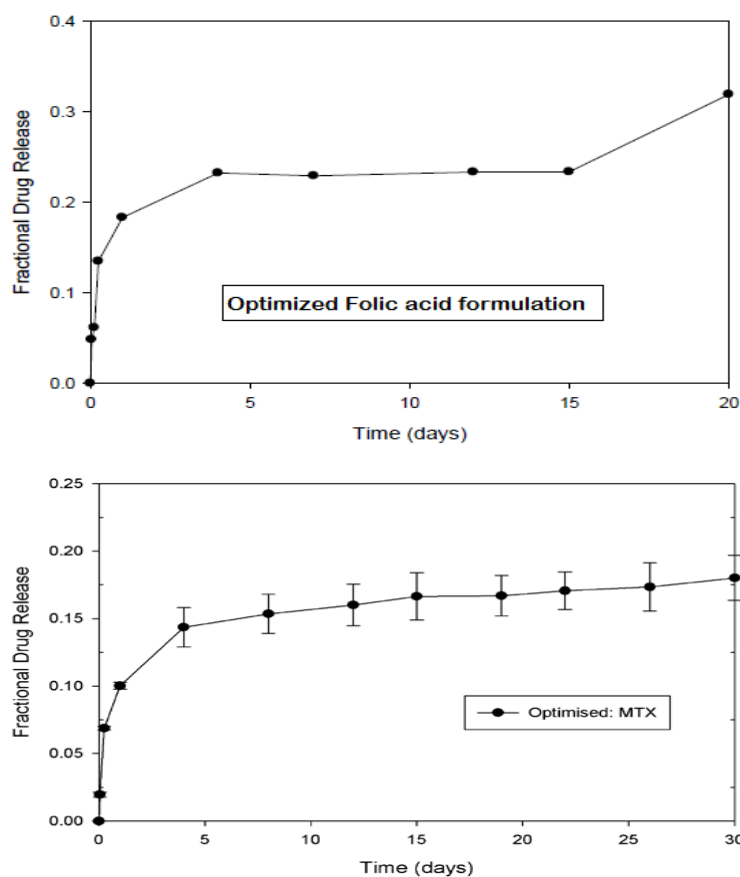


Figure 6.12: Folic acid and Methotrexate release profiles from the optimized formulation over a month (30 days) period.

The release of MTX from the formulation followed a pattern similar to that obtained for folic acid; however the MDT was 20.65 whereas formulations containing folic acid had a slighter higher MDT of 21.23. The pattern of release was also considered satisfactory, in that the formulation appears to have a fast release initially and then a steady release of drug followed by fast release. Weinberg et al. (2007) have suggested that a formulation would prove the best for the delivery of drug to solid tumors if it is able to provide an initial burst release at the specific site and then show continuous slow release of drug. MTX has a “time effect” i.e. the sensitivity of cells towards MTX increases with a time an implant releasing drug slowly will also be beneficial. The release of the drug *in vivo* will be discussed further in Chapter 7.

6.3.10 *Ex vivo* evaluation of the ISFI

6.3.10.1. Cytotoxicity analysis of the polymer framework on cell culture

The cytocompatibility and/or cytotoxicity of the functionalized nanomicelles, C-P-N hydrogel and ISFI in the presence of NIH:OVCAR-5 cells was evaluated using MTT assay as previously

discussed in section 5.2.6. MTT assay as depicted in Figure 5.5 generated for functionalized nanomicelles, C-P-N hydrogel and ISFI showed increasing cytotoxicity with regression in cell viability after incubation for 72 hours as the formulation concentration increased. While C-P-N hydrogel displayed superior biocompatibility *in vitro* even at the highest concentration of 0.01mg/mL a value of 86% cell viability was recorded, comparable to the observations in section 5.3.4. This high cell survival rate for PNIPAAm-b-PASP confirmed that the C-P-N hydrogel offers excellent biocompatibility for intracellular biomedical applications. Functionalized nanomicelles showed a low impact on cell viability or cytotoxicity $70\pm 1\%$, while the effect on the C-P-N hydrogel $86\pm 1\%$ and ISFI $76\pm 1\%$ were slightly higher. These results validate that functionalized nanomicelles, C-P-N hydrogel and ISFI have low effect on extracellular methotrexate release post-cultivation in a cellular environment (37°C in a CO_2 condition) over 30 days. Slightly lower methotrexate levels in the presence of the functionalized nanomicelles encapsulated with C-P-N may have been influenced by the C-P-N engineered to embed the nanomicelles. In addition, the presence of CHT also demonstrated a significant effect on sealing cell membrane damage through maintaining membrane integrity (Bhattarai et al., 2005; Heinemann et al., 2009).

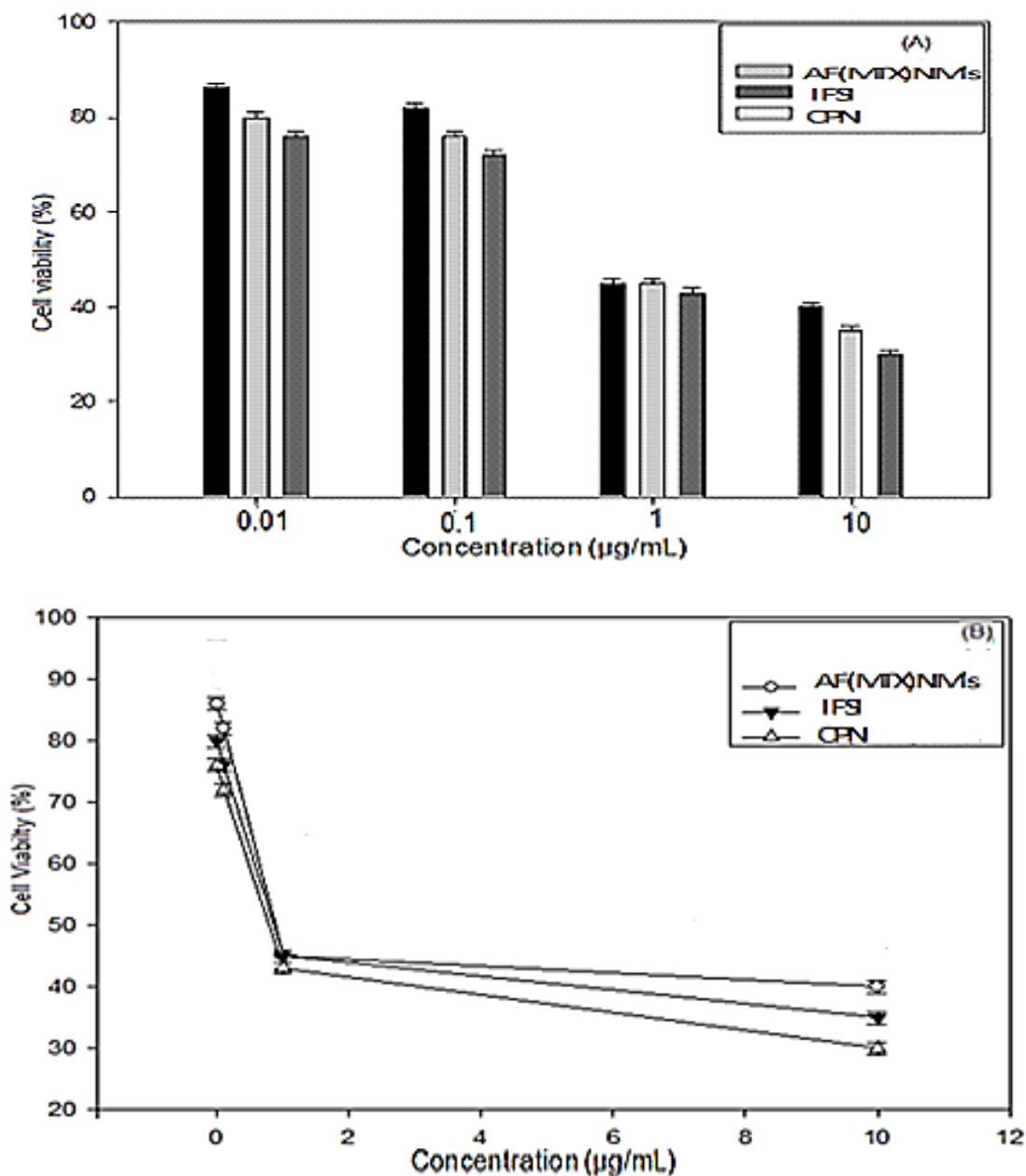


Figure 6.13: Tetrazolium salt MTT assay to evaluate the effect of AF(MTX)NM's, ISFI and C-P-N formulations (a) on percentage viability of NIH:OVCAR-5 cells. AF(MTX)NM's formulation, ISFI and C-P-N elutes were incubated with ovarian cells for 72 hours prior to cell viability evaluation in each treatment group. Each point depicts average \pm SD (n =3).

6.3.10.2. Fluorescence imaging of the fluorescence-labeled ISFI

Fluorescence labeling technology in nano-pharmaceuticals has been the most-often-used technology for validating the capability of targeting of the drug delivery system into a disease site (Martina et al., 2007; Wanga et al., 2010). In this chapter, fluorescence imaging was utilized for further validating ISFI formation and intracellular distribution. Figure 6.14 shows confocal fluorescence images of the ISFI. Unlabelled control micelles image (a), FITC-labeled functionalized nanomicelles (b-d) and C-P-N hydrogel stained with DAPI or trypan blue (e).

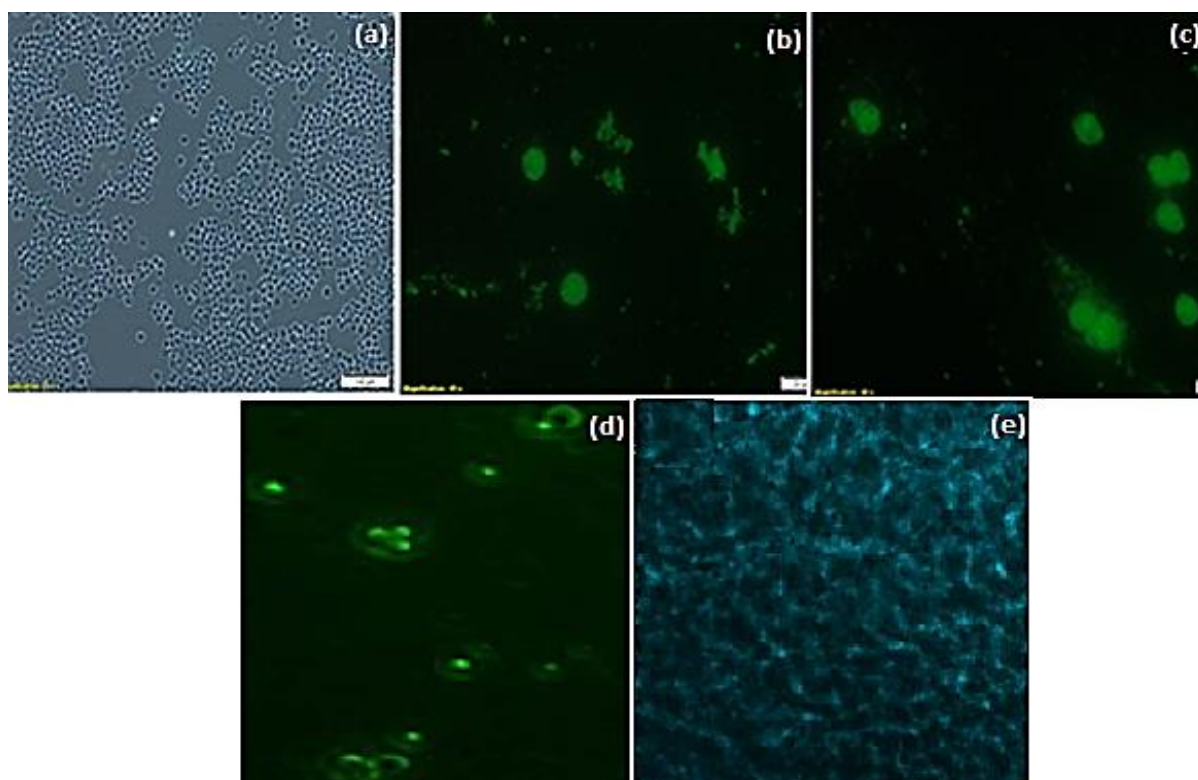


Figure 6.14: Confocal fluorescence images of the ISFI. Unlabelled control micelles image (a), FITC-labeled functionalized nanomicelles (b-d) and C-P-N hydrogel stained with DAPI or trypan blue.

6.4. Concluding Remarks

The formulated ISFI may provide an improvement to the available drug delivery systems and may provide adequate management of EOC in terms of chemotherapeutic efficacy, long-term pharmaceutical stability, specific targeted drug delivery and once-off drug administration. The data acquired in this chapter evidently confirmed the development of the ISFI formulated by encapsulating fluorescence-labeled functionalized nanomicelles within cross-linked C-P-N hydrogel. FTIR analysis revealed the existence of bands produced during molecular structural interactions or cross-linking of the polymers during the design of the C-P-N hydrogel. In addition, these results propose that biomechanical features must also be taken into consideration when designing the C-P-N drug delivery system. The mechanical properties of the permanent C-P-N hydrogel were influenced by gel flow which was observed in solid state rather than liquid state. In this case, G' was greater than G'' , indicating that strong intermolecular interactions were obtained during C-P-N hydrogel formulation. Fluorescence imaging exhibited the specificity of the FITC-labeled nanomicelles post-encapsulating within the double-labeled ISFI. Future studies are necessary to identify the ISFI's ability for diagnosis and/or targeted chemo-treatment for afflictions such as EOC, since functionalized moieties

have previously been observed to have the ability for directing nanomicelles to specific sites of EOC. The results in this chapter also confirmed that biomechanical activity and imaging techniques could be utilized as appropriate potential techniques for characterization of track-labeled drug delivery nanomicelles post-encapsulated into an ISFI.

CHAPTER 7

AN OPTIMAL MOUSE MODEL FOR HUMAN OVARIAN CARCINOMA RESEARCH AND EFFICACY OF VARIOUS CHEMOTHERAPEUTIC TREATMENT PROTOCOLS

7.1. Introduction

Epithelial ovarian cancer (EOC) is one of the most fatal gynaecological malignancies in which many patients are diagnosed at an advanced stage when the disease has already spread beyond the ovaries to the abdominal cavity (Whitehouse and Solomons, 2003; Wang et al., 2011; Cho et al., 2013). Thus, some of the significant goals of ovarian carcinoma research include the identification of molecular markers which can be used to prevent this malignant disease, facilitate its earlier detection and treat it more effectively (Vanderhyden, 2003; Chauhan et al., 2009; Jacobs et al., 1992)). Various biomarkers have been employed to assess the growth of epithelial ovarian cancer and to detect the disease at an early stage (Bast et al., 2005). Serum tumor biomarkers such as HE4, CA 72-4, EGFR, SMRP, mesothelin and various mucins (especially mucin 16-MUC16/CA125) have proven invaluable in the diagnosis and monitoring of treatment regimes in various types of ovarian cancer. MUC16 (CA125) is a well-established clinical marker for the assessment of epithelial ovarian cancer (EOC) progression, regression and therapeutic response and is evaluated by quantifying serum, and ascitic fluid levels of the MUC 16/CA 125 antigen (Yin et al 2002; Rump et al 2004; Moore et al 2007; Felder et al 2014). The monoclonal antibody OC125/Mab anti-MUC16 identifies this tumor-associated antigen which is over-expressed in epithelial ovarian cancer cells, but not in the epithelium of normal fetal and mature ovaries (Bast et al., 1981). Whilst being a sensitive biomarker, the role of CA125/MUC16 is restricted due to its elevated serum levels in some benign conditions including endometriosis, chronic liver disease, pleural, pericardial and peritoneal inflammation and pregnancy (first trimester), to mention a few (Ja"ger et al., 2007; Kafali et al., 2004). CA125/MUC16 in human ovarian carcinoma also forms a lubricating gel-like barrier that surrounds ovarian tumor cells, protecting them against chemotherapy agents (Wang et al., 2008; Th"eriauult et al., 2011).

Enzyme-linked immunosorbent assays/ELISAs for OC125 detect elevations in cancer antigen 125 (CA125) concentrations in greater than 80 percent of epithelial ovarian cancer (EOC) patients' sera but in less than 1 percent of control group sera from normal healthy women (Bast et al., 1983). The serum CA125/MUC 16 concentration is >35 U/ml in 60 percent of women with epithelial ovarian cancer. In the present study, quantification of MUC 16/CA 125 concentration was conducted utilizing the highly sensitive Cancer Antigen 125 (CA125)

Human ELISA Kit (Code No. ab108653, Abcam, Cambridge, USA) with a minimum detectable concentration value of 5 U/ml. As part of the validation of this assay, normal healthy women were estimated to have CA125 concentrations below 35 units per ml which was consistent with the aforementioned ELISA assays.

In evolving models of human ovarian malignancy, it is important to ascertain whether the selected model system mimics the biological behavior of ovarian cancer in human patients closely enough (Sallinen et al., 2006; Lin et al., 2007; Zhang et al., 2013). It has been established that, compared with cancer cell lines, only xenografts derived directly from fresh human ovarian cancer tissues are identical to the original malignancies in terms of MUC16/CA 125 over-expression. This may be ascribed to the fact that cancer cell lines have been shown to transform their protein expression profiles and lose the heterogeneity implicit in *in-vivo* human carcinoma through continued *in-vitro* culturing (Deraco et al., 2011; Streppel et al., 2012). A variety of mouse models of ovarian cancer have been developed, providing ample information regarding the genetic and developmental etiology of this disease (Denise and Connolly, 2009; Wang et al., 2008). There are three distinct applications for mouse model systems in cancer research: First, to support research into basic tumor biology (e.g. tumor tissue histomorphology including microvessel density/MVD and MUC 16 expression), secondly as a system for the refinement of chemotherapeutic drugs in preclinical trials, and lastly as a controlled system for testing novel clinical therapeutic agents and assays (Bruns et al., 2002). Intraperitoneal (IP) mouse model systems have proven essential in testing the therapeutic efficacy of a variety of intraperitoneal chemotherapies which has not been the case with the subcutaneous models. This is not altogether surprising, since peritoneal dissemination is the key feature of ovarian carcinomas, a feature which is thought to be related to MUC16 expression, since MUC16 is expressed by mesothelial cells lining the parietal and visceral peritoneum, as well as by the neoplastic ovarian carcinoma cells themselves. MUC16 mediates cell contact and adhesion by binding to apical surface of the mesothelin and this MUC16-mesothelin interaction has a significant role in dissemination of metastasizing EOC cells to the peritoneal cavity. On the other hand, the subcutaneous ovarian carcinoma nodules do not disseminate (Orsulic et al., 2002; Roberts et al., 2002).

Current treatment regimes for ovarian cancer make use of aggressive cytoreductive surgery, systemic chemotherapy and external beam radiotherapy (MacGibbon *et al.*, 1999; Murdoch and Van Kirk, 2002; Borgeest, et al., 2002). While many patients initially respond to surgery and chemotherapy, the long-term prognosis is generally unfavorable, with recurrence and development of chemo-resistant disease (Khayat *et al.*, 2000). Therefore, there is a dire need for improvement in early diagnosis and treatment strategies for this disease, which may

include the design and use of novel improved drug delivery systems that prolong drug bioavailability, thereby effectively minimizing the incidence of recurrent disease (Seiden, 2001; Cannistra, 2004). In this vein, the present study focused on the development of drug-loaded nanomicelles that specifically targeted MUC16/CA125 antigens on the surface of EOC cells, thereby improving drug bioavailability, minimizing drug-associated systemic side-effects and increasing overall survival rate in a mouse model.

7.2. Materials and Methods

7.2.1. Materials

Methotrexate (MTX), cisplatin [*cis*-dichlorodiammineplatinum(II); CDDP], 3-(4,5-dimethylthiazol-2-yl)-2,5-diphenyl-tetrazolium bromide (MTT), 100 IU/mL penicillin/100mg/mL streptomycin, RPMI 1640, Phosphate Buffered Saline (PBS), 10% heat-inactivated fetal bovine serum (FBS) and 0.25%w/v trypsin 0.03%w/v EDTA solution were purchased from Sigma Aldrich (St. Louis, MO, USA). NIH: OVCAR-5 cells were purchased from Dr. Tom Hamilton (Fox Chase Cancer Institute, PA, USA). RayBio® Human CA-125 (MUC16) Elisa Kit for serum, plasma, ascitic fluid, cell culture supernatants, and urine (96-wells) were purchased from Biocom Biotech (Pty) Ltd. (Centurion, Pretoria, RSA). Anti-MUC16 antibody [OC125] ab693 was procured from Abcam Inc. (Cambridge, USA). Purified deionized water was prepared by a Milli-Q System (Millipore Co., Billerica, MA, USA). 98% DMSO, N,N'-dimethylformamide (DMF), tetrahydrofuran (THF), ethyl ether and petroleum ether (30-60°C) was obtained from Merck Chemicals Co. (Pty) Ltd. (Darmstadt, Germany) and were of analytical grade. Culture plates were purchased from Corning Inc. (NY, USA). All OC cells were grown in an incubator from RS Biotechnological Galaxy (Irvine, UK) maintained at 37°C in a fully humidified atmosphere of 5% CO₂. All cell experiments were performed in the logarithmic phase of growth.

7.2.2. Mouse housing conditions and welfare

Four- to six-week-old female Swiss Athymic nude mice (purchased from Charles River Laboratories International, France, Inc.) were housed in a specific pathogen free (SPF) facility in IVC cages Air flow systems ® filter top cage Type 2 L (Bioscape Eboco + Ethet Fusion, Emmendingen, Germany) and placed in stainless steel racks (Figure 7.1). The SPF room temperature was kept at 25°C with 60-70 % relative humidity (RH) with a 12 hour light/dark rotation and then the nude mice were given a week of acclimatization before the experiments commenced, the details of the mice utilized in this study are illustrated in Table 7.1. Mice were fed ad libitum diet and water. All procedures were performed under sterile conditions in a

laminar flow hood. The animals were monitored daily for general health status. Animal ethics for *in vivo* studies was approved by Wits Animal Ethics Screening Committee, AESC Number: 2012/46/05 and the study protocol adhered to these guidelines and those of the South African Council on Animal Care. Furthermore, approval of modifications to the study can be presented in Appendix B2.

Table 7.1: Details of the optimal mouse model for human ovarian carcinoma research used in this study.

Species	Strain	Sex	Age/Body Mass	Number required	Location ¹
Mice	Swiss Athymic nude	F	4-6 weeks old, ~ 26g	120	Central Animal Services



Figure 7.1: Athymic nude mice were placed in inside sterile IVC cages air flow systems in SPF room at 25°C with 60-70°C relative humidity(RH), sterile fed ad libitum diet, water and bedding were also used to ensure the soothe-comfort and protection against infection.

The measures which were used if needed to ensure that the animal's welfare needs were met or enhanced and reduce suffering included doses, routes of administration, frequency of administration of analgesics. If the animals experience an anaphylactic response to the ISFI and its components, they were to be treated with the appropriate anti-anaphylactic agents and this was not encountered in this study. If the response is too severe, however, these mice were to be removed from the study. As a result of the growing cancer cells in the animals and chemotherapy, exclusion criteria included; a reduction in weight (>15%), animal distress possibly caused by hypersensitivity to the delivery system or drugs, characteristic sickly behaviour or deteriorating body condition and distinctive side effects such as neutropenia.

7.2.3. Cell Culture

The NIH:OVCAR-5 cell line is an established ovarian carcinoma cell line that expresses the MUC16 antigen (Hamilton et al., 1983). This ovarian cancer cell line (NIH:OVCAR-5) was purchased from Dr Tom Hamilton (Fox Chase Cancer Facility, USA, Jerkitown, CA). The NIH:OVCAR-5 cells were cultured to 80% density and allowed to adhere in plastic tissue culture flasks in Roswell Park Memorial Institute (RPMI) growth medium supplemented with heat-inactivated fetal calf serum (FCS 10%), glutamine (2mM), penicillin/streptomycin (50 units/mL) and insulin (50 units/mL), respectively. All the cancer cells were grown in an incubator from RS Biotechnological Galaxy (Irvine, UK) maintained at 37 °C in a fully humidified atmosphere of 5% CO₂. Cells were sub-cultured weekly, harvested by trypsination, washed twice in PBS, stained with Trypan Blue and counted. Experiments were conducted after 1–2 sub-culturing cycles. A sterile hemacytometer was the instrument used for counting and this was done using the trypan blue exclusion assay. Trypan blue is a dye that stains the nuclei of non-viable or dead cells isolating them from live viable ones and allowing this distinction to be observed under the light microscope. A 0.4 %w/v trypan blue solution in sterile PBS (0.1 M, pH 7.4) was prepared for cell counting. A cell volume of 20 µL and a trypan blue volume of 60 µL were mixed together. The percentage of viable cells was calculated as a function of number of cells counted per number of quadrants counted as shown in Equation 7.1. This was 1:3 ratio which produced a dilution factor of 4.

$$\% \text{ Viable cells} = \frac{\text{Number of cells counted}}{\text{Number of quadrants counted}} \times \text{dF} \times 10^4 \text{ cells/mL} \dots \dots \text{Equation (7.1)}$$

where DF is the dilution factor used and 10⁴ is a constant. Only samples that exhibited viability of greater than 95% were employed in subsequent testing.

7.2.4. Sterile preparation of ISFI formulations

The ISFI formulation were fabricated as per protocol described in Chapter 6, Section 6.2.6. The formulations were prepared under a horizontal laminar flow unit (Labotec®, Midrand, South Africa) fitted with a HEPA sterile filter in a sterile room. Sterile settle plates of Tryptone Soya Agar were placed at the corners of the laminar flow unit in order to determine the presence of possible contaminating micro-organisms. These plates were incubated at 37°C and 25°C for 24 hours to determine the presence of bacteria and fungi respectively. A small amount of the final formulation was also streaked onto a nutrient rich blood agar plate and incubated at 37°C for 24 hours to determine if the formulation was sterile.

7.2.5. Biocompatibility studies in mice

Mice received the once-off drug loaded implant (ISFI) on Day 1 and were sacrificed after 1 hour, 4 hours and then on days 2, 4, 6, 8 and 10. The area around the implant including skin and underlying muscle was resected. The flank opposite to the side of implant implantation was utilised as the control. The samples were preserved in formaldehyde (4%v/v) and were sent to IDEXX laboratories where they were analyzed using routine histopathological methods. Briefly, sections of the samples were processed in an automated tissue histological processor according to a routine standard operating procedure. Following overnight tissue processing, wax blocks were prepared and 5µm slides were cut on a microtome before the sections were mounted on a microscope slide. These sections were stained with the Haematoxylin and Eosin staining method and mounted before microscopy was performed.

7.2.6. Establishment of a model for induction of ovarian cancer using Athymic nude mice: Pilot study

A pilot study was first conducted in order to evaluate feasibility and validity of the experimental procedures that includes; intraperitoneal injections, ovarian cancer induction, implant tolerance and measurement techniques for targeted drug delivery prior to performance of main study. All experiments were conducted inside an Esco Frontier™ DuoFume Hood in the specific pathogen free (SPF) facility. This pilot study confirmed ovarian cancer induction and no deficiencies in the design of the main study.

7.2.7. Experimental design

The study design described how the animals were allocated to experimental and control groups, the number of animals in each group (n), the probability level of confidence adopted, and how the experimental treatments were assigned to each group. A flow diagram was used in Figure 7.2, and the experimental design is explained in detailed in the subsequent subsections.

In vivo animal studies
Athymic nude mice

Pilot Study*
23 mice (5 mice for each Group)

Main Study*
40 mice (10 mice for each Group)

Day 1: Inoculation, all mice injected subcutaneously with 5×10^6 NIH:OVACAR-5 cancer cells in 0.2 μ l RPMI in the peritoneal/s region.

10 days after inoculation
Tumor development will be measured using calipers and VEVO imager
a volume of 2 cm³ fluid was extracted from peritoneal region.

Experimental group 1

10 mice injected with IPSI containing Methotrexate -loaded PNIPAAM-b-PASP nanomicelles.

Experimental group 2

10 mice injected with IPSI containing anti-MUC16-targeted Methotrexate-loaded PNIPAAM-b-PASP nanomicelles.

Comparison group 3

10 mice treated with 15mg/Kg Methotrexate infused intravenously (i.v).

Placebo group 4

10 mice injected with placebo IPSI containing PNIPAAM-b-PASP nanomicelles

Anaesthesia

Anaesthesia achieved by subcutaneous intramuscular injection of Ketamine HCL (60mg/kg) and Xylazine HCL (10mg/kg).

Blood Sampling

Days 1, 4, 8, 16, 24, 32 after IPSI implantation
Peritoneal fluid (2 cm³) collected with fine needle inserted through the abdomen.

Anaesthesia and Euthanasia

- Mice will be intramuscular injected with anaesthetic followed thereafter by carbon dioxide inhalation to euthanize the mice after day 32. Blood sampled (4ml) collected via cardiac puncture

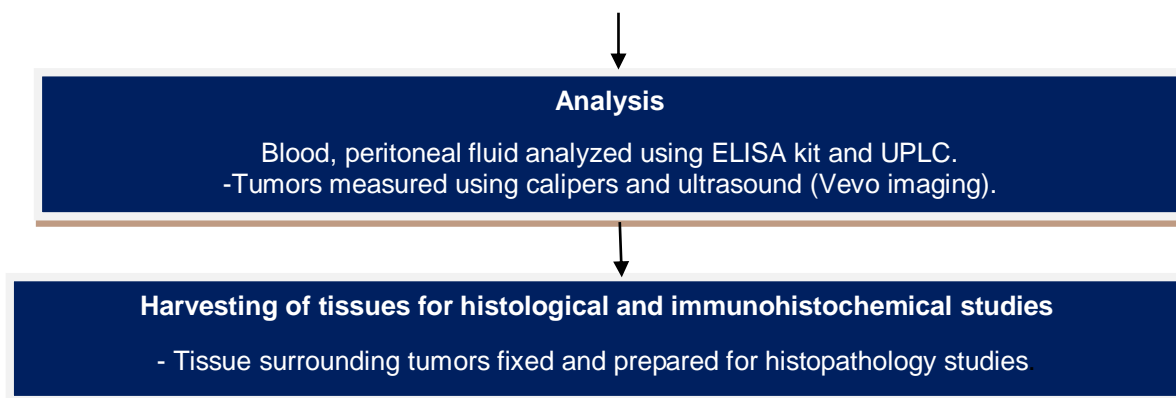


Figure 7.2: Schematic representing of the study design and number of mice required for the in vivo preclinical studies using PNIPAAM-b-PASP methotrexate-loaded with/without antibody nanomicelles for targeting ovarian cancer cells.

7.2.7.1. Intraperitoneal (IP) and Subcutaneous (SC) induction of Human Ovarian Carcinoma in Swiss Athymic Nude Mice – Pre-treatment Phase

The ovarian carcinoma induction stage of this study shall be referred to as the pre-treatment phase. All experiments were conducted inside an Esco Frontier™ DuoFume Hood in the specific pathogen free (SPF) facility. The model was generated by injecting female athymic 4- to 6-week-old nude mice SC and IP with 2×10^6 cells/ml and 2×10^8 cells/ml, respectively of NIH:OVCAR-5 cancer cell suspensions in 200 μ l RPMI media as shown in Figure 7.3 a and b and protocol in appendix (D5). Inoculations were performed using a 26G gauge needle and a 1 ml syringe.



Figure 7.3: a) Inoculation of 1×10^6 NIH:OVCAR-5 cells/ml into the flank (SC) and b) 2×10^8 cells/ml into the peritoneal cavity of immuno-deficient Swiss nude mice respectively.

7.2.7.2. Acquisition of adequate mice stock for human ovarian carcinoma research

Breeding of the nude was conducted in this study, for acquisition of sufficient stock for human ovarian carcinoma research. This was to surmount the cost challenges, since these animals are very expensive. Breeding of nude mice commenced with 15 breeders from Charles River France. However, breeding had its drawbacks: out of 8 litters produced only 1 or 2 were female nude mice and also out of 15 litters of in-bred mice only 5 or 6 survived, this was due to temperature fluctuations resulting in stress and cannibalism, although their ad libitum diet was supplemented with calcium.

7.2.7.3. SC-inoculated mice

To inoculate cells SC, the skin of the nude mouse was pinched between the index finger and thumb and the skin was dragged away from the soft-body of the mouse. Then, NIH:OVCAR-5 cells were inoculated slowly and uniformly into the pouch formed by fingers, creating a single-bubble of cells underneath the skin and avoiding excessive spread of the injected-cells. In the SC-inoculated mice, growths were observed under the skin and were measured using an electronic digital Vernier caliper and a Vevo 2100® imaging system (Visualsonics Inc, Toronto, Canada) (Figure 7.5a-c). All tumor-bearing mice were further monitored until the tumors developed to their target size of 80mm³-100mm³, which was regarded as the baseline for initiation of treatment. Tumor sizes were evaluated using the formula $0,5 \text{ (length} \times \text{breadth}^2)$ by measuring the surface length and breadth dimensions of the tumor every second day after tumor development, and also every second day after implantation of the AF(D)NMs treatment (Figure 7.5a). Using ultrasonography, tumor development was detected from day 1 PI-post-inoculation (at the site of induction) until day 10 PI, and thereafter mice were scanned every second day after implantation of the AF(D)NMs treatment (Figure 7.4 and 7.5d).

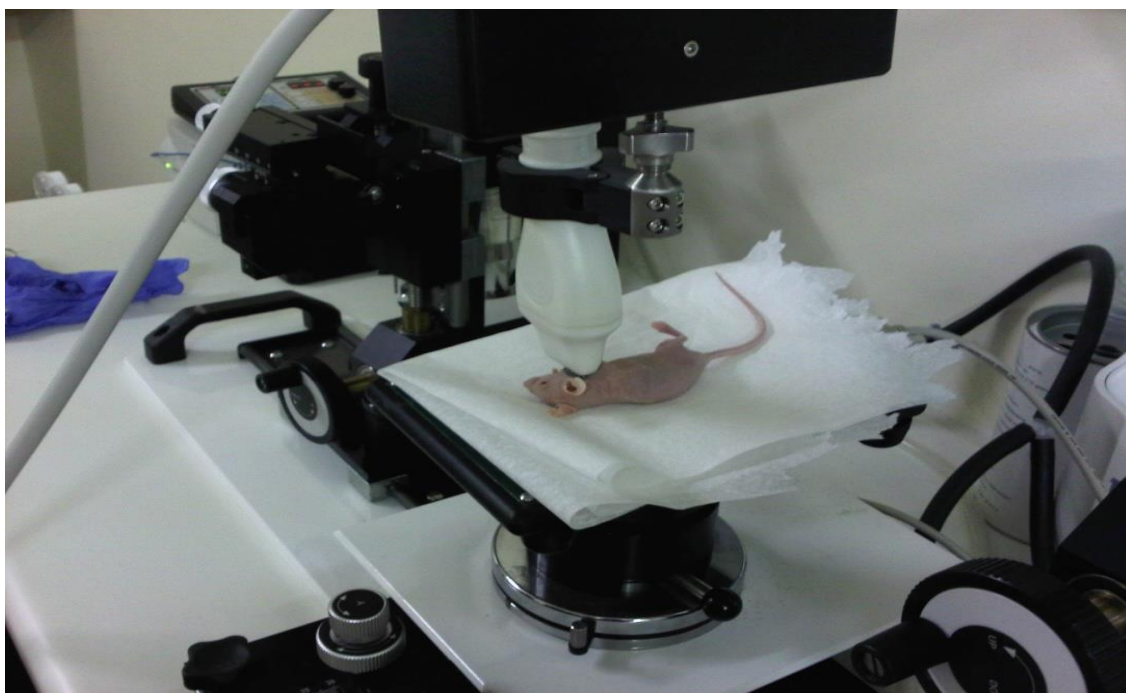


Figure 7.4: Digital-image of anaesthetized SC (neck region) inoculated mouse scanned for tumor development using ultra sound Vevo® 2100 Imaging system (Visualsonics Inc, Toronto,Canada).

7.2.7.4. IP-inoculated mice

Mice were inspected weekly and tumor development with peritoneal carcinomatosis in the IP-inoculated mice was monitored based on overall health using the following clinical positive indicators: presence of intra-abdominal nodular growths, distension of the abdominal cavity due to ascites, weakness, weight loss with extensive skin tenting due to dehydration and changes in behavior due to perceived pain (Figure 7.6a). One of the modalities used to assess IP tumor development was a Vevo 2100® imaging system (Visualsonics Inc, Toronto, Canada), which was used to detect early tumor development (Figure 7.4 and Figure 7.6b and c). Tumor-bearing mice were scanned from day 1 PI-post-inoculation (at the site of induction) until day 10 PI and thereafter mice were scanned every second day after implantation of the AF(D)NMs treatment, in order to evaluate treatment efficacy over the course of therapy (Figure.7.6b and c).

7.2.7.5. Description of the anaesthetics, analgesics and drugs employed

Mice were anaesthetized with Ketamine and Isoflurane before scanning for tumors using the Vevo® 2100 Imager. Description of the anaesthetics, analgesics and drugs used together with the doses and routes of administration are demonstrated in Table 7.2. Briefly, isoflurane is a

halogenated ether utilized for inhalational anesthesia; most common volatile anesthetic employed in veterinary medicine. The animals were placed in the clean induction chamber disinfected with 10% ethanol, and the chamber was closed securely. The oxygen was turned on so that flow rate is 1 liter/minute and the dial for isoflurane delivery was adjusted to 3-4 %. The induction chamber was always kept functionally air-tight and animals confined in the closed chamber with gas flow. When animal lost righting reflex, isoflurane flow was turned off and induction chamber was flushed with oxygen for 20 seconds. The anaesthetized animal was removed onto a surface of a clean stage fitted with a heated pad; and its snout snugly attached onto a nose cone placed in the opening of the tube dialing isoflurane concentration to 1.5-2.0% and oxygen flow rate to 0.8 liters/minute. A pre-warmed gel specific to ultrasound imaging was smoothly applied on the inoculated area of the mouse. The imaging probe was properly placed on the region of interest and imaging was conducted. The imaging procedure was conducted by CAS trained staff to ensure appropriate mice monitoring, and as described in the approved protocol (chapter 1 of this thesis).

Table 7.2: Details of the anaesthetics, analgesics and drugs used together with the doses and routes of administration

Drug/Substance	Route (e.g., I.V., I.M.)	Dose	Frequency
Cisplatin	Intravenous	4mg/kg	Weekly administration
	IPSI (intraperitoneal)	20 mg/kg	Once off injection of IPSI.
Methotrexate	Intravenous	10 mg/m ²	Weekly administration
	IPSI (intraperitoneal)	20mg/m ²	Once off injection of the IPSI
Xylazine	Intraperitoneal injection	10mg/kg	Administered before injection of cancer cells, IPSI and prior to euthanasia.
Ketamine	Intraperitoneal injection	60mg/kg	Administered before injection of cancer cells, IPSI and prior to euthanasia.
Carbon dioxide	Inhalant	5%	Administered Once off prior to euthanasia.
Sodium Pentobarbitone	Intracardiac injection	200mg/kg	Administered once off to euthanasia.
Isoflurine gas	Inhalant	1.5-2%	Once off prior to imaging
Medical Oxygen	Inhalant	12%	Once off prior to imaging



Figure 7.5: a, b, c and d are SC inoculated nude mice with a tumor diameter of 4mm, measured using an electronic digital Vernier caliper a) and Vevo® 2100 Imager d), respectively.

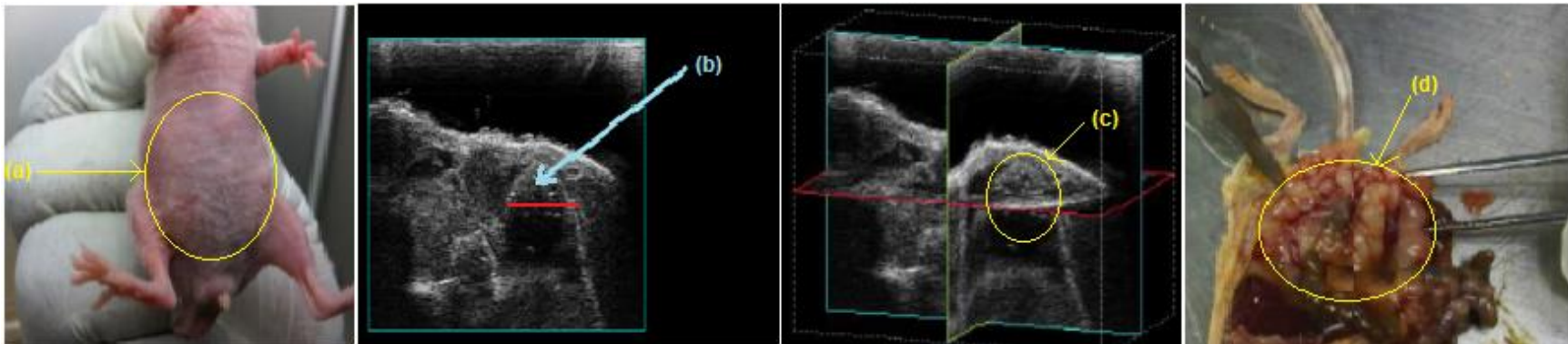


Figure 7.6: a) An IP-inoculated nude mouse with a moderately distended abdomen due to tumor growth, dissemination and ascites. b) Refers to an ultrasound image taken using the Vevo® 2100 Imager indicating a tumor diameter of 100 mm³ and c) is a 3D image of the circumference of the tumor. d) Reveals multiple coalescing tumor nodules disseminated throughout the peritoneal cavity (peritoneal carcinomatosis) as seen during the gross necropsy examination.

7.2.8. Experimental design

Nude mice with growing tumors 10 days post-inoculation were then randomly allocated to four experimental groups including two experimental groups (a drug loaded nanomicelles ((D)NMs) implant and an anti-MUC16/CA125 functionalized drug loaded nanomicelles (AF(D)NMs) implant group), a comparison group (I.V drug only) and a placebo group of 10 mice each (n=10/group) (Figure 7.2). Tumor-bearing mice in the pre-treatment group were euthanized by 5% carbon dioxide (CO₂) inhalation after 10 days once the tumors have developed to their target size of 80mm³-100mm³, which was regarded as the baseline-for initiation of treatment. Organs including the liver, intestines, omentum, mesentery, lungs, pancreas, uterus, oviduct and ovaries, kidney, body wall (skeletal muscle lined by parietal peritoneum) and spleen, as well as solid tumors were collected and ascitic fluid was stored in heparinised tubes (Improve® Improvacuter® Lithium Heparin collection tubes, GmbH, Hamburg, Germany) at -80°C. The 5mm³ tissue and organ samples were preserved in plastic containers filled 10% neutral buffered formalin for up to 5 days, whereafter the formalin- fixed (FF) samples were submitted to the Section of Pathology (SP), Department of Paraclinical Sciences (DPS), Faculty of Veterinary Science (FVS), University of Pretoria (UP), Onderstepoort (OP) for histopathology and MUC 16/CA125 immunohistochemistry/IHC. The tumor-bearing mice in the 2 experimental, as well as the control and placebo groups were further subjected to chemotherapeutic efficacy studies. Survival curves were calculated utilizing the Kaplan-Meier method (Guñther et al., 1999). Survival rate was evaluated as the number of days lapsed between the introduction of a chemo-treatment and euthanasia, and percentage (%) nude mice survival was the number of mice still alive in each test group following introduction of chemo-treatment.

7.2.8.1. Chemotherapeutic Efficacy Studies in EOC-inoculated Nude (NU/NU) Mice

Two intervention studies were conducted in this project and different model chemotherapeutic drugs and formulations were also employed. In the main study 1, implantable antibody-functionalized methotrexate-loaded PNIPAAm-b-PASP nanomicelles were utilized. While, in study 2, implantable antibody- functionalized cisplatin-loaded PEG-PBLG-PF68 nanomicellesemployed for the targeted treatment of ovarian cancer. Hence, invitro results on cisplatin as a model drug were an essential section of study 2 not of this study 1. However, for clinical significance, both optimized formulation from study 1 and 2 were utilized in the invivo studies. The two chemotherapeutic drugs utilized in study (1 & 2) were methotrexate (15mg/kg) and cisplatin (4mg/kg) respectively. In the main intervention study 1 with schematic representation

in Figure 7.2, anti-mucin 16/CA125 antibody-functionalized methotrexate-loaded PNIPAAm-b-PAsp nanomicelles implants were used whereas in intervention study 2 anti-mucin 16/CA125 antibody-functionalized cisplatin-loaded PEG-PBLG-PF68 nanomicelle implants were utilized for the targeted treatment of ovarian carcinoma in mice. PEG-PBLG-PF68, PNIPAAm-b-PAsp copolymers were utilized in the formulation of the drug-loaded nanomicelles and further encapsulated in hydrogel based implants. These implants were subsequently injected into the mice at a volume of 0.2 ml - (4mg/kg for cisplatin and 15mg/kg for Methotrexate) directly into the SC tumor or into a palpable tumor mass within the peritoneal cavity as depicted in Figure B(6f) Appendix B(6). Each mouse in the experimental group received a once-off implant (ISFI) treatment monitored for a period of 30 days whilst the comparison group (IV drug only) was administered treatment at 11-day intervals over the period of a month. Mice in all 4 groups were routinely weighed and tumor size was determined sonographically every five days. Mouse weights were consistently compared with weights at day 0 (first day of treatment administration) in order to determine the percentage weight variation. After a month of treatment the mice in the post-treatment groups were euthanized in same manner as those in the pretreatment group. There was no difference in post mortal sample collection post-treatment compared to pre-treatment.

7.2.8.2. Athymic nude mice Blood Sampling

Blood samples from the tail and sephanus vein, via intra-cardiac puncture were collected pre-inoculation, during the period of tumor growth, during the period of chemotherapeutic dosing and post-mortem respectively (Figure 7.7). This was to determine progression and regression of the MUC16 antigen and drug concentrations. At each time interval, 0.2 ml of blood was sampled. Mice were transported from the SPF unit in a closed, sterile IVC cage to the Vevo 2100 Imager for sonar imaging of tumor sizes. Thereafter, the mice were returned to an alternative sterile room in the CAS unit. Blood was sampled at each time point from different mice, to ensure that the maximum amount of blood was attained while simultaneously allowing each mouse to recuperate as shown in Appendix B2.

Different chemotherapeutic drugs and formulations were administered and blood samples were obtained via intra-cardiac puncture after 1 h, 4 h and 8 h. After 24 h, 48 h and 72 h, mice were euthanized by carbon dioxide inhalation to sample 5mls of blood, organs and tumors, and the wet weight of the tissues was measured. Blood samples were collected in vacutainer tubes containing clotting factor to draw out serum (Figure 7.7 e). The blood tubes were allowed to rest overnight at 4 °C for collection of plasma the following day. The supernatant, containing the plasma, was

carefully extracted and transferred into sterile 2 mL eppendorf tubes and were placed to freeze at -80 °C immediately till further analysis. The Blood and tissue immediately surrounding the implant samples obtained from mice were analysed with Ultra Performance Liquid Chromatography (UPLC) instrument and human ELISA kit, for detection of drug and MUC 16 antigen concentrations respectively. These were terminal procedures for each individual mouse to allow for adequate blood collection and organ excision (Beeton et al., 2007).

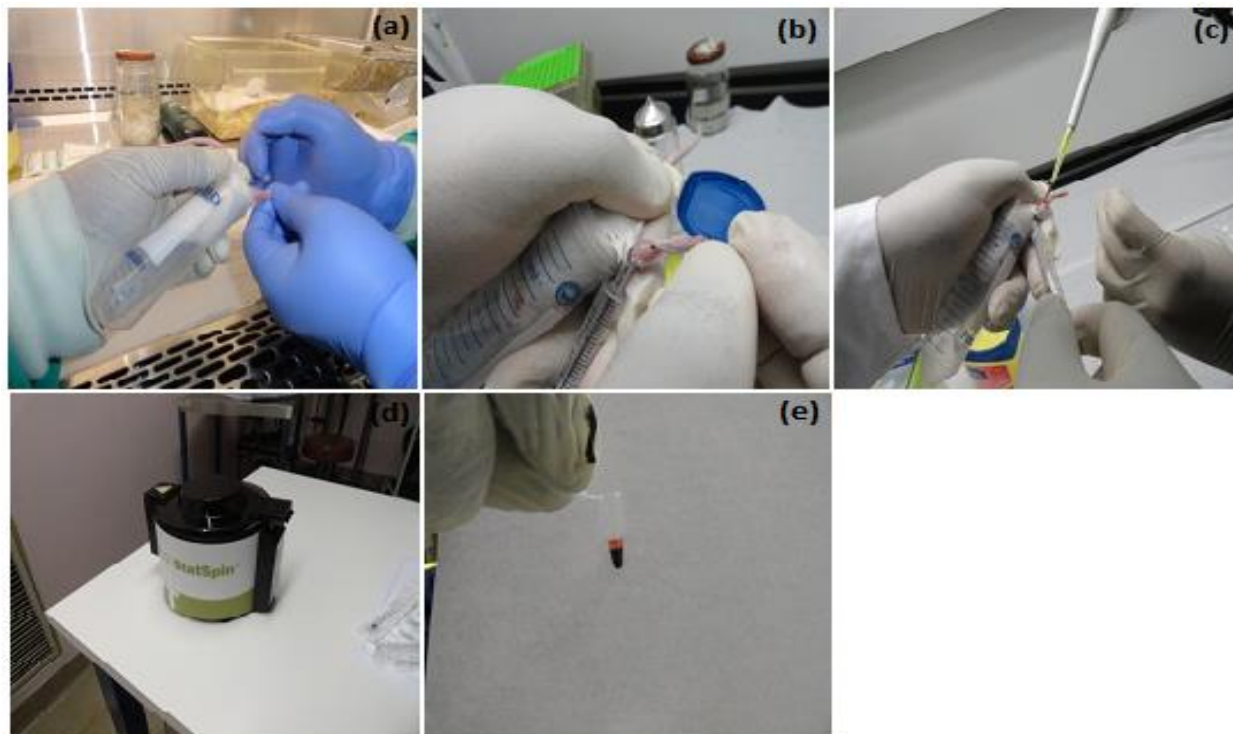


Figure 7.7: Blood collection through the sephanus vein, during pre-inoculation, during the period of tumor growth, during the period of chemotherapeutic dosing (a-c), subsequently serum/plasma samples were extracted employing exxstat spin centrifuge from Idexx laboratories (d-e).

7.2.8.3. Quantification of MUC16/CA 125 levels in Plasma and Ascitic Fluid

Quantification of the MUC16/CA125 antigen in plasma and ascitic fluid was performed by means of the Cancer Antigen CA125 Human ELISA Kit (Code No. ab108653, Abcam, Cambridge, USA), which is based on the solid-phase assay system. The minimum measurable concentration of mucin 16/CA125 in this Elisa assay was 5 units per ml. For the purpose of Elisa-analysis, ascitic fluid and whole blood (obtained from cardiac punctures) were collected in heparinised tubes for plasma, respectively (Improve® Improvacuter® Lithium Heparin collection tubes, GmbH, Hamburg, Germany). The tubes were centrifuged at 3000rpm for 5 minutes to separate the cells from the plasma using a desktop centrifuge (Model TD5A-WS, Shanghai Luxiangyi Centrifuge

Instrument Co.,Ltd., Shanghai, China). The ascitic fluid and plasma were stored at -80°C, pending further processing. The selected Elisa employs a mouse monoclonal anti-MUC16/CA125 antibody (Mab) against a distinctive antigenic determinant on the intact MUC16/CA125 molecule. The Mab was utilized for solid phase assay immobilization (on the microtiter-wells). A rabbit anti-MUC 16/CA125 antibody conjugated to horseradish-peroxidase (HRP) was incorporated in the antibody-enzyme-conjugate solution. The assay sample was permitted to react together with the two antibodies, causing the MUC16/CA125 molecules to be sandwiched in-between the solid-phase and enzyme-linked-antibodies. Following incubation at 37°C for 90 mins, the microtiter-wells were rinsed with Wash-Buffer to clear unbound-labeled-antibodies. Tetramethylbenzidine (TMB) reagent solution was introduced and incubated for 20 mins, resulting in the formation of a blue color. The color-formation was quenched with the introduction of Stop Solution transforming the color to yellow. The concentration of CA125 was directly proportional to the color intensity of the test sample. Absorbance was measured spectrophotometrically at 450 nm.

7.2.8.4. Histopathology and IHC

Formalin-fixed, paraffin-embedded (FFPE) organs from pre-and post-treatment mice (of both cisplatin-and methotrexate-treated nude mouse groups) and SC and IP ovarian carcinomas were sectioned at 3-4 µm and routinely stained with Haematoxylin and Eosin (H&E). Additional 3-4 µm-thick sections were submitted for IHC (specifically the immunoperoxidase labeling technique) to detect membrane-bound and extracellular/shed MUC16. Immunohistochemistry was performed by hand following validated protocols. The standard immunoperoxidase procedure for the detection of MUC16 included deparaffinization and hydration of slides, incubation with 3 % hydrogen peroxide in methanol for 15 minutes to quench endogenous peroxidase activity, heat-induced epitope retrieval/HIER (in a microwave using citrate buffer, pH of 6.0 for 14 min at 96 °C) followed by non-specific immunoglobulin binding^a, incubation for 40 minutes with the mouse monoclonal anti-MUC16^b antibody (diluted 1:50 in buffer ^c), with subsequent application of the Envision Polymer Detection System^d according to manufacturer's instructions. The reaction product was developed by incubating the tissue sections with a liquid 3,3'-diaminobenzidine (DAB) substrate/chromogen (included in the Envision Immunodetection System) for 1-2 minutes. Thereafter the sections were counterstained with Lilly Mayer's hematoxylin for 20 seconds, rinsed with water for 10 minutes, routinely dehydrated through increasing alcohol concentrations and xylol, mounted using Entellan™ (Code No. 1076, Merck Millipore, Darmstadt, Germany) and coverslipped for examination using an Olympus BX43 light microscope. Positive-tissue controls included sections of mouse-inoculated human ovarian carcinoma (NIH:OVCAR-5 cell line) and

negative-mouse tissue controls included normal spleen, liver, omental and mesenteric fat, uterus, oviduct, ovary and pancreas. For negative reagent control purposes, buffer^c was substituted for the primary antibody.

7.2.8.5. Immunohistochemical Quantification of MUC16/CA125 antigens in FFPE tissue sections

Positive labeling was identified as being brown in color and was observed in both cellular (cytoplasmic and cell membrane) and extracellular locations (in tubular lumina) throughout the neoplastic foci (Figure 7.8A). All IHC-labeled tissue slides (one slide per mouse) were scanned utilizing the Olympus dotSlide scanner (VS120-S6-W slide loader system in the Department of Anatomical Pathology at the Medical School, University of the Witwatersrand) for the generation of virtual slide images. The single neoplastic nodule with the most MUC16-specific positive labeling (as assessed with the naked eye) per slide was selected for quantification. The Dimension count and Measure module from the corresponding Olympus Cell Sens software (Wirsam Scientific and Precision Equipment PTY LD, Johannesburg, South Africa) was utilized to delineate and measure the area of each selected region of interest (ROI) per slide, and the calculation of the percentage IHC positive labeling within each ROI (per mouse) was performed with the assistance of the phase separation function (Figure 7.8A and B).

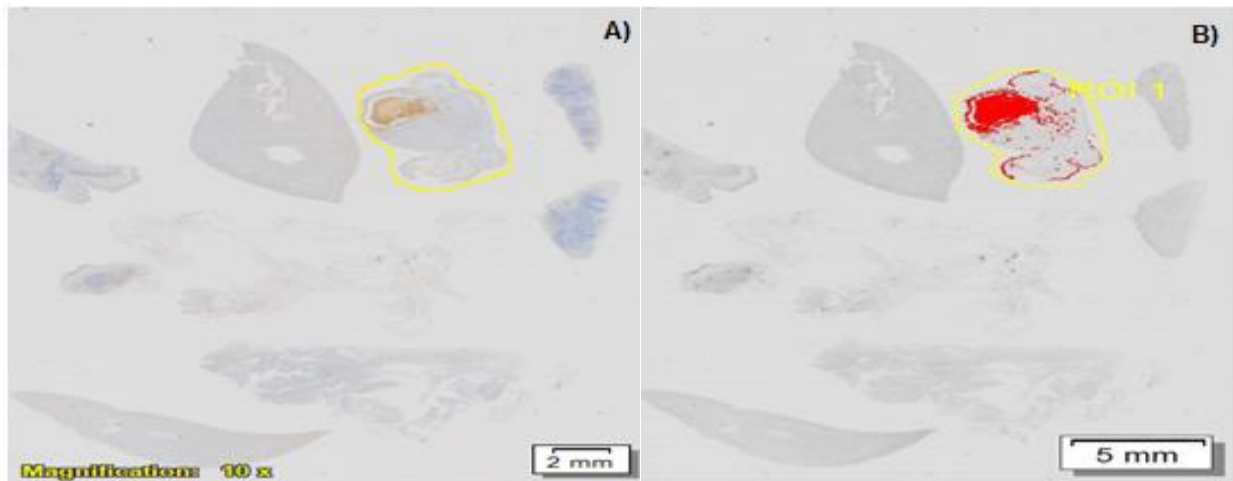


Figure 7.8: A) Scanned IP-implanted, AF(D)NM's-treated nude mouse tissue section showing a section (yellow ring) of ovarian carcinoma expressing MUC16/CA125 antigens (brown staining). MUC16/CA 125 IHC, DAB, chromogen, hematoxylin counterstain. B) Shows the region of interest/ROI delineated (yellow ring) and MUC16-positive signal (red) within the ROI for quantification using the Olympus Count and Measure function (Olympus cellSens software).

7.2.9. Applying Ultra Performance Liquid Chromatography (UPLC) to determine the Methotrexate content in blood and tissue samples

Simple and sensitive analytical techniques for quantification are necessary in order to develop the understanding toward the correlation between pharmacokinetics, pharmacodynamics, pharmacology and the bioavailability of drug/methotrexate within a drug delivery system (Wang et al., 2009). Ultra Performance Liquid Chromatography (UPLC) is an exploratory method utilised to measure and enhances the analysis of samples encountered in pharmaceutical development (Wren et al., 2006). The blood and tissue samples were analyzed to collect information about the drug molecule through UPLC to ascertain drug concentration against time.

7.2.9.1. UPLC analysis

Detection and analysis was conducted on an Acquity® Ultra Performance Liquid Chromatography system (Waters®, Milford, MA, USA) fitted with an Acquity UPLC® BEH Shield RP18 1.7µm VanGuard precolumn (2.1x5mm) and an Acquity UPLC® BEH Shield RP18 column (2.1 x100mm, 1.7µm particle size). The function of the guard column as the name implies was to prevent proteinaceous matter from reaching the column. Samples were run for 2 minutes and an injection volume of 15µL for plasma samples, or 10µL for tissue samples and implant samples was inoculated onto the column. Detection was via a photoiodide UV/Vis detector (PDA Detector). This allowed the recording of the full UV/Vis absorption spectra and determination of the highest absorption of the methotrexate as shown in Figure 7.9. Using this data, a wavelength of 310nm was used for the detection of methotrexate and pyrazinamide.

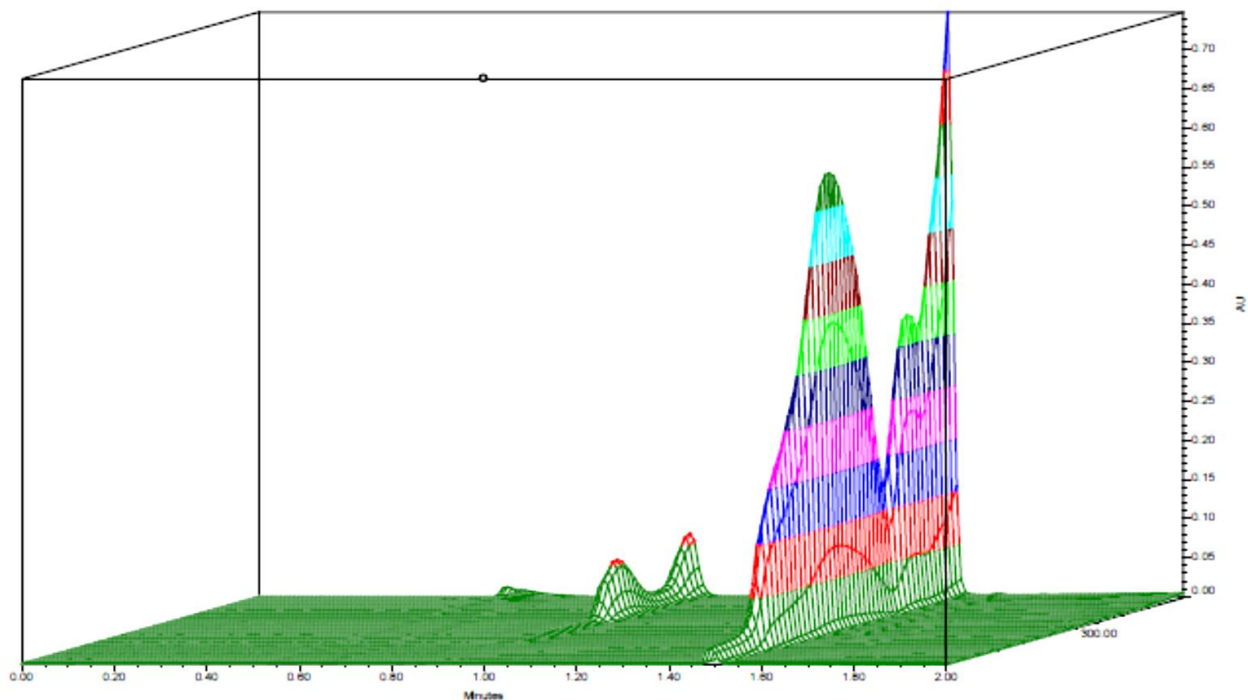


Figure 7.9: PDA plot showing the absorbance of MTX (retention time= 1.5mins) and PYZ (retention time= 1.1.mins).

7.2.9.2. Preparation of weak and strong washes and mobile phases

Considering the packing nature of the column, it can be easily understood that any particulate material in the system can cause blockages which would increase pressures and hence lead to failure of equipment. For this reason all solutions were prepared using double deionised water (DDW) (Milli-Q Gradient, Millipore, MA, USA, electrical conductivity 18.2M Ω .cm at 25°C) and all solutions were freshly prepared daily and filtered under vacuum using Durapore® membrane filters (Millipore, Ireland). Gloves were worn at all times to minimise contamination. Priming solutions consisted of a weak wash (10%v/v acetonitrile) and a strong wash (90%v/v acetonitrile). Gradient elution was achieved using acetonitrile and phosphoric acid (0.1%v/v) as mobile phases in a method described in Table 7.3.

Table 7.3: UPLC method for the elution of methotrexate and internal standard pyrazinamide.

Time (min)	Flow Rate(mL/min)	% Phosphoric Acid	% Acetonitrile
Initial	0.400	95	5
0.5	0.400	85	15
1.0	0.400	75	25
1.5	0.400	65	35
1.6	0.400	95	5

Precision and accuracy were determined by replicate injections of three concentrations of MTX. Intraday accuracy and precision was determined by multiple injections (n=3) of the three concentrations of MTX during the period of analysis on one day and inter-day accuracy and precision were determined by injecting the same three concentrations of MTX over 3 non-consecutive days (n=3). Peak area and retention time were noted for each of the analyte runs. In order to determine the precision, the % RSD (Equation 7.2) for retention time and peak area was calculated. Accuracy was determined by comparing the obtained amount with the theoretical quantity.

$$\% \text{ RSD} = \frac{\text{std dev}}{\text{mean}} \times 100 \dots \dots \dots \text{Equation (7.2)}$$

7.2.9.3. Determination of the optimal method of extraction of drug from plasma samples

Before samples of blood can be injected onto the UPLC column, proteins must be extracted. Two methods exist for achieving this: liquid-liquid extraction and solid phase extraction. Liquid-liquid extraction was chosen as solid phase extraction showed low levels of MTX in the final elute. Methanol was selected as the deproteinising agent in this study as other agents such as acetonitrile and perchloric acid proved ineffective.

Extraction yield was determined by spiking 400µL blank plasma samples with fixed quantities of drug sample (100µL of a 0.1mg/mL MTX solution). To these samples differing quantities of methanol was added and UPLC analysis conducted on these samples was compared with samples of the drug solution (100µL of a 0.1mg/mL MTX solution) in the same quantity of methanol. The ratio of plasma to methanol in order to obtain a recovery of 99% was found to be 1:4.2, and subsequently plasma samples were treated in this way. Plasma samples were dried completely under a gentle stream of nitrogen gas and reconstituted in 500µL methanol or samples

were dried to 500 μ L in a vacuum oven (Trade Raypa® Digital drying oven, Barcelona, Spain maintained at 50°C, -0.6bar).

7.2.9.4. Treatment of actual plasma samples

Using the obtained ratio of 1:4.2, 400 μ L samples of blood were pipetted into suitable centrifuge tubes and 1800 μ L of methanol was then added. The samples were vortexed (Vortex-Genie 2, Scientific Industries Inc., Bohemia, NY, USA) for 15 seconds to ensure adequate mixing of the methanol with the plasma. The samples were then centrifuged at 1500rpm for 5 minutes (Model TG16-WS, Shanghai Luxiangyi Centrifuge Instrument Co., Ltd., Shanghai, China) in order to precipitate the proteins. Supernatants were then decanted into Eppendorf microtubes (Eppendorf AG, Hamburg, Germany), placed in a vacuum oven and evaporated to 500 μ L. Samples were filtered using a 0.2 μ m filter (GHP Acrodisc filter, Pall Life Sciences, NY, USA). Pyrazinamide was used as an internal standard and 2 μ L of a 0.5mg/mL solution was added to each sample before analysis.

7.2.8.5. Construction of a calibration curve in order to quantify amounts of drug in actual plasma samples

A calibration curve was generated in order to quantify the amount of drug in the plasma samples. Briefly, blank plasma samples were spiked with known quantities of MTX and the procedure outlined above was followed. The ratio of the area under the (AUC) of the chromatogram of drug to the internal standard was plotted against the corresponding drug concentrations (μ g/500 μ L). The least squares method was used to determine the linearity equation and correlation coefficient (r^2). The limit of quantification (LOQ) was defined as the concentration which produces chromatographic peaks with heights at least 3 times that of the baseline noise.

7.2.9.6. Construction of a calibration curve in PBS

A calibration curve of MTX in PBS was also conducted. The ratio of the area under the (AUC) of the chromatogram of the drug to internal standard was plotted against the corresponding drug concentrations expressed in μ g/mL. The least squares method was used to determine the linearity equation and correlation coefficient (r^2).

7.2.9.7. Determination of the drug content in surrounding tissue

Tissue immediately surrounding the implant was collected from day 4 and day 10. The samples of tissue surrounding the implant were rinsed with PBS and then accurately weighed and cut into thin pieces using surgical scissors and/or a scalpel and placed in a mortar. Liquid nitrogen was then added to the mortar and a pestle was used to crush the tissue to a powder. PBS (5mL) was then added to the powder and the solution was homogenised for 15 seconds using a homogenizer (Polytron®, Kinematica Inc, Bohemia, NY, USA). The obtained solution was centrifuged at 3000rpm for 10 mins and the supernatant was collected and filtered using filter paper (Whatman filter paper, Kent, England) to remove any remaining pieces of flesh or fatty tissue and then refiltered using 0.22µm filters. To remove protein from the samples, 400µL of the obtained filtrate was treated with 800µL of methanol. At this ratio of methanol to tissue sample, protein precipitation was observed. Samples were then vortexed for 15 seconds and centrifuged for 5 minutes. Following final filtration of the supernatant through a 0.22µm filter into vials (Waters® LCMS certified vials with a pre-slit screw top, Waters, Milford, MA, USA) samples were injected onto the column.

7.2.9.8. Statistical analysis

All numerical data were expressed as the average of the values obtained, and the standard deviation (SD) was calculated. Statistical analysis was performed by repeated measures ANOVA. Significant differences between means of treated and untreated groups were analyzed for statistical significance using the two-tail Student's t-test for paired/unpaired observations. Two sided p-values < 0.05 were considered to be statistically significant. Kaplan-Meier mouse survival curves were prepared and were utilized to ascertain whether MUC16 expression correlated with mouse survival. Mouse Survival was calculated as the number of days lapsed between initiation of treatment and euthanasia, and percentage (%) of mice surviving was the number of mice remaining in each group (10) at the end of each week following initiation of appropriate treatment. Survival curves were evaluated, and the variance in mice survival was assessed for statistical significance. All statistical analyses were performed using the sigma plot 11 graphing software excel (Systat Software, Inc. Richmond, CA 94804. U.S.).

7.3. Results and Discussion

7.3.1. Sterile preparation of ISFI

Post-incubation of the plates (agar plates and streaked formulation plate) for 24 hours, plates were observed visually to determine the growth of contamination. None of these plates exhibited any contamination-growth indicative of the sterility of the prepared-formulation.

7.3.2. Bio-compatibility of the ISFI in the mouse model

7.3.2.1. Implantation area and tissue-necrosis

After one to six hours of inoculation of the ISFI, no inflammation was detected. Minimal, subacute and acute inflammation was also not detected in the 6th day samples, since it was the anticipated response of the tissue to a foreign material, this was indicative of the SFI superior biocompatibility *in vivo*. The ISFI was observed in the tissues of organs surrounding the implantation site (Figure 7.10). Persistent chronic inflammation usually follows and is usually part of the healing course. It is a continual inflammation that poses a problem (Anderson and Langone, 1999). The tissue necrosis particularly in the SC-fatty tissue was detected in practically all of the implantation areas as shown in Figure 7.11. Whilst, the reports of safety associated with the copolymer seem promising and indicate that the polymer itself is not the likely cause of toxicity, the polymer needs to be examined further. It is a possibility that the polymer is safe and the high calcium content of the ISFI is then most likely the causation of the necrotic regions. Further investigation in this regard is warranted.

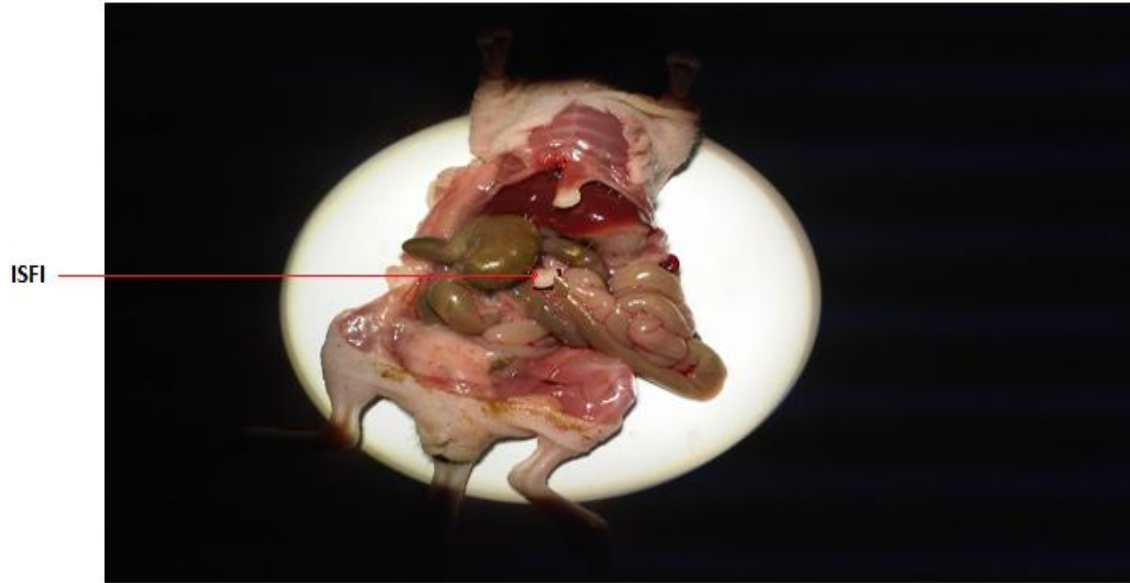


Figure 7.10: Intraperitoneal injected mice showing ISFI in the peritoneal cavity under biopsy microscope viewed with digital camera.

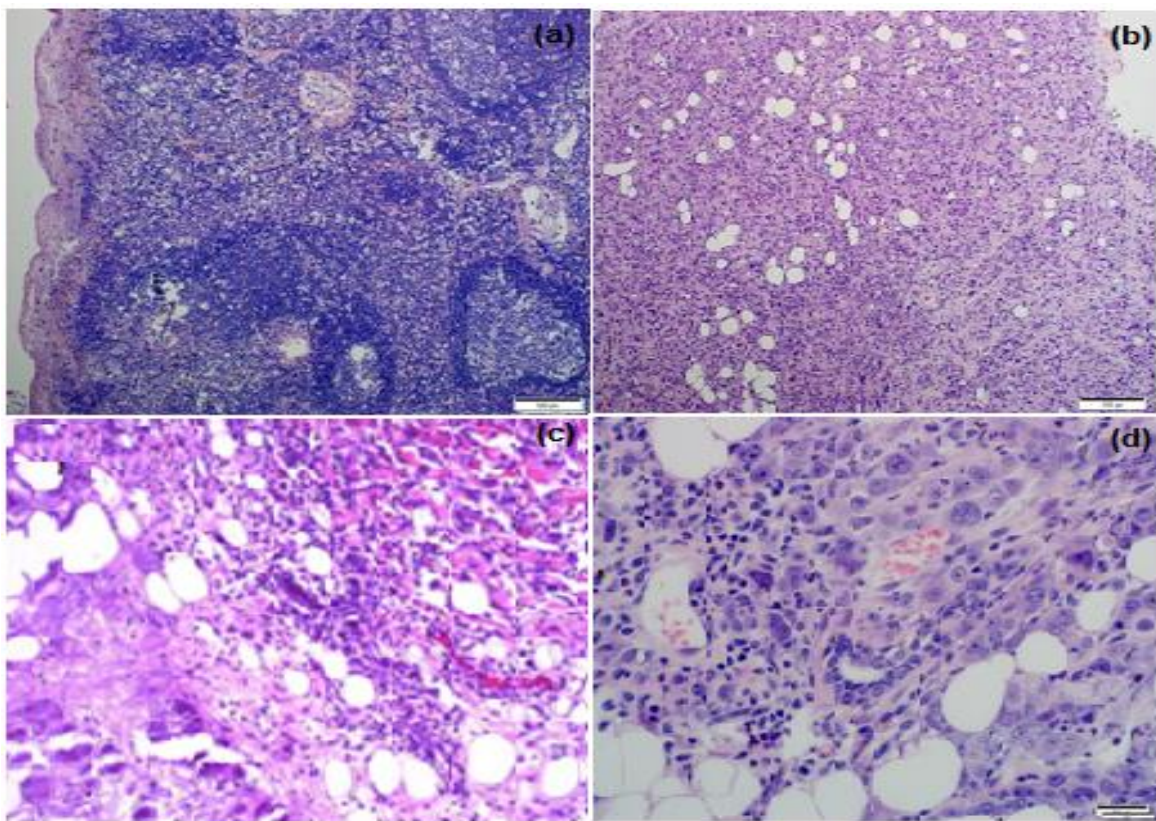


Figure 7.11: Histopathological analysis of tissue surrounding the site of implantation of the ISFI implant in a) control (non-treated normal mouse) b) after 4 days of implantation c) after 6 days of implantation and d) after 10 days of implantation.

7.3.3. Establishment of a model for induction of ovarian cancer using Athymic nude mice: Pilot study

Growth of cancer cells in the intra-peritoneal cavity and subcutaneous region of immunocompromised mice are a common procedure for evaluating tumorigenic potential *in vivo*. These procedures are also utilized to evaluate the effects of chemotherapeutic interventions on tumor cell lines. Twenty-five mice were used in the Pilot study, 22 were utilized in the induction of ovarian cancer and 3 were un-infected, health nude mice for correlation purposes. Table 7.4 provides information on the numbers, procedure and % of the nude mice used in this study. The 22 nude mice were used in the pilot study in order to increase the number of mice used in SC and IP induction of ovarian cancer, thereby ensuring statistically relevant results ($p < 0.05$) and also to validate the process of induction of human carcinoma in this mouse model. We have found the athymic nude mice to be most effective in all our attempts to induce ovarian cancer with a success rate of 22 out of 22 attempts: 12 mice were IP injected with 0.2ml containing 2×10^7 cells/ml of ovarian carcinoma suspension and the other 15 were SC injected with 0.2ml containing 2×10^6 cells/ml as shown in the protocol (Appendix 2). Charles River France Swiss nude mice were established as a suitable model for ovarian cancer as observed by the rapid growth of the NH:OVAR5 cell line *in vitro* (RPMI cell culture media) and formation of tumors *in vivo* in Swiss nude mice (Figure 7.5a-d and Figure 7.6a-d). There are no early detection methods for ovarian cancer in the clinical settings and this disease is usually diagnosed at an advanced untreatable stage, furthermore in the main study, emphasis was on early detection (using Vevo® 2100 imaging techniques) and treatment of ovarian carcinoma with various chemotherapeutic treatment protocols, when tumor size has reached 100 mm^3 .

Table 7.4: Procedures conducted in nude mice model used for induction of ovarian cancer.

Number of nude mice	Procedure	Percentage of nude mice
4	IP injected mice were euthanized and autopsies performed. No tumors or nodules were observed, but high levels of ascitic fluid accumulated in the peritoneal cavity, thus indicating possible ovarian cancer induction.	16%
8	IP injected. One died just before planned euthanasia, the others were euthanized for biopsy purposes. Both were biopsied	32%
5	SC injected, euthanized, mice had reached the maximum tumor diameter of 10mm ³ and were sickly (losing a lot of weight).	20%
5	SC injected, euthanized for biopsy purposes, had reached maximum tumor burden of 10 mm ³ and didn't were not sickly (gained a lot of weight).	20%
3	Normal nude mice, euthanasia for biopsy purposes.	12%
25	Total number of mice used in the Pilot	100%
Main study		
90	Healthy and un-infected.for the main study	100%

7.3.4. Main Study

7.3.4.1. Intraperitoneal (IP) and Subcutaneous (SC) Induction of Human Ovarian Carcinoma in Athymic Swiss Nude Mice

The main study was conducted in the same manner as the pilot study except that increased numbers of Athymic nude mice (n=80) were utilized in the induction of ovarian cancer. Charles River France Athymic Swiss nude mice (n=80) were also established as a simple, reproducible mouse model for the IP induction of human ovarian carcinoma using the NIH:OVCAR5 cell line, as was evidenced by the visible development *in vivo* of intra-abdominal tumor nodules with associated severe ascites (Figure 7.6a-c). This occurred within 10 days of inoculation. Advanced IP ovarian carcinoma disease in the athymic nude mice was consistently associated with peritoneal carcinomatosis/transcoelomic metastasis, which always preceded the formation of severe ascites. Solid tumor nodules coated all serosal surfaces, especially within the pelvis (Figure 7.6d). Due to the widespread dissemination of the IP tumors, it was not feasible to analyze specific regions of the peritoneum in order to assess the uptake of the antibody (anti-MUC16) and drug-loaded nanomicelles delivery system in the peritoneum.

7.3.4.2. Chemotherapeutic efficacy in the Treatment of Human Ovarian Carcinoma

The chemotherapeutic efficacy of the AF(D)NM's implant (the preferred chemotherapeutic model system) was evaluated against the non-functionalized (D)NM's and the comparison group (IV methotrexate/cisplatin only), as well as the control/placebo group. A variety of indices were assessed, including tumor size (measured with calipers and sonography), mouse weight, quantification of mucin 16 antigen expression levels as well as survival rate of mice post-treatment.

7.3.4.3. Tumor size

The tumor size was measured with calipers and sonography (Figure 7.5, Figure 7.6 and Figure 7.12), and two chemotherapeutic drugs utilized in this study were cisplatin (4mg/kg) and methotrexate (15mg/kg) as illustrated in nude mice growth curves in Figure 7.13a & b respectively. The average tumor size in the 3 treatment groups each with 10 mice (two experimental groups, a comparison group (i.v drug only)) decreased significantly ($p < 0.05$) from day 15 after implantation of the AF(D)NM's treatment (Figures 7.13 a-d) and Figure 7.13.1a-d). Conversely, in the placebo group, the average tumor size increased steadily, indicating biocompatibility of the blank nanomicelle implant delivery system (placebo) *in vivo*. During the

evaluation phase, nanomicelle implant ((D)NM's)-treated mice reached the ultimate point (of 100 mm³ average tumor diameter) within 21 days of treatment whilst the group of AF(D)NM's-implant treated mice survived until completion of the study. After necropsy examination of IP inoculated mouse post treatment, the AF(D)NMs implant treatment resulted in reduced average tumor size and ascitic fluid (Figure 7.12a-d and Figure 7.14 a-d).

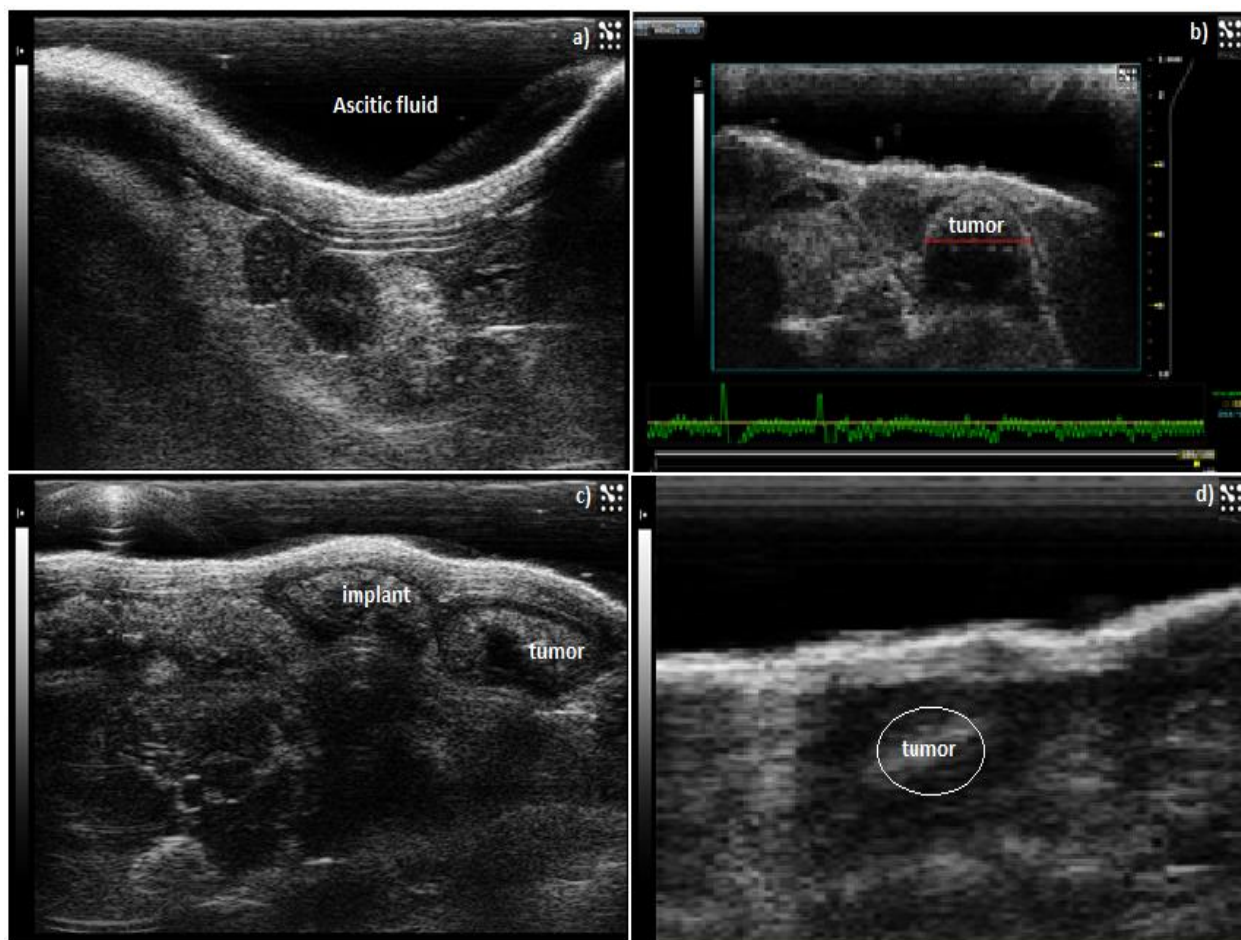


Figure 7.12: Sonographic representation of tumor growth and response to antibody-bound drug loaded nanomicelle hydrogel composite delivery system (AF(D)NMs). (a) Ascitic fluid development in a nude mouse 5 days post-induction, (b) Tumor growth 10 days post induction with NIH:OVAR-5 cell suspension, (c) Chemotherapeutic implant injected adjacent to tumor growth 11 days post-induction, (d) decrease in tumor size and only a small tumor nodule was noticeable 15 days after implementation of the (AF(D) NMs) treatment.

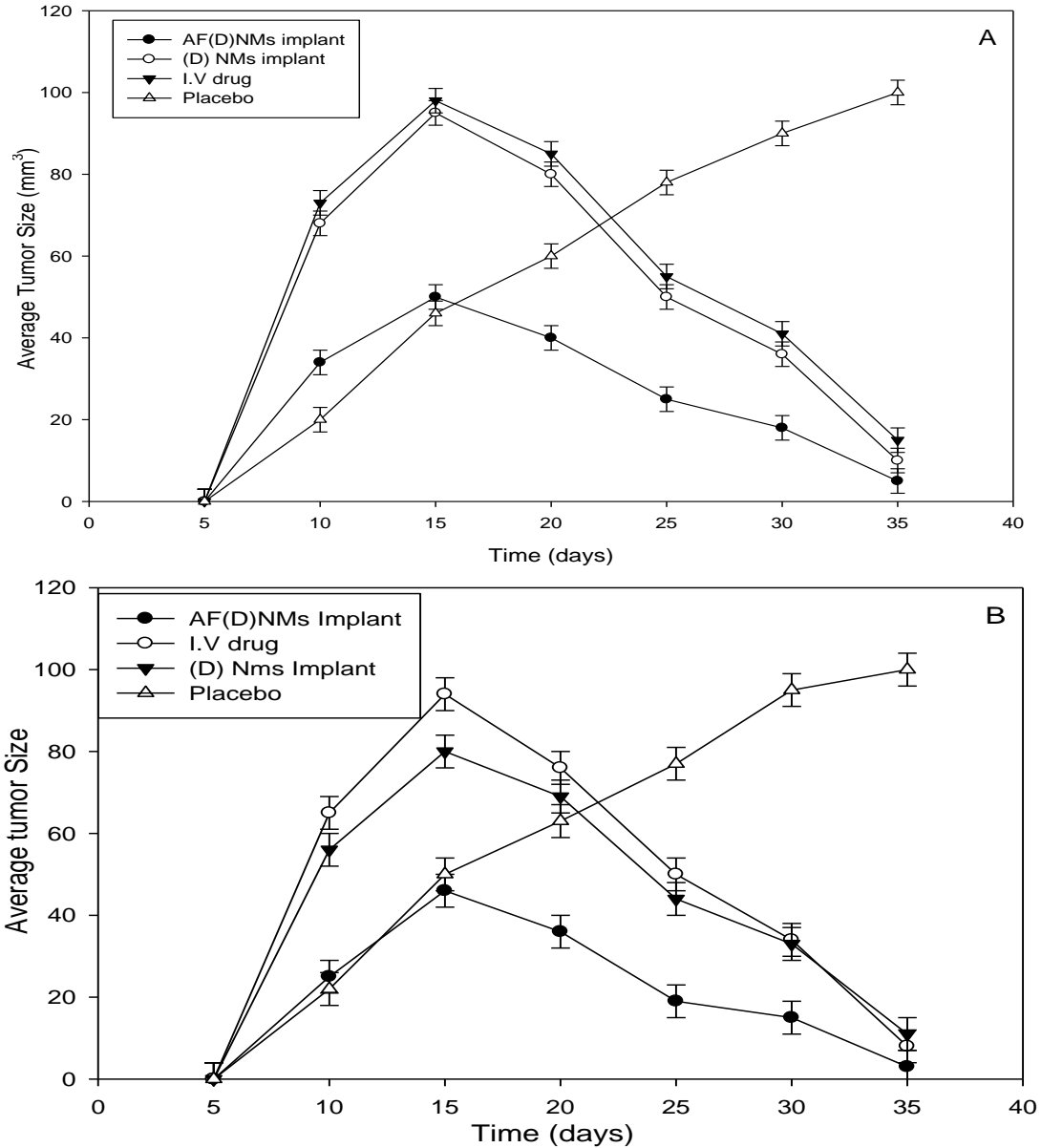


Figure 7.13: Nude mouse tumor growth curves illustrating chemotherapeutic efficacy of the three treatment groups vs the control/placebo group, expressed as average tumor sizes in NIH:OVCAR-5 EOC-bearing nude mice. A refers to the methotrexate- and B the cisplatin-loaded nanomicelle implant delivery system in NIH:OVCAR-5 EOC-bearing nude mice. Each point depicts mean (n=10/group); bar, \pm SD.

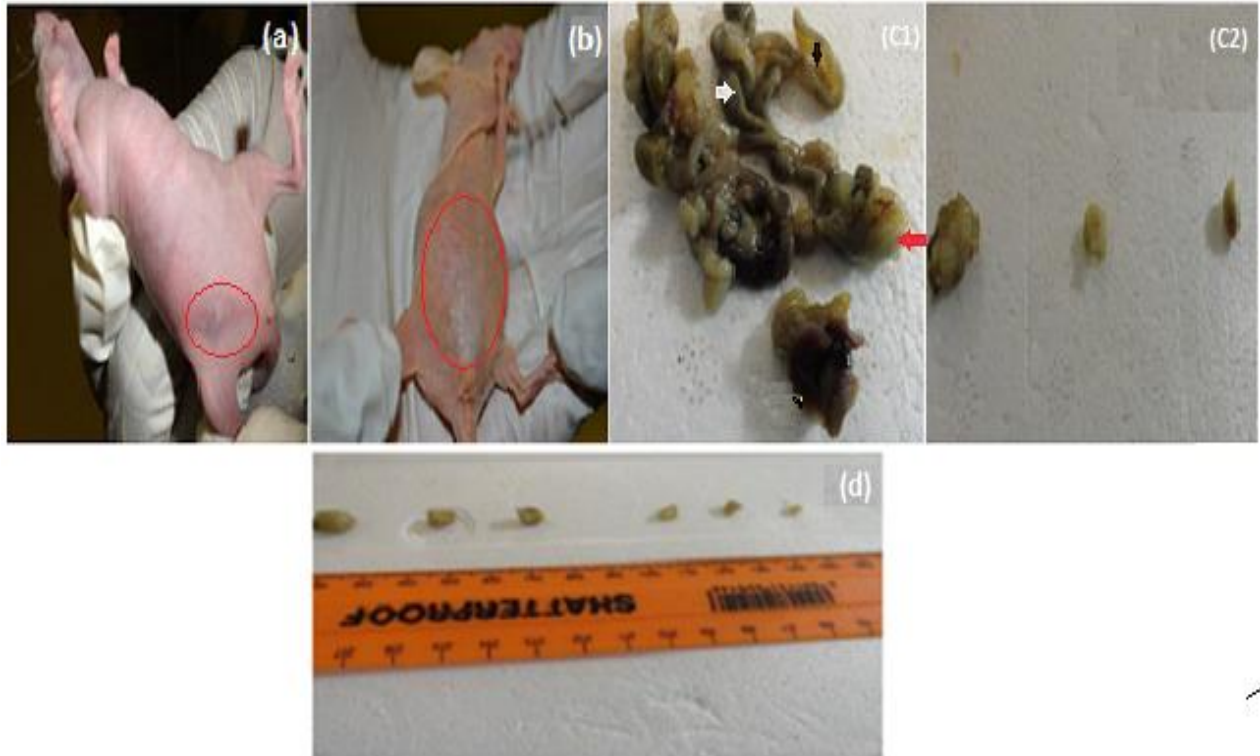


Figure 7.14: (a) An IP-inoculated mouse pre-treatment (red ring), (b) distended abdomen post-treatment (red ring), (c₁,c₂) after necropsy examination, displaying intestinal nodules (white and red arrows), nodules in omentum (black arrow), and (d) illustrates the reduction in tumor size after treatment with the antibody-bound drug loaded nanomicelle hydrogel composite delivery system (AF(D) NMs).

7.3.4.4. Whole mouse weight

Mouse weights in both the comparison and control groups (IV cisplatin and methotrexate only, respectively) and the 2 experimental treatment groups decreased during the course of this study ($p < 0.05$) (Figure 7.15a and b). While, in the placebo group body weights increased slightly and were normalized to baseline weight ($p < 0.05$). The final average weight of nude mice with NIH:OVCAR-5 tumor treated with AF(D)NM's formulations was $16,94 \pm 0.3$ g compared with $17,68 \pm 0.3$ g in mice treated with non-specific methotrexate/cisplatin-loaded nanomicelles ((D)NM's and 26.34 ± 0.36 g in mice administered with only the placebo injections ($p < 0.05$). The IV drug group final average weight was 22.62 ± 0.28 g. Baseline weights were 26.00 ± 0.40 g, 24.00 ± 0.33 g and 19.1 ± 0.35 g for placebo and (D)NMs, IV drug and AF(D)NMs, respectively. The body weight of the placebo group was normalized to 26.00 g on day 30, indicative of implant biocompatibility and low levels of cytotoxicity (Figure 7.15a and b).

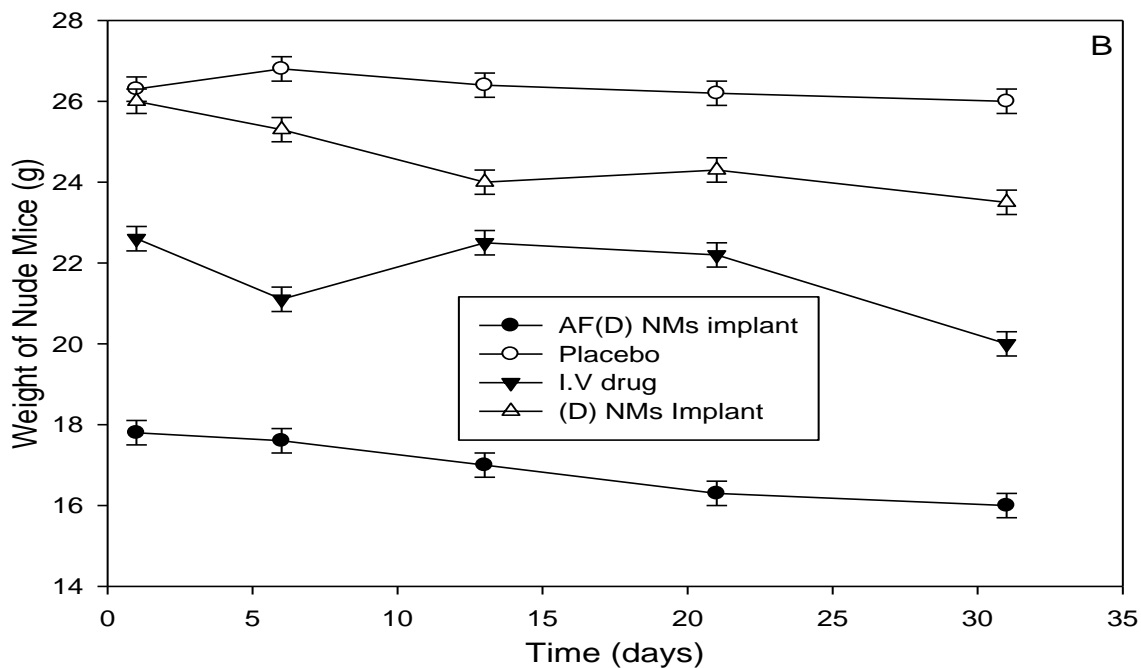
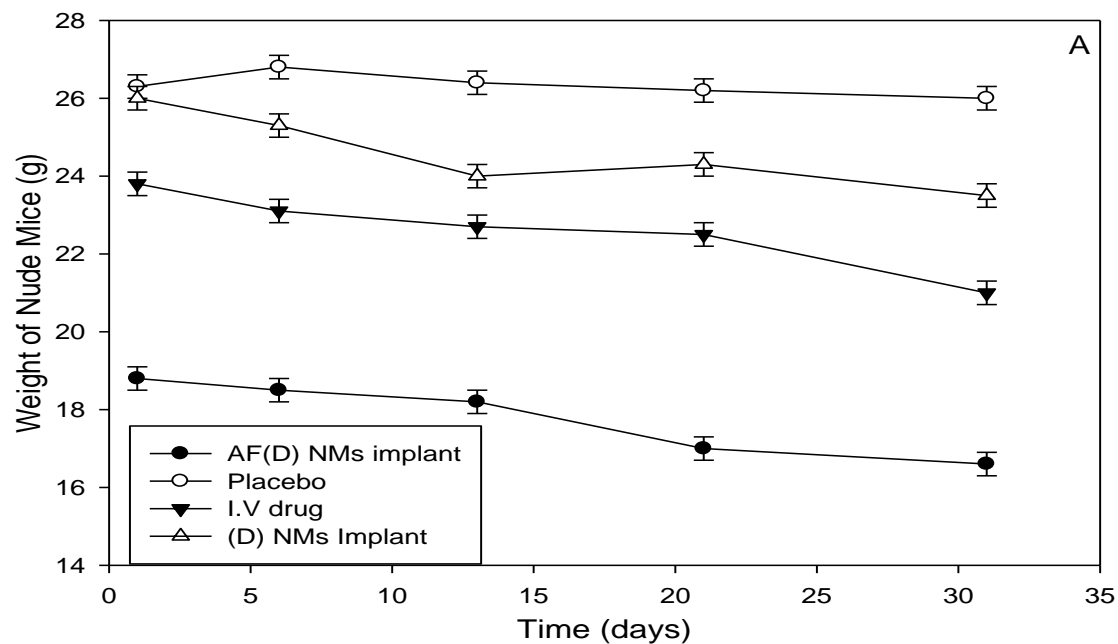


Figure 7.15: Nude mice average body weight curves illustrating chemotherapeutic efficacy in the 3 treatments and control (placebo) group. A refers to the methotrexate- and B the cisplatin-loaded PNIPAm-b-PASP nanomicelle implant delivery system in NIH:OVCAR-5 EOC-bearing nude mice. Each point depicts mean (n=10/group); bar, \pm SD.

The notable reduction in tumor size and corresponding mouse weights corresponded with decreased MUC16/CA 125 antigen expression levels employing the ELISA technique. These results indicated a significant difference ($p > 0.01$) in tumor burden between the different chemo-treatment groups and showed that antibody functionalized combination treatment significantly improved chemo-therapeutic efficacy as shown by inhibition of tumor growth ($p < 0.05$).

7.3.4.5. Quantification of plasma and ascitic fluid MUC16/CA125 antigen levels

Using the Cancer Antigen CA125 Human ELISA Kit, MUC16 antigen concentrations in IV-treated mouse plasma samples were significantly lower ($p < 0.05$) compared with the levels in plasma samples from mice in the pre-treatment group. However, MUC16 antigen concentrations in mice treated with (D)NM's and AF(D)NM's were all in low levels, i.e. 1.8 – 2.4 U/ml. The MUC 16 antigen concentration in the plasma samples was typically slightly higher than in the ascitic fluid, likely due to the fact that the AF(D)NM's are site-specific and are therefore localized in the peritoneal cavity; they target MUC16 antigens expressed on ovarian carcinoma cells within tumor nodules and in ascitic fluid. The AF(D)NM's group had significantly reduced MUC 16/CA125 antigen concentrations in plasma compared with the (D)NM's group and the IV chemotherapeutic drug only-group ($p < 0.05$) (Figure 7.16a and b). At the time of euthanasia, the average plasma MUC16/CA125 value in the AF(D)NM's group was 1,9460 U/ml, compared to the value of 2.0180 U/ml in the (D)NM's group, 2,077 U/ml in the IV drug group and 2,368 U/ml in the placebo group. The decrease in MUC 16/CA125 antigen concentration in ascitic fluid was consistent with the overall reduction in ascitic fluid production and average tumor size. These results indicate that the AF(D) NM's can specifically target MUC16/CA 125 antigens on the surface of EOC cells, thereby effectively decreasing their expression.

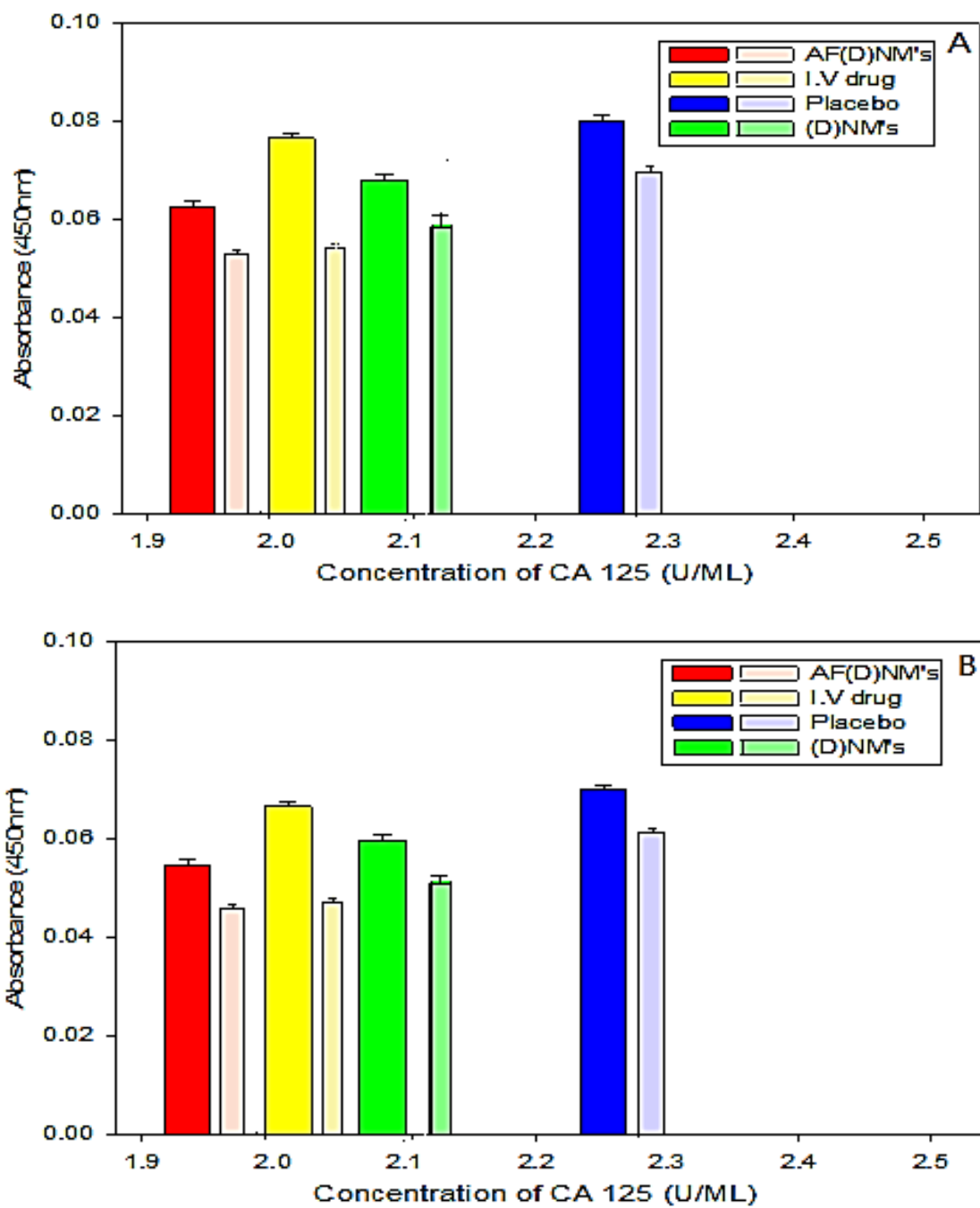


Figure 7.16: Point-of-euthenasia levels of MUC 16/CA 125 antigens in the plasma and ascitic fluid of mice in the experimental and control groups. (D refers to methotrexate (in graph A) and cisplatin (in graph B).

7.3.4.6. Histopathology and IHC

7.3.4.7. SC and IP tumor Macropathology

Gross necropsies were performed on all the pre-treatment animals that died or were euthanized by carbon dioxide (CO₂) inhalation after 10 days once the tumors have developed to their target size of 80mm³-100mm³, which was regarded as the baseline-for initiation of treatment. The tumor nodules were scattered throughout the omentum, mesentery and had infiltrated the body wall in the IP-inoculated mice (Figure 7.6d). There was no difference in histomorphological appearance of SC-and IP-inoculated tumors.

7.3.4.8. SC and IP tumor histopathology

Histopathology was subsequently performed on all SC/IP nodules and in all cases, the existence of anaplastic ovarian carcinoma(s) was confirmed histologically (Figure 7.17). The intra-abdominal tumors however, were far more infiltrative (widespread transcoelomic metastases and histopathology also revealed tumor emboli within lymphatic vessels) whilst SC tumors were localized/non-infiltrative. After a month of chemotherapy, the mice in the post-treatment groups were euthanized in same manner as those in the pretreatment group and full histopathology performed. There was no difference in post mortal sample collection post-treatment compared to pre-treatment.

7.3.4.9. Liver histopathology

Histopathology performed on IP nude mice implanted with experimental, conventional and placebo treatments displayed multifocally coalescing neoplastic nodules throughout the peritoneal cavity, as well as multiple random foci of hepatocellular coagulative necrosis associated with bile 'lakes' (so called 'bile infarcts') likely due to biliary outflow obstruction by ovarian carcinomas ((viz. in several instances, carcinomatous foci were observed immediately abutting extra-hepatic biliary cysts (Figure 7.17a and b). There was also evidence of neoplastic emboli in some sections in the placebo post-treatment group. There was very mild bile ductule proliferation within the liver sections as well as occasional extra-hepatic biliary cysts (lined by hyperplastic epithelium), the latter also embedded within an increased fibrous connective tissue stroma. Numerous bile ductules within the liver were bile-laden and some bile ductules were severely distended in portal areas and lined by hyperplastic (in places, pseudoepitheliomatous) epithelium. There was a mild portal peri-ductular infiltration of mature (small) lymphocytes and neutrophils and there was evidence of a mild to moderate multifocal portal fibrosis. There was

also a venous thrombus in one section of liver. All these observations are illustrated in Figure 7.17a and b.

7.3.4.10. Renal histopathology

Widespread but quite subtle (mild/moderate) cortical and medullary intra-tubular cast formation – basophilic, granular and variably vacuolated (derived from degenerate tubular epithelial cells) cellular detritus that filled some tubules. Outer cortex – multifocal (patchy) severe nephrosis-lytic necrosis of proximal convoluted tubular epithelial cells, as evidenced by clumps of ragged, mineralized (due to dystrophic calcification) cell debris and occasional karyolytic nuclei in affected tubular epithelium. In the deeper cortex there was widespread desquamation/shedding of PCT epithelial cells into tubular lumens, with slight condensation of nuclear chromatin in the affected epithelial cells. There was mild distension of occasional PCT lumens, which were lined by mildly attenuated epithelial cells. All these observations are illustrated in Figure 7.17c and d.

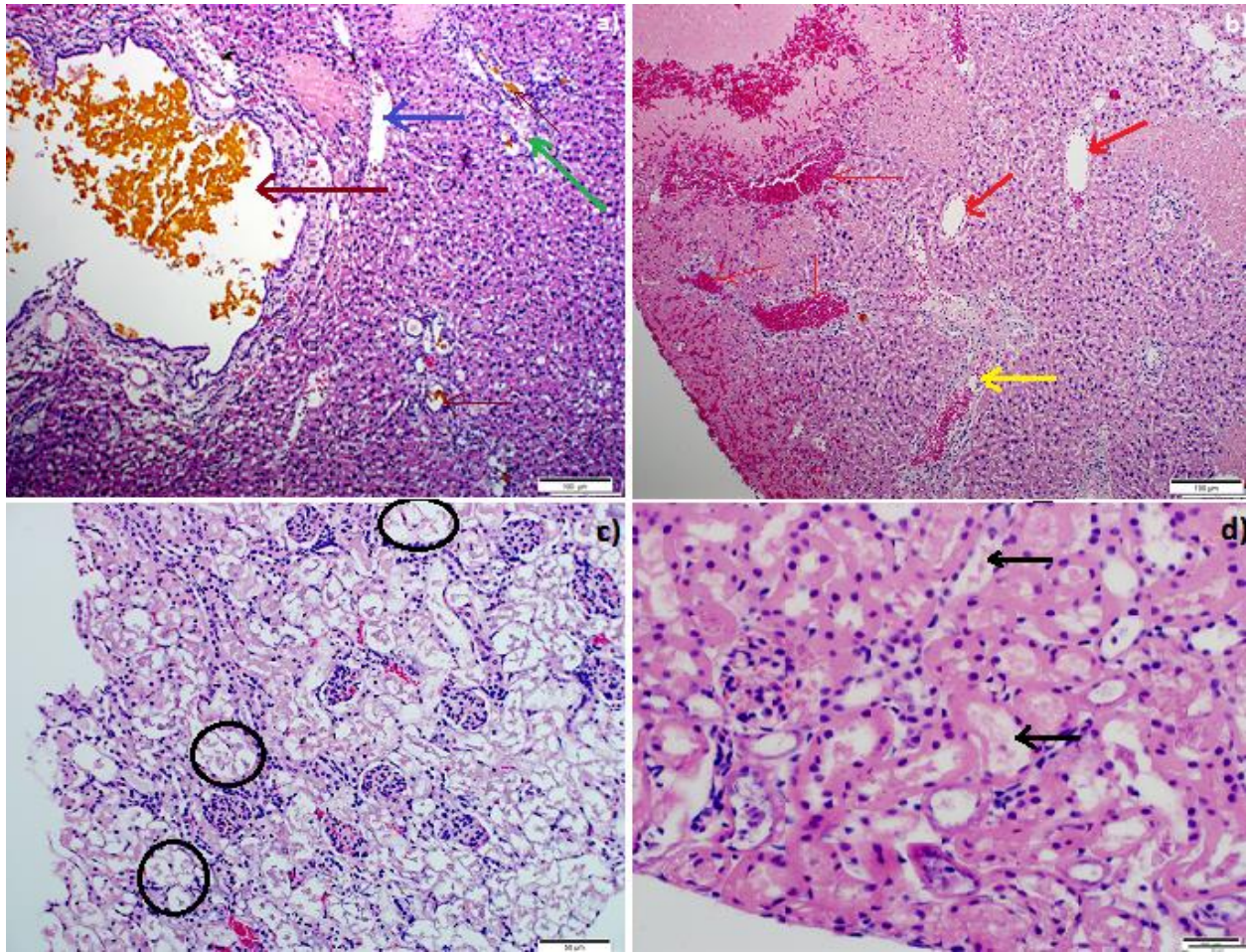


Figure 7.17: Microscopic view of the liver (a-b) and kidney (b-c) in AF(D)NMs, (D)NMs and IV-drug only treatment groups, stained with H&E. (a) Cystic distension of bile ductule containing bile (dark brown thick arrows), foci of hepatocellular necrosis (dark blue arrow), mild bile ductule proliferation (dark brown thin arrows) and mild lymphocytic infiltration into portal areas (green arrow). (b) Multifocal to coalescing hepatocellular coagulative necrosis with (red thin arrows) or without associated haemorrhage (red thick arrows). (c) Severe nephrosis as evidenced by ragged intraluminal clumps of cell debris (black rings), HE. (d) Basophilic (calcified), granular intra-tubular cellular detritus (black arrow), multifocal (segmental) karyolysis in some tubular epithelial cells, and multifocal mild distension of proximal convoluted tubular lumens (lined by slightly attenuated epithelium) HE.

7.3.4.11. Immunohistochemistry

MUC 16/CA 125 IHC revealed positive labeling of 1-10% of the area within the specified regions of interest (ROI) (Figure 7.18c-h). Generally, throughout these tumors, variably-sized clusters of neoplastic cells labeled with the MUC16/CA 125 antibody. Labeling was both cellular (cytoplasmic and cell membrane) and extracellular (around shrunken apoptotic-like cells and in tubular lumina lined by irregularly branching papillae of neoplastic epithelial cells). There was occasional distinct membranous labeling of epithelial cells lining the papillary projections in some sections. However, most labeling appeared extracellular in the majority of tumor sections, and there was more cytoplasmic labeling of neoplastic cells compared to membranous labeling (Figure 7.18c-h).

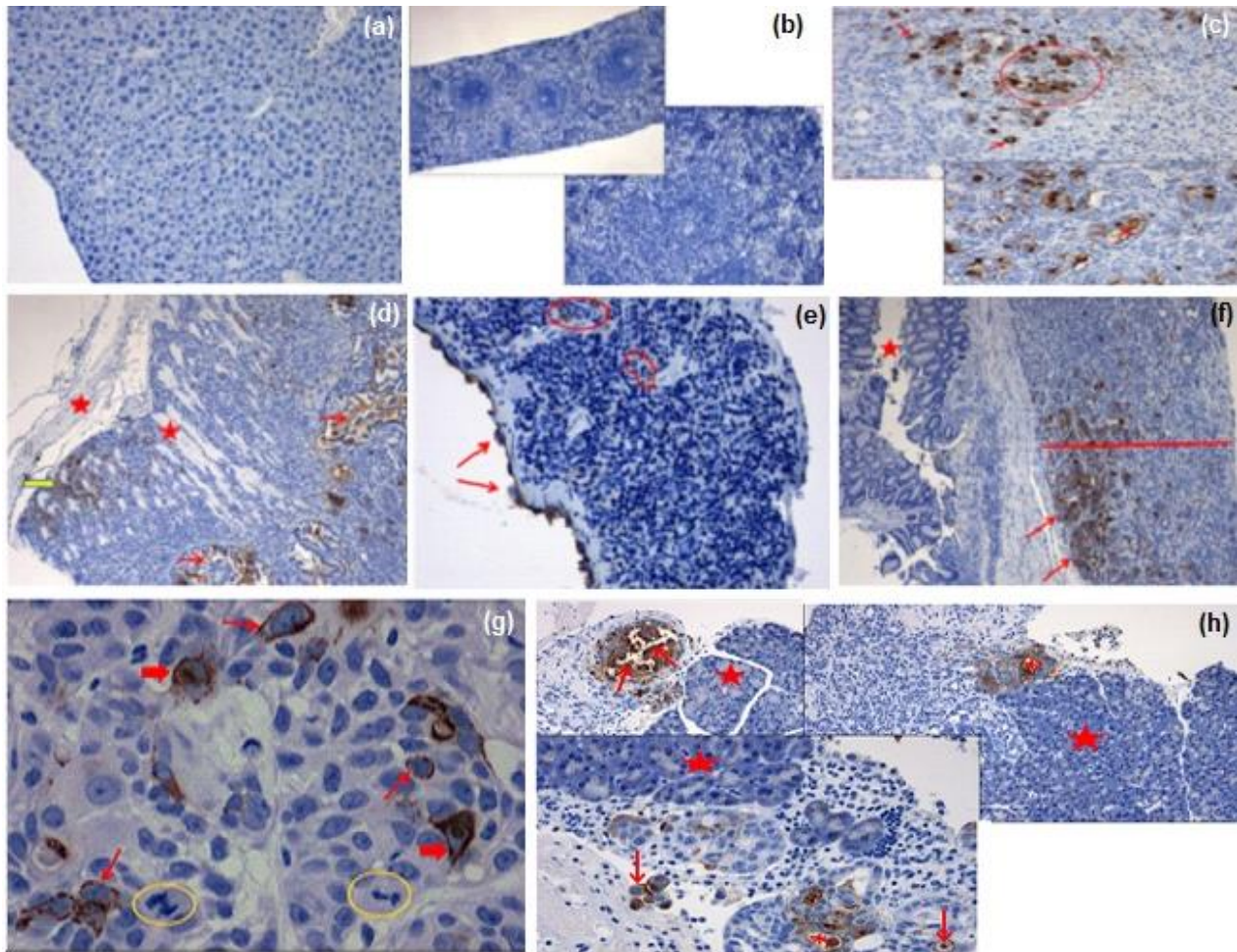


Figure 7.18: MUC16/CA125-positive labeling of EOC cells in mouse tissues and tumor foci in IP-inoculated nude mice.

Individual Figure 2.3 Legends

Figure 7.18 (a): Negative tissue control (normal mouse liver). MUC16/CA125 immunolabeling, DAB chromogen, hematoxylin counterstain.

Figure 7.18 (b): Negative tissue control (normal mouse spleen). MUC16/CA125 immunolabeling, DAB chromogen, hematoxylin counterstain.

Figure 7.18 (c): SC ovarian carcinoma. MUC16/CA125 positivity associated with EOC cells and extracellularly (arrows). MUC16/CA125 immunolabeling, DAB chromogen, hematoxylin counterstain.

Figure 7.18 (d): IP ovarian carcinoma infiltrating skeletal myofibres (stars) of the body wall. EOC cell-associated (yellow arrow) and extracellular (red arrows) MUC16-positive labeling. MUC16/CA125 immunolabeling, DAB chromogen, hematoxylin counterstain.

Figure 7.18 (e): IP-inoculated mouse. MUC16-positive labeling of reactive mesothelial cells on the visceral peritoneal (serosal) surface of the spleen (arrows). MUC16/CA125 immunolabeling, DAB chromogen, hematoxylin counterstain.

Figure 7.18 (f): MUC16-positive neoplastic cells (arrows) within the IP-inoculated ovarian carcinoma (red line) impinging on the serosal surface of the intestine (star indicates intestinal lumen). MUC16/CA125 immunolabeling, DAB chromogen, hematoxylin counterstain.

Figure 7.18 (g): SC anaplastic ovarian carcinoma with MUC16-positive labeling of cytoplasmic membranes of EOC cells (thin arrows) and of extracellular spaces around shrunken EOC cells (fat arrows). Note the mitoses (yellow circles). MUC16/CA125 immunolabeling, DAB chromogen, hematoxylin counterstain.

Figure 7.18 (h): IP-inoculated ovarian carcinoma infiltrating the pancreas (stars) with MUC16-positive labeling of cytoplasmic membranes of neoplastic cells (arrows). MUC16/CA125 immunolabeling, DAB chromogen, hematoxylin counterstain.

7.3.4.12. MUC 16/CA125 IHC analysis on FFPE EOC tissue sections

The percentage of MUC16-positive labeling per square centimeter of each selected EOC tissue section (one per mouse) was determined with the help of the phase separation function for both pre- and post-treatment mice (Figure 7.8). MUC 16 expression in pre- and post-treatment groups using both drugs (methotrexate and cisplatin) was up-regulated and displayed an increasing trend in the placebo (4.31-5.11-%), AFNM's (D) (6.13-6.36%) and IV-drug groups (7.67-8.14%) ($p < 0.05$), whilst in the NM's (D) group, MUC 16 expression was down-regulated (2.67-3.3%) (Figure 7.19a & b).

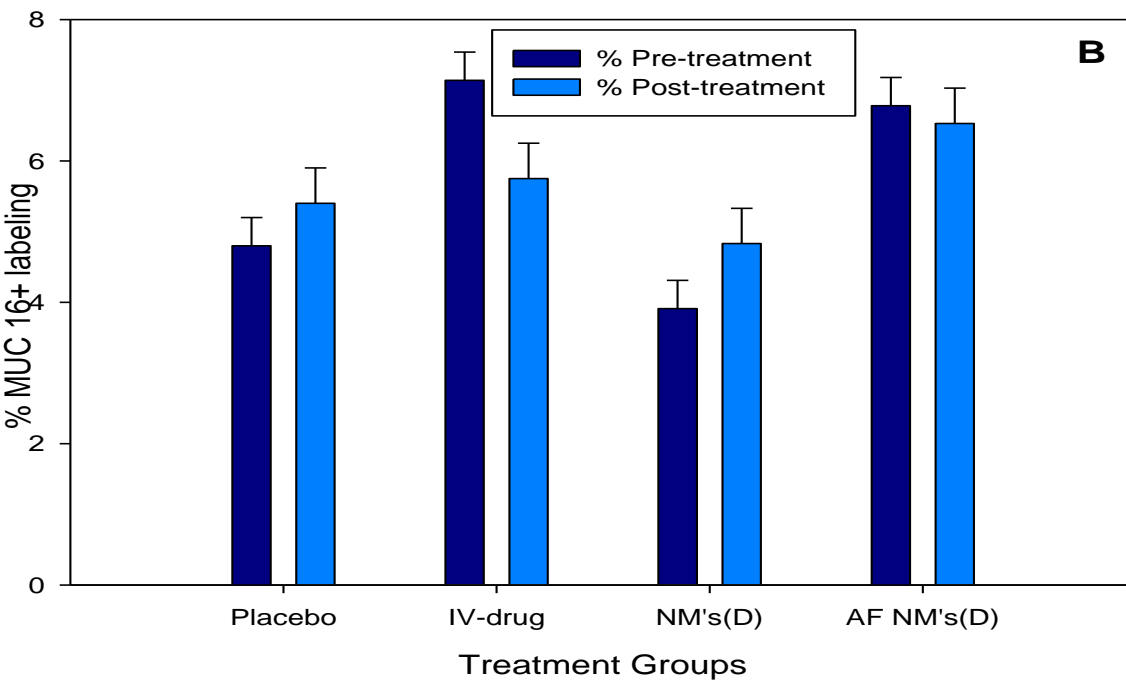
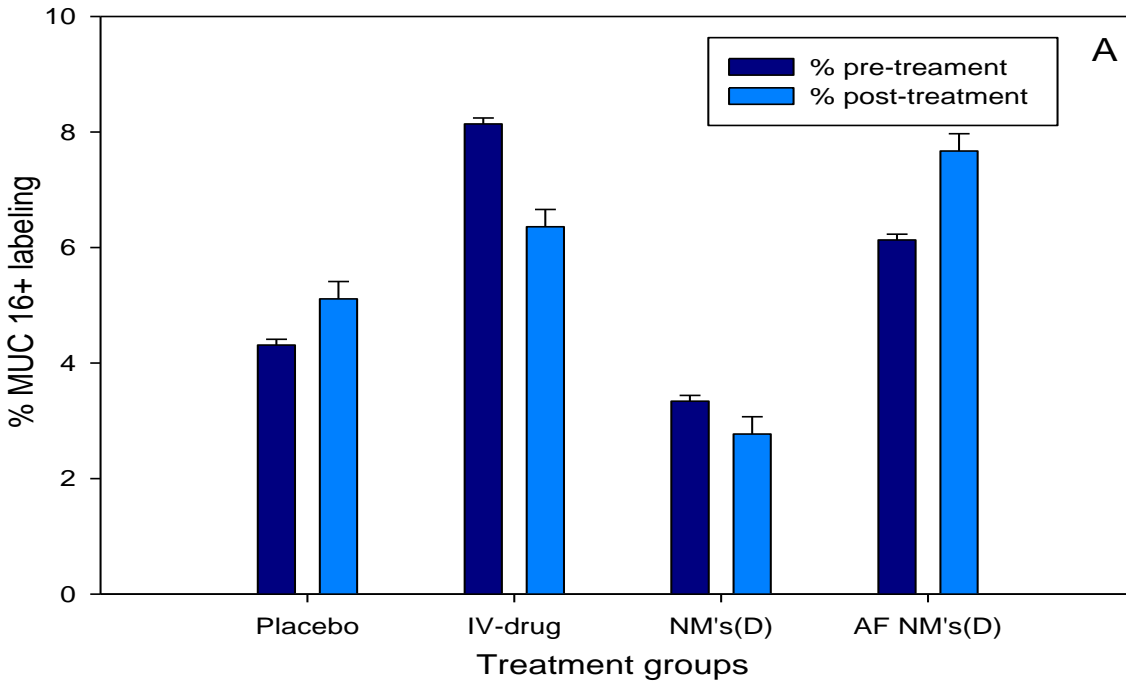


Figure 7.19: ROI (regions of interest) measurement of IHC images on the stained slides for each treatment group, and the MUC 16 density in each image was calculated as percentage of MUC16-positive labeling per square centimeter of each selected EOC tissue section (one per mouse). (D refers to methotrexate (in graph A) and cisplatin (in graph B).

The survival rate in response to various chemotherapeutic protocols was a significant index for comparing antitumor efficacy between the groups. Nude mice survival rates were significantly different ($p < 0.05$) between the experimental treatment and control/placebo and comparison (IV chemotherapy) groups as shown by means of Kaplan-Meier analysis. Mouse survival was significantly improved (100% over 35 days) in the AF(D)NMs test group compared to the placebo group, as well as all the other groups (Figure 7.20). The data also indicated that the mice in the AF(D)NMs test group exhibited the greatest overall reduction in tumor size and had the longest survival times (Figure 7.13A and B, Figure 7.20).

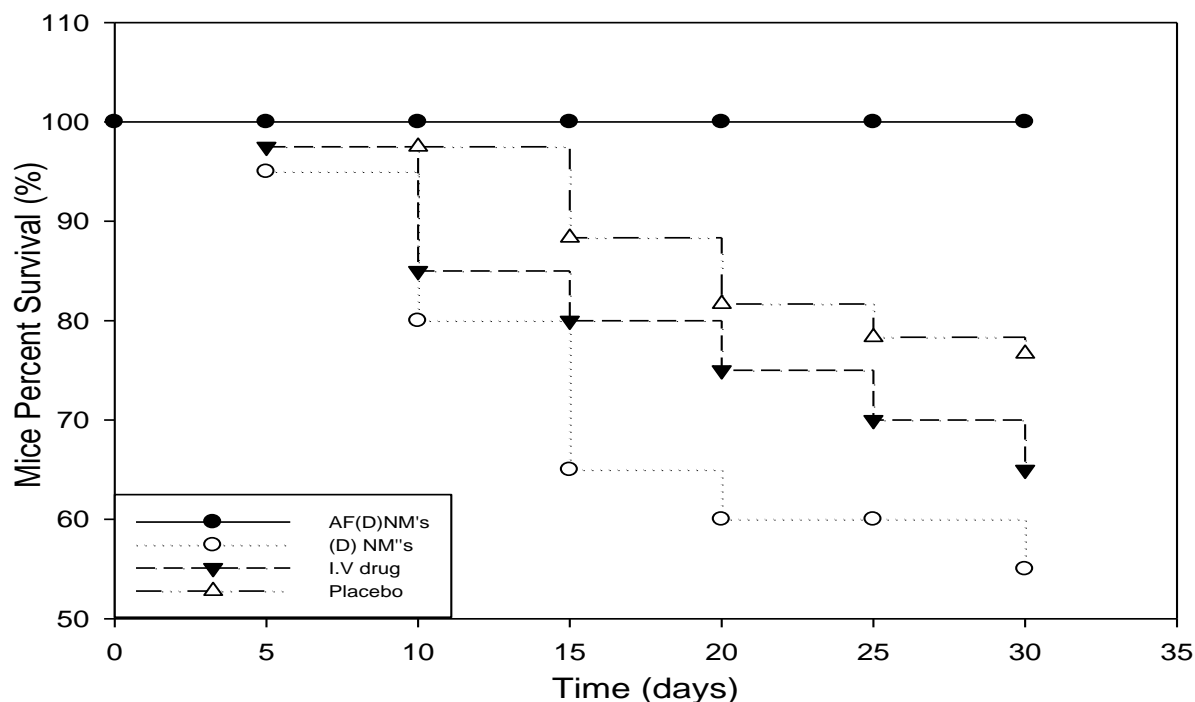


Figure 7.20: Kaplan–Meier mouse survival curves, showing the three chemo-treatment groups ($n = 10$) including nude mice injected with AF(D)NM's, (D)NM's and IV chemotherapeutic drugs and a control placebo implant treatment group. The survival rate of mice in the AF(D)NM's test group was significantly improved compared with the other groups ($p < 0.05$).

7.3.5. Construction of a calibration curve in order to measure the quantity of methotrexate in blood and tissue samples and precision and accuracy of the UPLC method

Figure 7.21 shows the typical chromatograms acquired for the drug, methotrexate and the internal standard, pyrazinamide. As shown in Figure 7.22, a calibration curve with a high coefficient of determination was obtained. Table 7.5 shows the calculated precision and accuracy of the method when three replicate injections of three samples with known concentrations were made on the

same day and on three non-consecutive days. As should be noted the accuracy remained high even between days and % RSD remained relatively low indicating that the method had good precision and accuracy. The limit of quantification was determined to be 0.50ng/mL.

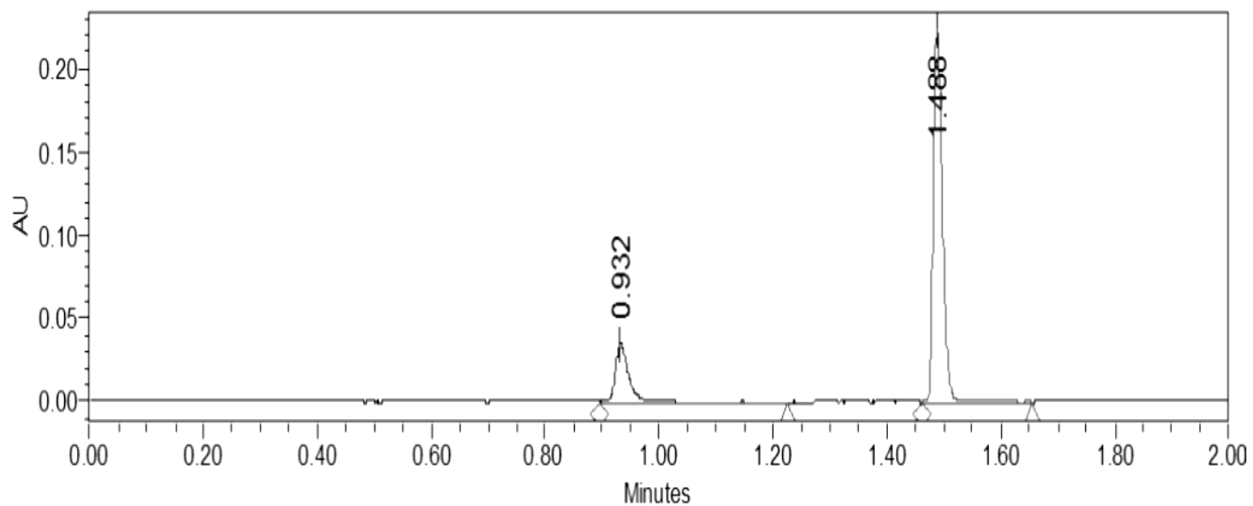


Figure 7.21: Typical chromatogram obtained for methotrexate (retention time=1.408min) and internal standard, pyrazinamide (retention time=0.932min).

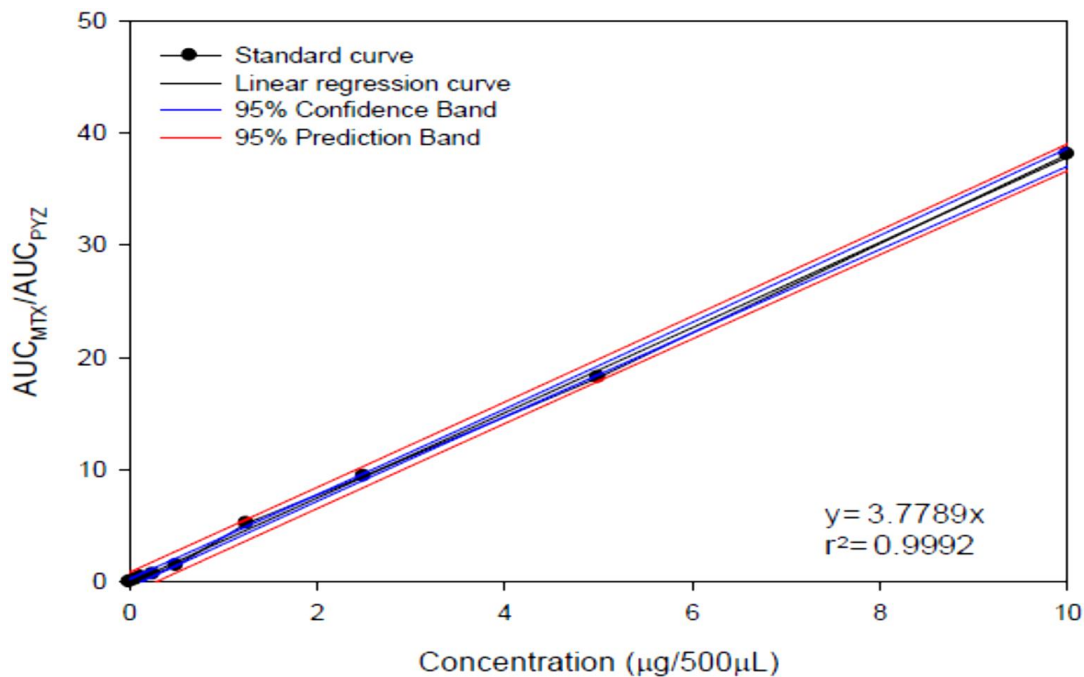


Figure 7.22: Calibration curve of Methotrexate obtained in blank plasma

Table 7.5: Inter- and intra- day precision and accuracy of the method were determined (only one set of interday data is shown).

	%RSD (TR)	%RSD (AUC)	Accuracy
Intraday			
1	0.154	0.583	99%
2	0.143	0.433	99%
3	0.166	0.494	99
Interday			
1	0.61	0.290	97%
2	0.54	0.540	98%
3	0.49	0.667	96%

%RSD= Percentage relative standard deviation; TR= Retention Time; AUC= Area under the curve

The amount of MTX in the blood was low when using standard UPLC method. This could be indicative that the majority of the drug being released at later stages was retained at the site of implantation rather than distributing into the blood as depicted in Figure 7.23.

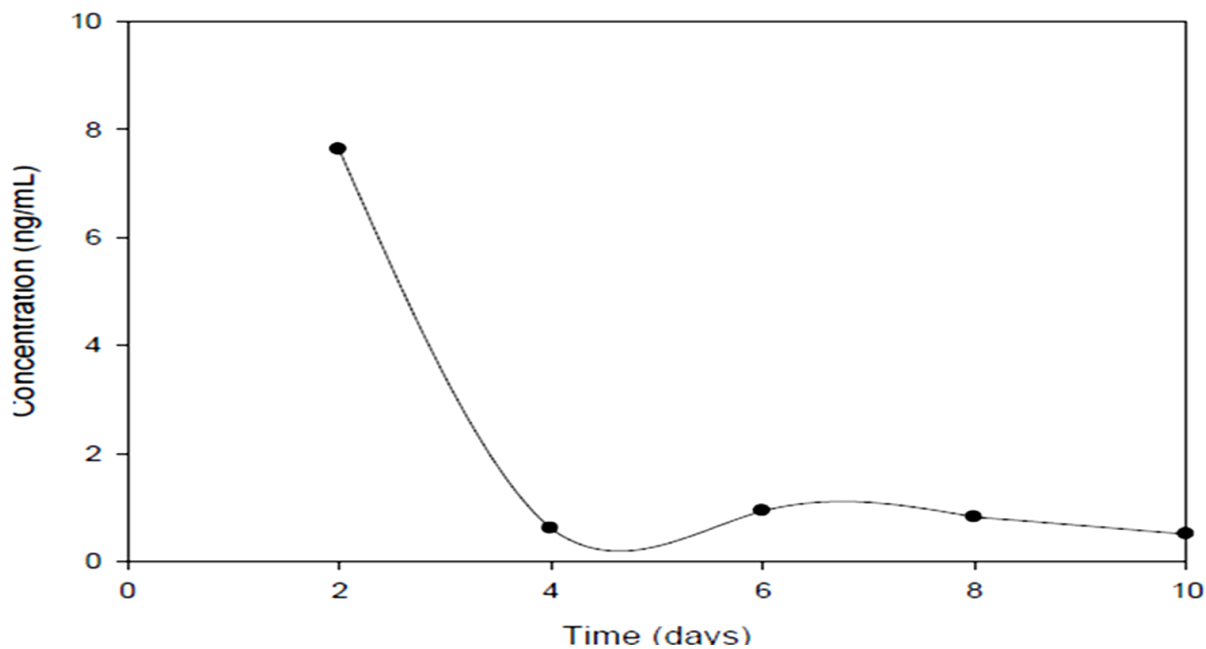


Figure 7.23: Blood methotrexate levels in experimental nude mice (SD< 0.044).

7.3.5.1. Determination of methotrexate concentration in surrounding tissue

Figure 7.24a and b depict the calibration curves acquired for PBS and methanol respectively. The area around the implant (Figure 7.24c) showed relatively high quantities of drug was still present at the site after 10 days.

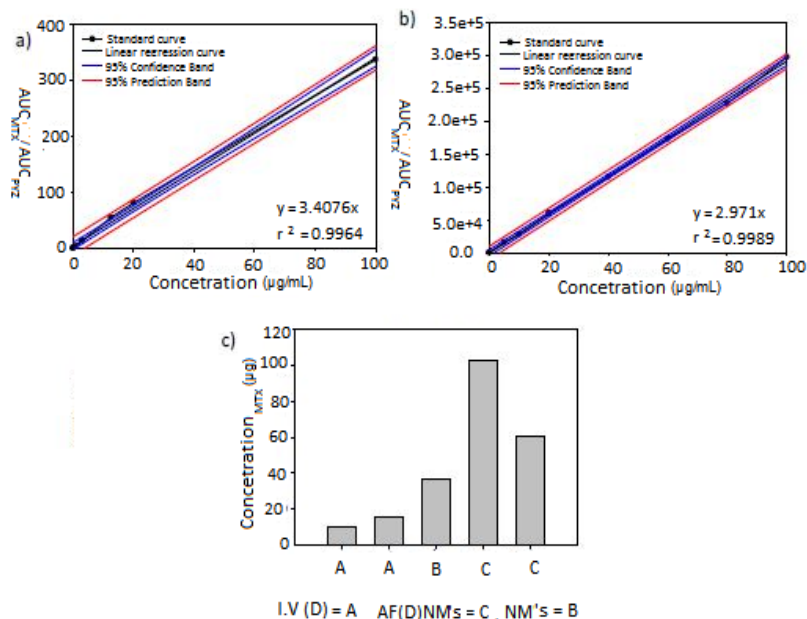


Figure 7.24: a) Calibration graph of MTX in PBS b) calibration curve of MTX in methanol c) drug in the surrounding tissue after 4 or 10 days.

7.3.6. Mechanism of Intraperitoneal ISFI Delivery for human ovarian carcinoma targeting

ISFI was fabricated by encapsulating a nanomicelle comprising of anti-MUC 16 (antibody) functionalized methotrexate (MTX)-loaded PNIPAAm-b-PASP nanomicelles (AF(MTX)NM's) within C-P-N hydrogel (Figure 7.25a-b) as per protocol described in Chapter 5, Section 6.2.6.. Given that the peritoneal cavity is the principal site of disease in ovarian cancer, the ISFI was injected and released nanomicelles into the peritoneal cavity (Figure 7.25c₁,c₂). Following the release of nanomicelles from the hydrogel, the nanomicelles (formulated to circulate for prolonged periods in the peritoneal fluid) targeted specific mucin antigens significantly over-expressed on ovarian cancer cells circulating in the peritoneal fluid (when patients are usually diagnosed) and cancer cells forming nodules at distant sites in the peritoneal cavity (Figure 7.25d₁,d₂,e₁,e₂&f). This targeting system reduced the tumor load responsible for adhesion at the sites of secondary metastasis (peritoneal and abdominal surfaces). The anti-MUC16 antibody functionalized nanomicelles has great potential in improvement of tumor selectivity, eliminate/ reduce the tumor

load while improving the recovery, long term survival rate of the majority of patients suffering from ovarian cancer.

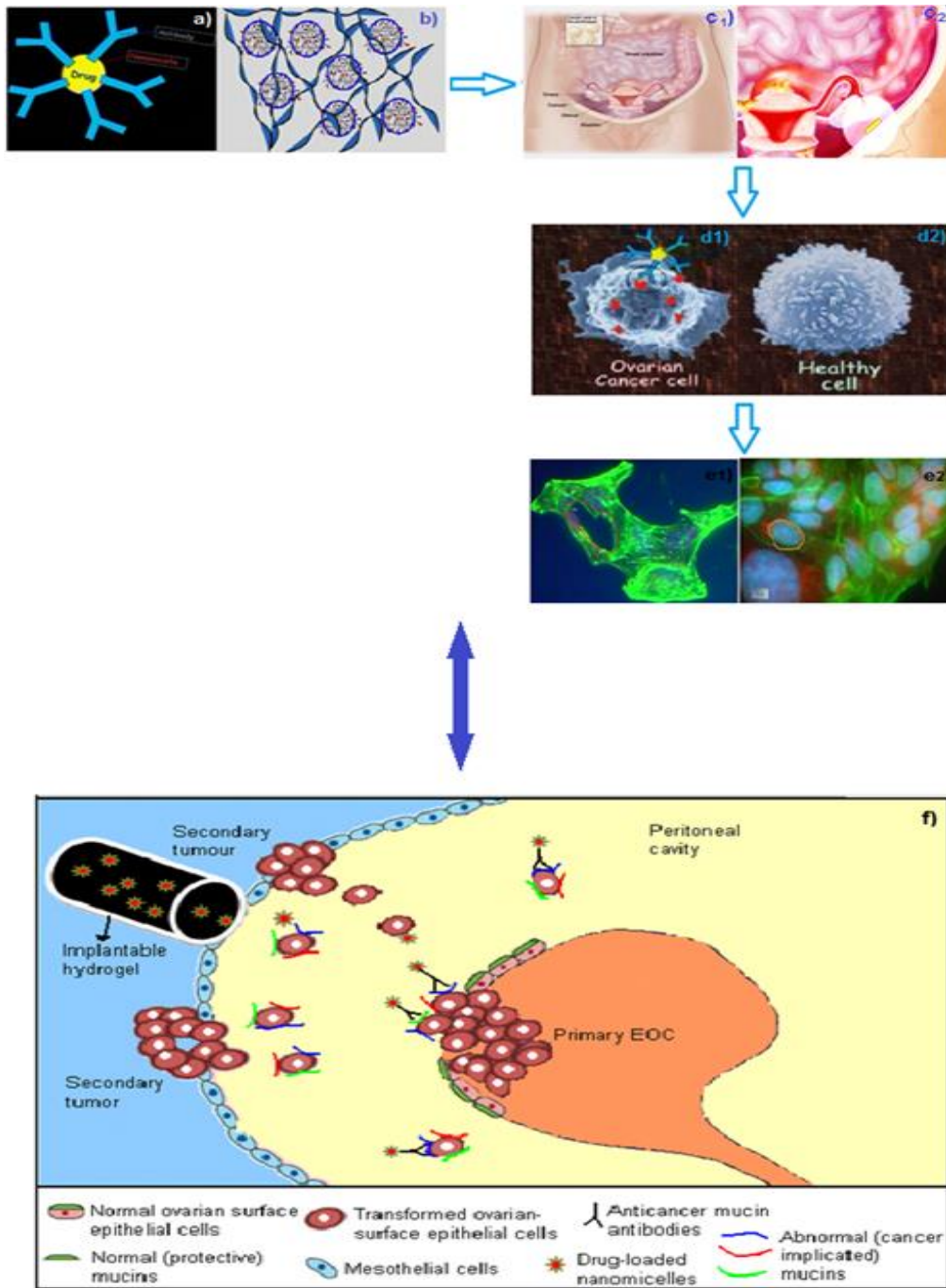


Figure 7.25: (a)-Antibody functionalized drug loaded nanomicelles AF(D)NMs/nanomicelle. (b)- AF(D)NMs encapsulated in an optimized implantable composite C-P-N delivery system (ISFI). (c₁,c₂)-ISFI injected and release nanomicelles into the peritoneal cavity. (d₁,d₂)-Specific antibody-muc16 interaction or binding. (e₁,e₂)- Fluorescence images of targeted chemotherapy of human ovarian carcinoma cells. (f)-Intraperitoneal targeted chemotherapeutic mechanism congruently depicted.

7.4. Discussion

Epithelial ovarian cancer (EOC) is the most insidious gynaecological malignancy that is asymptomatic during its early stages and is therefore diagnosed at an advanced, often untreatable stage when the disease has spread beyond the ovaries throughout the abdominal cavity and even further afield (Whitehouse and Solomons, 2003; Wang et al., 2011; Cho et al., 2013). Thus, deaths due to ovarian cancer could be significantly lowered by developing new, ultrasensitive, yet reliable methods for early diagnosis and by developing improved treatment protocols. Mucins are amongst the most promising molecular biomarkers for EOC and have proven invaluable in the diagnosis and monitoring of treatment regimes in various types of ovarian cancer. Increased mucin expression, otherwise known as 'mucin switching' that occurs during the neoplastic transformation of ovarian surface epithelium to ovarian carcinoma is important in the progression of this disease (Rump et al., 2004; Gubbels et al., 2006; Tamada et al., 2007). MUC16 is an important clinical biomarker of ovarian cancer and it is a target for various immuno-chemotherapies currently under investigation (Liu et al., 1998; Gullery et al., 2008; Oei et al., 2008; Rustin et al., 2001).

Blood serum, plasma and ascitic fluid levels of MUC16 in mice and humans have been well-researched and are now commonly used as diagnostic markers when evaluating the effect of various chemo-treatments and for establishing the advent of relapse in EOC (Rustin et al., 2001; Nishida et al., 2004). In this study, quantification of MUC 16/CA 125 concentration was conducted utilizing the highly sensitive Cancer Antigen 125 (CA125) Human ELISA Kit with a date-to-date coefficient of sensitivity >5%. Progressively increasing MUC16/CA125 values are correlated with ovarian malignancy, whilst steady MUC/CA125 values, even when raised, are correlated with some benign conditions. Significantly, in the pre- vs post-treatment groups of mice with induced EOC, the MUC16 antigen levels in the blood measured 2,368 in the placebo group, compared to 1,9460 U/ml in the (AF(D)NMs) post-treatment group (Figure 7.16). Our findings also showed that plasma MUC16 antigen levels were consistent with tumor growth, ascitic fluid development and mouse survival with distinct and combination chemo-treatments, indicative of MUC16 as a valuable biomarker to investigate the effect of chemo-treatment or relapse in the NIH:OVCAR-5 mice model.

Histopathology was subsequently performed on all SC/IP nodules and in all cases, the existence of anaplastic ovarian carcinoma(s) was confirmed histologically (Figure 7.17). Our findings

revealed foci of coagulative necrosis but necrotic foci were most often associated with cholestasis and bile infarcts thought to be due to obstruction to bile outflow by tumor nodules. In prior studies, additional toxic side effects that were observed in association with the use of methotrexate/cisplatin included chronic interstitial, obstructive pulmonary disease, severe renal outer cortex nephrosis (Malonnea et al., 2005; Li et al., 2014). Immunohistochemical analysis of epithelial ovarian tumors in the present study confirmed an apparent over-expression MUC16 in all induced tumors. Significantly, cellular labeling of MUC 16 was detected both in cytoplasmic granular and/or (to a lesser extent) cytoplasmic membrane labeling of neoplastic cells. Our results showed that MUC 16 is up-regulated in most of the tumor tissue samples analyzed (Figure 7.19). As has been shown in previous studies, we also detected a down-regulation of MUC16 expression in ovarian tumors post-treatment as compared to the pretreatment stage. At euthanasia, MUC16 antigen expression in the ovarian carcinoma tissues significantly decreased post-treatment with the AF(D)NMs and only a few small pieces of cell debris stained positive in these sections (Figure 7.8). These data indicated that the AF(D)NMs treatment can specifically target (MUC16) antigen-associated EOC tissue. The improved survival rate associated with the AF(D)NMs treatment was probably at least partly due to the profound decrease in ascitic fluid formation in this group ($p < 0.01$). The reduction in ascitic fluid probably occurred due to the specific and prolonged retention of AF(D)NMs hydrogels intra-peritoneally close to the tumor burden; intra-peritoneal tumor cells had close and prolonged exposure to the chemotherapeutic drugs, no doubt resulting in increased drug efficacy *in situ*.

The novel aspect of the study was the design and implementation of an antibody-functionalized nanomicelles hydrogel composite to specifically target MUC 16 antigens known to be over-expressed on ovarian cancer cells. Following the release of antibody-bound nanomicelles from the hydrogel, said nanomicelles targeted specific MUC 16 antigens over-expressed on ovarian carcinoma cells within the ascitic fluid and within neoplastic nodules at distant sites within the peritoneal cavity. This MUC 16 targeting system reduced the mass of neoplastic cells capable of adhering to parietal and visceral peritoneal surfaces at sites distant to the original tumor implant (Niloff et al., 1986; Mogensen et al., 1990). Chemo-treatment with AF(D)NM's significantly (via reducing MUC 16 antigen expression on tumor xenografts) inhibit growth of and transcoelomic metastasis of EOC and reduce the production of ascitic fluid, thereby increasing longevity in patients with ovarian carcinoma.

7.5. Conclusion Remarks

The present study has shown for the first time that combining anti-MUC16 antibodies with drug-loaded nanomicelles in a hydrogel composite can inhibit intra-peritoneal tumor growth (and therefore peritoneal carcinomatosis), reducing the consequent production of ascites, resulting in increased survival of animals in a Swiss nude mouse xenograft EOC model. This functionalized nanomicelle treatment may provide the basis for reducing the quantity of cisplatin or methotrexate utilized, thereby minimizing potentially harmful (toxic) side effects without significantly impacting on treatment efficacy. As a result, this antibody-bound nanotherapeutic implant drug delivery system may be a potent immuno-chemotherapeutic treatment that can be effectively employed in cases of advanced, and/or recurring, metastatic EOC.

CHAPTER 8

CONCLUSION AND RECOMMENDATIONS

9.1. Conclusions

In view of the burden of ovarian cancer and the numerous challenges associated with the systemic treatment of solid tumors in particular, the development of an *in situ* forming implant capable of delivering chemotherapeutics directly to tumors is certainly required. The aim of this study was to design and develop a novel drug delivery system employing antibody- ligand functionalized to drug-loaded nanomicelles encapsulated into implantable C-P-N hydrogel to form an *in situ* forming implant (ISFI) for cancer cell-targeting following intraperitoneal implantation to increase the residence time of the nanomicelles at tumor sites, enhancing tumor uptake of drugs and prevent recurrence and chemo-resistance. There is no record of an implantable, biodegradable intra-peritoneal chemotherapeutic formulation employing mucin antibodies hence this study yielded the first of its kind. Novel nanomicelles that are biodegradable, biocompatible, stable and have prolonged circulation for superior stability longer than a month in the peritoneum were developed.

ISFI formulation was prepared and release fractions tested for activity against NIH:OVCAR-5 cell lines. *In vivo* testing of the implant was conducted in Athymic nude mouse model. Methotrexate was the model antineoplastic drug that was loaded into anti-MUC16 conjugated nanomicelle and reduced the tumor size. Results showed that several animals that received the ISFI loaded with methotrexate developed diarrhea. Animals in the control group receiving methotrexate intraperitoneally did not show this side-effect. Hence the side-effects were indicative of prolonged release of drug from the implant compared to the intraperitoneal delivery of methotrexate which was cleared rapidly. This was confirmed by the blood levels found in the animals receiving the implant. In addition, animals receiving the placebo implant did not show this side-effect either indicating that the diarrhea was a side-effect of the drug and not of the implant material itself.

The drug delivery system surmounted cisplatin (key drug for chemotherapy) related disadvantages by offering a better selective accumulation. The use of antibody-bound-nanomicelles improved tumor tissue penetration and intracellular retention of chemotherapeutic drug to avoid P-glycoprotein efflux of the drugs. This resulted in increased cytotoxicity at

suboptimal doses and improved the safety profiles of the drug. Peritoneal spread of ovarian tumors was decreased by formulating IP implantation of a biodegradable hydrogel responsive to pH and temperature and fabricated for controlling the release of drug-loaded nanomicelles over an extended period of time, preventing multiple surgeries and injections. The formulated drug delivery system has clinical potential to reduce the titer of malignant cells floating in the peritoneum, to reduce metastatic implantation and increase the 5-year survival rates of ovarian cancer patients. Optimal therapeutic efficacy was attained to eradicate the population of cells in the tumor that have been developed via MDR design of novel hydrogel networks for delivery of drug-loaded nanomicelles. The drug delivery system was also administered intravenously to target mucin antigens that are strongly expressed on disseminated ovarian carcinoma cells. Our strategy of employing monoclonal antibodies for targeting ovarian cancer cells generated specificity to cancer cells that express MUC16. The development of this novel implantable drug delivery system may circumvent the treatment flaws experienced with conventional systemic therapies, effectively manage recurrent disease and ultimately prolong disease-free intervals in ovarian cancer patients.

In conclusion, *in vitro* and *in vivo* work showed promising results with the prolong release of drug from the implant exceeding a month and improved biocompatibility of the ISFI.

9.2. Recommendations and future outlook

To date there is no data on the pharmaceutical use of Chitosan-Poly(N-vinylpyrrolidone)-Poly(N-isopropylacrylamide) (C-P-N) *in situ* forming implant. It is recommended that the polymer be investigated further. The actively targeted nature of this drug delivery system lends applicability to other solid tumors since targeting modalities that are specific to ovarian cancer have been employed. Hence, potential for use in other solid tumors should be investigated. The implant may offer combinational chemotherapy (as an alternative to current commercial approaches) to enhance the therapeutic efficacy and translate to treatment doses below those currently administered. The delivery system could be used for the treatment of a variety of cancers associated with aberrant mucin expression: pancreatic, prostate, metastatic breast cancer, bladder and lung. Moreover, *ex vivo* studies should extend to the respective cell lines that are applicable to other tumor subtypes. It is recommended that antineoplastic drugs to which resistance has been identified be incorporated into the ISFI and tested against resistant cell lines. Furthermore, the potential of phytochemical incorporation in overcoming drug resistance should be considered. Other targeted therapy will be especially beneficial for antineoplastic drugs since

site-specific delivery enhances cytotoxicity at the desired site while maintaining the condition of healthy tissue. Considering the calcification of tissues caused and the slow *in vivo* degradation of the implant, the implant (as currently formulated) is perhaps also suited for the potential delivery of cells (such as osteoblasts) to areas where bone formation is required. Nanomicelles, as described in this thesis, have theranostic potential and may be combined with ultrasound technology for tumor detection, imaging and monitoring the progress of therapy. Historically it has been acknowledged that biodegradable devices (with relative ease of implantation and lower side effects profile) are more applicable for short-term (hours, days) or intermediate-term (weeks, months) drug delivery and is all that is required to treat acute disease and where chronic therapy is required (>1 year) non-biodegradable devices may provide superior control of drug release, improved retrievability in the case of serious side-effects, and fewer invasive procedures than a biodegradable device.

REFERENCES

1. Abolmaali SS, Tamaddon AM, Dinarvand R. A review of therapeutic challenges and achievements of methotrexate delivery systems for treatment of cancer and rheumatoid arthritis. *Cancer Chemotherapy Pharmacology* 2013, 71:1115–1130.
2. Adams ML, Lavasanifar A. Kwon GS. Amphiphilic block copolymers for drug delivery. *Journal Pharmaceutical Science* 2003, 92:1343-55.
3. Akao T, Kimura T, Hirofuji YS, Matsunaga K, Imayoshi R, Nagao JI. A poly(γ -glutamic acid)-amphiphile complex as a novel nanovehicle for drug delivery system. *Journal Drug Target* 2010, 18(7):550-6.
4. Alexisa F, Rhee JW, Richieb JP, Radovic-Moreno A.F, Langer R, Farokhzada O.C, New frontiers in nanotechnology for cancer treatment. *Urologic Oncology: Seminars and Original Investigations* 2008, 26:74–85.
5. Alexis F, Pridgen EM, Langer R, and Omid C. Farokhzad O.C. Nanoparticle Technologies for Cancer Therapy. M. Schäfer-Korting (ed.). Drug Delivery, Handbook of Experimental Pharmacology, Springer-Verlag Berlin Heidelberg 2010, 197: 55-77.
6. American Cancer Society. Cancer Facts and Figures. Atlanta, GA: American Cancer Society 2010, 50:3.
7. Anderson, J. M. & Langone, J. J. Issues and perspectives on the biocompatibility and immunotoxicity evaluation of implanted controlled release systems. *Journal of Controlled Release* 1999, 57:107-113.
8. Aranovich, G., Donohue, M. Determining Surface Areas from Linear Adsorption Isotherms at Supercritical Conditions. *Journal. Colloid. Interface Science* 1997, 194:392-397.
9. Arimura H, Ohya Y, Ouchi T. Macromolecules, Rapid Commun 2004, 25:743–747.

10. Arimura H, Ohya Y, and Ouchi T. Formation of core-shell type biodegradable polymeric micelles from amphiphilic poly(aspartic acid)-block-poly(lactide) diblock copolymer. *Biomacromolecules* 2005, 6: 720-725.
11. Auersperg N, Edelson MI, Mok SC, Johnson SW, Hamilton TC. The biology of ovarian cancer. *Seminars in Oncology* 1998, 25: 281-304.
12. Auersperg N, Ota T, Mitchell GW. Early events in ovarian epithelial carcinogenesis: progress and problems in experimental approaches. *International Journal of Gynecological Cancer* 2002, 12:691-703.
13. Auersperg N, Wong AS, Choi KC, Kang SK, Leung PC. Ovarian surface epithelium: biology, endocrinology, and pathology. *Endocrine Review* 2001, 22: 255-288.
14. Bae Y, Nishiyama N, Kataoka K. In vivo antitumor activity of the folate conjugated pH-sensitive polymeric micelle selectively releasing adriamycin in the intracellular acidic compartments. *Bioconjugates Chemistry* 2007, 18:1131-9.
15. Bae Y, Kataoka K. Intelligent polymeric micelles form functional poly(ethylene glycol)-poly(amino acid) block copolymers. *Advanced Drug Delivery Review* 2009;61:768-84.
16. Bae K. H., Lee J. Y., Lee S. H., Park T. G., and Nam Y. S., "Optically traceable solid lipid nanoparticles loaded with siRNA and paclitaxel for synergistic chemotherapy with in situ imaging," *Advanced Healthcare Materials* 2013, 4:576–584,.
17. Bae H.S, Kim H. J, Hong J.H, Lee J.K, Lee N.W and Song J.Y. Obesity and epithelial ovarian cancer survival: a systematic review and meta-analysis, *Journal of Ovarian Research* 2014, 7:41.
18. Babu A, Templeton AK, Munshi A and Ramesh R. Nanoparticle-Based Drug Delivery for Therapy of Lung Cancer: Progress and Challenges. *Journal of Nanomaterials* 2013, 11: <http://dx.doi.org/10.1155/2013/863951>.
19. Barbucci, R., Leone, G. & Vecchiullo, A. Novel carboxymethylcellulose-based microporous hydrogels suitable for drug delivery. *Journal. Biomaterials. Science. Polymer Edition* 2004, 15:607-619.

20. Bast RC, Feeney M, Lazarus H, Nadler LM, Colvin RB, Knapp RC. Reactivity of a monoclonal antibody with human ovarian carcinoma. *Journal of Clinical Investigation* 1981, 68:1331–1337.
21. Bast RC, Klug TL, St. John E, Jenison E, Niloff JM, Lazarus H. A radioimmunoassay using a monoclonal antibody to monitor the course of epithelial ovarian cancer. *N England Journal Medine* 1983, 309: 883–7.
22. Bast., R.J. Status of tumor markers in ovarian cancer screening. *Journal Clinical Oncology* 2003, 21:200s-205s.
23. Bast, R.C., Badgwell J.R.D., Lu, Z., Marquez R., Rosen, D., Liu, J., Baggerly, K.A., Atkinson, E.N., Skates, S., Zhang, Z., Lokshin A., Menon U., Jacobs, I. & Lu, K. New tumor markers: CA125 and Beyond. *International Journal Gynecological Cancer* 2005, 15 (Suppl. 3):274–281.
24. Bastakoti BP, Wu KCW, Inoue M, Yusa S, Nakashima K, Yamauchi Y. Multifunctional Core-Shell-Corona-Type Polymeric Micelles for Anticancer Drug-Delivery and Imaging. *Chemistry. European. Journal.* 2013, 19:4812-4817.
25. Batrakova EV, Li S, Li YL, Alakhov VY, Elmquist WF, Kabanov AV. Ditrubution kinetics of a micelle-forming block copolymer Pluronic P85. *Journal Control Release* 2004, 100: 389-97.
26. Bawa P, Pillay V, Choonara Y E, du Toit LC, Ndesendo, VMK, Kumar P A. Composite polyelectrolyte matrix for controlled oral drug delivery. *American Pharmaceutical Sciences Technology* 2011, 12: 227–238.
27. Bayó-Puxan N, Dufresne M.H, Felber A.E, Castagner B, Leroux J.C, Preparation of polyion complex micelles from poly(ethylene glycol)-block-polyions. *Journal of Controlled Release* 2011, 156: 118–127.
28. Benamer, S., Mahlous, M., Boukrif, A., Mansouri, B. & Youcef, S. L. Synthesis and characterisation of hydrogels based on poly(vinyl pyrrolidone). *Nuclear Instruments and Methods in Physics Research B* 2006, 248:284–290.
29. Bergbreiter D E, Case B L, Liu YS, Caraway J W Poly(N-isopropylacrylamide) Soluble Polymer Supports in Catalysis and Synthesis. *Journal of Macromolecules* 1998, 31: 6053-6062.

30. Bertrand N, Fleischer JG, Wasan KM, Leroux JC. Pharmacokinetics and biodistribution of N-isopropylacrylamide copolymers for the design of pH-sensitive liposomes. *Biomaterials* 2009, 30:2598–2605.
31. Biswas, Swati, Onkar S.Vaze, Sara Movassaghian. and Vladimir P. Torchilin. "Polymeric Micelles for the Delivery of Poorly Soluble Drugs" Drug Delivery Strategies for Poorly Water Soluble Drugs Douroumis/Drug 2013, Article ID 863951: 11 pages.
32. Blanco. E. C. W., Kessinger. B. D. Sumer. and J. Gao. "Multifunctional Micellar Nanomedicine for Cancer Therapy". *Experimental Biology and Medicine* 2009, 2: 123–131.
33. Bonina P, Petrova T, Manolova N. pH-Sensitive hydrogels composed of chitosan and polyacrylamide-preparation and properties. *Journal. Bioactive Compatibility. Polymer* 2004, 9:101–116.
34. Borgeest, C., Symonds, D., Mayer, L.P., Hoyer, P.B., Flaws, J.A. Methoxychlor may cause ovarian follicular atresia and proliferation of the ovarian epithelium in the mouse. *Toxicological Science* 2002, 68:473-478.
35. Brem H, Gabikian P. Biodegradable polymer implants to treat brain tumors. *Journal of Control Release* 2001, 74:63–67.
36. Bronstein LM, Chernyshov DM, Timofeeva GI *et al.* Interaction of polystyrene-block-poly (ethylene oxide) micelles with cationic surfactant in aqueous solutions. Metal colloid formation in hybrid systems. *Langmuir* 2000, 16: 3626-32.
37. Bruns, C.J., Shrader, M., Harbison, M.T. Effect of the vascular endothelial growth factor receptor-2 antibody DC101 plus gemcitabine on growth, metastasis and angiogenesis of human pancreatic cancer growing orthotopically in nude mice. *International Journal Cancer* 2002, 102:101- 8.
38. Buller RE, Berman ML, Bloss JD, Manetta A, DiSaia PJ. CA125 regression: A model for epithelial ovarian cancer response. *American Journal of Obstetrics & Gynecology* 1991, 165:360-367.

39. Cammas, S., Kataoka, K. Functional poly(ethylene oxide)-co-(beta-benzyl-aspartate) polymeric micelles—block-copolymer synthesis and micelles formation, *Macromolecules. Chemistry. Physics* 1995, 196:1899–1905.
40. Cancer Association of South Africa (CANSA). Research, Educate and support. Fact Sheet on Ovarian Cancer 2014, 1:1-15.
41. Cannistra SA. Cancer of the Ovary. *New England Journal of Medicine* 2004, 351:2519-2529.
42. Cantaert B, Beniash E, Meldrum FC. The role of poly(aspartic acid) in the precipitation of calcium phosphate in confinement, *Journal. Material. Chemistry. B* 2013, 1:6586-6595.
43. Chang D, Chiu C, Kuo S, Lin W, Lo A, Wang Y, Li P, Wu H. Antiangiogenic Targeting Liposomes Increase Therapeutic Efficacy for Solid Tumors. *The journal of biological chemistry* 2009, 19: 2905–12916.
44. Chauhan, SC, Singh, AP, Ruiz F, Johansson SL, Jain M, Smith LM, Moniaux N, Batra SK. Aberrant expression of MUC4 in ovarian carcinoma: diagnostic significance alone and in combination with MUC1 and MUC16 (CA125). *Modern Pathology* 2006, 19:1386–1394.
38. Chauhan, S.C., Kumar, D., Jaggi, M. Mucins in ovarian cancer diagnosis and therapy. *Journal of Ovarian Research* 2009, 2:21.
45. Chan JK, Pham H, You XJ, Cloven NG, Burger RA, Rose GS, Van Nostrand K, Korc M, DiSaia PJ, Fan H. Suppression of ovarian cancer cell tumorigenicity and evasion of cisplatin resistance using a truncated epidermal growth factor receptor in a rat model. *Cancer Research* 2005, 65:3243-3248.
46. Chen, H.B., Khemtong, C., Yang, X.L., Chang, X.L., Gao, J.M. Nanonization strategies for poorly water-soluble drugs. *Drug Discovery. Today* 2011, 16:354–360.
47. Chen Y, Lo C, Hsiue G. Multifunctional nanomicellar systems for delivering anticancer drugs. *Journal of Biomedical Materials Research* 2014, 102: 6.
48. Cheng N, Liu W, Cao Z, Ji W, Liang D, Goo G, Zhang JA. Study of thermoresponsive poly(N-isopropylacrylamide)/polyarginine bioconjugate non-viral transgene vectors. *Biomaterials* 2006, 27:4984–4992.

49. Cheng FY, Su CH, Wu PC, Yeh CS. Multifunctional polymeric nanoparticles for combined chemotherapeutic and near-infrared photothermal cancer therapy in vitro and in vivo. *Chem Commun (Camb)* 2010, 46: 3167-9.
50. Chithrani DB, Jelveh S, Jalali F, van Prooijen M, Allen C, Bristow RG, et al. Gold nanoparticles as radiation sensitizers in cancer therapy. *Radiat Res* 2010, 173:719-28.
51. Cho H, Lai TC, Kwon GS. Poly (ethylene glycol)-block-poly(ϵ -caprolactone) micelles for combination drug delivery: evaluation of paclitaxel, cyclophosphamide and gossypol in intraperitoneal xenograft models of ovarian cancer. *Journal of controlled Release* 2013, 166: 1-9.
52. Choi SJ, Oh JM, Choy JH. Biocompatible nanoparticles intercalated with anticancer drug for target delivery: pharmacokinetic and biodistribution study. *J Nanosci Nanotechnology* 2010, 10: 2913-6.
53. Chung J.E, Yokoyama M, Suzuki K, Aoyagi T, Sakurai Y, Okano T. Reversibly thermo-responsive alkyl-terminated poly(N-isopropylacrylamide) core-shell micellar structures. *Journal of Colloids and Surfaces B: Biointerfaces* 1997, 9:37-48.
54. Chung, M. Yokoyama, T. Aoyagi, Y. Sakurai, T. Okano. Effect of molecular architecture of hydrophobically modified poly (N-isopropylacrylamide) on the formation of thermoresponsive core-shell micellar drug carriers, *Journal. Controlled Release* 1998, 53:119-130.
55. Chung, J.E., Yokoyama, M., Okano, T. Inner core segment design for drug delivery control of thermo-responsive polymeric micelles. *Journal of Controlled Release* 2000, 65:93-103.
56. Condon, J.B. Chapter 1 - An Overview of Physisorption, Surface Area and Porosity Determinations by Physisorption. *Elsevier Science, Amsterdam* 2006, 1:296.
57. Costa, P., Sousa Lobo, J.M. Modeling and comparison of dissolution profiles. *European. Journal. Pharmaceutical. Science* 2001, 13:123-133.
58. Daman Z, Ostad SN, Amini M, Gilani K. Preparation, optimization and in vitro characterization of stearyl-gemcitabine polymeric micelles: A comparison with its self-assembled nanoparticles. *International Journal of Pharmaceutics* 2014, 468: 142-151.

59. Dash PR, Read ML, Fisher KD, Howard KA, Wolfert M, Oupicky D, Subr V, Strohal J, Ulbrich K, and Seymour LW. Decreased binding to proteins and cells of polymeric gene delivery vectors surface modified with a multivalent hydrophilic polymer and retargeting through attachment of transferrin. *J. Biol. Chem* 2000, 275: 3793-3802.
60. Davis A, Tinker A.V, Friedlander M. Platinum resistant” ovarian cancer: What is it, who to treat and how to measure benefit? *Journal of Gynecologic Oncology* 2014, 133: 624–631.
61. Dayananda K, Pi BS, Kim BS, Park TG, Lee DS, Synthesis and characterization of pH/temperature-sensitive block copolymers via atom transfer radical polymerization, *Polymer* 2007, 48: 758–762,.
62. Denise C. Connolly, DC. Animal Models of Ovarian Cancer, in M.S. Stack, Fishman, D.A. (Eds.), *Ovarian Cancer, Cancer Treatment and Research*. Fox Chase Cancer Center, Philadelphia, PA, USA 2009, 3:1053–1064.
63. Deraco, M., Baratti, D., Laterza, B., Balestra, M.R., Mingrone, E., Macrì, A., Virzi, S., Puccio, F., Ravenda, P.S., Kusamura, S. Advanced cytoreduction as surgical standard of care and hyperthermic intraperitoneal chemotherapy as promising treatment in epithelial ovarian cancer. *European Journal Surgical Oncology* 2011, 37:4–9.
64. Desseyn, JL, Tetaert D, Gouyer V. *Gene (Amst.)* 2008, 410: 215–222.
65. Díaz M.R and Vivas-Mejia P.E, Nanoparticles as Drug Delivery Systems in Cancer Medicine: Emphasis on RNAi-Containing Nanoliposomes. *Journal of Pharmaceuticals* 2013, 6: 1361-1380.
66. Ding Y, Kang Y, Zhang X. Enzyme-responsive polymer assemblies constructed through covalent synthesis and supramolecular strategy. *Chemistry. Commun* 2015, 51: 996.
67. Du Bois A, Luck HJ, Meier W, Adams HP, Mobus V, Costa S, Bauknecht T, Richter B, Warm M, Schroder W, Olbricht S, Nitz U, Jackisch C, Emons G, Wagner U, Kuhn W, Pfisterer J. A randomized clinical trial of cisplatin/paclitaxel versus carboplatin/ paclitaxel as first-line treatment of ovarian cancer. *Journal of the National Cancer Institute* 2003, 95: 1320–1329.

68. Duncan R. Polymer conjugates as anticancer nanomedicines. *Nat Rev Cancer* 2006, 6(9):688–701.
69. Eeckman F, Amighi K, J. Moe's AJ. Effect of some physiological and non-physiological compounds on the phase transition temperature of thermoresponsive polymers intended for oral controlled-drug delivery. *International Journal of Pharmaceutics* 2001, 222: 259–270.
70. ElBayoumi T.A and Torchilin V.P. Tumor-Targeted Nanomedicines: Enhanced Antitumor Efficacy In vivo of Doxorubicin Loaded, Long-Circulating Liposomes Modified with Cancer-Specific Monoclonal Antibody. *Clin Cancer Res* 2009, 15:1973-1980.
71. Fei, B., Wach, R. A., Mitomo, H., Yoshii, F. & Kume, T. Hydrogel of biodegradable cellulose derivatives. I. Radiation-induced crosslinking of CMC. *Journal of Applied Polymer Science* 2000, 78:278-283.
72. Feki A, Berardi P, Bellingan G, Major A, Krause K-H, Petignat P, Zehra R, Pervaize S, Irminger-Finger I. Dissemination of intraperitoneal ovarian cancer: discussion of mechanisms and demonstration of lymphatic spreading in ovarian cancer model. *Critical Reviews in Oncology/Hematology* 2009, 72:1-9.
73. Felder M, Arvinder Kapur A, Gonzalez-Bosquet J, Horibata S, Heintz J, Albrecht R, Fass L, Kaur J, Hu K, Shojaei H, Whelan R.J and Manish S Patankar M.S. MUC16 (CA125): tumor biomarker to cancer therapy, a work in progress. *Journal of Molecular Cancer* 2014, 13:129.
74. Fernandes LP, Morais WA, Santos AIB, dos Santos AML, dos Santos DES, Pavinatto, FJ, Oliveira, O.N, Dantas, TNC, Pereira MR. The influence of oxidative degradation on the preparation of chitosan nanoparticles. *Colloids Polymer Science* 2005, 284:1–9.
75. Frank Alexis F, Pridgen E.M, Langer R, Farokhzad O.C. Nanoparticle Technologies for Cancer Therapy M Schäfer-Korting (ed.). Drug Delivery, Handbook of Experimental Pharmacology 197, Springer-Verlag Berlin Heidelberg 2010, 197: 55-87.
76. Fournier E, Dufresne MH, Smith DC, Ranger M, Leroux JC. A novel one-step drug-loading procedure for water-soluble amphiphilic nanocarriers. *Pharm Res* 2004, 6:962-8.

77. Gaucher G, Dufresne MH, Sant VP, Kang N , Maysinger D, Leroux JC. Block copolymer micelles: preparation, characterization and application in drug delivery. *Journal of Controlled Release* 2005, 109:169–188.
78. Giuntoli RL, Rodriguez GC, Whitaker RS, Dodge R, Voynow JA. Mucin gene expression in ovarian cancers. *Cancer Research* 1998, 58:5546-5550.
79. Gabizon AA. Liposome circulation time and tumor targeting: implications for cancer chemotherapy. *Adv. Drug Delivery. Review* 1995, 16:285-294.
80. Gao J, Wang Yu J, Lin TW. The accelerated degradation of aqueous polyacrylamide at low temperature. *Journal of Applied. Polymer Science* 1998, 69:791–797.
81. Giammona, G., Pitarresi, G., Tomarchio, V., Cavallaro, G., Mineo, M. Crosslinked alpha, beta polyasparthydrazide hydrogels: effect of crosslinking degree and loading method on cytarabine release rate, *J. Controlled Release* 1996, 41:195–203.
82. Giammona, G., Cavallaro, G., Fontana, G., Pitarresi, G. Carlisi, B., Coupling of the antiviral agent zidovudine to polyaspartamide and in vitro drug release studies, *J. Controlled Release* 1998, 54:321–331.
83. Goa, Guang Hui, Yi Li, and Doo Sung Lee, “Environmental pH sensitive polymeric micelles for cancer diagnosis and targeted therapy”. *Journal of Controlled release* 2013, 169 :180-184.
84. Govender, S., Pillay, V., Chetty, D.J., Essack, S.Y., Dangor, C.M., Govender, T. Optimization and characterisation of bioadhesive controlled release tetracycline microspheres. *International Journal of Pharmaceutics* 2005, 306:24-40.
85. Gubbels JA, Belisle J, Onda M, Rancourt C, Migneault M, Ho M, Bera TK, Connor J, Sathyanarayana BK, Lee B, Pastan I, Patankar MS. Mesothelin-MUC16 binding is a high affinity, N-glycan dependent interaction that facilitates peritoneal metastasis of ovarian tumors. *Molecular Cancer* 2006, 5:50.
86. Gulley, J.L., Arlen, P.M., Tsang, K.Y., Yokokawa, J., Palena, C. Pilot study of vaccination with recombinant CEA-MUC-1-TRICOM poxviral-based vaccines in patients with metastatic carcinoma. *Clin Cancer Res* 2008, 14:3060–3069.

87. Güney G, Genç L, Dikmen G. Use of Nanocarrier Systems in Cancer Therapy. *Journal of Materials Science and Engineering* 2011, 5:577-582.
88. Guenther J.H, Jurczok A, Wulf T, Brandau S, Deinert I, Jocham D, Böhle A. Optimizing Syngeneic Orthotopic Murine Bladder Cancer (MB49)¹. *Cancer Research* 1999, 59:2834–2837.
89. Guo S, Huang L. Nanoparticles containing insoluble drug for cancer therapy. *Biotechnology Advances* 2014, 32: 778–788.
90. Gupta, A. K., Madan, S., Majumdar, D. K., Maitra, A. “Ketorolac entrapped in polymeric micelles: preparation, characterisation and ocular anti-inflammatory studies”. *International Journal of Pharmaceutics* 2000, 209:1–14.
91. Harries M, Kaye SB. Recent advances in the treatment of epithelial ovarian cancer. *Exp Opin Investig Drugs* 2001, 10: 1715–1724.
92. Hennink, W. E. & Nostrum, C. F. v. Novel crosslinking methods to design hydrogels. *Advanced Drug Delivery Reviews* 2002, 54:13–36.
93. Hobbs SK, Monsky WL, Yuan F, Roberts WG, Griffith L, Torchilin VP, Jain RK, Regulation of transport pathways in tumor vessels: role of tumor type and microenvironment, *Proc. Natl. Acad. Sci. U. S. A.* 1998; 95: 4607–4612.
94. Hoffman, A. S. Hydrogels for biomedical applications. *Advanced Drug Delivery Reviews* 2002, 43:3–12.
95. Horacio Cabral. “Smart Nanoassemblies of Block Copolymers for Drug and Gene Delivery”. *Advanced Nanomaterials* 2009, 1: 014109 (9pp).
96. Hoskins, WJ, McGuire WP, Brady MF, Homesley HD, Creasman WT, Berman M, Ball H, Berek JS. The effect of diameter of largest residual disease on survival after primary cytoreductive surgery in patients with suboptimal residual epithelial ovarian carcinoma. *American Journal of Obstetrics & Gynecology* 1994, 170:974–979.
97. Hou, D., Xie, C.S., Huang, K. J., Zhu, C. H. “The production and characteristics of solid lipid nanoparticles (SLNs)”. *Biomaterials* 2003, 24:1781–1785.

98. Huang CJ, Chang FC. Polypeptide Diblock Copolymers. Syntheses and Properties of Poly(N-isopropylacrylamide)-b-Polylysine. *Macromolecules* 2008, 41:7041-7052.
99. Hu, B., Pan, C., Sun, Y. "Optimization of fabrication parameters to produce chitosan-tripolyphosphate nanoparticles for delivery of tea catechins". *Journal of Agricultural and Food Chemistry* 2008, 56:7451–7458.
100. International Federation of Gynecology and Obstetrics (FIGO) staging for ovarian, fallopian tube and peritoneal cancer. *Journal of Gynecologic Oncology* 2014, 133: 401–404.
101. Instruments and Methods in Physics Research B 2001, 175–177: 1-818.
102. Iwata, H., Matsuda, S., Mitsuhashi, K., Itoh, E., Ikada, Y. A novel surgical glue composed of gelatin and N-hydroxysuccinimide activated poly(L-glutamic acid): Part 1. Synthesis of activated poly(L-glutamic acid) and its gelation with gelatin, *Biomaterials* 1998,19:1869–1876.
103. Jacobs IJ, Oram DH, Bast RC. Strategies for improving the specificity of screening for ovarian cancer with tumor-associated antigens CA 125, CA 15-3, and TAG 72.3. *Obstetrics and Gynecology* 1992, 80:396–399.
104. Jaeger K, Wu G, Sel S, Garreis F, Brauer L, Paulsen FP;. MUC16 in the lacrimal apparatus. *Histochem Cell Biology* 2007, 127:433–438.
105. Jain RK. Transport of molecules, particles, and cells in solid tumors. *Annu Rev Biomed Eng* 1999, 1:241–263.
106. Jeong, Y., Seo,D.H., Kim, D.G., Choi, C., Jang, M.K., Nah, J.W. Methotrexate-Incorporated Polymeric Micelles Composed of Methoxy Poly(ethylene glycol)-Grafted Chitosan. *Macromolecular Research* 2009, 17:538-543.
107. Jemal A, Siegel R, Xu J, Ward E (2010) Cancer statistics. *CA Cancer Journal for Clinicians* 2010, 60: 277–300.
108. Jemal A, Murray T, Ward E, Samuels A, Tiwari RC, Ghafoor A, Feuer EJ, Thun MJ. Cancer statistics, CA: A Cancer. *Journal for Clinicians* 2005, 55:10–30.

109. Jiang T, Mo R, Bellotti A, Zhou J, Gu Zhen. Gel–Liposome-Mediated Co-Delivery of Anticancer Membrane Associated Proteins and Small-Molecule Drugs for Enhanced Therapeutic Efficacy. *Advanced Functional Material* 2014, 24: 2295–2304.
110. Jin Q, Maji S, Agarwal S. Novel amphiphilic, biodegradable, biocompatible, cross-linkable copolymers. Synthesis, characterization and drug delivery applications. *Polymer Chemistry* 2012, 3: 2785.
111. Jones. M.C. "Polymeric micelles - a new generation of colloidal drug carriers". *European Journal of Pharmaceutics and Biopharmaceutics* 1999, 48:101-111.
112. Jule E, Nagasaki Y, Kataoka K. Lactose-installed poly (ethylene glycol)-poly(D,L-lactide) block copolymer micelles exhibit fast-rate binding and high affinity toward a protein bed simulating a cell surface. A surface plasmon resonance study. *Bioconjug. Chem* 2003, 14:177-186.
113. Kabanov AV, Alakhov VY. Micelles of amphiphilic block copolymers as vehicles for drug delivery. In: Alexandris P, Lindman B, editors. Amphiphilic block copolymers: self-assembly and applications. *The Netherlands: Elsevier* 1997, 19:1-72.
114. Kobayashi. H. "Characterization of CA 125 antigen identified by monoclonal antibodies that recognize different epitopes". *Clinical Biochemistry* 1993, 13(8): 9942–9958.
115. Kaneko. S.J. "CA125 and UOCRF51 FISH studies of ovarian carcinoma". *Gynecologic Oncology* 2003, 90(1):29-36.
116. Kang H S, Yang S R, Kim JD, Han SH, Chang HIS. Effects of Grafted Alkyl Groups on Aggregation Behavior of Amphiphilic Poly(aspartic acid). *Langmuir* 1997, 17:7501-7506.
117. Kang, H., Kim, J. D., Han, S. H., Chang, I. S., *J. Control. Release* 2002, 81:135.
118. Kang N, Perron M.E., Prud'homme R.E, Zhang Y, Gaucher G, Leroux J.C., Stereocomplex block copolymer micelles: core-shell nanostructures with enhanced stability, *Nano Lett* 2005, 5:315– 319.

119. Kafali, H., Artuc, H., Demir, N. Use of CA125 fluctuation during the menstrual cycle as a tool in the clinical diagnosis of endometriosis; a preliminary report. *Eur J Obstet Gynecol Reproductive Biology* 2004, 116:85-88.
120. Katz, Josh. "Chemical modifications to vesicle forming diblock copolymers: Development of smart functional polymersome membranes". *J. Phys. Chem. B.* 2012 106 (11), 2848–2854
121. Karel Petrak. "Targeted Drug Delivery Quo Vadis?. Targeted Drug Delivery". *Drug Development Research* 2012, 3: 7-46.
122. Kedar U, Phutane, Shidhaye S, Kadam V, U. "Advances in polymeric micelles for drug delivery and tumor targeting", *Nanomedicine: Nanotechnology, Biology, and Medicine* 2010, 6: 714–729. doi:10.1016/j.nano.2010.05.005.
123. Khayat, D, Antoine EC, Coeffic D. Taxol in the management of cancers of the breast and the ovary. *Cancer Investigation* 2000, 18:242–260.
124. Kim, J.Y., Kim, S., Papp, M., Park, K., Pinal, R. Hydrotropic solubilization of poorly water-soluble drugs. *J. Pharm. Sci* 2011, 99: 3953–3965.
125. Kohori F, Sakai K, Aoyagi T, Yokoyama M, Sakuraib Y, Okano T. Preparation and characterization of thermally responsive block copolymer micelles comprising poly (N-isopropylacrylamide-b-DLlactide). *Journal of Controlled Release* 1998, 55:87–98.
126. Krupka TM, Weinberg BD, Ziats NP, Haaga JR, Exner AA. Injectable polymer depot combined with radiofrequency ablation for treatment of experimental carcinoma in rat. *Invest Radiol* 2006, 41: 890–897.
127. Kumar, Pradeep, Yahya Choonara, Lisa Toit, Girish Modi, Dinesh Naidoo, Viness Pillay. "Novel High-Viscosity Polyacrylamidated Chitosan for Neural Tissue Engineering: Fabrication of Anisotropic Neurodurable Scaffold via Molecular Disposition of Persulfate-Mediated Polymer Slicing and Complexation". *International Journal of Molecular Sciences* 2012, 13(11): 13966–13984.
128. Lastoskie, C.M., Gubbins, K.E. Characterization of Porous Materials Using Molecular Theory and Simulation. *Adv Chem Eng* 2001, 28:203-250.

129. Le Garrec D, Gorib S, Luob L, Lessard D, Smith D.C, Yessinea M.A, Rangera M, J.-C. Leroux J.C. Poly(N-vinylpyrrolidone)-block-poly(D,L-lactide) as a new polymeric solubilizer for hydrophobic anticancer drugs: in vitro and in vivo evaluation. *Journal of Controlled Release* 2004, 99: 83– 101.
130. Lee SC, Chang Y, Yoon JS, Kim C, Kwon IC, Kim YH, Jeong SJ. Synthesis and Micellar Characterization of Amphiphilic Diblock Copolymers Based on Poly(2-ethyl-2-oxazoline) and Aliphatic Polyesters. *Macromolecules* 1999, 32:1847-1852.
131. Lin, X.J., Chen, X.C., Wang, L., Wei, Y.Q., Kan, B., Wen, Y.J., He, X., Zhao, X. Dynamic progression of an intraperitoneal xenograft model of human ovarian cancer and its potential for preclinical trials. *J Exp Clin Cancer Res* 2007, 26:467–474.
132. Li, W., Tu, W.X., Cao, D.P. Synthesis of thermo-responsive polymeric micelles of PNIPAAm b-OMMA as a drug carrier for loading and controlled release of prednisolone. *J. Appl. Polym. Sci* 2008, 111:701–702.
133. Li N, Li Na, Yi Q, Luo K, Chunhua Guo, Dayi Pan, Zhongwei Gu. Amphiphilic peptide dendritic copolymer doxorubicin nanoscale conjugate self-assembled to enzyme-responsive anti-cancer agent. *Journal of Biomaterials* 2014, 35:9529-45.
134. Liang M, Liu X, Cheng D, Liu G, Dou S, Wang Y, Rusckowski M, Hnatowich DJ. Multimodality Nuclear and Fluorescence Tumor Imaging in Mice Using a Streptavidin Nanoparticle. *Bioconjug Chem* 2010, 21:1385–1388.
135. Liao C, Sun Q, Liang B, Shena J, Shuai X. Targeting EGFR-overexpressing tumor cells using Cetuximab-immunomicelles loaded with doxorubicin and superparamagnetic iron oxide. *European Journal of Radiology* 2011, 80: 699– 705.
136. Lin KF, Hsu CY, Huang TS, Chiu WY, Lee YH, Young TH. A novel method to prepare chitosan/montmorillonite nanomicelles. *Journal of Applied Polymer Science* 2005, 98:2042–2047.

137. Lin J, Li Y, Li Y, Cui F, Yu F, Wu H, Xie L, Luo F, Hou Z, Lin C. Self-targeted, bacillus-shaped, and controlled-release methotrexate prodrug polymeric nanoparticles for intratumoral administration with improved therapeutic efficacy in tumor-bearing mice, *Journal of Materials Chemistry B* 2015, 3:7707-7717.
138. Liu, M., Dong, J., Yang, M, Y., Yang, X., H. Xu, H. "Characterization and release of triptolide-loaded poly (D, L-lactic acid) nanoparticles". *Journal of European Polymer* 2005, 41:375–382.
139. Liu, H., Rajasekaran, A.K., Moy, P., Xia, Y., Kim, S. Constitutive and antibody-induced internalization of prostate-specific membrane antigen. *Cancer Res* 1998, 58:4055–4060.
140. Liu. Rang. M Laird Forrest. and Glen Koon. "Micellization and Drug Solubility Enhancement Part II: Polymeric Micelles". *Water-Insoluble Drug Formulation Second Edition* 2008, 2:688 – 252.
141. Liu C, Chen Y, Chen J. Synthesis and characteristics of pH-sensitive semi-interpenetrating polymer network hydrogels based on konjac glucomannan and poly (aspartic acid) for in vitro drug delivery. *Carbohydrate Polymers* 2010, 79:500–506.
142. Lu Ying and Kinam Park. Polymeric micelles and alternative nanonized delivery vehicles for poorly soluble drugs. *International Journal of Pharmaceutics* 2012, 8:1-17.
143. Lu HF, Lim WS, Wang J, Tang ZQ, Zhang PC, Leong KW, et al. Galactosylated PVDF membrane promotes hepatocyte attachment and functional maintenance. *Biomaterials* 2003, 24:4893-903.
144. Ma D, Zhang H, Tua K, Zhang L. Novel supramolecular hydrogel/micelle composite for co-delivery of anticancer drug and growth factor. *This journal is a The Royal Society of Chemistry* 2012, 8: 3665–3672.
145. MacGibbon A, Bucci J, MacLeod C, Solomon J, Dalrymple C, Firth I, Carter J. Whole Abdominal Radiotherapy Following Second-Look Laparotomy For Ovarian Carcinoma. *Gynecologic Oncology* 1999, 75:62 – 67.
146. Malonnea H, Eeckman F, Fontainea D, Ottoa A, De Vos L, Moe's A, Fontainea J, Amighi K. Preparation of poly(N-isopropylacrylamide) copolymers and preliminary assessment of

- their acute and subacute toxicity in mice. *European Journal of Pharmaceutics and Biopharmaceutics* 2005, 61:188–194.
147. Menon U, Jacobs I. Screening for ovarian cancer. Best Practice and Research. *Clinical Obstetrics and Gynaecology* 2002, 16:469–482.
 148. Miller MT, "In Vitro Evaluation of Cytotoxicity and Cellular Uptake of Alternating Copolymers for use as Drug Delivery Vehicles", Thesis, Massachusetts Institute of Technology 2009, 1:25.
 149. Madaswamy S Muthu. "Stimulus-responsive targeted nanomicelles for effective cancer therapy". *Nanomedicine* 2009, 4(6):657-67.
 150. Mahmud A, Xiong XB, Aliabadi HM, Lavasanifar A. Polymeric micelles for drug targeting. *Journal of Drug Targeting* 2007, 15: 553-84.
 151. Mall AS. "Analysis of mucins: role in laboratory diagnosis". *Journal of Clinical Pathology* 2008, 61:1018–1024. doi:10.1136/jcp.2008.058057.
 152. Mishra. B.. "Colloidal nanocarriers: a review on formulation technology. Types and applications toward targeted drug delivery". *Nanomedicine: Nanotechnology. Biology and Medicine* 2010, 6(1):9-24. doi: 10.1016/j.nano.2009.04.008. Epub 2009.
 153. Mogensen O, Mogensen B, Jakobsen A. Predictive value of CA125 during early chemotherapy of advanced ovarian cancer. *Gynecologic Oncology* 1990, 37:44-46.
 154. Mogensen O. Prognostic Value of CA 125 in Advanced Ovarian Cancer. *Gynecologic Oncology* 1992:44: 207-212.
 155. Moore RG, Brown AK, Miller MC, Skates S, Allard WJ, Verch T, Steinhoff M, Messerlian G, DiSilvestro P, Granai CO, Bast RC. The use of multiple novel tumor biomarkers for the detection of ovarian carcinoma in patients with a pelvic mass. *Gynecologic Oncology* 2007, 108:402–408.
 156. Mourya VK, Inamdar Nazma, Nawale R B, Kulthe SS, Polymeric Micelles: General Considerations and their Applications. *Indian Journal Pharmaceutical Education and Research* 2011, 45: 2.

157. Mukherjee, B., Santra, K., Pattnaik, G., Ghosh, S. "Preparation, characterization and in-vitro evaluation of sustained release protein-loaded nanoparticles based on biodegradable polymers". *International Journal of Nanomedicine* 2008, 3: 487–496.
158. Mukherjee I, Moulik SP, Rakshit AK. Tensiometric determination of Gibbs surface excess and micelle point: A critical revisit. *Journal of Colloid and Interface Science* 2013, 394: 329–336.
159. Murdoch, W.J., Van Kirk, EA. Steroid hormonal regulation of proliferative, p53 tumor suppressor, and apoptotic responses of sheep ovarian surface epithelial cells. *Mol Cell Endocrinol* 2002, 186:61-67.
160. Musacchio T, Laquintan V, Latrof A, Trapani G, Torchilin VP. PEG-PE micelles loaded with paclitaxel and surface-modified by a PBR-ligand: Synergistic anticancer effect. *Mol Pharm* 2009, 6: 468-79.
161. Mura S, Nicolas J, Couvreur P. Stimuli-responsive nanocarriers for drug delivery. *Journal of Nature materials* 2013, 12. DOI: 10.1038/NMAT3776.
162. Nakato T, Yoshitake M, Matsubara K, Tomida M. Relationships between Structure and Properties of Poly(aspartic acid)s. *Macromolecules* 1998, 31:2107-2113.
163. Nakayama M, Okano T, Miyazaki T, Kohori F, Sakai K, Yokoyama M. Molecular design of biodegradable polymeric micelles for temperature-responsive drug release, *J. Controlled Release* 2006, 115:46–56.
164. NanoCarrier Co. (4571). SR Research Report, 2014/2/1.
165. Nho, Y.-C. & Lee, J.-H. Reduction of postsurgical adhesion formation with hydrogels synthesized by radiation. *Nuclear Instruments and Methods in Physics Research B* 2005, 236:277–282.
166. Niloff JM, Knapp RC, Levin PT. The CA125 assay as a predictor of clinical recurrence in epithelial ovarian cancer. *American Journal of Obstetrics & Gynecology* 1986, 155:56-60.

167. Nishida, N., Yano, H., Komai, K., Nishida, T., Kamura, T. Vascular endothelial growth factor C and vascular endothelial growth factor receptor 2 are related closely to the prognosis of patients with ovarian carcinoma. *Cancer* 2004, 101: 1364–1374.
168. Nita LE, Chiriac AP, Bercea M, Neamtu I. The Temperature Influence upon the Complexation Process between Poly(aspartic acid) and Poly(ethylene glycol). *Journal of Industrial. Engineering. Chemistry. Res* 2011, 50:5369–5375.
169. Nobs L, Buchegger F, Gurny R, Alle´mann E. Current Methods for Attaching Targeting Ligands to Liposomes and Nanoparticles. *Journal of Pharmaceutical Sciences* 2004, 93:1980–1992.
170. Nori A, Yim EKF, Hen S, Leong KW. Cell Substrate Interactions. In *Principles of Regenerative Medicine*; Atala, A., Lanza, R., Thomson, J.A., Nerem, R.M., Eds.; Academic Press: New York, NY, USA. 2010, 666–685.
171. Nudelman F, Pieterse K, George A, Bomans PHH, Friedrich H, Brylka LJ, Hilbers PAJ, de With G, Sommerdijk N. *Nat. Mater* 2010, 9:1004–1009.
172. Oberoi. Hardeep S. "Polymer micelles with cross-linked ionic cores for delivery of platinum anticancer agents". *International Journal of Nanomedicine* 2012, 7:2557–2571. doi: 10.2147/IJN.S29145.
173. Oei, A.L., Moreno, M., Verheijen, R.H, Sweep, F.C., Thomas, CM.,. Induction of IgG antibodies to MUC1 and survival in patients with epithelial ovarian cancer. *Int J Cancer* 2008, 123:1848–1853.
174. Oerlemans C, Bult W & Bos M, Storm G, Nijssen J. F W, Hennink W E. Polymeric Micelles in Anticancer Therapy: Targeting, Imaging and Triggered Release. *Pharm Res* 2010, 27: 2569–2589.
175. Orsulic, S., Li, Y., Soslow, R.A., Vitale-Cross, L.A., Gutkind, J.S., Varmus, H.E. Induction of ovarian cancer by defined multiple genetic changes in a mouse model system. *Cancer Cell* 2002, 1:53-62.

176. World Cancer Research Fund / American Institute for Cancer Research. Continuous Update Project Report. Food, Nutrition, Physical Activity, and the Prevention of Ovarian Cancer 2014. Available at http://www.dietandcancerreport.org/cup/cup_resources.php!
177. Owens III, D.E., Peppas, N.A. Opsonization, biodistribution, and pharmacokinetics of polymeric nanoparticles. *International Journal of Pharmaceutics* 2006, 307:93–102.
178. Palivan G.C, Fischer-Onaca O, Delcea M, Iteľ F and Wolfgang Meier W. Protein–polymer nanoreactors for medical applications. *Chem. Soc. Rev* 2012, 41: 2800–2823.
179. Panyam, J., Zhou, W. Z., Prabha, S., Sahoo, S. K., Labhasetwar, V., 2002. “Rapid endosomal escape of poly(DLlactide- co-glycolide) nanoparticles: implications for drug and gene delivery” . *The FASEB Journal* 16, 1217– 1226.
180. Park E. K, Kim SY, Lee SB, and Lee YM. Folate conjugated methoxy poly(ethylene glycol)/poly(epsilon-caprolactone) amphiphilic block copolymeric micelles for tumor-targeted drug delivery. *J. Control. Release* 2005, 109:158-168.
181. Parveen. S.. "Nanoparticles: a boon to drug delivery. Therapeutics,diagnostics and imaging". *Nanomedicine: Nanotechnology. Biology and Medicine* 2012, 8:147–166. doi:10.1016/j.nano.2011.05.016.
182. Pasc A, Blin J, ´ Ste´be´ M and Ghanbaja J. Solid lipid nanoparticles (SLN) templating of macroporous silica beads. *RSC Advances* 2011, 1:1204–1206.
183. Pignatello, R., Bucolo, C., Spedalieri, G., Maltese, A., Puglisi, G. “Flurbiprofen-loaded acrylate polymer nanosuspensions for ophthalmic application”. *Biomaterials* 2002, 23: 3247–3255.
184. Prabakaran M, Grailer JJ, Pilla S, Steeber DA, Gong S. Folate-conjugated amphiphilic hyperbranched block copolymers based on Boltorn H40, poly(Llactide) and poly(ethylene glycol) for tumor-targeted drug delivery. *Biomaterials* 2009, 30(16):3009–19.
185. Prat J, for the FIGO Committee on Gynecologic Oncology. Staging classification for cancer of the ovary, fallopian tube, and peritoneum. *International Journal of Gynecology and Obstetrics* 2014, 124: 1–5.

186. Preetham, A.C., Satish. Formulation of a poorly water-soluble drug sirolimus in solid dispersions to improve dissolution. *J. Dispers. Sci. Technol* 2011, 32:778–783.
187. Qian F, Saidel GM, Sutton DM, Exner A, Gao J. Combined modeling and experimental approach for the development of dual-release polymer millirods. *J Control Release* 2002, 83:427–435.
188. Qiao P, Niu Q, Wang Z, Cao D. "Synthesis of thermosensitive micelles based on poly(N-isopropylacrylamide) and poly(L-alanine) for controlled release of adriamycin". *Journal of Chemical Engineering* 2010, 159:257–263.
189. Roberts, D., Williams, S.J., Cvetkovic, D., Weinstein, J.K., Godwin, AK. Johnson SW and Hamilton TC: Decreased expression of retinolbinding proteins is associated with malignant transformation of the ovarian surface epithelium. *DNA Cell Biol.* 2002, 21:11-19.
190. Rapoport. N.. "Physical stimuli-responsive polymeric micelles for anti-cancer drug delivery". *Progress in Polymer Science* 2007, 32:962–990. doi:10.1016/j.progpolymsci.2007.05.009.
191. Rosiak, J. M., Ulanski, P. & Rzeinicki, A. Hydrogels for biomedical purposes. *Nuclear and Methods in Physics Research B* 1995, 151:56-64.
192. Rosiak, J. M. & Yoshii, F. Hydrogels and their medical applications. *Nuclear Instruments and Methods in Physics Research B* 1999, 105:335-339.
193. Rhyner. Matthew N. "Development of cancer diagnostics using nanoparticles and amphiphilic polymers". *Nanomedicine* 2006, 1:2. <https://doi.org/10.2217/17435889.1.2.209>.
194. Rivory, L.P. "Molecular, cellular, and clinical aspects of the pharmacology of 20(S) camptothecin and its derivatives". *Pharmacology and therapeutics* 1995, 68: 269-296.
195. Rimmer S, Carter S, Rutkaite R, Haycockb J.W, Swanson L. Highly branched poly-(N-isopropylacrylamide)s with arginine–glycine–aspartic acid (RGD)- or COOH-chain ends that form sub-micron stimulus-responsive particles above the critical solution temperature. *Journal of Soft Matter* 2007, 3: 971–973.

196. Rodríguez-Ayala G, Romaguera J, López M and Ortiz A.P. Ovarian Cancer Screening Practices of Obstetricians and Gynecologists in Puerto Rico. Hindawi Publishing Corporation. *Journal of BioMed Research International* 2014, 6. <http://dx.doi.org/10.1155/2014/920915>.
197. Roßler A, Vandermeulen GW, Klok HA. Advanced drug delivery devices via self-assembly of amphiphilic block copolymers. *Adv Drug Deliv Rev* 2001, 53: 95–108.
198. Roweton S, Huang SJ, Swift G. Poly (aspartic Acid): Synthesis, Biodegradation, and Current Applications Acid): Synthesis, Biodegradation, and Current Applications. *Journal of Environmental Polymer Degradation* 1997, 5:3.
199. Rump A, Morikawa Y, Tanaka M, Minami S, Umesak N, Takeuchi M, Miyajima A. Binding of ovarian cancer antigen CA125/MUC16 to mesothelin mediates cell adhesion. *Journal of Biological Chemistry* 2004, 279:9190–9198.
200. Rustin, G.J., Marples, M., Nelstrop, A.E., Mahmoudi, M., Meyer, T. Use of CA-125 to define progression of ovarian cancer in patients with persistently elevated levels. *J Clin Oncol.* 2001, 19: 4054–4057.
201. Saadat, E, Amini, M, Khoshayan M.R, Dinarvand, R, Dorkoosh, F.A. Synthesis and optimization of a novel polymeric micelle based on hyaluronic acid and phospholipids for delivery of paclitaxel, in vitro and in-vivo evaluation. *International Journal of Pharmaceutics* 2014, 475: 163–173.
202. Said, H. M., Alla, S. G. A. & El-Naggar, A. W. M. Synthesis and characterization of novel gels based on carboxymethyl cellulose/acrylic acid prepared by electron beam irradiation. *Reactive & Functional Polymers* 2004, 61:397–404.
203. Sallinen, H., Anttila, M., Narvainen, J., Ordén, MR., Ropponen, K., Kosma, V.M, Heinonen, S., Ylä Herttua, S. A highly reproducible xenograft model for human ovarian carcinoma and application of MRI and ultrasound in longitudinal follow-up. *Gynecol Oncol.* 2006, 103:315–320.
204. Sanna V, Pala N, Sechi M. Targeted therapy using nanotechnology: focus on cancer. *International Journal of Nanomedicine* 2014, 9: 467–483.

205. Santos A N, Soares D.A.W, Queiroz A.A.A. Low Potential Stable Glucose Detection at Dendrimers Modified Polyaniline Nanotubes. *Materials Research* 2010, 13(1): 5-10.
206. Sapa P, Allen T.M. Ligand-targeted liposomal anticancer drugs. *Progress in Lipid Research* 2003, 42: 439–462.
207. Sawant. R. M. J.P. Hurley. S. Salmaso. A. Kale. E. Tolcheva. T. S. Levchenko. and V. P. Torchilin. ""SMART" Drug Delivery Systems: Double-Targeted pH-Responsive. Pharmaceutical Nanocarriers". *Bioconjugate Chemistry* 2006,17:943-949.10.1021/bc060080h.
208. Sawant RR, Jhaveri AM, Torchilin VP, Jhaveri AM, Torchilin VP. Immunomicelles for advancing personalized therapy. *Advanced Drug Delivery Reviews* 2012, 64:1436–1446.
209. Seiden, M.V., 2001. Ovarian cancer. *Journal of Oncologist*. 6:327–332.
210. S. Sharma, A. Dua, A. Malik, Superabsorbent Polymer Gels based on Polyaspartic Acid and Polyacrylic Acid, *Journal of Material Sciences & Engineering* 5 (2016) 235 ISSN: 2169-0022.
211. Shim WS, Kim JH, Kim K, Kim YS, Park RW, Kim IS, Kwon IC, Lee DS. pH- and temperature temperature sensitive, injectable, biodegradable block copolymer hydrogels as carriers for paclitaxel. *Int J Pharm* 2007, 331:11–18.
212. Singh, B., Kumar, R., Ahuja, N. Optimizing drug delivery systems using systematic design of experiments. Part I: Fundamental Aspects. *Critical ReviewsTM in Therapeutic Drug Carrier Systems* 2005, 22:27-105.
213. Skarda, V., Rypacek, F., Ilavsky, M. Biodegradable hydrogel for controlled release of biologically-active macromolecules. *J. Bioact. Compat. Polym.* 1993, 8:24–40.
214. Song H, He R, Wang K, Ruan J, Bao C, Li N, Ji J, Cui D. Anti-HIF-1a antibody-conjugated pluronic triblock copolymers encapsulated with Paclitaxel for tumor targeting therapy. *Biomaterials* 2010, 31: 2302–2312.

215. Soppimath, K. S., Aminabhavi, T. M., Kulkarni, A. R., Rudzinski, W. E. "Biodegradable polymeric nanoparticles as drug delivery devices". *Journal of Controlled Release* 2001, 70:1–20.
216. Soppimath, K.S., Tan, D.C.W., Yang, Y.Y. pH-triggered thermally responsive polymer core–shell nanoparticles for drug delivery. *Adv. Mater* 2005, 17:318–323.
217. Sumer B, Gao J. Theranostic nanomedicine for cancer. *Nanomedicine* 2008, 3:137–140.
218. Sun TM, Du JZ, Yan LF, Mao HQ, Wang J. Self-assembled biodegradable micellar nanoparticles of amphiphilic and cationic block copolymer for siRNA delivery. *Biomaterials* 2008, 29(32):4348–55.
219. Sutton D, Nasongkla N, Blanco E, and Gao J. Functionalized Micellar Systems for Cancer Targeted Drug Delivery. *Pharmaceutical Research* 2007, 24: 6.
220. Sutton. Damon M. "pH sensitive RNA and drug delivery systems". PhD Thesis 2011. https://etd.ohiolink.edu/rws_etd/document/get/case1179847644/inline.
221. Sinha, S., Ali, M., Baboota, S., Ahuja, A., Kumar, A., Ali, J. Solid dispersion as an approach for bioavailability enhancement of poorly water-soluble drug ritonavir. *AAPS PharmSciTech* 2010, 11: 518–527.
222. Smetana, K. Cell biology of hydrogels. *Biomaterials* 1993, 14:1046-1050.
223. Solaro. Roberto. Federica Chiellini. and Antonella Battisti. "Targeted Delivery of Protein Drugs by Nanocarriers". *Materials* 2010, 3:1928-1980; doi:10.3390/ma3031928.
224. Soliman. Ghareb Mohamed. "Polysaccharide-based polyion complex micelles as new delivery systems for hydrophilic cationic drugs". PhD Thesis 2011. https://papyrus.bib.umontreal.ca/xmlui/bitstream/handle/1866/3844/Soliman_Ghareb_M_2009_these.pdf.
225. Smolle E, Taucher V, haybaeck J. Malignant Ascites in Ovarian Cancer and the Role of Targeted Therapeutics. *Anticancer Research* 2014, 34: 1553-1562.

226. Song H, He R, Wang K, Ruan J, Bao C, Li N, Ji J, Cui D. Anti-HIF-1 α antibody-conjugated pluronic triblock copolymers encapsulated with Paclitaxel for tumor targeting therapy. *Biomaterials* 2009, 1–11. doi:10.1016/j.biomaterials.2009.11.067.
227. Stimpfl M. "Exoexpression of mucins and cytokeratins in ovarian cancer cell lines". *Cancer Letters* 1999, 18; 145(1-2):133-41.
228. Stohlbach LA, Pitt L, Gandhir B, Dorsett H, Barber H, Iochim H. Ovarian cancer patient antibodies and their relationship to ovarian cancer associated markers. In *Compendium of Assays for Immunodiagnosis of Human Cancer*, Elsevier North-Holland, Inc., New York. 1979, 553-557.
229. Streppel, M.M., Vincent, A., Mukherjee, R., Campbell, N.R., Chen, S., Konstantopoulos, K., Goggins, M.G., Seuningen, I., Maitra, A., Elizabeth A. Montgomery, E.A. Mucin 16 (cancer antigen 125) expression in human tissues and cell lines and correlation with clinical outcome in adenocarcinomas of the pancreas, esophagus, stomach, and colon. *Human Pathology* 2012, 43:1755–1763.
230. Sudimack B.A.J, Lee R.J. Targeted drug delivery via the folate receptor. *Journal of Advanced Drug Delivery Reviews* 2000, 41:147–162.
231. Syed K. H. Gulrez, Saphwan Al-Assaf and Glyn O Phillips. *Hydrogels: Methods of Preparation, Characterisation and Applications, Progress in Molecular and Environmental Bioengineering. Analysis and Modeling to Technology Applications*, Prof. Angelo Carpi (Ed.), 2011, ISBN: 978-953-307-268-5.
232. Tamada Y, Takeuchi H, Suzuki N, Susumu N, Aoki D, Irimura T. Biological and therapeutic significance of MUC1 with sialoglycans in clear cell adenocarcinoma of the ovary. *Cancer Science* 2007, 98:1586–1591.
233. Tanya J. Shaw, Mary K. Senterman, 3, 4 Kerri Dawson, 1 Colleen A. Crane, and Barbara C. Vanderhyden. Characterization of Intraperitoneal, Orthotopic, and Metastatic Xenograft Models of Human Ovarian Cancer. *Molecular Therapy* 2004, 10:6.
234. Teicher BA. Antibody-Drug Conjugate Targets. *Current Cancer Drug Targets* 2009, 9: 982-1004.

235. Thassu. Deepak. Yashwant Pathak. and Michel Deleers. "Nanoparticulate Drug-Delivery Systems: An Overview', Drugs and the Pharmaceutical Sciences, A Series of Textbooks and Monographs. Executive Editor James Swarbrick. *PharmaceuTech, Inc.* 2007. http://ajprd.com/download ebooks_pdf/50.pdf.
236. Thériault, C., Pinard, M., Comamala, M., Migneault, M., Beaudin, J., Matte I., Boivin M., Piché A., Rancourt, C. MUC16 (CA125) regulates epithelial ovarian cancer cell growth, tumorigenesis and metastasis. *Gynecologic Oncology* 2011, 121: 434–443.
237. Thomas, C., Hamilton, Robert, C., Young, Karen, G., Louie, Brent, C., Wilma BM. McKoy, R. G., Ozols R.F. Characterization of a Xenograft Model of Human Ovarian Carcinoma Which Produces Ascites and Intraabdominal Carcinomatosis in Mice. *CANCER RESEARCH*. 1984, 44: 5286-5290.
238. Thünemann, A. F., Beyermann, J., Kukula, H. *Macromolecules* 2000, 33:5906.
239. Tong R, Yala L, Fan TM, Cheng J. The formulation of aptamer-coated paclitaxel-poly lactide nanoconjugates and their targeting to cancer cells. *Journal of Biomaterials* 2010, 31: 3043-53.
240. Topp M. D. C, Dijkstra P. J, Talsma H, Feijen J. Thermosensitive Micelle-Forming Block Copolymers of Poly(ethylene glycol) and Poly(*N*-isopropylacrylamide). *Macromolecules* 1997, 30: 8518-8520.
241. Torchilin. V.P. "Polymeric micelles in diagnostic imaging". *Colloids and Surfaces B: Biointerfaces* 1999, 16: 305-319. PII: S0927-7765(99)00081-8.
242. Torchilin. V.P. "Polymeric Contrast Agents for Medical Imaging". *Current Pharmaceutical Biotechnology* 2000, 1:183 – 215. DOI: 10.2174/1389201003378960.
243. Torchilin. V.P. "Structure and design of polymeric surfactant-based drug delivery systems". *Journal of Controlled Release* 2001, 73:137-72. [https://doi.org/10.1016/S0168-3659\(01\)00299-1](https://doi.org/10.1016/S0168-3659(01)00299-1).
244. Torchilin VP, PEG-based micelles as carriers of contrast agents for different imaging modalities. *Advanced. Drug Delivery. Review.* 2002, 54:235–252.

245. Torchilin V. P. "Targeted polymeric micelles for delivery of poorly soluble drugs". *Cellular and Molecular Life Sciences CMLS* 2004, 61: 2549–2559.
246. Tsubokawa, N., Nagano, Y., Sone, Y. Grafting of poly-beta-alanine onto carbon black the hydrogen transfer polymerization of acrylamide catalyzed by normal-butyllithium in the presence of carbon-black. *J. Appl. Polym. Sci* 1984, 29:985–993.
247. Tyrrell. Zacha. "Near-critical fluids for the preparation of nanosized micelles for cancer drug delivery". *Journal of Physical Chemistry* 2011, *J. Phys. Chem. C* 2011, 115, 11951–11956. [dx.doi.org/10.1021/jp202335r](https://doi.org/10.1021/jp202335r).
248. Vanderhyden Barbara C, Tanya J Shaw and Jean-François Ethier. Animal models of ovarian cancer. *Journal of Reproductive Biology and Endocrinology* 2003, 1:67.
249. Venugopal KN, Abhilash M. Study of hydration kinetics and rheological behaviour of guar gum. *International Journal of Pharma Sciences and Research (IJPSR)* 2010, 1: 28-39.
250. Veronese F.M., Ceriotti G., Caliceti P, Lora S, Carenza M. Slow release of narciclasine from matrices obtained by radiation-induced polymerization. *J. Controlled Release* 1991, 16:291–298.
251. Vadia, N., Rajput, S. Study on formulation variables of methotrexate loaded mesoporous MCM-41 nanoparticles for dissolution enhancement. *European Journal of Pharmaceutical Sciences* 2012, 45:8–18.
252. Vladimir P. Torchilin. "Passive and Active Drug Targeting: Drug Delivery to Tumors as an Example". *Handbook of Experimental Pharmacology* 2010, 276:1937 – 2017. <https://link.springer.com/bookseries/164>.
253. Vyas, T. K., Shahiwala, A., Amiji, M. M. "Improved oral bioavailability and brain transport of Saquinavir upon administration in novel nanoemulsion formulations," *International Journal of Pharmaceutics* 2008, 347:93–101
254. Wang M, Zhang G, Chen D, Jiang M, Liu S. Noncovalently connected polymeric micelles based on a homopolymer pair in solutions. *Macromolecules* 2001, 34: 7172-78.

255. Wang YZ, Li YJ, Han LM, Sha XY, Fang XL. Difunctional Pluronic copolymer micelles for paclitaxel delivery: synergistic effect of folate-mediated targeting and Pluronic-mediated overcoming multidrug resistance in tumor cell lines. *Int J Pharm* 2007, 337: 63-73.
256. Wang TW, Xu Q, Wu Y, Zeng A.J, Li M, Gao H. Quaternized chitosan (QCS)/poly (aspartic acid) nanoparticles as a protein drug-delivery system. *Carbohydrate Research* 2009, 344: 908–914.
257. Wang L, Hongmin Chen, Mohammad H. Pourgholami, Julia Beretov, Jingli Hao, Hongtu Chao, Alan C. Perkins, John H. Kearsley. Anti-MUC1 Monoclonal Antibody (C595) and Docetaxel Markedly Reduce Tumor Burden and Ascites, and Prolong Survival in an in vivo Ovarian Cancer Model 2011, <https://doi.org/10.1371/journal.pone.0024405>.
258. Wang A. Z, Langer R, and Farokhzad O. C., “Nanoparticle delivery of cancer drugs,” *Annual Review of Medicine* 2012, 63:185–198.
259. Wang J, Yin C, Tang G, Lin X and Wu Q. Synthesis, characterization, and in vitro evaluation of two synergistic anticancer drug-containing hepatoma targeting micelles formed from amphiphilic random copolymer. *Journal of Biomaterials Science* 2013, 1: 774–782.
260. Weers JG, Scheuing DR. Characterization of viscoelastic surfactant mixtures, I: fourier transform infrared spectroscopic studies. *Colloids Surf B: Biointerfaces* 1991, 1(55):41–56.
261. Wei H, Zhang XZ, Cheng H, Chen WQ, Cheng SX, Zhuo RX. Self-assembled thermo- and pH-responsive micelles of poly (10-undecenoic acid-b-N isopropylacrylamide) for drug delivery. *Journal of Controlled Release* 2006, 116: 266–274.
262. Wei Li, Tu W, Cao D. Synthesis of Thermoresponsive Polymeric Micelles of PNIPAAm-b-OMMA as a Drug Carrier for Loading and Controlled Release of Prednisolone. *Journal of Applied Polymer Science* 2009, 111: 701–708.
263. Weinberg BD, BLANCO E, GAO J. Polymer Implants for Intratumoral Drug Delivery and Cancer Therapy. *Journal of Pharmaceutical Sciences* 2008, 97:1681–1702.

264. Weinmann HJ, Ebert W, Misselwitz B, Schmitt-Willich H. Tissue-specific MR contrast agents. *Eur J Radiol* 2003, 46:33–44.
265. Westphal M, Ram Z, Riddle V, Hilt D, Bortey E. Gliadel wafer in initial surgery for malignant glioma: Long-term follow-up of a multicenter controlled trial. *Acta Neurochir (Wien)* 2006, 148:269–275; discussion 275.
266. Whitehouse C, Solomon E. Current status of the molecular characterization of the ovarian cancer antigen CA125 and implications for its use in clinical screening. *Gynecologic Oncology* 2003, 88:152 –157.
267. William Jr WN, Heymach JV, Kim ES, Lippman SM. Molecular targets for cancer chemoprevention. *Nat Rev Drug Discov* 2009, 8: 213–25.
268. Stewart BW, Wild CP, editors. *World Cancer Report 2014*. Lyon, France: International Agency for Research on Cancer 2014. https://www.iarc.fr/en/media-centre/pr/2014/pdfs/pr224_E.pdf.
269. Wu Y. "Synthesis and characterization of a novel amphiphilic chitosan-poly lactide graft copolymer". *Carbohydrate Polymers A* 2005, 59:167-171.
270. Xie J, Lee S, Chen X, Nanoparticle-based theranostic agents, *Adv. Drug Deliv. Rev.* 2010, 62:1064–1079.
271. Xiong XB, Mahmud A, Uludag H, Lavasanifar A. Conjugation of arginine-glycine-aspartic acid peptides to poly(ethylene oxide)-b-poly(-caprolactone) micelles for enhanced intracellular drug delivery to metastatic tumor cells. *Biomacromolecules* 2007, 8:874- 84.
272. Xuan. T. "HPLC method for determination of SN-38 content and SN-38 entrapment efficiency in a novel liposome-based formulation. LE-SN 38" .*Journal of Pharmaceutical and Biomedical Analysis* 2006, 41(2):582-8. Epub. <https://doi.org/10.1016/j.jpba.2005.10.051>.
273. Yallapu M.M, Jaggi M, Chauhan S.C. Scope of nanotechnology in ovarian cancer therapeutics. *Journal of Ovarian Research* 2010, 3:19.

274. Yap TA, Carden CP, Kaye SB. Beyond chemotherapy: targeted therapies in ovarian cancer. *Nat Rev Cancer* 2009, 9:167–181.
275. Yin BW, Dnistrian A, Lloyd KO. Ovarian cancer antigen CA125 is encoded by the MUC16 mucin gene. *International Journal of Cancer* 2002, 98:737–740.
276. Yoksan R, Akashi M, Miyata M, Chirachanchai S. Optimal γ -ray dose and irradiation conditions for producing low-molecular-weight chitosan that retains its chemical structure. *Radiation. Res* 2004, 161:471–480.
277. Zana R, editor. Dynamics of surfactant self-assemblies micelles, microemulsions, vesicles, and lyotropic phases. Boca Raton, Taylor and Francis Group, FL 33487-2742, CRC Press 2005, 2:16-130.
278. Zhang, Y., Jin, T., Zhuo, R. Methotrexate-loaded biodegradable polymeric micelles: Preparation, physicochemical properties and in vitro drug release. *Colloids and Surfaces B: Biointerfaces* 2005, 44:104–109.
279. Zhang G, Zhang R, Wen X, Li L, Li C. Micelles based on biodegradable poly(L-glutamic acid)-b-poly lactide with paramagnetic Gd ions chelated to the shell layer as a potential nanoscale MRI-visible delivery system. *Biomacromolecules* 2008, 9:36–42.
280. Zhang Y, Huo M, Zhou J, Yu D, Wu Y. Potential of amphiphilically modified low molecular weight chitosan as a novel carrier for hydrophobic anticancer drug: Synthesis, characterization, micellization and cytotoxicity evaluation. *Journal of Carbohydrate Polymers* 2009, 77: 231–238.
281. Zhang W, Shi Y, Chen YZ, Yu SY, Hao JG, Luo JQ. Enhanced antitumor efficacy by Paclitaxel-loaded Pluronic P123/F127 mixed micelles against nonsmall cell lung cancer based on passive tumor targeting and modulation of drug resistance. *Eur J Pharm Biopharm* 2010, 75: 341-53.
282. Zhang J, Chen X, Shi G, Xie X, Liu H, Zhang X, Lai Y, Zuo Y, Chen Z, Liu S, Wang H. Establishment of a new representative model of human ovarian cancer in mice. *Journal of Ovarian Research* 2013, 6:9.

283. Zhao Y, Kang J, Tan T. Salt-, pH- and temperature-responsive semi-interpenetrating polymer network hydrogel based on poly(aspartic acid) and poly(acrylic acid). *Polymer* 47 (2006) 7702-7710.
284. Zhong C, Chu CC. Biomimetic mineralization of acid polysaccharide-based hydrogels: towards porous 3-dimensional bone-like biocomposites. *J. Mat. Chem* 2012, 22:6080-6087.
285. Zhou DH, Zhang J, Zhang G, Gana ZN. Effect OF Surface Charge of Polymeric Micelles on *in vitro* Cellular uptake. *Chinese Journal of Polymer Science* 2013, 31: 1299–1309.
286. Zhu J, Liao, Zhu L , Zhang P , Guo K, Kong J, Ji C, Baohong Liu. Size-dependent cellular uptake efficiency, mechanism, and cytotoxicity of silica nanoparticles toward HeLa cells. *Talanta* 2013, 107:408–415.

APPENDICES

APPENDIX A

ASSESSMENT OF C-P-N HYDROGEL PROPERTIES

TGA LIFE TIME KINETICS

Tabulation of degradation temperature of the native polymers (CHT, PVP NIPAAm) components and cross-linked C-P-N hydrogel

Components	Decomposition points		Offset point DT °C	Derivative temperature	
	Onset point *DT °C	^a Delta Weight Loss (%)		Peak # Tp °C	Inflection point °C
Chitosan	279.41	54.28	350.00	377.67	349.39
PVP	293.88	66.31	374.29	329.17	331.20
NIPAAm	281.27	95.24	318.71	298.18	298.85
CPN hydrogel	382.28	93.82	417.27	402.56	404.24

RESEARCH PUBLICATIONS

APPENDIX B (1)

A Review of Nanomicellar Technologies for Targeted Drug Delivery in Ovarian Cancer Chemotherapeutics, Jonathan Pantshwa, Viness Pillay, Yahya E Choonara, Lisa C du Toit, Lomas K Tomar, Charu Tyagi, Pradeep Kumar, Clement Penny 2015. Submitted to Journal of Pharmaceutics South Africa.

REVIEW

Nanomicellar Technologies for Targeted Drug Delivery in Ovarian Cancer Chemotherapeutics

JONATHAN PANTSHWA¹, VINESS PILLAY¹, YAHYA E CHOONARA¹, LISA C DU TOIT¹, LOMAS K TOMAR¹, CHARU TYAGI¹, PRADEEP KUMAR¹, CLEMENT PENNY²

¹Wits Advanced Drug Delivery Platform Research Unit, Department of Pharmacy and Pharmacology, Faculty of Health Sciences, School of Therapeutics Sciences, University of the Witwatersrand, Johannesburg, 7 York Road, Parktown 2193, South Africa

²Department of Medical Oncology, Division of Oncology, Faculty of Health Sciences, University of the Witwatersrand, Johannesburg, 7 York Road, Parktown 2193, South Africa

ABSTRACT: In spite of the advancements in medicine, cancer still has detrimental side-effects with ovarian cancer (OC) accounting for numerous deaths among females. The provision of safe and effective treatment of OC continues to be a challenge to clinicians, despite the development of novel antineoplastic drugs. Micelles have progressively made their mark in the diagnosis and chemotherapy of various cancers due to their ideal size; improved drug encapsulation within the nanomicellar core; the potential to minimize drug degradation; improve *in vivo* drug release kinetics; and prolong blood circulation times. However, micelles have a few limitations with regard to the accuracy of tumor targeting and the ability to provide sustained drug release. Therefore, a rational design impetus has focused on micelle attachment to antibody-based ligands to selectively enhance cellular uptake of antineoplastic drugs for an improved chemotherapy. In this context, antibody-functionalized micelles are excellent technologically engineered candidates with broad spectrum of effectiveness to directly target tumor tissue while leaving healthy cells untouched. This article comprehensively reviews and provides perspective on the current status of nanotherapeutic applications using micellar technologies for treating OC. In addition, biomarkers for nanosystems may provide important prospects as a therapeutic strategy to increase the survival rate of patients with OC.

Keywords: Ovarian cancer, diagnostics, biomarkers, chemotherapeutics, toxicity, targeted drug delivery, micelle technologies

APPENDIX B (2)

Synthesis of new superior-viscosity amphiphilic poly N-isopropylacrylamide-block-poly aspartic acid copolymer for ovarian cancer chemotherapeutics. Submitted to Journal of Nanoparticles, Jonathan Pantshwa, Pradeep Kumar, Yahya Choonara, Lisa Du Toit, Clement Penny, Viness Pillay 2016.

Synthesis of Novel Amphiphilic poly (N-isopropylacrylamide)-b-poly (Aspartic acid) Micelles for Potential Targeted Chemotherapy in Ovarian Cancer

Jonathan Pantshwa¹, Yahya E. Choonara¹, Pradeep Kumar¹, Lisa C. du Toit¹, Clement Penny²
and Viness Pillay^{1*}

¹Wits Advanced Drug Delivery Platform Research Unit, Department of Pharmacy and Pharmacology, School of Therapeutic Sciences, Faculty of Health Sciences, University of the Witwatersrand, Johannesburg, 7 York Road, Parktown, 2193, South Africa.

²Department of Medical Oncology, Division of Oncology, Faculty of Health Sciences, University of the Witwatersrand, Johannesburg, 7 York Road, Parktown 2193, South Africa

ABSTRACT: The purpose of this study was to merge amino terminated poly N-isopropylacrylamide (PNIPAAm-NH₂) with L-Aspartic acid-N-carboxyanhydride (L-Asp-NCA) using thermal ring-cleavage polymerization to form a pH and thermo-responsive amphiphilic PNIPAAm-b-PAsp copolymer as a framework for producing self-assembling nanomicelles. The stimuli-responsive nanomicelles are intended for application as a targeted system for the delivery of methotrexate (MTX). Rheological profiles of various concentrations of the block copolymer were evaluated. The thermal ring-opening polymerization of L-Asp-NCA onto PNIPAAm-NH₂ yielded a copolymer with an inherent viscosity of 494.527mPas that was confirmed by advanced rheometry with a high mean molecular weight ($M_w=2.217 \times 10^6$ kDa) computed by the partially-proportional Mark-Houwink formula. SEM elucidated the copolymer topography and pore distribution. Vibrational FTIR spectra, NMR, DSC and TGA analysis confirmed the synthesis of the amphiphilic block copolymer. The PNIPAAm-b-PAsp nanomicelles were 90nm in size with a zeta potential value of -0.539mV (Pdl ≤ 0), a yield of 94% and a DEE value of >77%. The *in vitro* release profile of MTX displayed constant release of MTX over 72 hours. The CMC value was computed to be 0.09mg/mL. Overall, results demonstrated that the new PNIPAAm-b-PAsp copolymer synthesized was practical for nanomicelle formation and for the potential application as a stimuli-responsive nanocarrier system for the targeted delivery of MTX in OC.

Keywords: Ovarian cancer, targeted chemotherapy, methotrexate, poly(N-isopropylacrylamide), poly(aspartic acid), ring-opening polymerization, amphiphilic di-block copolymeric nanomicelles.

APPENDIX B (3)

Optimized Design of Combinational Poly N-isopropylacrylamide-block Poly Aspartic Acid Copolymeric Nanomicelles for Methotrexate Delivery. International Journal of Pharmaceutics, 2016, 448:267-281, Jonathan Pantshwa, Yahya Choonara, Pradeep Kumar, Lisa du Toit, Clement Penny, Viness Pillay 2016.

Optimized Design of Combinational Poly N-isopropylacrylamide-block Poly Aspartic Acid Copolymeric Nanomicelles for Methotrexate Delivery

Jonathan Pantshwa^a, Yahya Choonara^a, Pradeep Kumar^a, Lisa du Toit^a, Clement Penny^b and Viness Pillay^a

^aWits Advanced Drug Delivery Platform Research Unit, Department of Pharmacy and Pharmacology, School of Therapeutic Sciences, Faculty of Health Sciences, University of the Witwatersrand, Johannesburg, 7 York Road, Parktown, 2193, South Africa,

^bDepartment of Medical Oncology, Division of Oncology, Faculty of Health Sciences, University of the Witwatersrand, Johannesburg, 7 York Road, Parktown 2193, South Africa

Abstract

The aim of this article was to fabricate poly N-isopropylacrylamide-block- poly aspartic acid copolymeric nanomicelles with improved efficacy and prospective to offer as methotrexate (MTX) nanocarriers employed in intraperitoneal chemotherapeutics of ovarian cancer. MTX- loaded nanomicelle formulations were synthesized by dialysis method and optimized by employing a 3²-Factorial Box-Behnken experimental screening design approach. For the purpose of further drug entrapment efficacy enhancement, a solvent evaporation method was also employed. Investigations of micelle size, zeta potential, polydispersity index (PDI), morphology, drug-encapsulation efficacy (DEE), structural transformation utilizing Fourier Transform Infrared (FTIR) spectroscopy, and MTX release behaviour also ascertained. Nanomicelles with sizes ranging from 51.67 to 76.45 nm, a yield/recovery of 46.8–89.8 mg and polydispersity index (PDI ≤ 0.5) were obtained. Drug encapsulation efficacy (DEE) was initially (65.3 ±0.5%) and was ultimately optimized to 80.6±0.3%. FTIR spectroscopy investigations verified the encapsulation of the model drug (MTX) in the nanomicelles. The micelle formulation showed a rapid release at first, then a stable release period of MTX within and over 72 hours. Scanning Electron Micrographs showed spherical nanomicelles, and Transmission Electron Micrograph (TEM) images confirmed the presence of MTX in the nanomicelles. The results of this study suggest that the optimized stable nanomicelle formulation developed may have prospective application as an antineoplastic drug carrier nanosystem for ovarian cancer chemotherapeutics.

APPENDIX B (4)

Anti-muc 16 Functionalized Pnipaam-b-Pasp Nanomicelles for the Targeted Delivery of Methotrexate to Human Ovarian Carcinoma Cells. Submitted to Journal of Nanoparticles, Jonathan Pantshwa, Yahya Choonara, Pradeep Kumar, Lisa du Toit, Clement Penny, Viness Pillay 2016.

ANTI-MUC 16 FUNCTIONALIZED PNIPAAM-B-PASP NANOMICELLES FOR THE TARGETED DELIVERY OF METHOTREXATE TO HUMAN OVARIAN CARCINOMA CELLS

Jonathan Pantshwa¹, Yahya E. Choonara¹, Pradeep Kumar¹, Lisa C. du Toit¹, Clement Penny² and Viness Pillay^{1*}

¹Wits Advanced Drug Delivery Platform Research Unit, Department of Pharmacy and Pharmacology, School of Therapeutic Sciences, Faculty of Health Sciences, University of the Witwatersrand, Johannesburg, 7 York Road, Parktown, 2193, South Africa.

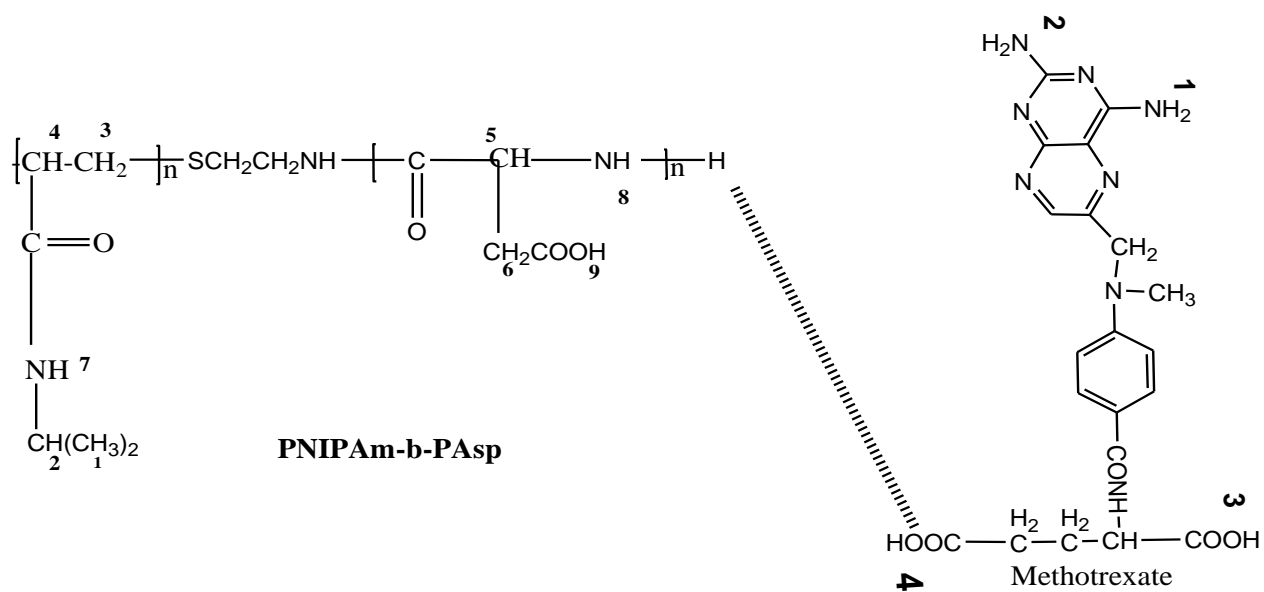
²Department of Medical Oncology, Division of Oncology, Faculty of Health Sciences, University of the Witwatersrand, Johannesburg, 7 York Road, Parktown 2193, South Africa

ABSTRACT:

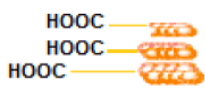
Ovarian cancer (OC) is lethal and challenging to treat since it presents with few early symptoms and is usually diagnosed late in advanced stages. The purpose of this study was to engineer a NanoComposite comprising anti-MUC 16 (antibody) functionalized methotrexate (MTX)-loaded PNIPAAm-b-PASP nanomicelles for the targeted delivery of MTX to NIH:OVCAR-5 OC cells that express MUC 16 as a preferential form of intraperitoneal OC chemotherapy. MUC16 is a well-known cell surface antigen in OC that is shed into the serum and therefore used clinically to diagnosis and treat epithelial OC. Amphiphilic MTX-loaded nanomicelles were prepared by self-assembly and thereafter functionalized with anti-MUC 16. The resulting NanoComposite was fully characterized by FT-IR, ZetaSizing analysis (DLS), TEM and SEM to ensure the pharmaceutical stability of the system before incubation with OC cells (NIH:OVAR-5). The treated cells were analyzed via a MTT assay and confocal microscopy for cellular uptake. The MTX-loaded nanomicelles produced were 75nm with spherical morphology with no significant influence on size and morphology post-functionalization with anti-MUC 16 on the nanomicelle surface. The results also confirmed that the NanoComposite successfully interacted with the OC cells and was internalized by MUC 16-mediated endocytosis with MTX release within the OC cell cytoplasm. *In vitro* cytotoxicity, cell apoptosis/death and cell cycle evaluations also showed that the functionalized NanoComposite was more potent than the non-functionalized MTX-loaded nanomicelles. In conclusion, the NanoComposite shows promise for direct MTX targeting to reduce or eliminate OC cells with over-expression of MUC 16 and thus may be an option for the clinical detection and targeted chemotherapy in OC.

KEYWORDS: Ovarian cancer; drug targeting; polymeric nanomicelles; methotrexate; cell uptake; antibody functionalization.

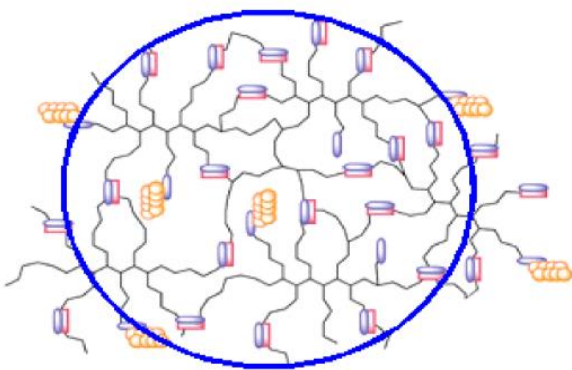
GRAPHICAL ABSTRACT



Micellization by solvent evaporation method to form Methotrexate loaded micelles



Functionalization by antibody attachment (NHS/EDC)



Antibody functionalized Drug Copolymer Nanomicelles

APPENDIX B (5)

In-vitro Synthesis, Characterization and assessment of a Bio-responsive IPN nanomicelle/hydrogel composite based implant for ovarian carcinoma treatment. To be submitted to Journal of Pharmaceutical Sciences. Jonathan Pantshwa, Yahya Choonara, Pradeep Kumar, Lisa du Toit, Clement Penny, Viness Pillay 2016.

IN-VITRO SYNTHESIS, CHARACTERIZATION AND EVALUATION OF A BIO-RESPONSIVE IPN NANOMICELLE/HYDROGEL COMPOSITE BASED IMPLANT FOR OVARIAN CARCINOMA TREATMENT

Jonathan Pantshwa, Divya Bijukumar, Yahya Choonara, Lisa Du Toit, Pradeep Kumar, Clement Penny, Viness Pillay 2016.

¹Wits Advanced Drug Delivery Platform Research Unit, Department of Pharmacy and Pharmacology, School of Therapeutic Sciences, Faculty of Health Sciences, University of the Witwatersrand, Johannesburg, 7 York Road, Parktown, 2193, South Africa.

²Department of Medical Oncology, Division of Oncology, Faculty of Health Sciences, University of the Witwatersrand, Johannesburg, 7 York Road, Parktown 2193, South Africa

ABSTRACT:

Chemotherapeutic agents such as cytotoxic drugs are limited by toxicity to healthy body cells that surround the tumor cells. An implant employed at the site of the tumor instead of an intravenously delivered chemotherapeutic agent may overcome this problem. The systemic side effects are much reduced due to the localized therapy exerted by the implant. Further, the implant can be formulated to release drug over a number of weeks or even months decreasing the need for the patient to return to the hospital for systemic treatment or eliminating the need to take medication daily and hence improving patient acceptability and compliance. A stimuli-responsive hydrogel, as an in situ forming implant (ISFI), can be synthesized using biodegradable NIPAAm, DMAEM and PMA to form a stable dual-sensitive (temperature and pH) hydrogel that swells once introduced into the simulated peritoneal environment (pH~7). In this study a new ternary interpenetrating polymeric networks (IPN) systems containing chitosan, poly (N-vinylpyrrolidone) and poly (N-isopropylacrylamide) polymers were prepared. This stimuli-responsive IPN hydrogel was synthesized by radical polymerization of NIPAAm monomers in presence of glutaraldehyde (G) and N,N-methylenebisacrylamide as crosslinkers and the other polymers (i.e., chitosan and poly(N-vinylpyrrolidone)). This IPN hydrogel was named as C-P-N. The ISFI was fabricated by encapsulating a nanocomposite comprising anti-MUC 16 (antibody) functionalized methotrexate (MTX)-loaded PNIPAAm-b-PASP nanomicelles within the synthesized bio-responsive C-P-N hydrogel followed by freeze drying. FTIR, NMR, Textual, Rheological, porosimeter and SEM studies were utilized to characterize the ISFI in vitro. Hydration and degradation studies were conducted within simulated peritoneal environment. Images were acquired using a bench-top MRI over a period of 50 days. Labelled – nanocomposites distribution within the ISFI was examined by micro- ultrasound imaging (Vevo ® 2100) and CLSM. SEM images validated the porous surface morphology of the hydrogel, with pores that are relatively uniform in size and shape. Rheological and textual parameters demonstrated that the cross-linked hydrogel was more firm and resilient when compared with the non cross-linked hydrogel. MRI images showed complete hydrogel hydrated within 3 min after submergence within a FCS, however the hydrated hydrogel exhibited swelling and slight erosion. Fluorescence patterns postulate intact vesicles after ISFI lyophilization. Ultrasound images confirmed that more even nanocomposites distribution was achieved in the slightly less viscous rather than highly viscous ISFI. Conclusion: The results validated that evaluation of ISFI physicochemical transitions is a useful tool for further investigations of optimized formulation designed for prolonged delivery of drugs into the targeted tumor tissue in ovarian cancer.

APPENDIX B (6)



Poster Title: An Optimal Mouse Model for Human Ovarian Carcinoma Research and Efficacy of various chemotherapeutic Treatment Protocols. The formatted research paper is to be submitted to the Journal of Oncology.

An Optimal Mouse Model for Human Ovarian Carcinoma Research and Efficacy of various chemotherapeutic Treatment Protocols

Jonathan Pantshwa¹, Khadija Rhoda¹, Sarah Clift², Divya Bijukumar, Yahya Choonara¹, Lisa Du Toit¹, Pradeep Kumar¹, Clement Penny¹ and Viness Pillay¹

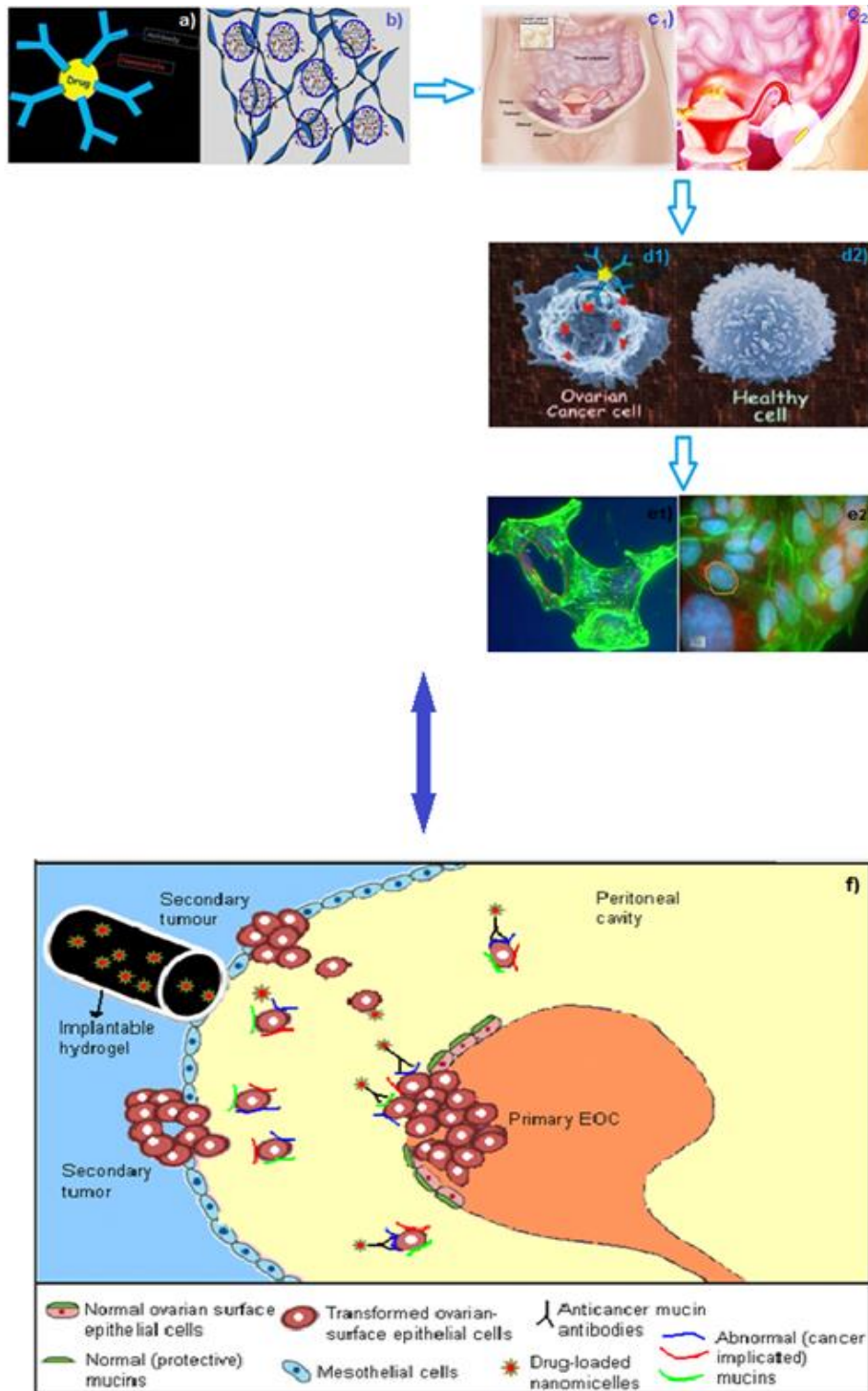
¹Wits Advanced Drug Delivery Platform Research Unit, Department of Pharmacy and Pharmacology, Faculty of Health Sciences, School of Therapeutics Sciences, University of the Witwatersrand, Johannesburg, 7 York Road, Parktown 2193, South Africa

²Section of Anatomical Pathology, Department of Paraclinical Sciences, Faculty of Veterinary Science, University of Pretoria, Onderstepoort, 0110, Republic of South Africa

ABSTRACT:

The purpose of this study was to validate an optimum mouse model for human ovarian carcinoma research and to utilize the model to assess the efficacy of various chemotherapeutic treatment protocols. The NIH:OVCAR-5 cell line from an ovarian carcinoma of a 47-year-old woman was established in tissue culture and in nude mice. NIH:OVCAR-5 cell suspensions (10^8 , 10^7 cells/ml) were injected intraperitoneally (IP), and subcutaneously (SC), respectively into 6-8-week-old Swiss athymic nude mice. Human ovarian carcinomas (NIH:OVCAR-5) were induced within 10 days of inoculation. As NIH:OVCAR-5 mainly proliferated within the peritoneal cavity and over-expressed mucin 16 (MUC16/CA 125) as compared to normal tissue, thus it was rational to conclude that the IP growth mimicked human clinical disease. Clinically advanced ovarian carcinoma disease was characterized by several positive indicative signs which included an extensive solid tumour burden with evidence of transcoelomic metastasis (peritoneal carcinomatosis), and the development of severe ascites. Histopathology later confirmed induction of malignant anaplastic ovarian carcinomas, with evidence of metastatic tumour emboli within lymphatic vessels. An optimized implant containing various experimental treatments was injected either IP or SC into the mice at 0.2 ml (volume) at the site of tumour growth. An implantable drug-loaded antibody functionalized nanomicelles delivery system was compared with both placebo and clinical chemotherapeutic groups. The chemotherapeutic drugs utilized in this model system were cisplatin and methotrexate. Each mouse in the experimental group received a once-off implant treatment monitored for a period of 30 days whilst the IV chemotherapy group was treated at 11-day intervals for a period of a month. In order to assess the response of induced ovarian carcinomas to the various treatment modalities, a variety of indices were assessed, including whole mouse weight, tumour size (measured with calipers and sonography), quantification of mucin 16 antigen expression levels (using immunohistochemistry in formalin-fixed, paraffin-embedded ovarian carcinoma tissues and sandwich quantitative CA125 Human ELISA Kit on serum, plasma and ascitic fluid), as well as survival rate of mice post-treatment. Results demonstrated tumour regression including reduction in mouse weight and tumour size, as well as a significant ($p < 0.05$) reduction in mucin 16 levels in serum and ascitic fluid and improved survival in mice after treatment with the experimental anti-MUC16/CA125 antibody-bound nanotherapeutic implant drug delivery system ($p < 0.05$). Based on the results of this study, the antibody-bound nanotherapeutic implant drug delivery system should be considered a potentially important immuno-chemotherapeutic agent that can be employed in human clinical trials of advanced, and/or recurring, metastatic epithelial ovarian cancer (EOC).

GRAPHICAL ABSTRACT



APPENDIX C

ANIMAL ETHICS CLEARANCE

CLEARANCE CERTIFICATE (C1)

AESC3



STRICTLY CONFIDENTIAL

ANIMAL ETHICS SCREENING COMMITTEE (AESC)

CLEARANCE CERTIFICATE NO. 2012/46/05

APPLICANT: Mr. J Pantshwa

DEPARTMENT: Pharmacy & Pharmacology

PROJECT TITLE: *In vivo* intraperitoneal delivery of an injectable hydrogel-based implant for ovarian cancer treatment in the Fischer 344 rat model.

Number and Species

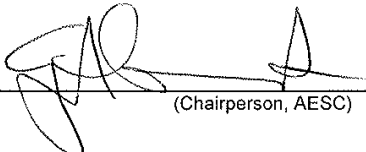
Approved: Pilot study to establish model for the induction of ovarian cancer, 5 mice per strain investigated.

Approval was given for to the use of animals for the project described above at an AESC meeting held on **27 November 2012**. This approval remains valid until **30 November 2014**.

The use of these animals is subject to AESC guidelines for the use and care of animals, is limited to the procedures described in the application and to the following additional conditions:


Conditions of approval:

- Mice or rats from any of the following strains may tested: Hsd:Athymic Nude-Foxn1nu, Hsd:RH-Foxn1rnu, BALB/cOlaHsd-Foxn1nu, Swiss Nude, NMRI Nude, CD1 Nude, BALBc AnN Nude, Rowett Nude (RNU) Rat | A T-Cell-Deficient, Athymic Nude Rat Model, NCr nude, B6 nude, HRN™ nude, NIH Nude, BALB/cA nude, BALB/c nude. Note that the availability of strains is not guaranteed.
- Work should proceed with close communication with Dr Eide of CAS.

Signed:  _____
(Chairperson, AESC)

Date: 5/12/12

I am satisfied that the persons listed in this application are competent to perform the procedures therein, in terms of Section 23 (1) (c) of the Veterinary and Para-Veterinary Professions Act (19 of 1982)

Signed:  _____
(Registered Veterinarian)

Date: 5/12/12

cc: Supervisor:
Director: CAS

MODIFICATIONS TO THE STUDY: CLEARANCE (C2)

AESC 2012 M&E

Please note that only typewritten applications will be accepted.

UNIVERSITY OF THE WITWATERSRAND ANIMAL ETHICS SCREENING COMMITTEE MODIFICATIONS AND EXTENSIONS TO EXPERIMENTS

- a. Name: Jonathan Pantshwa
b. Department: Pharmacy and Pharmacology

c. Experiment to be modified / extended

	AESC NO		
Original AESC number	2012	46	05
Other M&Es :			

- d. Project Title: *In vivo* intraperitoneal delivery of an injectable hydrogel-based implant for ovarian cancer treatment in the Balb/c mouse model.

	No.	Species
e. Number and species of animals originally approved:	144	<i>Swiss Nu/Nu</i> <i>Athymic nude mice</i>
f. Number of additional animals previously allocated on M&Es:	0	
g. Total number of animals allocated to the experiment to date:	40	<i>Swiss Nu/Nu</i> <i>Athymic nude mice</i>
h. Number of animals used to date:	29	<i>Swiss Nu/Nu</i> <i>Athymic nude mice</i>

- i. Specific modification / extension requested:

We request the use of athymic hairy mice for the inoculation of NIH:OVCAR5 ovarian cancer cell line in addition to that of the nude athymic mice currently being used.

In addition, blood sampling from the sephanus vein will be collected pre-inoculation, during the period of tumour growth, during the period of chemotherapeutic dosing and post-mortem. This is to determine progression and regression of the MUC16 antigen as well as presence of drug concentrations.

At each time interval, 0.2ml of blood will be sampled. Mice will be transported from the SPF unit in a closed, sterile IVC cage to the Vevo 2100 Imager for sonar imaging of tumour sizes (on the 8th floor). Thereafter, the mice will be returned to an alternative sterile room in the CAS unit. Blood will be sampled at each time point from different mice, to ensure the maximum amount of blood is attained while simultaneously allowing each mouse to recuperate (as shown in Table 1 below).

Table 1: Timeline for the blood sampling

Time in days	Procedure
0	1 st blood sampling.
3	IP inoculation of NIH:OVCAR5 cells in mice.
20	Vevo sonar imaging of tumour size and 2 nd blood sampling.
27	Delivery system injected in inoculated mice.
29	3 rd blood sampling on alternative mice.
31	4 th blood sampling on alternative mice.
35	5 th blood sampling on alternative mice.
39	6 th blood sampling on alternative mice.
41	7 th blood sampling on alternative mice.
43	Euthanasia of all mice and final blood sample via cardiac puncture.

j. Motivation for modification / extension:


Our rationale for requesting this adjustment is that Athymic Nude mice are very expensive and the use of hairy Athymic mice will surpass the need for any further purchases. These hairy Athymic mice are of Balb/c mouse background which is ideal for a general multipurpose model for hybridoma development, monoclonal antibody production and infectious diseases according to our Supplier (Charles River France: <http://www.criver.com/products-services/basic-research/find-a-model/balb-c-mouse>). In previous studies, hairy Balb/c mice have been used for epithelial ovarian cancer studies as well as malignant gliomas (Walter *et al*, 1994, Rose *et al*, 1996). Blood sampling is necessary in order to accurately determine fluctuations in MUC16 antigen concentrations as well as effective drug presence. This would provide pharmacokinetic and pharmacodynamic parameters of the chemotherapeutic drugs in ovarian cancer treatment.

References

- Rose GS, Tocco LM, Granger GA, DiSaia PJ, Hamilton TC, Santin AD, Hiserodt JC, 1996. Development and characterization of a clinically useful animal model of epithelial ovarian cancer in the Balb C mice. *American Journal of Obstetrics and Gynecology*. 3, 593-599.
- Walter KA, CahmMA, Gur A, Tyler B, Hilton J, Cohin O M, Burger P C, Domb A, Brem H, 1994. Interstitial Taxol delivered from a biodegradable polymer implant against experimental malignant glioma. *Cancer Research*. 54, 2207 – 2212.

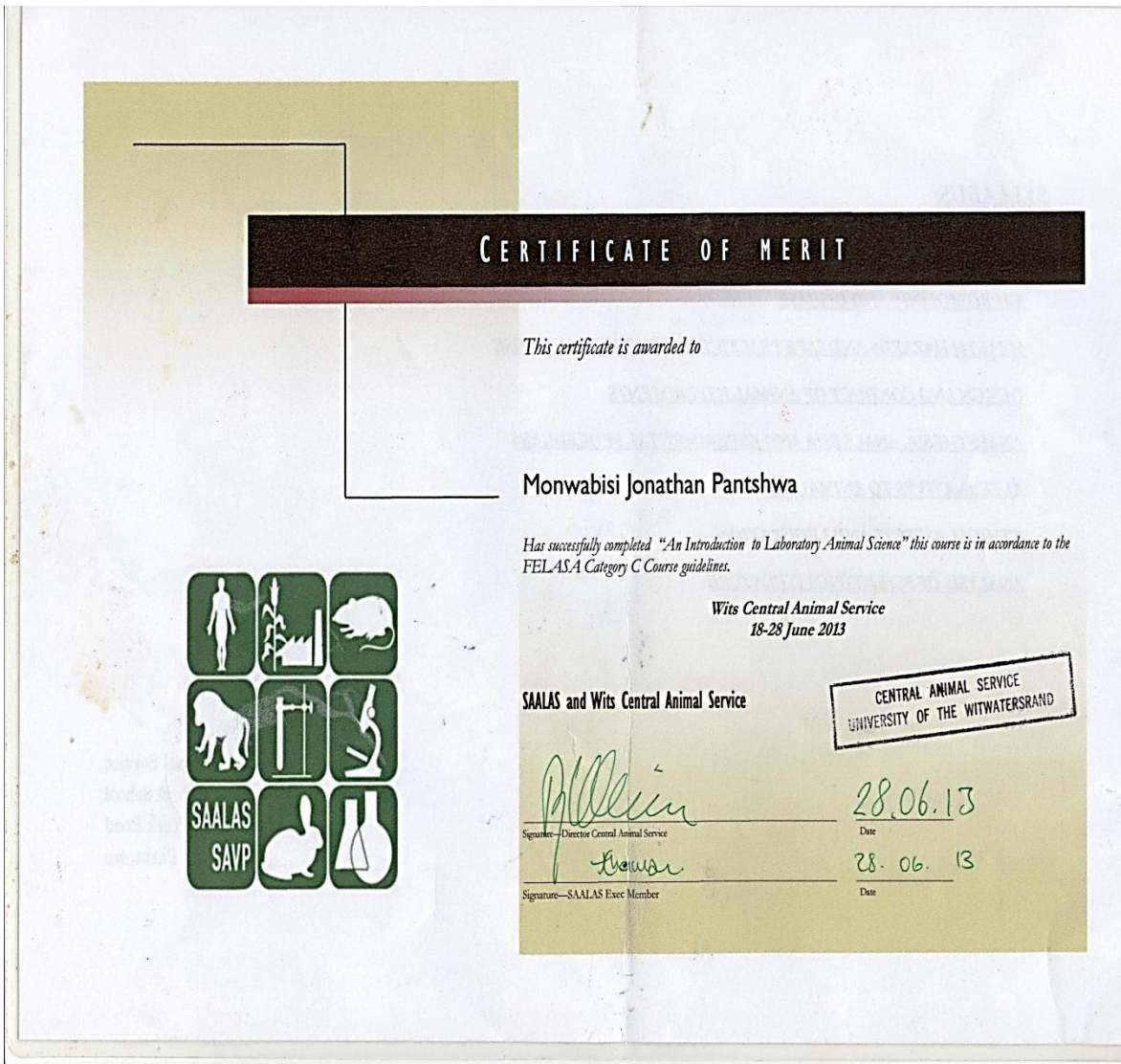
Date: 19 December 2013

Signature: 

Signature: 
Chairman, AESC

APPENDIX D

FELASA COURSE CERTIFICATE



APPENDIX (E)

IMPORT PERMITS AND SOP's

IMPORT PERMIT FOR THE ATHYMIC NUDE (E1)



agriculture, forestry & fisheries

Department:
Agriculture, Forestry and Fisheries
REPUBLIC OF SOUTH AFRICA

Directorate of Animal Health
Import-Export Policy Unit
Private Bag X138
Pretoria, 0001
Republic of South Africa

Tel: (27)-012-3197514
Fax: (27)-012-3298292

IMPORTER:
JONATHAN PANTSHWA
PHARMACY & PHARMACOLOGY WITS-DEPT OF
PHARMACY ROOM 8M08 MEDICAL SCHOOL
7 YORK ROAD SOUTH AFRICA
PARK TOWN
2193



PERMIT NO: 13/1/1/30/2/1/2-491
Valid from: 2013-02-25
Expiry date: 2013-05-25

VETERINARY IMPORT PERMIT FOR LABORATORY MICE/RATS [Issued in terms of the Animal Diseases Act, 1984 (Act 35 of 1984)]

Authority is hereby granted for you to import into Republic of South Africa.

180 NUDE MICE MICE, 20 BOXES IN TOTAL
from: CHARLES RIVER LABORATORIES FRANCE, BP 0109 69592 L'ARBRESLE CEDEX FRANCE

subject to the following conditions :

- Each consignment must be accompanied by:
 - This original permit;
 - a certificate issued by the Veterinary Authority of the country of export, certifying:
 - the origin of the 180 NUDE MICE;
 - that the 180 NUDE MICE do not constitute any danger of introducing infectious or contagious diseases into South Africa;
 - that the 180 NUDE MICE were securely packed in leakproof containers, sealed under official Veterinary supervision.
- the consignment is to be airfreighted through port of entry **O.R. TAMBO INTERNATIONAL AIRPORT**. The mice/rats may only be imported as manifest cargo under an airwaybill number and may not be imported as personal luggage.
- the 180 NUDE MICE must be kept and used for purposes of testing/research at the laboratories of **CENTRAL ANIMAL SERVICES FACULTY OF MEDICINE , UNIVERSITY OF THE WITWATERSRAND** under the personal supervision of **DR DAG MARCUS EIDE**
- On completion of tests/research the 180 NUDE MICE are to be euthanized and destroyed by incineration;
- The State Veterinarian: **KEMPTON PARK** Tel: **(011)973 2827** must be advised timeously of the arrival of the consignment.
- This permit is subject to amendment or cancellation by the Director **Animal Health** at any time and without prior notice being given.
- This permit is valid for three (3) months from date of issue and **FOR ONE CONSIGNMENT ONLY**.


DIRECTOR: ANIMAL HEALTH

NOTE:

From 1st January 2005 any consignment imported into South Africa packed with either wood packing material or dunnage, will require treatment to remove any pests present (by heat or methyl bromide fumigation). Treatment must be indicated on packing material. [Enquiries: Directorate Plant Health & Quality Fax: 012 319 6350 or www.daff.gov.za]

STANDARD OPERATING PROCEDURES FOR HANDLING NUDE MICE (E2)

Purpose:

Nude and other immunocompromised mice are at greater risk than conventional mice for the development of infectious disease. Frequently, infectious pathogens are transferred to nude mice by contaminated equipment or exposure to contaminated environments. The procedures described here are implemented to minimize the risk of infectious disease to nude mice.

General Procedures:

1. All equipment and caging is sterilized prior to using with the nude mice. See the *“Preparation of Nude Mouse Caging”* for details.
2. The night prior to manipulating the mice under the laminar flow hood, the hood is sprayed with 70% ethanol with the blower on. After each use, the hood is sprayed with a disinfectant and wiped of all debris and again sprayed with the 70% ethanol.
3. The hood blower is left on at all times. The light is turned off when the hood is not in use.
4. All individuals handling the nude mice must wear a steam sterilized gown, mask, hair bonnet, and sterile gloves. Optimally, two individuals are present during the handling of the mice, one that is designated as the animal handler and maintains sterility, while the other handles the non-sterile items and opens the sterile materials for the handler.
5. It is required that persons reaching into the hood wear a clean long-sleeved gown, lab coat or smock, mask and bonnet and the required gloves to prevent contamination of the sterile interior.
6. Aseptic technique should be used at all times when handling the nude mice. Any objects or surfaces that will come in contact with the mice should have been sterilized by steam, UV radiation, or contact with 70% ethanol for at least 30 minutes.

Unpacking Newly Arrived Mice:

1. Prepare laminar flow hood as previously described. Animal handlers must be prepped, as described above.
2. Shipping labels, health reports, cable ties and animal information are removed and recorded.
3. Shipping containers are sprayed with a chlorine dioxide solution before they are placed in the hood.
4. The designated animal handler opens the sterile food and water under the hood.
5. The non-sterile person opens the cage and shipping box under the hood. Care must be taken by the non-sterile person to avoid contact with the inner surfaces of the hood and the inside of the shipping box and cage.
6. The animal handler then adds food and water to the cage top and removes the mice from the shipping box and places them in the cage. JAG cages are limited to 5 mice per cage; Nalgene cages will accommodate 7 mice per cage; Innovive cages allow 5 mice per cage. The non-sterile person will close the cage and remove it from the hood.

7. The animal handler should re-glove after each shipping container to avoid possible cross contamination of groups of animals in case the shipping container has been damaged.
8. Container number is recorded on the cage card to track origin of the animals in case of illness.
9. Place the water bottle onto the cage BEFORE removing from the hood.
10. Unused water bottles are resealed in the container and will be stored in the room for future use. Unused food is given to FLSC personnel for use in the breeding colony rooms.
11. Mice will undergo a two week acclimation period prior to experimental use.

Cage changing:

1. Follow all previous steps for hood preparation, gowning of personnel and cage handling.
2. The designated animal handler should re-glove after every 6-10 cages or if gloves are torn, contaminated or if a cage has ill animals.
3. Any cages with animals appearing sick will be placed at the end of the cage changing order to avoid possible exposure of healthy animals to pathogens or contaminants.
4. The mouse cages are changed at least once weekly or more often, if deemed necessary. JAG and Nalgene cages are sterilized as a complete unit consisting of a bedded cage, cage top with feeder and filter bonnet and will be replaced as a unit weekly. Innovive products come separately as empty cages, feeders, and cage tops. Animals housed in the Innovive caging will require weekly cage changes. Feeders will be reused changing them every 4 weeks and cage bonnets will be reused and changed every 8 weeks unless there is a break in sterility necessitating replacement of the contaminated component.
5. If food and/or water must be added between the scheduled cage changes, it must be done aseptically under the prepared hood.
6. Water bottle preparation and sterilization are the responsibility of the PI. Water is acidified by adding 2 drops of 12M HCl to 8 liters of RO water. Water is sterilized in individual bottles covered with foil. Bottle lids are sterilized separately in an autoclave bag. Innovive water bottles are pre-sterilized and are replaced weekly unless acidified in which case they are changed every other week. To acidify Innovive™ water bottles, place 0.15 ml of 12M HCl into each bottle through the lid opening. Any special diets must be provided by the PI. If diets are not sterilized by the manufacturer, the PI is responsible for autoclaving or sterilization of the food.
7. Food and water are stored in the room with the hood.
8. Gowns are laundered, wrapped and sterilized by FLSC staff. Should an experiment require daily gowning by multiple persons, disposable sterile gowns should be purchased by the PI and stocked in the storage cabinet in the room with the hood.

Routine Inspection of the Mice:

1. All animals will be checked daily, including on the weekends and holidays.
2. Examine the mice by viewing them through the cage. The micro-isolator top should not be opened without the permission of the investigator or the Associate Director or the Director of FLSC and NEVER outside the sterile hood.
3. In the event of a problem, the investigator (see the contact list on the door) should be called. Emergencies should also be directed to Jonathan Pantshwa or Khadija Rhoda.

IMPORT PERMIT FOR NIH:OVCAR-5 CANCER CELL LINE (E3)



health

Department:
Health
REPUBLIC OF SOUTH AFRICA

Private Bag X828, PRETORIA, 0001
Civitas Building Corner Andries and Struben Street, PRETORIA, 0001
Tel (012) 395 0922 • Fax (012) _____

(012) 395 8366/9197

Ms Lineo Motopi

0866326815/2606

J1/2/4/1 No 1/13

IMPORT PERMIT

In terms of Section 68 of the National Health Act 2003 (Act No. 61 of 2003) –

Jonathan Pantsha
PhD Researcher
Pharmacy and Pharmacology Wits
Pharmacy Room 8 M 08 Medical School
7 York Road
PARKTOWN
2193 South Africa
Tel: (011) 717 1302 Fax: (011) 717 2199

is hereby authorised to import into the Republic of South Africa –
Human ovarian cancer cell line, NIH: OvcAR - 5

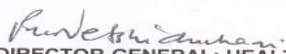
from –

Pamela Nakajima, PhD (Staff Scientist)
Fox Chase Cancer Center
Corporate Alliances, 610 York Road, Suite
400 Jerkitown, PA 19046
UNITED STATES OF AMERICA
Tel: + Fax:

for – Research.

This import permit is subject to the following conditions:

1. The material shall be exported from the country specified above, within the legal requirements of that country.
2. The material shall be imported into South Africa and handled in accordance with the provisions of the National Health Act 2003 (Act No. 61 of 2003), and the regulations made in terms of the Act.
3. The import permit shall not be used for any trade or advertising purposes.
4. **This import permit shall expire on 28 February 2014.**


DIRECTOR-GENERAL: HEALTH
Date: 01/03/2013
Ms P Netshidzivhani

NIH:OVCAR-5 CANCER CELL LINE MATERIAL TRANSFER AGREEMENT (E4)



TEMPLE HEALTH

*Kurt Schwinghammer, Ph.D.
Vice President
Research & Development Alliances*

*610 Old York Road, Suite 400
Jenkintown, Pennsylvania 19046*

*215 214 3985
FAX 215 214 1440
Kurt.Schwinghammer@fcc.edu*

March 7, 2013

Jonathan Pantshwa
University of the Witwatersrand
Pharmacy and Pharmacology
Wits-dept of pharmacy
ROOM 8M03
MEDICAL SCHOOL, 7 YORK ROAD
SOUTH AFRICA
PARKTOWN
2193

Dear Dr. Pantshwa:

On behalf of The Institute for Cancer Research d/b/a The Research Institute of Fox Chase Cancer Center (hereinafter "FOX CHASE") hereby acknowledges the request of University of the Witwatersrand (hereinafter "REQUESTER") for OVCAR-5 (hereinafter "ORIGINAL MATERIAL") and agrees to provide such specimens to REQUESTER, subject to the following terms and conditions:

1. Legal title to the ORIGINAL MATERIAL, its progeny, unmodified derivatives and any accompanying know-how or data (collectively, the "MATERIALS") is to remain in FOX CHASE.
2. This agreement and any transfer of the MATERIALS made pursuant hereto constitute a license to REQUESTER for use of the MATERIALS for purposes of internal research only, such research to be conducted under the exclusive supervision and control of Dr. Jonathan Pantshwa (hereinafter REQUESTER'S PI). The MATERIALS shall not be used in human subjects, clinical trials, or for diagnostic purposes involving human subjects without FOX CHASE's prior written consent.
3. REQUESTER specifically agrees to make no use of the MATERIALS for any profit-making or other commercial purposes, including use of MATERIALS to perform contract research, to screen compound libraries, to produce or manufacture products for general sale, or to conduct research activities that result in any sale, lease, license, or transfer of the MATERIALS or substances created there from containing or incorporating said MATERIALS.
4. No specimen of the MATERIALS is to be given, made available or otherwise distributed to another party without FOX CHASE's prior written consent. All such specimens are to remain under the immediate and direct control of REQUESTER'S PI unless said prior written consent is obtained.
5. REQUESTER'S PI agrees to inform FOX CHASE of all experimental results, discoveries

333 Cottman Avenue – Philadelphia, Pennsylvania 19111 – foxchase.org

and/or inventions arising out of REQUESTER'S PI's research using the MATERIALS and the role, if any, of all FOX CHASE personnel involved in the research, discovery or invention, as the case may be. All such information may be used by FOX CHASE for research purposes or for submissions to regulatory agencies, but shall otherwise be held in confidence by FOX CHASE.

6. This Agreement shall not be interpreted to prevent or delay publication of research findings resulting from the use of the MATERIALS or substances created there from containing or incorporating said MATERIALS. REQUESTER PI agrees to provide appropriate acknowledgement of the source of the MATERIALS in all publications.

7. The MATERIALS are experimental and are provided to REQUESTER WITHOUT WARRANTY OF MERCHANTABILITY OR FITNESS FOR PARTICULAR PURPOSE OR ANY OTHER WARRANTY, EXPRESS OR IMPLIED. FOX CHASE MAKES NO REPRESENTATION OR WARRANTY THAT THE USE OF THE MATERIALS WILL NOT INFRINGE ANY PATENT, COPYRIGHT, TRADEMARK, OR OTHER PROPRIETARY RIGHTS.

8. In no event shall FOX CHASE be liable for any use of the MATERIALS by REQUESTER or its employees, or any loss, claim, damage or liability of whatever kind or nature which may arise from, or in connection with this agreement, or the use, handling or maintenance of the MATERIALS, except to the extent permitted by law when caused by the gross negligence or willful misconduct of FOX CHASE.

9. REQUESTER will use the MATERIALS in compliance with all applicable laws and governmental regulations.

10. The MATERIALS in the possession of REQUESTER are subject to return upon demand by FOX CHASE at any time after 12 months from the date of acceptance of this agreement, if they are no longer being employed for purposes of research.

11. This agreement is not assignable, whether by operation of law, or otherwise, without FOX CHASE's prior written consent.

12. This Agreement shall be construed, interpreted and governed by, and the rights and obligations of the parties determined in accordance with, the laws of Commonwealth of Pennsylvania, U.S.A., without giving effect to any conflict of laws provision(s).

13. This agreement constitutes the entire understanding between the parties with respect to the subject matter hereof; there are no representations, promises, warranties, or understandings relied upon by either party which are not contained herein.

14. In consideration of providing the MATERIALS herein granted by FOX CHASE to REQUESTER, REQUESTER is responsible to pay to FOX CHASE a One Hundred-Fifty U.S. Dollar (\$150.00) handling fee in addition to paying the shipping costs. Shipping information, along with proper account number is to be emailed directly to Dr. Pamela Nakajima at Pamela.Nakajima@fcc.edu. The handling fee is payable in advance to FOX CHASE. Payments may be made by check payable to:

Institute for Cancer Research
Attention: Chief Financial Officer
Office of Business Operations
604 Cottman Avenue
Cheltenham, PA 19012

333 Cottman Avenue – Philadelphia, Pennsylvania 19111 – foxchase.org

Or, the payment may be delivered via wire to the following account:

Bank Name: PNC Bank
Bank Address: 1600 Market Street
Philadelphia, PA 19103
Bank ABA #: 031000053
Bank SWIFT #: PNCCUS33
Bank Account Name: Institute for Cancer Research
333 Cottman Avenue
Philadelphia, PA 19111
Bank Account #: 8601786447

If the foregoing terms and conditions are acceptable, please so indicate by signing and dating one original of this agreement and returning the same to me.

Very truly yours,

Institute for Cancer Research

Kurt Schwinghammer, Ph.D.
Vice President
Research & Development Alliances

Accepted:



Signature of Authorized Representative

YAGNA E. CHOONARA

Printed Name

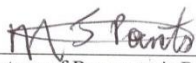
PROF.

Title

8/3/2013

Date

Reviewed and Acknowledged:



Signature of Requester's Principal Investigator

JONATHAN PANTSHWA

Printed Name

MR

Title of Requester

08/03/2013

Date

**Disclaimer: Temple Health refers to the health, education and research activities carried out by the affiliates of Temple University Health System, Inc. and by Temple University School of Medicine.

333 Cottman Avenue – Philadelphia, Pennsylvania 19111 – foxchase.org

PROTOCOL FOR INTRA-PERITONEAL AND SUBCUTANEOUS INDUCTION OF (NIH:OVCAR-5) OVARIAN CARCINOMA CELLS (E5)

Growth of cells in the peritoneal cavity and subcutaneous space of immunocompromised mice are a common method for assaying tumorigenic potential in vivo. These techniques are also used to assess the effects of therapeutic interventions on cancer cell lines.

Materials and Reagents

1. Trypsin (Invitrogen; 25300-054)
2. RPMI media
3. L-glutamine, (Invitrogen; 11965-092)
3. Streptomycin/Penicillin antibiotics
4. FBS (Invitrogen; 16000-044)
5. Insulin
4. PBS
5. Trypan blue (Invitrogen;15250-061)
6. Charles River France Swiss nude Mice
7. Isoflurane (usually purchased through animal facility at institution)

Equipments

1. Centrifuges
2. Insulin syringe
3. Hemocytometer
4. Cell culture hood
5. Incubator
6. Microscope

Procedure

1. 45mL RPMI media with ingredients: 100 μ L-L-glutamine, 100 μ L Streptomycin/Penicillin antibiotics, 5mL FBS, 100 μ L insulin was prepared.
2. Remove growth medium from cells and wash with 5 mL of PBS.
3. Aspirate PBS, add 2 mL of trypsin and incubate for 5 min, or until cells have detached, at 37 °C
4. Quench trypsin by adding the RPMI medium with ingredients.
5. Pellet cells by centrifugation for 5 min at 1100 RPM and 37 °C.
6. Aspirate medium, wash cells with 10 mL sterile PBS, mix well with pipette and save 50 μ L aliquot of cells for counting.
7. Pellet cells by centrifugation for 5 min at 1100 RPM and 37 °C.
8. Aspirate PBS, resuspend cells in fresh PBS to a concentration: 1×10^6 cells/100 μ L for subcutaneous injections and 1×10^7 cells/100 μ L for intraperitoneal injections.
9. Transfer cells to a sterile eppendorf tube. Note, the cell number required depends upon the aggressiveness of the tumor cells and can vary by an order of magnitude.
10. (Optional) Add an equal volume of RPMI media without ingredients to cells and mix carefully with pipette.
11. Slowly pull up 100 μ L of cells alone or 200 μ L of cell/RMPI mixture using an insulin syringe. Note, cells can be damaged by the small gauge of the insulin needle; however, insulin syringes provide a more accurate volume measurement. If significant death is observed, 1mL syringes with 22 gauge needles can be substituted.

12. Inject 1×10^6 cells into the flanks or necks and 1×10^7 cells into the peritoneal cavity of immune deficient mice, preferably Swiss nude mice. To do this, pinch the skin of the mouse between your index finger and thumb and pull the skin away from the body of the mouse. Inject slowly and evenly into the pouch created by your fingers, creating a single bubble of cells beneath the skin and avoiding too much spread of the cells. Anesthetizing the mice using isoflurane makes the injection process significantly less stressful for the both the mice and the researcher.

Recipes

1. Trypsin (0.05%)
2. RPMI cultural medium: supplemented with 10% fetal bovine serum, 100 μ L-glutamine, 100 μ L Streptomycin/Penicillin antibiotics.